Cellular Senescence in Non-Small Cell Lung Cancer: from mechanisms to therapeutic opportunities

by

Estela González-Gualda

Queens' College

September 2021

This thesis is submitted to the University of Cambridge for the degree of Doctor of Philosophy

Department of Oncology

CRUK Early Detection Programme, Cambridge Cancer Centre

University of Cambridge

DECLARATION

This thesis is the result of my own work and includes nothing which is the outcome of work done in collaboration except as specified in the text and declared here:

- Bioinformatics analyses of RNA-seq data were performed in collaboration with Dr Ezequiel Martín Rodríguez (Department of Oncology, University of Cambridge), Dr Guy Slater (CRUK Cambridge Institute) and Dr Ioana Olan (CRUK Cambridge Institute)
- Computed Tomography (CT) imaging analysis was performed in collaboration with the Molecular Imaging Unit from the Spanish National Cancer Research Centre (CNIO)
- Synthesis and validation of novel senolytic Nav-Gal presented in this work was performed by Dr Beatriz Lozano-Torres (Polytechnic University of Valencia)
- *In vivo* validation of Nav-Gal in xenograft mouse model was performed with the help of Dr Marta Paez-Ribes (CRUK Cambridge Institute)
- Platelet toxicity analyses were performed by Dr David Macías (Department of Oncology, University of Cambridge) and Dr Beatriz Lozano-Torres (Polytechnic University of Valencia)

This thesis is not substantially the same as any work that has already been submitted before for any degree or other qualification.

The word count of this thesis is 59,144 and it does not exceed the prescribed word limit for the Degree Committee.

ABSTRACT

Lung cancer is the leading cause of cancer-related deaths in our society due to the inefficiency of early detection strategies and the high rate of treatment failure. Therefore, a better understanding of the mechanisms underlying its origin and the response to current treatment paradigms are crucial to improve lung cancer survival. Cellular senescence is a powerful tumour-suppressive mechanism whereby cells stably enter a cell-cycle arrest in response to oncogenic stress. However, the accumulation of senescent cells can alter the tumour microenvironment through a strong paracrine secretion of factors that can lead to detrimental and tumour-promoting effects. Intriguingly, senescence has been reported to be a defining feature of early lesions in Non-Small Cell Lung Cancer (NSCLC), a subtype that accounts for over 80% cases of lung cancer. In addition, senescence has also been reported to occur in response to the standard of treatment for this disease. It is thus conceivable that senescence may play a role in the origin and progression of this disease, despite a causal connection remains to be deciphered. Pharmacologic therapeutics that preferentially target senescent cells, known as senolytics, have been successful in preventing and even reversing senescence-driven detrimental effects in multiple pathological processes. However, their suboptimal specificity and toxicities hamper their clinical translation. Therefore, the targeting of senescent cells through the development of second-generation senolytics that can overcome these obstacles has the potential to revolutionise cancer treatment. The aim of this work is to define the role of cellular senescence at the origin and progression of lung cancer and in response to chemotherapy, and to develop safer and more effective therapeutic approaches to eliminate senescent cells in the context of lung malignancies.

In this thesis, we studied the accumulation of senescent cells during the development of lung adenocarcinoma using a $Kras^{G12V}$-driven lung cancer mouse model. We demonstrate that senolytic treatment of early lesions results in a significant reduction in lung tumour burden and increased survival, providing evidence of the tumour-promoting effect of senescence in early stages of NSCLC. Our research also reveals that platinum-based chemotherapy of human and murine lung adenocarcinoma cells induces

senescence, which in turn promotes malignant phenotypes on untreated cancer cells in a paracrine manner *in vitro*, in xenografts and in orthotopic models of lung adenocarcinoma. Through high throughput unbiased transcriptomic and proteomic approaches, we show that secreted TGF-β ligands activate the Akt/mTOR pathway in untreated cells resulting in enhanced tumour growth. We further demonstrate that senolytic treatment and pharmacologic inhibition of TGFβR1 in tumours can prevent increased proliferation and enhance survival of lung tumour-bearing mice. In order to develop a novel approach for improved senolytic treatment, we show that the galacto-conjugation of senolytic ABT-263 (navitoclax) in the form of an activatable pro-drug significantly enhances cytotoxicity in combination with cisplatin, resulting in reduced lung cancer tumour growth. Importantly, our approach demonstrates decreased navitoclax-associated toxicities, including platelet apoptosis in human and murine blood treated *ex vivo* and decreased thrombocytopenia in mouse lung cancer models.

In summary, this PhD thesis provides evidence of the incidence and role that cellular senescence plays in promoting the progression of early and advanced NSCLC and demonstrates that cisplatin chemotherapy drives pro-tumorigenic phenotypes in a paracrine fashion, which can be prevented with senolytic and TGFβR1 inhibitory treatments. Lastly, it proposes a novel second-generation therapeutic approach to mitigate senolytic toxicities and enhance the efficiency of targeting senescence in the context of lung cancer.

ACKNOWLEDGEMENTS

I would like to express my most heartfelt gratitude to my supervisor Dr Daniel Muñoz-Espín for his invaluable support and advice during these four years, for believing in my potential and for giving me the opportunity to become a doctor under his exceptional guidance and admirable expertise.

I would like to give a special thanks to Dr David Macias, for helping me find the way to move my project forward and acting as an outstanding mentor, providing crucial input and invaluable resources, and making me a better researcher in the process. I would like to also express my warmest gratitude to past and current members of the lab, including Marta, Hui-Ling, Drew, Zhenguang, Cristina, Samir, Sofía and Georgina, for their priceless help in my projects, the moral support and the yummy treats. I couldn't have asked for better colleagues in my PhD journey.

Thank you to all collaborators that have provided critical contributions, expertise and support during the development of this thesis, including the groups of Prof Martínez-Barberá (UCL), Prof Martínez-Máñez (Polytechnic University of Valencia), Dr Jim Korkola (OHSU) and Dr Narita (CRUK Cambridge Institute), who has also been my PhD co-adviser. A particular thanks to Dr Scott Haston, Dr Beatriz Lozano-Torres and Dr Ezequiel Martín for their work and collaborations and for showing me how extraordinary science can be when great teams come together to achieve a common goal.

I can't thank my Cambridge friends (Compango CDR and beyond) enough for their constant encouragement, for taking care of me and for reminding me to prioritise myself at all times. Thank you for your endless assistance and friendship throughout this process. You made Cambridge feel like home, and provided a safe space when this PhD seemed to carry me away.

A mi familia y amigos en Barcelona, gracias por vuestro apoyo incondicional durante cada etapa de mi vida. En especial, gracias a mis padres, Mari y Francis, que a pesar de que aún no entiendan bien qué es un doctorado, priorizaron mi educación por encima de todo, y me enseñaron a no tener miedo a soñar en grande y a luchar incansablemente por lo que me apasiona, a pesar de las adversidades. Gracias por hacerme creer que los límites no existen.

Finally, I would like to give my whole gratitude to my partner, Ettore, who has been my biggest supporter and listener, and has celebrated every of my achievements during this PhD as his own. Thank you for being my rock over the years, for showing interest in my research, for bringing clarity when things seemed dark and for your endless encouragement to make me become the best version of myself as a scientist and as a woman.

Thank you all.

TABLE OF CONTENTS

LIST OF FIGURES

LIST OF TABLES

ABBREVIATIONS

AAH	atypical adenomatous hyperplasia
ABC	ATP-binding cassette
ADC	adenocarcinoma
AIS	adenocarcinoma in situ
ALDH	aldehyde dehydrogenase
AMH	anti-muellerian protein
AP	alkaline phosphatase
AT1	alveolar type 1
AT2	alveolar type 2
ATM/ATR	ataxia-telangiectasia mutated and Rad3-related homologue
ATR	attenuated total reflectance
B2M	beta-2 microglobulin
BCA	bicinchoninic acid
BCL-2	B-cell lymphoma 2
BMP	bone morphogenetic proteins
BSA	bovine serum albumin
C/EBPβ	CCAAT/enhancer binding protein beta
CAFs	cancer-associated fibroblasts
CAR	chimeric antigen receptor
CCL2	chemokine ligand 2
CCl_4	carbon tetrachloride
CDDP	cisplatin
CDI	coefficient of drug interaction
CDK	cyclin-dependent kinase
CDK4/6	cyclin-dependent kinase 4/6
CM	conditioned medium
CMs	conditioned media
COPD	chronic obstructive pulmonary disease

COSY	correlated spectroscopy
CSC	cancer stem cells
CTR1	copper transport protein 1
D + Q	dasatinib and quercetin
DAB	3,3′-diaminobenzidine tetrahydrochloride
DAPI	4′,6-diamidino-2-phenylindole
DAPK	death-associated protein kinase
DDR	DNA-damage response
DMSO	dimethyl sulfoxide
DNA	deoxyribonucleic acid
DNA-SCARs	DNA segments with chromatin alterations reinforcing senescence
DT	dihpteria toxin
ECAR	extracellular acidification rate
ECM	extracellular matrix
EDTA	ethylenediaminetetraacetic acid
EFNB	Ephrin-B
ELISA	enzyme-linked immunoassay
FBS	foetal bovine serum
FCCP	carbonyl cyanide-p-trifluoromethoxyphenylhydrazone
FGF	fibroblast growth factor
FSC	forward scatter
Gal	2,3,4,6-tetra-O-acetyl-α-D-galactopyranosyl bromide
GalNPs	nanoparticles conjugated with galacto-oligosaccharides
GAPDH	glyceraldehyde 3-phosphate dehydrogenase
GDFs	growth and differentiation factors
GM-CSF	granulocyte-macrophage colony-stimulating factor
GRB2	growth factor receptor-bound protein 2
GRO	growth-related oncogene
GzmB	granzyme B
HDAC	histone deacetylase

hEGF	human recombinant epidermal growth factor
HPLC	High-performance liquid chromatography
HRMS	high-resolution mass spectrometry
HSP90	heat shock protein 90
i.p.	intraperitoneal
i4F	inducible four factors
IF	immunofluorescence
IFN	Interferon
IHC	immunohistochemistry
IL	interleukin
KP	KRas-LSL$^{G12D/WT}$;p53$^{-/-}$
LAP	latency-associated protein
LCC	large-cell carcinoma
LSD1	lysine-specific histone demethylase 1A
MAPK	mitogen-activated protein kinase
MCPs	monocyte chemoattractant proteins
MEFs	mouse embryonic fibroblasts
MHC	major histocompatibility complex
MIA	minimally invasive adenocarcinoma
MICA	MHC class I polypeptide-related sequence A
MMP	metalloprotease
mTOR	mammalian target of rapamycin
MUT	mutant
NGS	next-generation sequencing
NK	Natural Killers
NMR	nuclear magnetic resonance
NPs	nanoparticles
NSCLC	non-small cell lung cancer
o.g.	oral gavage
OCR	oxygen consumption rate
OD	optical density

OIS	Oncogene-induced senescence
OSKM	Oct4, Sox2, Klf4 and Myc
PBS	phosphate buffered saline
PcG	polycomb group
PCR	polymerase chain reaction
PD-L1	Programmed death-ligand 1
PFA	paraformaldehyde
PGC-1a	peroxisome proliferator-activated receptor-γ coactivator-1a
PI3K	phosphoinositide 3 kinase
PNEC	Pulmonary neuroendocrine cell
polyI:C	polyinosinic–polycytidylic acid
pRB	retinoblastoma protein
PTEN	phosphatase and tensin homolog
PVDF	polyvinylidene fluoride or polyvinylidene difluoride
rhFGF	recombinant human FGF basic
RIPA	radioimmmunoprecipitation assay
ROS	Reactive oxygen species
RT-qPCR	real-time quantitative polymerase chain reaction
RTK	receptor tyrosine kinase
SA-β-gal	senescence-associated beta-galactosidase
SABR	steoreotactive ablative radiotherapy
SAHFs	senescence associated heterochromatic foci
SASP	senescence-associated secretory phenotype
SCC	squamous cell carcinoma
SCID	severe combined immunodeficiency disease
SCLC	small cell lung cancer
SDS	sodium dodecyl sulphate
SPC	Surfactant protein C
SSC	side scatter
TBS	tris buffered saline
TBS-T	tris buffered saline with Tween 20

TERT	telomease reverse transcriptase
TFs	transcription factors
TGF-b	transforming growth factor-beta
TLR3	toll-like receptor 3
TMRM	tetramethylrhodamine, methyl ester
TNM	tumour-node-metastasis system
TS	tumour suppressor
TTF-1	thyroid transcription factor-1
WT	wildtype

CHAPTER 1:
GENERAL INTRODUCTION

1.1. The lung

1.1.1. Anatomy and physiology of the lung

The lungs are a complex and highly specialised paired organ that allow for oxygen and carbon dioxide gas exchange in order to oxygenate the blood. They are located in the thoracic region, above the diaphragm, divided by the heart and surrounded and protected by the pleural membrane. The left human lung is structurally divided into two lobules, while the right one is divided into three. In contrast, the murine right lung is divided into four lobes, while the left one is comprised of just one. Despite these differences, the function and structure of the lower respiratory tract is largely conserved between the two species [1].

The lower respiratory tract comprises the conducting airways that drive the air from the trachea into the respiratory zone and *vice versa*. The trachea branches into the two primary bronchi, which then enter the lungs and continue to subdivide into bronchioles (**Figure 1.1**). Each of the lobules contains a branch of terminal bronchioles that eventually give rise to different respiratory bronchioles, which then in turn divide into the alveolar ducts. Within each duct, the primary functional units of gas exchange known as alveoli are clustered into alveolar sacs, and they are separated from one another by a layer of epithelial cells overlaid by small capillaries that carry blood from other parts of the body (**Figure 1.1**). There are two main types of cells in the alveoli: (1) alveolar type I cells (AT1), which allow the gas exchange and account for around 95% of the total alveolar surface area, and (2) alveolar type II cells (AT2), whose main role is the production of surfactant to control surface tension in the alveoli. Of note, these cells have also been reported to proliferate and divide, giving rise to type I alveolar cells and

providing alveoli homeostasis upon damage. In addition to these cell types, alveolar macrophages also reside within the inner surface of the alveoli and provide crucial immune surveillance. Overall, however, there are more than 40 different cell types in the lungs, which not only provide a structural and functional interface to allow gas exchange, but also serve as physical barriers against pathogens, synthesise host-defence compounds, remove particles and pathogens and release cytokines and chemokines to enable crosstalk with immune cells [1] (**Figure 1.1**).

Given the nature and function of the lungs, these organs are particularly exposed to potentially toxic chemicals or substances, infectious organisms and damaging debris. Despite the robust physiology in the lungs, these environmental factors can substantially contribute to the development of inflammatory processes and the acquisition of genetic mutations that can give rise to neoplastic lesions and tumorigenesis.

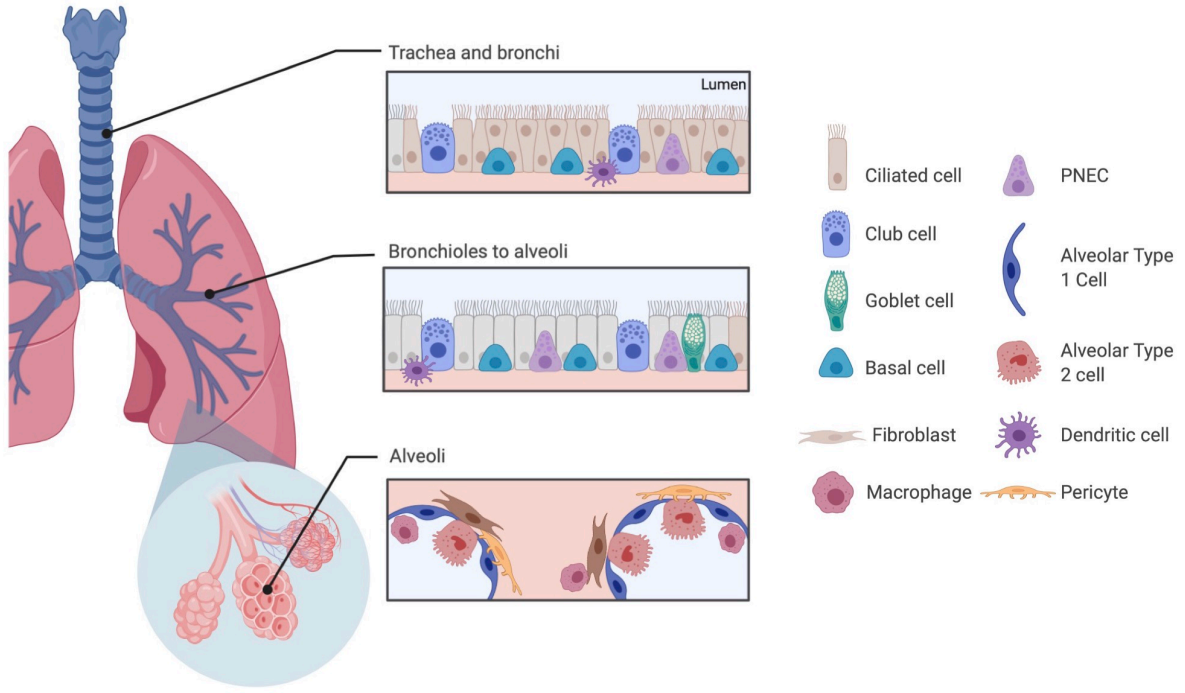

Figure 1.1. Respiratory tract anatomy and cell components of the respiratory system. The lower respiratory tract includes the trachea, bronchi, bronchioles and alveoli. In the lung, each bronchus divides into bronchi and continues to branch into smaller airways (bronchioles). The bronchioles end in the alveoli which form alveolar sacs. Tracheobronchial airways are formed by pseudostratified epithelium harbouring basal, ciliated, and secretory club cells. Intralobular bronchioles are lined by a simple columnar epithelium containing ciliated and club cells. The alveoli are lined by squamous AT1 and cuboidal AT2 cells. Alveolar

epithelial cells are closely associated with mesenchymal cells such as fibroblasts and endothelial cells. PNEC: pulmonary neuroendrocine cells. Picture created in BioRender.com.

1.1.2. Lung cancer

Lung cancer is the deadliest type of cancer around the world, accounting for more deaths than the three most common cancers (colon, breast and pancreatic) combined, and approximately 13% of all new cancers each year. The prognosis for lung cancer is very poor. In the UK, only around 16% of patients will survive 5 years post-diagnosis, and less than 10% will survive 10 years post-diagnosis [2].

The underlying processes promoting malignant transformation in the lung remain poorly understood. Despite lesions preceding the cancerous state and early stages of lung cancer have been defined, less is known about their nature and vulnerabilities, and as a consequence, the available tools for early diagnosis developed so far have not been efficient enough to tackle the disease. In addition, early stages of the disease are usually characterised by the absence of signs or symptoms. Only in later stages of lung cancer, patients generally display symptoms such as dyspnoea (shortness of breath), haemoptysis (coughing up blood) and a persistent cough [3]. As a result, almost three quarters of the patients are incidentally diagnosed at stages III and IV of lung cancer [4]. This delay in diagnosis is associated, as in many cancers, with a significantly worsened prognosis, and is thus believed to significantly contribute to the low five-year relative survival of lung cancer patients.

It is widely accepted that smoking is the main risk factor for lung cancer, accounting for up to 80% of the cases. Other lung cancer risk factors include exposure to radon and certain chemicals such as asbestos, silica and exhaust fumes, air pollution and previous lung conditions and diseases, including tuberculosis, pulmonary fibrosis and chronic obstructive pulmonary disease (COPD) [5]. Despite having a family history of lung cancer does increase the risk of lung cancer, lung damage is the most eminent risk factor in lung tumorigenesis. In this context, the association between chronic inflammation derived from unresolved injury and the increased risk of lung cancer is indeed well described [5], further supporting its impact in lung tumorigenesis.

1.1.2.1. Lung cancer classification and clinical features

Lung tumours are classified into two major histological subtypes: non-small cell lung cancer (NSCLC), which accounts for almost 85% of all the cases, and small cell lung cancer (SCLC). NSCLCs are in turn further divided into three different subtypes, namely squamous cell carcinoma (SCC), large-cell carcinoma (LCC) and adenocarcinoma (ADC) [6].

SCC is characterised by a marked differentiated phenotype, defined by the expression of SOX2 and p63 transcription factors and cytokeratin 5 and 6. Probably given its highly differentiated status, SSC is poorly metastatic in comparison to other subtypes of lung cancer, as well as it is highly heterogenous. If the tumour does not present a histological phenotype and markers specific to SCC or ADC, such as thyroid transcription factor 1 (TTF-1) and p40 [7], it is classified as LCC. In contrast with SSC, cancer cells in LCCs are poorly differentiated, and therefore have a higher ability for proliferation, progression and metastasis at earlier stages compared to other NSCLCs. This is likely to be the underlying reason why prognosis for LCC patients is particularly poor, with a five-year relative survival of approximately 13-21% [8].

ADC accounts for nearly 40% of all lung tumours around the world and it is therefore the most common subtype of NSCLC [9]. Histologically, mucin-producing cancerous glandular structures are one of the main features of ADCs. Of note, the morphology of these glands is highly heterogeneous and can drastically differ between tumours, from micropapillary formations to well-established acini. ADCs usually develop in the periphery of the lungs and express the biomarkers TTF1 and KRT7. In addition, ADCs are highly aggressive and metastatic, which contributes to the high mortality of ADC patients. Nearly 8% of patients present with lung cancer cell invasion into the pleural cavity in early stages [10], as well as metastasis to the brain and other distant tissues are very common.

Lung ADC will be the main focus of this thesis.

1.1.2.2. NSCLC tumorigenesis and progression

Recent advances in technologies such as next-generation sequencing (NGS) have provided greater insights into lung cancer most common mutations. Notably, a comprehensive whole-exome sequencing of 230 patients allowed the breadth of the array of mutations in ADC, with alterations detected in a total of 18 common genes [11]. Of note, the most frequently mutated gene was *TP53* (47%), which encodes for the tumour suppressor protein p53. Other commonly mutated tumour suppressor genes were *STK11* (17%), *KEAP1* (17%) and *NF1* (11%). More generally, further alterations were also detected in various oncogenes, such as *KRAS* (32%), *EGFR* (11%), *BRAF* (7%), *ROS1* (1.7%) and *ALK* (1.3%) [11].

With the identification of these mutations, many of them have been proposed for prognostic evaluation as well as for response prediction to particular treatments. Nevertheless, except for very few of them (such as *EGFR* mutations and *EML4-ALK* translocations), they have all failed to be translated into the clinic. It is for this reason that histological subtyping and grading remain the basis of most clinical evaluations.

The current consensus sequence of the development of lung adenocarcinoma comprises three preneoplastic lesions or stages: (I) atypical adenomatous hyperplasia (AAH), characterised by the growth of atypical epithelial cells with a slight thickening of the alveolar wall; (II) adenocarcinoma *in situ* (AIS) and (III) minimally invasive adenocarcinoma (MIA), with a small focus of invasion (usually smaller than 5 mm of diameter) (**Figure 1.2**) [12, 13]. Importantly, most stages of human lung cancer have been reported to be accurately recapitulated in lung cancer mouse models widely in use in research [14], where the development of lung adenocarcinoma comprises hyperplasia (corresponding to AAH), low- and high-grade adenoma (a stage that correlates to AIS or MIA, depending on its progression) and adenocarcinoma (human lung ADC).

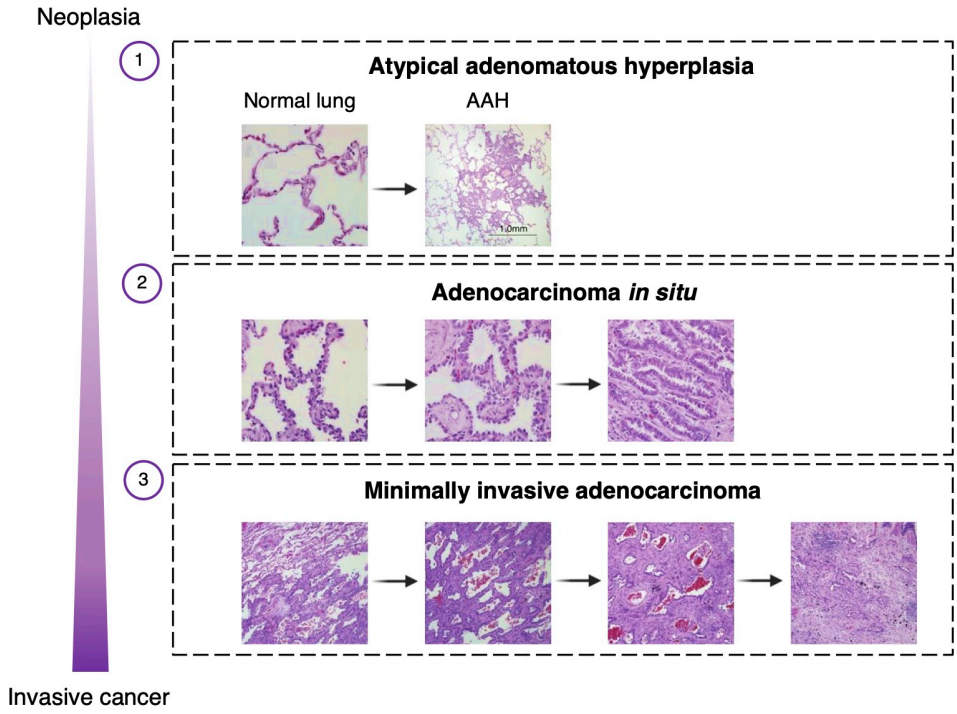

Figure 1.2. Histological representation of the different pre-cancerous lesions of ADC.. AHH is the first histological alteration featured by the proliferation of rather atypical epithelial cells surrounding the parenchyma. AIS is characterised by atypical cells with an increased size surrounding an intact alveolar wall in the periphery of the lesion. Towards the centre of it, the wall becomes more thickened and the cellular atypia is more marked and distinct. In MIA lesions, wall thickening and atypia are even more pronounced, increasing with progression from the periphery (zone 1) towards the centre (zones 2 and 3). Importantly, MIA exhibits a small focus of invasion in its centre (zone 4). Picture adapted from [15].

Despite a general characterisation of pre-neoplastic lesions during ADC development has long been recognised [16], the underlying biological mechanisms driving malignant transformation and progression remain poorly understood. The study of lesions found to be associated with malignancies or in individuals with an increased risk for cancer development, as well as the identification of genetic similarities between advanced tumours and pre-malignant lesions have shed some light onto the nature of early lung ADC development. This has not only allowed the description of the sequential pre-neoplastic steps in lung cancer as presented above, but also their general histology and molecular pathology [16, 17]. For instance, abnormal expression of p53 appears to be increased in AAH [16], and up to 40% of this type of pre-neoplastic lesions have also

been reported to display *KRAS* mutations on codon 12 [17]. Nevertheless, only a limited number of molecular alterations have been described, and many processes in lung tumorigenesis remain to be elucidated.

In this context, the identification of the cell or cells that give rise to NSCLC, as well as the molecular and cellular processes promoting its progression, still remains a challenge. The significant genetic alterations and the heterogeneity of the histological subtypes found in the tumours are major confounding factors [6]. Initial observations pointed at bronchioalveolar stem cells (BASCs) as potential precursors of lung tumours *in vivo* following oncogenic *Kras* activation [18]. However, successive studies that targeted oncogenic *Kras* to specific cell types markers showed that BASCs cells were only able to give rise to bronchiolar hyperplasias but did not progress to more malignant stages [19]. In addition, subsequent reports showed that adenocarcinomas only derived from surfactant protein C (SPC)-expressing AT2 cells in the alveoli upon *Kras* activation or *Pten* loss [18, 20, 21]. It is since then believed that lung adenocarcinomas most likely arise from AT2 cells [22-24], but it is worth noting that these studies are the result from the targeted activation of a single oncogene or the loss of a single tumour suppressor in such specific cell type. It is thus conceivable that other oncogenic mutations, insults or drivers that occur in alternative cell types, or a combination of them, can also lead to the development of lung adenocarcinoma. In addition, it remains largely unknown how these acquired mutations drive the progression of the disease in the early stages. Further work is therefore needed to elucidate not only the cell of origin of lung adenocarcinoma, but also the intrinsic and extrinsic mechanisms in the niche whereby this cell gives rise to a tumour and tumorigenesis is ensued and supported.

1.1.2.3. NSCLC management

Except for tumours that present known driver mutations or fusion proteins, including EGFR-TK, ALK and ROS-1, for which specific targeted therapies are available and under extensive clinical development, lung cancer management currently depends on the stage at which it is diagnosed and the general health of the patient [25]. Staging of NSCLC is performed using the Tumour-Node-Metastasis (TNM) classification system. For patients

diagnosed at stages I-III, surgery and platinum-based systemic adjuvant or neoadjuvant therapy, sometimes in combination with radiotherapy, constitute the standard of care treatment. More than half of the patients, however, present with stage IV disease, for which the indicated first-line standard management if the PD-L1 levels detected in the tumour is lower than 50% is platinum-doublet chemotherapy (cisplatin or carboplatin in combination with third-generation chemotherapy agents, such as docetaxel, paclitaxel or pemetrexed) [25]. In addition, the same combination of chemotherapy is indicated as a second-line regime when targeted therapies fail. Overall, a large proportion of lung cancer patients receive chemotherapy, and most relapse within 2 years after treatment and die from systemic metastases, which indicates flaws in the current standard of care of lung cancer [3].

Cisplatin, also known as cisplatinum, is a chemotherapeutic drug that enters the cell by binding to CTR1 copper membrane transporter. Once inside the cell, the chloride atoms in the molecule are displaced by water molecules, which makes it become a very potent electrophile and therefore it is considered to become activated, as it can react with any nucleophile. Cisplatin binds to the N7 reactive centre of purine residues and causes DNA damage within cells, blocking cell division and inducing apoptosis or cellular senescence. Depending on the amount of drug, the adducts formed as a result of cisplatin DNA damage are GpG (90%) or ApG (<10%), although GpXpG are sometimes also formed and they are a sign of severe cytotoxicity [26]. Cisplatin-based chemotherapeutic regimens for the treatment of lung cancer were first implemented in the 1970s, and they have since then been pivotal in the management for NSCLC as a single agent and in combination with second- and third-generation agents [27].

Docetaxel is an antineoplastic agent that acts by disrupting the microtubular network in cells that is essential for mitotic and interphase cellular functions. It binds to free tubulin and promotes the assembly of tubulin into stable microtubules while simultaneously inhibiting their disassembly. This leads to the production of microtubule bundles without normal function and to the stabilisation of microtubules, which results in the inhibition of mitosis in cells, therefore leading to cell death or senescence [28]. Docetaxel as a single agent is indicated for the treatment of patients with locally advanced

or metastatic non-small cell lung cancer, after failure of prior platinum-based chemotherapy [25].

Alternative chemotherapeutic drugs which are effectively used to treat other cancers are also being assessed for the treatment of lung cancer, such as the selective CDK4/6 selective inhibitor palbociclib. By targeting CDK4/6, this drug results in RB hypophosphorylation and inhibits the cell cycle, effectively inducing cellular senescence in tumour cells [29]. Palbociclib is currently under evaluation in a Phase I clinical trial in combination with the MEK inhibitor PH-0325901 to determine the maximally tolerated dose. The aim is to study the effect of this treatment for cancers with *KRAS* mutations for non-small cell lung cancer (NCT02022982). It is also under examination in a Phase II clinical trial as a second-line therapy in treating cell cycle gene alteration positive patients with recurrent stage IV squamous cell lung cancer (NCT02785939).

As stated earlier, despite significant changes and advances over the past decades in NSCLC management, benefits have been limited to a subset of advanced patients, and the low rate of lasting responses together with the emergence of treatment resistance remain a concern. The mechanisms whereby chemotherapeutic agents like cisplatin, docetaxel and palbociclib exert their anti-tumorigenic effects have been extensively studied *in vitro*. However, despite recent advances have shed light into the effects of different anti-cancer treatments at the genetic and transcriptomic levels [30, 31], the physiological response to chemotherapy at the cellular and microenvironmental layers remains largely unclear. Consequently, continued research is important to obtain an enhanced perception of the tumour biological response to chemotherapeutic therapies, in order to overcome complications from ineffective tumour response and treatment failure.

1.1.2.4. Mouse models of lung cancer

Despite noticeable functional, physiological and structural differences between the human and murine lung [32], mouse models have been demonstrated to be valuable tools to recapitulate human disease and allow a better understanding of the underlying mechanisms. To date, a wide array of lung cancer models have been developed to mimic

both human NSCLC and SCLC tumorigenesis in mice, including genetically engineered models, chemically-induced lung cancer models, strains that have a higher predisposition to developing lung cancer spontaneously and subcutaneous and orthotopic transplantation models using both mouse and human lung cancer cells [33, 34]. While the nature of the molecular changes that occur in human lung cancer development still remains to be fully elucidated, both the histological and genetic profiles of the developing tumours can be at least partially recapitulated in murine systems.

A wide range of genetically-engineered mouse models of lung cancer have been developed, with the use of different cell-specific promoters and other inducible systems that allow the spacial-temporal control of the activation or loss of the oncogene/tumour-suppressor that will initiate tumorigenesis in the lung. These have been designed largely based on recombination systems, such as the Cre/Lox and FLP/frt technologies, which induce the expression of mutated versions of genes that been generated to mimic lung cancer development, including *Kras*, *Tp53*, *Egfr* and *Braf*, among others [35].

In this study, the genetically engineered FLP/frt-inducible *Kras*-driven lung adenocarcinoma and the $Kras^{G12D;p53-/-}$ orthotopically-transplanted mouse models were employed.

1.1.2.4.1. Inducible model of NSCLC: *Kras-FSF*^{G12V}

Transgenic or genetically engineered mouse models rely on the introduction of dominantly acting oncogenes, or the loss of tumour suppressors, linked to appropriate regulatory or tissue-directed tools with the aim to target their altered expression to a specific tissue or cell type in a timely manner. It is widely accepted that for a tumour to develop, a sequence or combination of acquired mutations is needed, following the multistep model of tumorigenesis described by Hanahan and Weinberg [36]. While we do not have a full detailed landscape of the mutations that occur in the human lung and their specific sequence [37], the analysis of well-defined human lesions at different stages of NSCLC progression has allowed a deeper understanding of the early and late events in adenocarcinoma development. Despite the order of such events in human lung NSCLC is hard to establish, it is believed that the most frequent mutations found in patient

samples, such as *TP53* and *KRAS* mutations, are most likely the main drivers during early events of tumorigenesis.

Genetically modified *Kras* mouse models are the most commonly and successfully used models in lung cancer research, and a wide array of these models have been developed since 2001, with varying mutations, method of oncogene expression induction, phenotypes and tumour latency times [38]. Around 91% of the activating *KRAS* mutations in human NSCLC occur in the glycine residue of codon 12 of exon 1 (G12). Of these, approximately 44% result in the substitution by a cysteine (G12C), 23% in the substitution by a valine (G12V) and 17% by aspartate (G12D) [39].

The $Kras^{FSF\text{-}G12V}$ mouse model was developed by Barbacid's laboratory through the insertion of an *frt*-flanked PGK-neo-STOP cassette upstream of the endogenous *Kras* initiation codon and the simultaneous introduction of two point mutations, resulting in a G12V mutation [40]. As shown in **Figure 1.3a**, this insertion primarily prevents the expression of endogenous *Kras*, meaning the $Kras^{FSF\text{-}G12V}$ allele is null and thus homozygous $Kras^{FSFG12V}$ embryos are non-viable. In order to induce lung cancer development in this model, heterozygous $Kras^{FSFG12V/+}$ mice are infected with adenoviral particles expressing FLP Recombinase (Adeno-FLp) via intranasal or intratracheal instillation. When the particles infect the cells in the lungs, the FLP recombinase is synthesised and cleaves the STOP region flanked by *frt* sequences upstream the *Kras* initiation codon, allowing the expression of mutant $Kras^{G12V}$ under the constitutively expressed PGK promoter (**Figure 1.3b**). The aberrant expression of $Kras^{G12V}$ results in the continuous activation of the Ras-Raf-Mek-Erk signalling cascade, which activates essential genes implicated in cell growth and division (**Figure 1.3c**). Of note, the development of lung adenocarcinoma in the *Kras*-driven model was reported to be transcriptionally and histologically analogous to that of human ADC [14], rendering it a very useful tool to model human lung cancer progression *in vivo*.

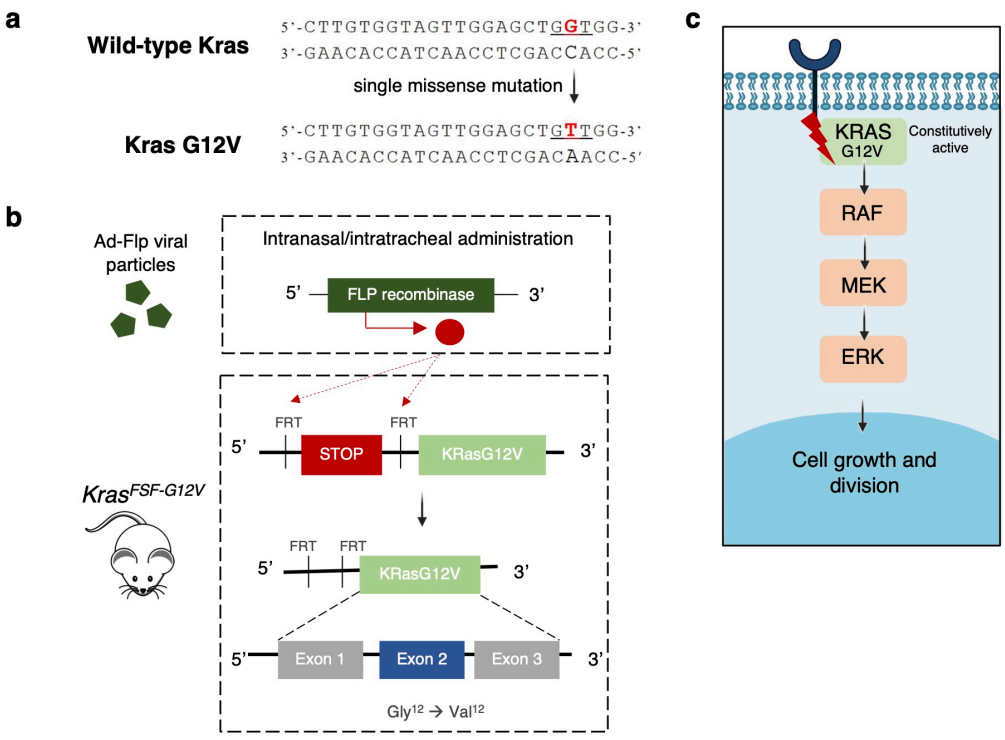

Figure 1.3. Description of the *Kras*$^{FSF-G12V}$ inducible model of NSCLC. a. Diagram depicting single missense mutation described as KrasG12V, which results in the substitution of a glycine amino acid by a valine residue that is normally translated as part of codon 12 of exon 2 in *Kras.* As described above, approximately one in five KRAS alterations in human NSCLC follow this substitution. **b.** Graphical representation of the *FSF-G12V* construct and how the administration of Ad-Flp viral particles drives the expression of *Kras-G12V* in the target tissue. **c.** Constitutively active oncogenic *KrasG12V* drives the aberrant overactivation of the Ras-Raf-Mek-Erk signalling cascade, resulting in uncontrolled cell growth and division.

1.1.2.4.2. Orthotopic model of NSCLC: *Kras*$^{G12D;p53-/-}$

Orthotopic murine models of lung cancer are valuable tools that can present significant advantages over genetically engineered mouse models. While in the latter the development of tumours usually takes up to several months, orthotopic models provide rapidly growing lung cancer tumours in significantly shorter timeframes. In addition, compared to xenograft models, orthotopic transplantation of cancer cells allow for the investigation of relevant *in vivo* processes and mechanisms in a more relevant tissue and microenviroment [41]. In this thesis, we employ an orthotopic model described and validated in detail by Kerr and colleagues [42] through the transplantation of murine cancer cells harvested from advanced lung tumours from *Kras*$^{G12D/+}$*;p53-null* mice [43].

Importantly, however, this model might not recapitulate normal lung cancer progression as faithfully as genetically-engineered mouse models, given the rapid nature of the development of the lesions. In addition, sublethal irradiation is needed prior to transplantation to avoid tumour cell rejection, which may also represent significant differences compared to genetically-engineered models, where the immune system remains unaltered.

1.2. Cellular Senescence

1.2.1. Definition of cellular senescence

In 1961, a seminal study by Leonard Hayflick and Paul Moorhead introduced cellular senescence for the first time, and described it as a state of irreversible cell cycle arrest after observing that serial passaging of human diploid fibroblasts resulted in replicative exhaustion [44]. This was followed by an additional report, where the "Hayflick limit", referring to the maximum number of potential cell doublings of cells *in vitro*, was established [45]. The limited proliferative capacity was subsequently attributed to the gradual attrition of the telomeres at both ends of the chromosome that occurred through gradual division [46]. However, research over the past decades has demonstrated that this cell programme can be induced by many different triggers, and the concept, perception and understanding of the biology of senescence has greatly evolved over the years.

As of today, senescence is described as a cellular programme characterised by a stable cell-cycle arrest elicited in response to multiple types of damage and stress, and, generally, by the implementation of a complex pro-inflammatory secretory phenotype. Despite being elicited by different insults, several traits and mechanisms are generally preserved among the different types of senescence, and they constitute the so-called *hallmarks of senescence* (**Figure 1.4**) [47, 48]. This stable proliferative arrest at the G1 phase of the cell cycle is driven by the activation and cooperation of different proteins involved in the $p21^{CIP1}$/p53 and $p16^{INK4a}$/Rb pathways [49, 50]. Senescent cells also present epigenetic changes and chromatin reorganisation, which includes the formation of well-

established structures named SAHFs (Senescence-Associated Heterochromatin Foci) [51] and DNA-SCARS (DNA Segments with Chromatin Alterations Reinforcing Senescence), as well as the disruption of the nuclear membrane by the downregulation of Lamin B1 expression and the presence of more than one nucleus in the cell (multinucleation) [52, 53]. These chromatin alterations derive from distinct histone modifications, including elevated trimethylation of lysine 9 or lysine 20 on histone H3 (H3K9me3 or H3K20me3) [54, 55].

In addition, senescent cells are characterised by metabolic changes and the accumulation of macromolecular damage, which results in higher ROS levels and dysfunctional mitochondria [56]. An additional hallmark is the well described resistance to apoptosis, which results from the upregulation and activation of pro-survival signalling pathways [57, 58]. Senescent cells also display an increased lysosomal compartment and the overexpression of SA-β-gal (Senescence-Associated β-galactosidase) [59], resulting in an enzymatic activity commonly used for the detection of senescence through a colorimetric reaction *in vitro* and in tissues. The senescent programme also features the implementation of a strong paracrine secretion of factors (including cytokines, chemokines, proteases, growth factors and other tissue remodelling factors) affecting the surrounding tissue, termed SASP (Senescence-Associated Secretory Phenotype) [60-62]. Further to these traits, senescent cells *in vitro* generally present a flattened and enlarged cellular morphology, probably derived from the adoption of a number of structural and metabolic changes. Finally, senescent cells have more recently been described to induce the expression of what is now surging as the senescent surfaceome (**Figure 1.4**) [63].

While all these elements are strongly associated to the senescent phenotype, they may not always be present or detected in senescent cells, as the majority are not exclusive nor indispensable for the implementation of the senescent programme, except for the cell cycle arrest. As a consensus in the field, the presence of more than two of the hallmarks described are generally sufficient to confirm the induction of cellular senescence *in vitro* and *in vivo*, as long as a stable cell cycle arrest is assessed.

For decades, cellular senescence has been described as a biological mechanism related to ageing and essentially aimed at preventing the growth of potential premalignant cells. However, during the past few years, it has become evident that this

process involves more than a simple loss of proliferative capacity, which has put senescence in the spotlight for a wide number of physiological and pathological processes [64], which will be dissected in the following sections.

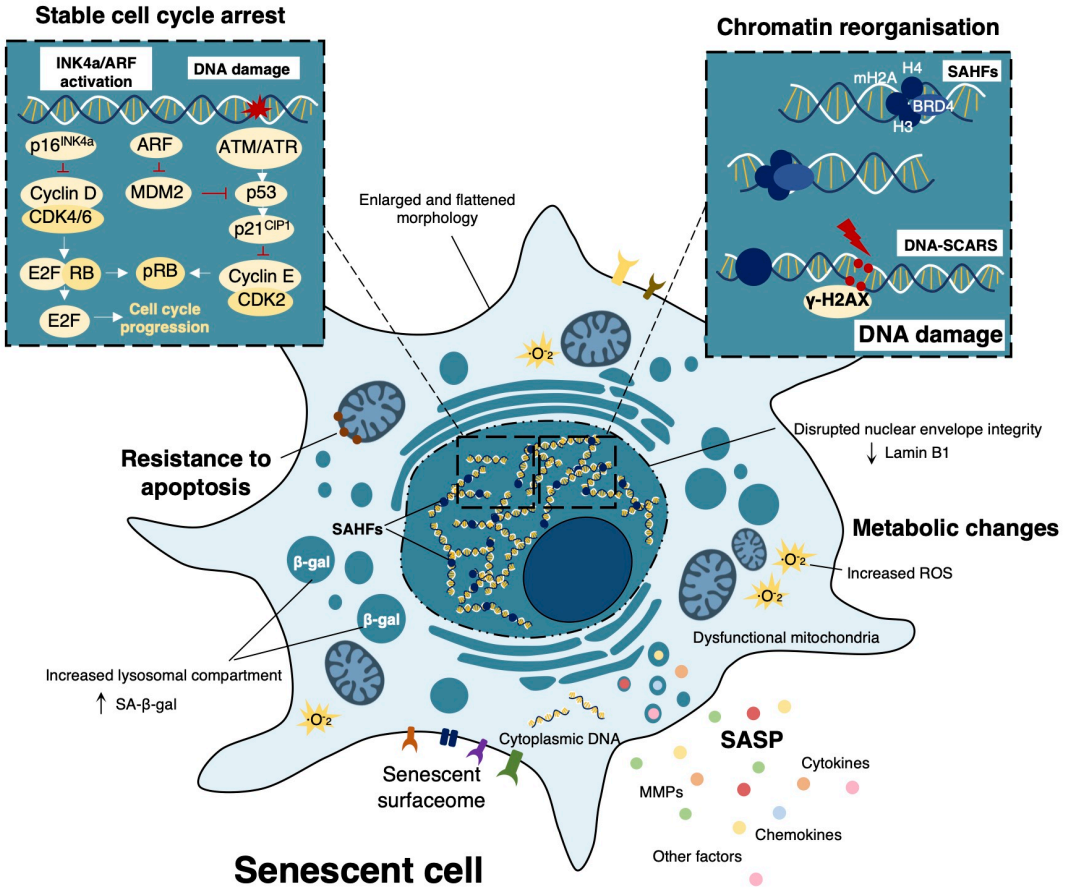

Figure 1.4. Hallmarks of cellular senescence. Several morphologic, metabolic and biochemical changes have been described in senescent cells, which are generally used for the detection and validation of the senescent phenotype *in vitro* and in tissues. These traits include the increased expression of lysosomal SA-β-gal, the upregulation of key cell cycle regulators, including $p16^{Ink4a}$, $p21^{CIP1}$ and p53, epigenetic markers of chromatin reorganisation and DNA damage (SAHFs and DNA-SCARS), disrupted integrity of the nuclear envelope due to decreased levels of lamin B1, upregulation of pro-survival pathways that result in apoptosis resistance, increased intracellular ROS levels and metabolic shifts, and the implementation of a strong secretion of factors, chemokines and metalloproteases termed SASP. DNA-SCARS, DNA segments with chromatin alterations reinforcing senescence; SA-β-gal, senescence-associated β-galactosidase activity; SAHFs, senescence associated heterochromatic foci; SASP, senescence-associated secretory phenotype.

1.2.2. Mechanisms of cellular senescence

Depending on the trigger or the insult that a dividing cell receives, the senescent programme can be generally classified into different types, including, but not limited to: (i) replicative senescence, which takes place when telomeres shorten or become dysfunctional after a number of replications [65]; (ii) stress-induced senescence, which can be further subdivided into different types including chemotherapy-induced senescence [66], DNA damage-induced senescence [67] or oxidative stress-induced senescence [56], and (iii) oncogene-induced senescence, which occurs after the activation of an oncogene, such as RAS, or the loss of a tumour suppressor, such as PTEN [68]. Despite being triggered by different mechanisms, the molecular cascades that are activated in response (including DNA-damage response (DDR) [69] and mitogen-activated protein kinase (MAPK) pathways [70, 71]) mostly converge in the activation of the tumour suppressor p53 and the cyclin-dependent kinase (CDK) inhibitors p16 (or INK4A), p21 (CIP1/WAF1), p15 (also known as INK4B) and p27 (see [50] for review). This ultimately results in a permanent cell cycle arrest, in the G1 cell-division phase, which is further reinforced by the hypo-phosphorylation of the tumour suppressor protein retinoblastoma (pRB) (**Figure 1.5**) [50].

When halted, unlike quiescent cells, senescent cells remain refractory to external mitogenic signals. Importantly, despite senescent cells can no longer replicate, they remain metabolically active, exerting a complex secretome that includes a wide number of pro-inflammatory cytokines, growth factors and matrix proteases.

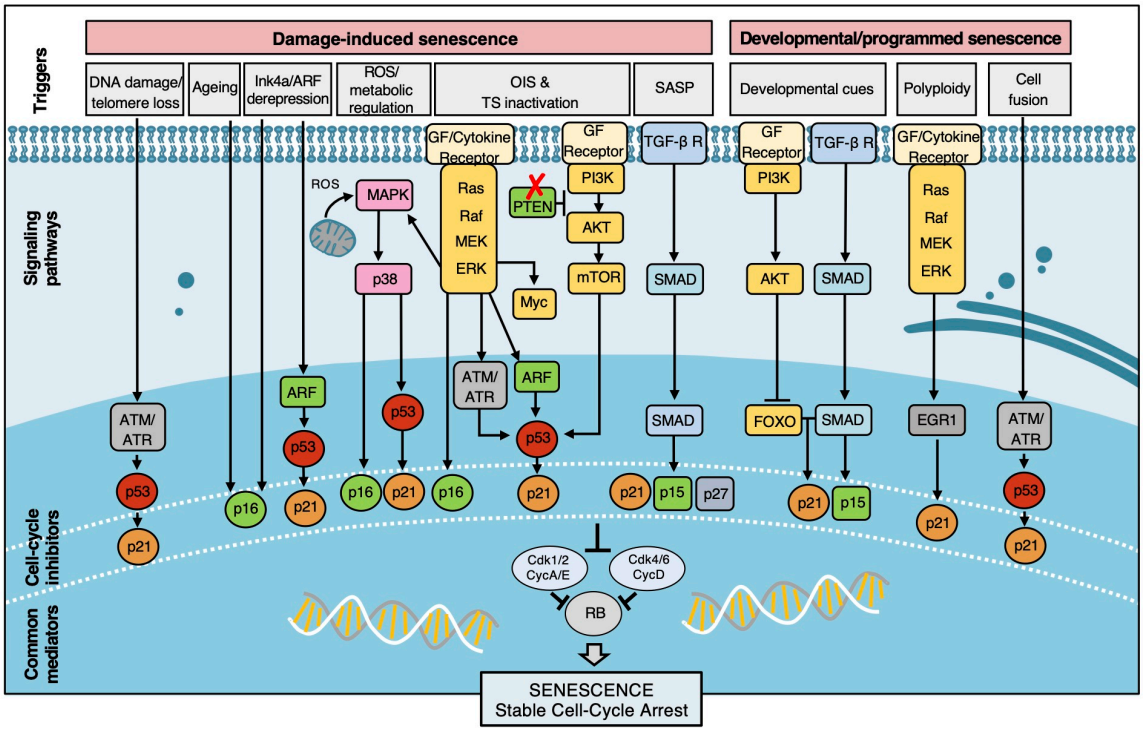

Figure 1.5. Molecular pathways of cellular senescence. Most senescence-inducing triggers converge in the activation of the cell-cycle inhibitor pathways p53/p21 and/or $p16^{INK4a}$. These result in the inhibition of cyclin-dependent kinase 1 (CDK1), CDK2, CDK4 and CDK6 which prevents the phosphorylation of the retinoblastoma protein (RB), leading to the suppression of S-phase genes and an ensuing stable cell cycle arrest. DNA damaging triggers activate the DNA-damage response (DDR) pathway resulting in the activation of p53 and p21. Ageing and epigenetic de-repression of the *Ink4a/ARF* locus also lead to the activation of cell cycle inhibitors p16 and p21. ROS lead to the activation of the MAPK signalling pathway and its downstream effector p38. The aberrant expression of oncogenes or the loss of tumour suppressors lead to p53 activation through the Ras-Raf-MEK-ERK or AKT signalling pathways, and TGF-β, and important factor of the SASP, leads to p15, p21 and p27 upregulation via SMAD signalling. Other triggers such as developmental cues and polyploidy activate the AKT, SMAD and/or Ras-Raf-MEK-ERK pathway for p21 upregulation, while processes such as cell fusion signal through the DDR for p53 activation.

1.2.3. The Senescence-Associated Secretory Phenotype (SASP)

This newly adopted cellular status is referred to as the Senescence-Associated Secretory Phenotype (SASP), a complex secretome that is orchestrated by the activation of various signalling pathways, including key drivers such as the mammalian target of rapamycin

(mTOR) [72, 73], the mitogen-activated protein kinase (MAPK) signalling [74], the phosphoinositide 3 kinase (PI3K) pathway [75], Notch signalling pathway [76] and GATA4/p62-mediated autophagy [77] (**Figure 1.6**). Despite the diversity in downstream activated cascades, most drivers have shown to converge in the activation of the NF-κB and the CCAAT/enhancer binding protein beta (C/EBPß) transcription factors pathways [78] (**Figure 1.6**). This results in the transcription, translation and secretion of a wide array of cytokines, chemokines, growth factors and proteases forming a local inflammatory milieu that attracts the immune system in order to resolve the damage created by the insult, while other factors impact nearby cells and contribute to signalling and intercellular communication processes. Some of the factors reported to be part of the SASP include the cytokines interleukin-6 (IL-6) and IL-8, IL-1α and IL1-β, transforming growth factor-β (TGF-β), TNFα, monocyte chemoattractant proteins (MCPs), granulocyte-macrophage colony-stimulating factor (GM-CSF), serine proteases and metalloproteinases, such as urokinase plasminogen activator and MMP-3 (reviewed in [79]).

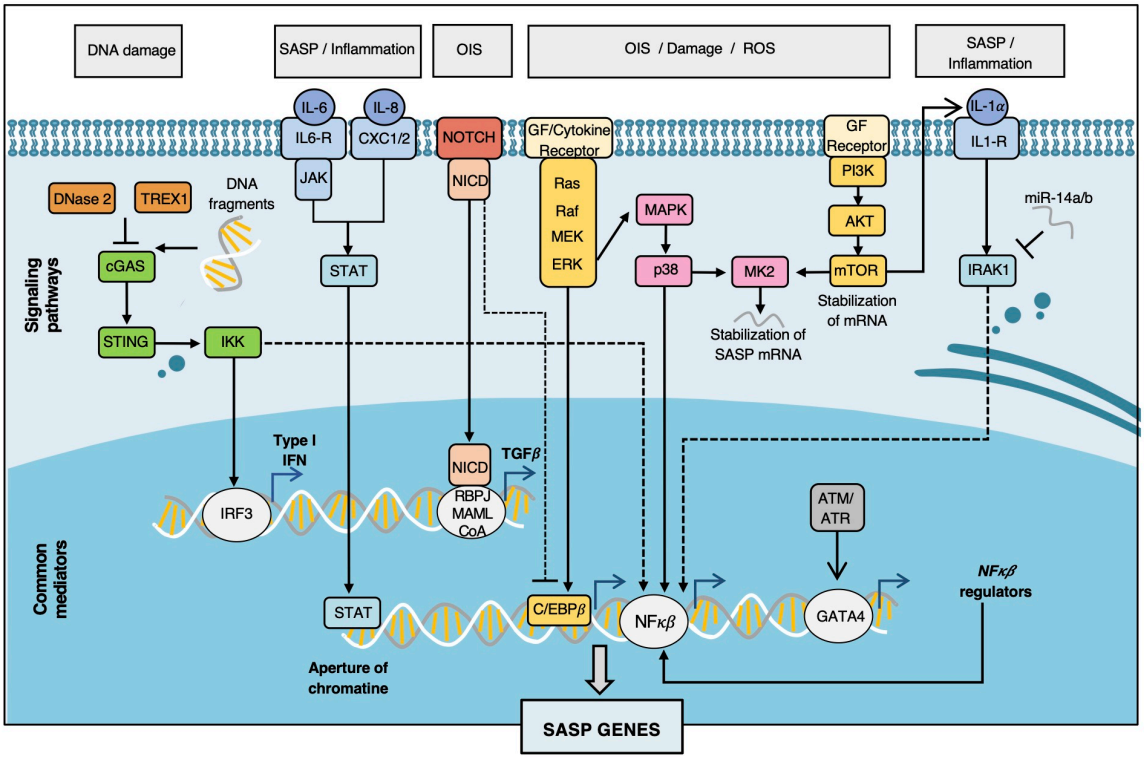

Figure 1.6. Regulation of the inflammatory SASP in the induction of cellular senescence. SASP implementation is orchestrated by the activation of the transcription factors NF-κB and C/EBPß through upstream signalling pathways. DNA-damaging agents, ROS and OIS generally activate the expression of SASP

TFs via the AKT and/or the Ras-Raf-MEK-ERK axis. In addition, DNA fragments are also known to trigger the activation of the cGAS/STING signalling, resulting in the activation of the IRF3 TF and subsequent transcription of Type 1 IFN. OIS-derived SASP is dynamic and can also be orchestrated by NOTCH signalling, a process that restrains the inflammatory secretion by inhibiting C/EBPß at initial stages, and allows the activation of SASP-related super enhancers through NF-κB later on. Finally, accumulating increased levels of TFs reinforce the senescent phenotype through autocrine and paracrine signalling. SASP-derived inflammatory chemokines such as IL-6 and IL-8 promote epigenetic modifications reinforcing the cell cycle arrest through the JAK/STAT cascade, while IL-1α stimulates the activity of NF-κB and C/EBPß promoting a positive feedback loop on the secretion of other cytokines. ATM/ATR, ataxia-telangiectasia mutated and Rad3-related homologue; IFN, interferon; OIS, oncogene-induced senescence; ROS, reactive oxygen species; SASP, senescence-associated secretory phenotype; TFs, transcription factors; TS, tumour suppressor.

The array of pleiotropic effects that cellular senescence can have in surrounding cells have been mostly attributed to the implementation of this secretory phenotype. It is believed that when senescence takes place in an acute manner, in response to an intense and sudden insult, such as oncogene activation and occasional physical or chemical damage (including chemotherapy), SASP production promotes tissue regeneration, immunosurveillance and has an overall beneficial and tumour-suppressing impact (**Figure 1.7**). However, when the immune-driven senescence clearance is impaired, such as during ageing, prolonged and persistent damage or in certain pathological conditions, senescence accrual drives chronic inflammation, and the persistent secretion of SASP factors may promote several detrimental effects, including fibrosis, degeneration and even cancer promotion (**Figure 1.7**) (reviewed in [80]).

Of note, the molecular processes governing these antagonistic effects, the factors responsible for them and the impact other elements may have on the resulting SASP remain broadly unknown. It remains to be fully elucidated to what extent the surrounding microenvironment, intrinsic cellular phenotypes or signatures or the senescence driver itself can determine the resulting secretion of factors that is implemented. A more refined understanding of the SASP is certainly needed in order to determine whether a certain insult or potential treatment may have beneficial or detrimental effects in our organism.

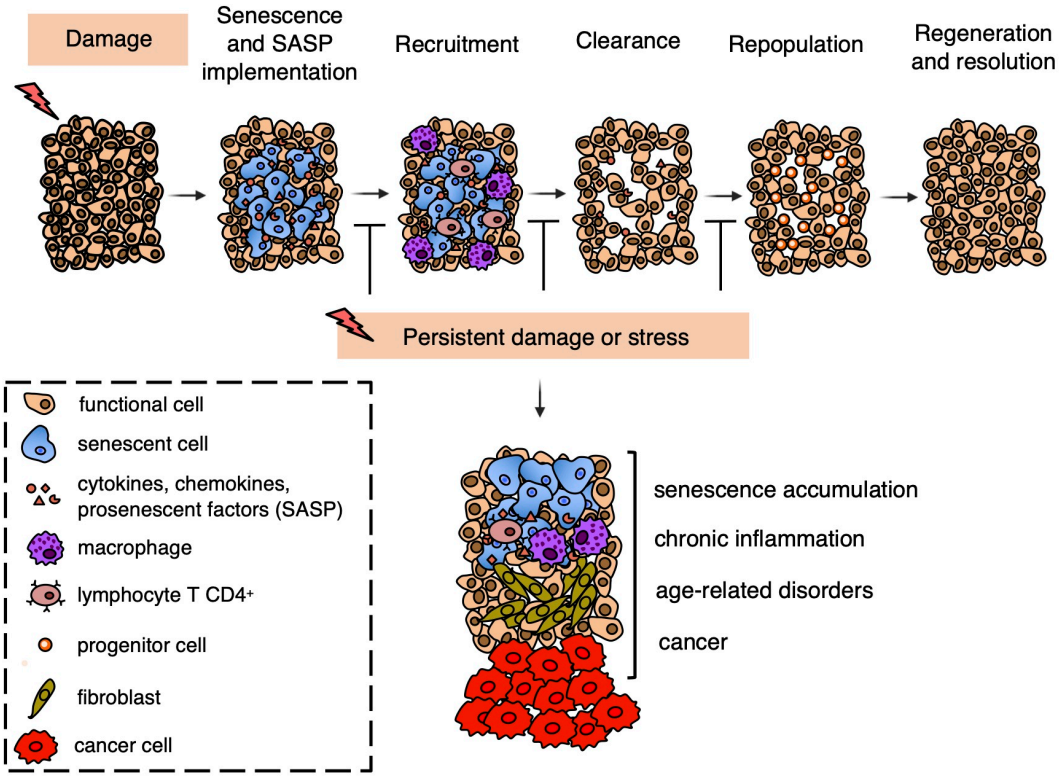

Figure 1.7. Unified model of the impact of resolved and unresolved senescence. Senescence is elicited in response to damage or stress and drives the recruitment of immune cells through the SASP to initiate a tissue remodelling and regenerative process. Recruited macrophages clear the senescent cells, and progenitor cells in the area subsequently repopulate and regenerate the damaged tissue. However, uoon persistent damage, stress or during ageing and certain pathological conditions, this sequence of senescence–clearance–regeneration may be impaired. In such scenario senescent cells are not effectively cleared by the immune system and the tissue is not fully regenerated. Resolution of the damage in these cases involves a fibrotic scar with senescent cells, inflammatory cells and fibrotic tissue, resulting in chronic inflammation and the exertion of detrimental effects derived from senescence accrual. Adapted from [64].

1.2.4. Biological impact of cellular senescence

Hayflick and Moorgate first described cellular senescence in fibroblasts as a phenomenon through which replicating cells reach their proliferative exhaustion and become arrested while metabolically active [44]. We now know that this observation relates to a particular type of senescence commonly referred to as replicative-induced senescence, which is implemented upon telomere shortening. However, as described earlier, a wide variety of stimuli, stressors and damaging factors can elicit the senescent response, and its

resulting biological impact significantly depends on the extent of the senescent burden, the physiological context, the tissue of origin and the senescent inducer itself. For this reason, cellular senescence is regarded as a double-edge sword, contributing to both beneficial and detrimental effects in the surrounding tissue in health and disease (**Figure 1.8**).

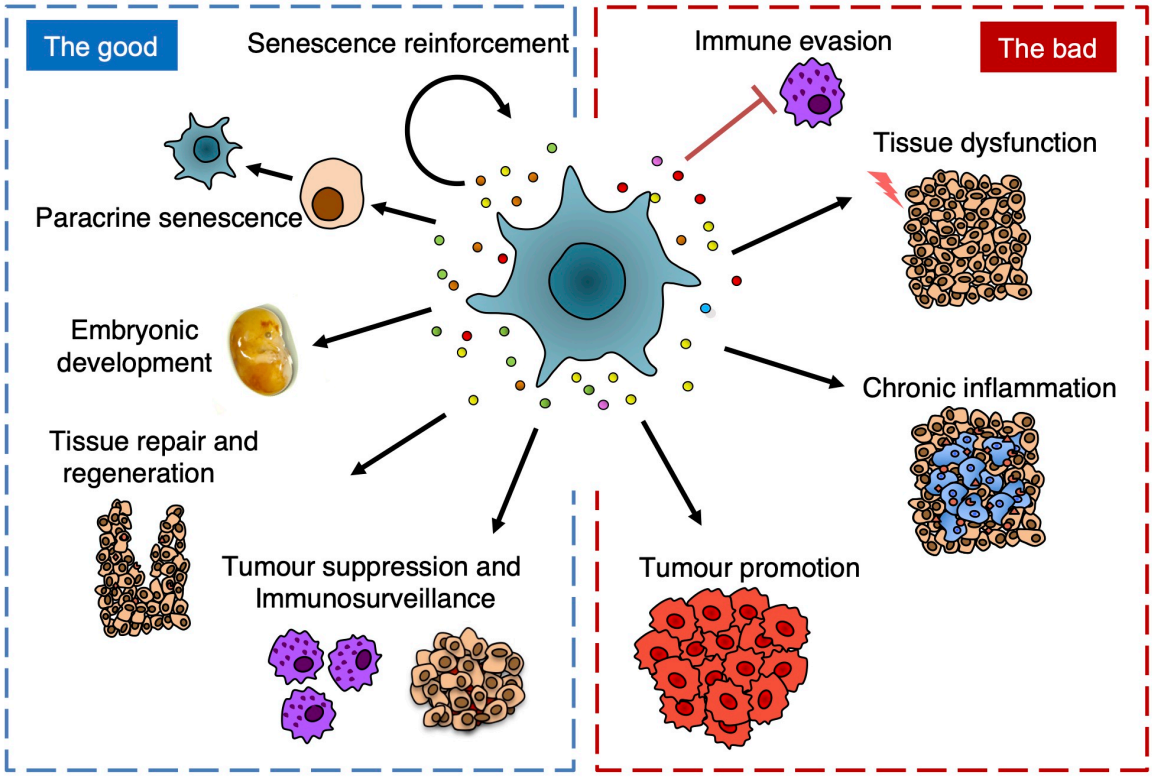

Figure 1.8. Antagonistic roles and functions of cellular senescence in physiology and pathology. Cellular senescence has been reported to play dual roles in physiology and disease. Senescent cells can implement a particular combination of factors as part of the elicited SASP that drives crucial developmental processes during embryogenesis, tissue repair and regeneration, and drive immune cell recruitment to promote immunosurveillance and tumour suppression. Importantly, the SASP can also induce cellular senescence in nearby cells, as well as it has also been reported to reinforce the senescent state and cell cycle arrest in an autocrine manner. Conversely, in chronic conditions, under persistent damage or stress and during ageing, as exemplified earlier via the unified model of resolved and unresolved senescence, the SASP can promote immune evasion, tissue dysfunction, chronic inflammation and even drive tumour promotion and metastasis.

1.2.4.1. Beneficial effects of cellular senescence

Research in the past decade has provided compelling evidence of the presence and beneficial role of senescence in pathological and non-pathological conditions, where it has even been described to play key physiological roles.

A pivotal study demonstrated that senescent stellate cells restrict liver fibrosis by limiting the fibrogenic response to acute damage [81]. In addition to its role in limiting fibrosis, this work suggested the potential of cellular senescence to drive tissue repair. Indeed, functions related to tissue repair were subsequently reported by other groups, which demonstrate that senescent cells play a key role in wound healing through the secretion of SASP reparative factors, such as PDGF-AA in the context of cutaneous fibrosis [82, 83].

In addition, senescence was also reported as a potential tissue regeneration driver when senescent cells were found accumulated in sectioned limbs in the salamander, an injury model that is able to fully regenerate them. It was then proposed that regeneration was driven by the recruitment of macrophages following the implementation of paracrine reparative signalling in senescent cells [84]. In addition to its roles in fibrosis restriction, tissue repair and regeneration, cellular senescence is also known to drive the acquisition of plasticity in surrounding cells, which in turn has been reported to drive the regeneration of different tissues, including the skeletal muscle [85], the skin and the liver [86].

Intriguingly, cellular senescence has also been described as a key player during embryonic development, where it is more commonly known as *developmentally-programmed senescence* and can regulate structural embryonic processes, remodelling and morphogenesis [87-89]. In adult tissues, programmed senescence has also been described in megakaryocytes and placental syncytiotrophoblasts, suggesting physiologically relevant functions in preventing myeloproliferative disorders and in placenta formation, respectively [90, 91].

In addition to fibrosis as described above, senescent cells have also been associated with several advantageous outcomes in other pathological conditions. For instance, senescence mitigates renal as well as cardiac fibrosis following infarction in

different mouse models [92, 93]. Reports also show that senescence can protect against atherosclerosis [94], and that deficiencies in senescence genetic drivers result in an increased susceptibility to this condition [95-97]. Importantly, senescence can further attenuate pulmonary hypertension [98-100], and promote tumour clearance through SASP-driven immune activation [101, 102].

After the establishment of the direct connection between telomere shortening and cell cycle arrest [103, 104], researchers in the 90s hypothesised that senescence could also be elicited through oncogenic stress and play a role as a tumour suppressive response by preventing uncontrolled growth. In 1997, Serrano and colleagues demonstrated that oncogenic Ras signalling triggers premature senescence through the accumulation of $p16^{INK4}$ and p53 [105]. Remarkably, this conceptually introduced what is known as *oncogene-induced senescence* (OIS) and demonstrated senescence-associated tumour suppressive effect. The role of senescence as an anti-tumour barrier will be described in the subsequent sections.

It is important to note, as described earlier (**Figure 1.7**), that the physiological and beneficial roles of senescence in pathological contexts require an efficient SASP-mediated immunoclearance of senescent cells. When they are not effectively cleared, such as in chronic conditions or under persistent damage or stress, unresolved senescence may result in detrimental effects as described next.

1.2.4.2. Detrimental effects of cellular senescence

As previously introduced, the first evaluations of cellular senescence *in vitro* and *in vivo* suggested a connection between this cell mechanism and ageing, given that an accumulation of arrested cells were found in the skin of aged individuals as opposed to young donors [106]. This functional association was demonstrated in an early study that showed that the senescence-mediator *INK4a/ARF* is a biomarker and an effector of ageing [107]. Indeed, a large body of literature has since then demonstrated that senescent cells accumulate during ageing in multiple tissues and organisms [108-111], and, most importantly, that this accrual results in detrimental effects when senescence is not effectively cleared by the immune system (**Figure 1.7**).

This chronic, persistent senescence has largely been reported to contribute to the progression and even the onset of age-related pathologies. Most of these detrimental effects have been effectively demonstrated through the genetic or pharmacologic ablation of senescent cells in different models. In this context, the benefit of senescent cell removal was demonstrated for the first time in a progeroid mouse model by Baker and colleagues in 2011 [112]. In this study, the authors markedly showed that accelerated ageing, linked to high senescent accumulation in tissues, could be reverted through the ablation of *Cdkn2a*-positive cells [112].

Further examples of age-related pathologies where senescence is known to be a key promoter include idiopathic pulmonary fibrosis. This condition has been linked to increased levels of senescence-related markers, such as SA-β-gal and p16, in both human and murine pulmonary fibrosis tissues [113-116]. Impaired senescence and SASP response through Caveolin-11 deficiency partially protected mice from bleomycin-induced pulmonary fibrosis [116], and inhibition of NOX4, which contributes to lung fibrosis through high levels of ROS in a different model, decreased senescence-related markers and reverted the fibrotic phenotype [113]. Senescence in adipocytes has also been associated with conditions such as obesity, where the stress response recruits high levels of macrophages to the adipose tissue, triggering obesity-related systemic complications [117]. The use of mouse models demonstrated that abrogation of *Trp53* gene prevented senescence accrual in adipose tissue, and that deletion of *Trp53* in the adipose tissue protected mice from insulin resistance [118].

The list of pathological conditions where senescence has been reported to be associated and even causative is extensive and keeps growing as the field advances. In addition to the pathologies described above, senescence has further been described to contribute to type 2 diabetes [119, 120], sarcopenia [121, 122], neurological disorders [123], osteoarthritis [124, 125] and atherosclerosis [126], among many others.

Of particular interest for this work, however, is the impact of cellular senescence in cancer. In this context, the dual role of cellular senescence is intriguingly maintained. Despite its undeniable role as a tumour suppressive mechanism by means of preventing the uncontrolled expansion of potential malignant cells, it can also promote tumour progression, immune suppression and metastasis [62, 127-130]. However, the processes

governing these antagonistic effects are not completely understood, and its complexity remains to be deciphered in many conditions, including lung cancer initiation, progression and management.

1.2.5. Cellular senescence and cancer

1.2.5.1. Oncogene-induced senescence in early tumorigenesis

As with other conditions in which senescence is implicated, the activities of this cellular response in cancer are context- and stage-dependent. Oncogene-induced senescence (OIS) was first documented in cells ectopically expressing *HRAS*^{G12V} [105], and subsequent investigations demonstrated that p53 and p16INK4a networks downstream of the Raf/MEK/MAPK pathway are the main drivers in its implementation [131], providing the first evidence of senescence acting as a barrier to tumour progression upon oncogene activation *in vitro*. Importantly, as introduced in previous sections, *in vivo* validation emerged in 2005, when several groups reported the presence and accumulation of senescence in various human and murine pre-malignant lesions [132-136]. Overexpression of E2F3 in pituitary cells and *BRAF*^{V600E} in skin melanocytes was found to initially boost cell proliferation in the short term, but this was then followed by a prominent cell cycle arrest and the acquisition of senescence-related features, resulting in a marked senescence accumulation in nevi and pituitary hyperplasias, respectively [134, 136]. Further studies independently demonstrated that the deficit of Suv39h1 and the combined loss of Pten and p53, which abrogated the ability of the cells to effectively undergo OIS, resulted in the earlier onset and accelerated progression of cancer in *NRas*-driven lymphoma [132] and prostate cancer models [133].

In the context of lung tumorigenesis, Collado and colleagues also found that pre-malignant adenomas in the *KRas*^{G12V} mouse model of lung cancer presented a marked increase in the expression of senescence markers, including p16^{INK4a}, p15^{INK4b}, DcR2, Dec1, SAHFs and SA-β-gal activity, along with decreased levels of the proliferative marker Ki67 [135]. Importantly, the authors demonstrated that such senescence-related markers

were scarce in lung adenocarcinomas, indicating the presence of cellular senescence in preneoplastic lesions but not in subsequent malignant stages.

While these pivotal studies established senescence as a defining feature of pre-malignant lesions and further supported the notion that this cell response serves as a barrier against oncogene-driven tumorigenesis, the fact that some of these lesions progress and give rise to malignant and invasive disease suggests that senescence or its dysregulation may contribute to tumorigenesis, which certainly warrants further investigations.

1.2.5.2. Chemotherapy-induced senescence

Increasing evidence supports the induction of senescence as a response to anti-cancer treatment, which, together with apoptosis, is generally perceived as a positive outcome, as it hampers the proliferation of cancer cells and promotes their clearance through the immunosurveillance of senescent cells [137]. Radiotherapy, which is commonly used in the clinic, has been reported to effectively elicit a senescent response in a wide variety of cells *in vitro* and *in vivo*, including lung adenocarcinoma, glioblastoma, neuroblastoma and breast and colorectal cancer cells [138-141]. On the other hand, an extensive number of anti-cancer drugs have also been described to induce senescence both in culture and living animals through varying mechanisms of action, including DNA damage and the inhibition of cell cycle inhibitor, DNA methyltransferases, tyrosine kinases and histone acetyltransferases [137]. Such agents include cisplatin, palbociclib, bleomycin, cyclophosphamide, doxorubicin, docetaxel and etoposide, among many others.

Importantly, as opposed to the limited evidence of OIS in humans, reports have also demonstrated the implementation of chemotherapy-induced senescence (CIS) in specimens retrieved from patients upon neoadjuvant or palliative therapeutic cancer treatment [137]. In 2001, the first of these reports demonstrated increased levels of senescence markers, including SA-β-gal, p21 and p16, in breast cancer samples from patients that had received neoadjuvant chemotherapy [142]. Cisplatin and gemcitabine/pemetrexed neoadjuvant also demonstrated the upregulation of SA-β-gal activity and increased levels of PAI-1 and p21 expression in prostate cancer samples

[143]. Likewise, chemotherapeutic treatment with mitoxantrone in prostate cancer patients as a neoadjuvant regimen resulted in increased transcription levels of p16, p21, IL-6, IL-8 and IL-1β [144]. Intriguingly, increased circulating mRNA levels of senescence markers have also been detected in peripheral blood collected from breast patients undergoing chemotherapeutic treatment [145].

With regards to NSCLC, chemotherapeutic agents commonly used for its management can effectively induce senescence *in vitro*, as described in **section 1.1.2.3**. Importantly, in 2005, Roberson and colleagues provided the first evidence in humans, when they analysed the expression of SA-β-gal in samples obtained during resection surgery of a small cohort of lung cancer patients [146]. The levels of this enzymatic was compared between patients who had undergone neoadjuvant chemotherapy of carboplatin combined with taxol to those that were not treated with chemotherapy before the procedure. Remarkably, the authors provided evidence of the accumulation of SA-β-gal-positive cells in lung cancer patients undergoing neoadjuvant chemotherapy (**Figure 1.9a**). But most interestingly, a follow-up of those cases indicated that patients that presented the highest levels of SA-β-gal relapsed within 14 months after treatment, while patients that had no or lower levels of senescent cells showed no evidence of recurrent disease during that period of time. Survival analysis demonstrated that patients whose samples were SA-β-gal-negative after neoadjuvant chemotherapy had a significantly increased survival compared to patients presenting SA-β-gal activity in the tumours (**Figure 1.9b**). Although it is unknown to what extent other factors may have impacted the outcome of the treatment, these data, together with the increasing evidence of tumour-promoting activities derived from senescence, as described in the next section, may suggest an implication of the accumulation of senescent cells during lung cancer chemotherapy in treatment failure.

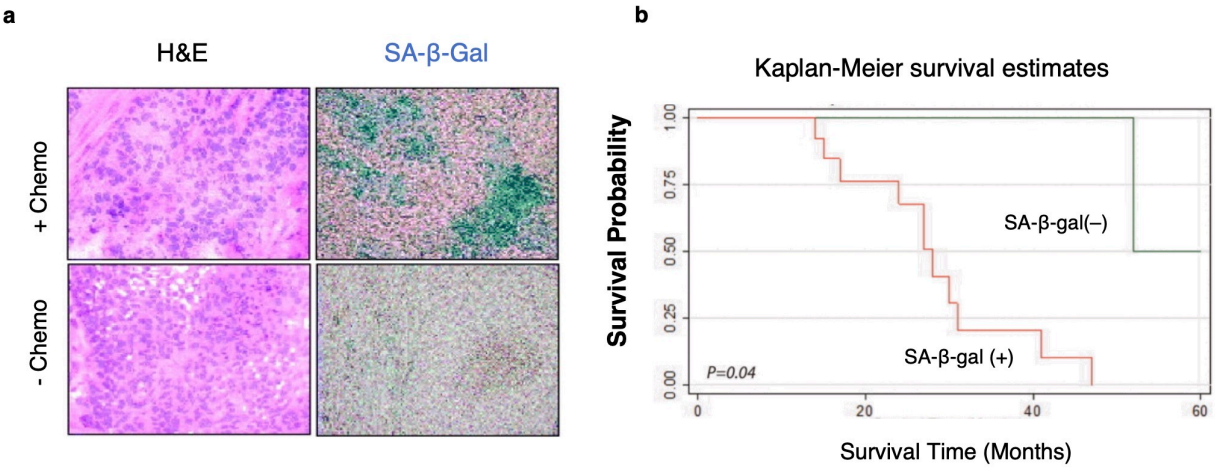

Figure 1.9. Neoadjuvant chemotherapeutic treatment in NSCLC results in increased levels of SA-β-gal in tumours and decreased survival. a. Representative histological images stained for Haematoxylin and Eosin (H&E) and Senescence-Associated β-galactosidase (SA-β-gal) activity in lung adenocarcinoma specimens resected from a patient upon completion of neoadjuvant chemotherapeutic treatment with carboplatin and taxol (+Chemo) and from an untreated patients (-Chemo). **b.** Survival analysis of NSCLC patients classified as SA-β-gal-positive or negative after histological assessment upon neoadjuvant chemotherapy (n = 11). Data adapted from [146].

1.2.5.3. Senescence as a tumour promoter in cancer

The activation of cellular senescence in response to oncogenic stress or therapeutic damage acts as a tumour-suppressive mechanism in the first instance. In addition, multiple reports demonstrate that its anti-tumour activities extend beyond the implementation of the cell cycle arrest. The SASP reinforces the senescent programme both in an autocrine [147, 148] and paracrine manner through IL-1 and NF-κB signalling [149]. Senescence can also drive immune stimulation in the local microenvironment, promoting the clearance of pre-cancerous and cancerous cells through the SASP, by promoting the infiltration and activation of different immune cells, including T lymphocytes and Natural Killers (NK) [101, 102, 150, 151]. Collectively, the halt of proliferation of pre-/cancerous cells, together with the amplification of the senescent response and the modulation of immunosurveillance through the SASP, thus provide a robust barrier against tumorigenesis. However, growing evidence demonstrates that when these mechanisms are compromised, senescence may also contribute to tumour development and advancement.

1.2.5.3.1. Senescence bypass

In the context of OIS during early tumorigenesis, the progression to malignant phenotypes from pre-neoplastic lesions, in which senescence accumulates, suggests that pre-malignant senescent cells can either bypass or revert the senescent state. However, evidence of such mechanisms is scarce, especially with regards to OIS, and how tumour progression ensues within an arrested pre-malignant lesion remains to be fully elucidated.

It is believed that while senescence may be implemented in most pre-malignant cells, a fraction of transformed cells that present a proliferative advantage during the early stages of tumorigenesis can acquire subsequent alterations or mutations that can abrogate their ability to undergo apoptosis or cellular senescence. In such cells, the loss of the tumour suppressive response will be favoured, and they will continue to proliferate and promote the progression to malignant stages, while cells that effectively entered the senescent programme will remain under persistent growth arrest and be eventually cleared by the immune system. This scenario can be recapitulated *in vitro* and in genetic mouse models, where the loss of a tumour suppressor integral to the senescence response, such as p53 [152] and the p16/Rb axis [153], can bypass the induction of the programme. Additional tumour suppressors the loss of which can circumvent senescence induction during tumorigenesis include components of the DNA damage response (DDR), such as Atm or Chk2 [154, 155], Hmga [156] and the methyltransferase Suv39h1 [132], which are needed for the formation of SAHFs.

In the context of CIS, the complexity and heterogeneity of the genetic background of cancerous cells place senescence bypass as an almost inevitable response to genotoxic stress. Indeed, recent reports indicate that CIS can be incomplete in cancer cells, owing to the inactivation of tumour suppressor genes or the instability of epigenetic marks in full-blown malignant cells [157]. However, despite the abundance of studies using cell culture and genetic mouse models that pose senescence bypass as a plausible event, clinical evidence is still lacking due to the challenging nature of capturing this scenario in the human settings.

1.2.5.3.2. Senescence escape or reversion

Alternatively, senescence reversion or escape has emerged as a potential mechanism whereby senescence facilitates tumour progression. The long-standing perception of senescence as an irreversible state has been challenged by different groups, and some studies indicate that the withdrawal from an established state of cellular senescence may be possible.

Early observations of cell cultures exposed to clinically relevant concentrations of chemotherapeutic drugs, including doxorubicin, etoposide and cisplatin, revealed that emergent colonies can be observed 3 to 4 weeks after removal of the drug, despite the senescent programme was initially established [146, 158-162]. Of note, these were mostly observed in breast, colorectal, ovarian and lung cancer lines that lacked pivotal senescence regulatory proteins, such as p53 and $p16^{Ink4a}$, indicating the importance of such factors in maintaining the senescent state. These reports demonstrate, however, that the frequency of escape was around 1 in 10^3-10^6 cells, suggesting that the stability of the senescent cell cycle arrest is largely predominant and senescence reversion is a rare event [146, 163].

Strikingly, some of these studies demonstrated that emergent clones presented increased resistance (i.e., decreased sensitivity) to the chemotherapeutic drug they had previously been exposed to [146] and that the so-called *escapers* displayed increased levels of cell cycle promoters, including *PCNA*, *E2* and *cyclin B1* [158]. Interestingly, additional reports associate senescence with the acquisition of stem-like features, as detected through the increased expression of the cancer stem cell markers CD34 and CD117 [163] and CD133 [159].

More recently, in agreement with these observations, Milanovic and colleagues showed that doxorubicin treatment of Eμ-Myc–Bcl2-overexpressing lymphoma cells induced a robust induction of cellular senescence, which was accompanied by an enhanced expression of markers associated with stem cell functions, including ALDH and ABC [164]. The authors subsequently used an inducible model to force senescence escape through the deactivation of p53 and Suv39h1, and determined that reverted

senescent cells entered the cell cycle with a more aggressive phenotype, forming rapidly growing colonies *in vitro* and more malignant tumours *in vivo* [164]. Additional instances of senescence escape have also been reported following inducers other than chemotherapeutic drugs, such as ionising radiation [165], but evidence of such reversal upon OIS implementation remains more limited.

It is worth noting that studies reporting senescence reversion have been conducted mostly *in vitro*, and the outcomes observed in *in vivo* models were obtained through the forced genetic manipulation of key senescence epigenetic and cell-cycle arrest drivers [164]. Therefore, evidence of such reversion occurring spontaneously in living organisms is still lacking, particularly in the context of OIS. However, despite not in the context of cellular senescence, research has demonstrated that mutations can occur in non-proliferating cells, and that these can lead to the re-establishment of the cell cycle [166]. It is thus conceivable that persistent stress or oncogenic damage on arrested senescent cells leads to the acquisition of mutations that inactivate the senescent programme and subsequently allow re-entry into the S phase of the cell cycle, ensuing tumour progression.

Taking into consideration the prevailing paradigm that senescence is irreversible, however, a major point of discussion in the field is whether the so-called senescence *escapers* fully implemented the senescent programme, or, alternatively, they were in a transient quiescent state displaying senescent-like traits and eventually bypassed the induction of senescence. While this still remains unclear, the development of multi-marker tracking approaches that allow the tracing of *bona fide* senescent cells, especially *in vivo*, will be crucial to answer the question and fully uncover the impact of senescence reversion as a tumour-promoting mechanism during tumorigenesis and upon chemotherapeutic treatment.

1.2.5.3.3. The dark side of the SASP

As with many processes in cancer biology, the SASP programme is likely to generate heterogeneous responses, especially *in vivo*. Importantly, the composition of the SASP has been shown to vary depending on the cell type, the inducing stressor and the time

passed since the initiation of the programme, indicating that there is not a unique secretome (reviewed in [61, 127]). This is therefore likely to hinder the ability of predicting with certainty how a specific SASP programme will affect the surrounding tissue microenvironment in tumour biology, an aspect to be considered in certain situations such as the use of senescence-inducing chemotherapeutic drugs. Despite the SASP is in principle elicited as a way of promoting senescent cell clearance and restore homeostasis in the surrounding tissue, compiling evidence suggests that cellular senescence, both in cancer and stromal cells, can also promote tumorigenesis, impacting different aspects of cancer cell behaviour, including:

(I) Cellular proliferation. A significant number of studies have shown that cells undergoing senescence within the tumour niche, such as fibroblasts, can induce cell growth of cancer cells *in vitro* [62]. This effect has also been observed in *in vivo* contexts, where the co-injection of senescent fibroblasts with tumour cells resulted in a greater progression of the tumour mass in xenograft models [167]. Examples of factors shown to stimulate cell growth include growth-related oncogene (GRO)-α and amphiregulin.

(II) Invasion, angiogenesis and metastasis. Several studies have demonstrated that the conditioned medium of senescent cells can promote epithelial-to-mesenchymal transition (EMT) *in vitro* [168]. In addition, the elimination of senescent cells in *in vivo* settings has recently been demonstrated to delay the dissemination of cancer cells to distal tissues and tumour relapse [169]. Notably, the two major cytokines of the SASP, IL-6 and IL-8, have been shown to disrupt cell adhesion, enhancing invasive properties of breast cancer cells [170].

(III) Tumour-initiating cells and cellular reprogramming. The gain of stem cell traits, defined as the loss of differentiation markers and/or the gain of progenitor markers, is an important hallmark of cancer progression. Of note, the presence of less differentiated cancer cells in the tumour has been linked to an increased aggressiveness and a poorer outcome. In this context, the SASP has recently been linked to the inhibition of differentiation processes and the acquisition of markers of stemness [164, 171, 172]. Although not in an oncogenic setting, the senescent secretome has further been proved to induce cellular reprogramming of neighbouring cells *in vivo* [85, 86, 173]. Importantly, the first formal connection between senescence and tumour initiation through SASP-

driven reprogramming was reported in a model of pituitary tumorigenesis, where reduced senescence and SASP was linked to decreased tumour-inducing potential of pituitary stem cells, resulting in abrogated cell transformation and tumour initiation [127, 174].

(IV) Immunomodulation. Senescent cells implement a strong pro-inflammatory environment to promote their own clearance through the secretion of cytokines and chemokines, such as CCL2. However, it has also been reported that they can have an opposite effect and evade immunosurveillance, by increasing the infiltration of tumour-suppressive immune cells and inhibiting anti-tumour T-cell responses [128, 175].

It is important to note that the mechanisms described above are not mutually exclusive, and it is therefore likely that more than one takes place during early tumorigenesis and/or chemotherapeutic stress within a tumour. In such scenario, the tumour-promoting effects of the SASP could impact emergent populations that derive from senescence bypass or reversion. This can provide a survival niche that notoriously favours tumour progression, further increasing the complexity of the tumour dynamics. Therefore, understanding the impact of senescence in early disease and upon therapeutic treatment is imperative to predict potential detrimental effects and develop strategies that can deter, prevent or revert them for improved patient outcomes. In this context, senotherapies, or the use of senolytics, are emerging as treatment options that can have the potential to revolutionise cancer care.

1.3. Senotherapies as potential anti-cancer treatments

1.3.1. Therapeutic approaches to target senescence

Over the past 15 years, along with the continuous increase in the number of studies demonstrating the detrimental impact of accumulated senescence in age-related disorders and other conditions, including cancer, efforts to find strategies to clear senescent cells in tissues have multiplied notoriously. The first formal demonstration of the potential of senescent cell abrogation was published by Baker and colleagues, who

showed that genetically-mediated eradication of *p16*^{Ink4a}-positive cells resulted in the amelioration, delay and even reversion of age-associated disorders [112].

After establishing the therapeutic potential of senolysis (induction of cell death in senescent cells), several research groups and companies have focused on the design, synthesis, development and validation of this treatment modality. In 2004, the first attempts to develop anti-senescence approaches utilised high-throughput compound library screens and resulted in the generation of fusion proteins containing a domain that could bind to a senescent-specific cell surface receptor coupled to toxins [176]. However, after failing to provide the first ever senescence-abrogating drug, research centred on depleting senescent-specific mechanisms, such as the activation of pro-survival pathways that render senescent cells resistant to apoptosis.

Consequently, in 2015, Zhu and colleagues performed a bioinformatics analysis to search for anti-apoptotic nodes essential for senescent cells in a RNA interference screening. After testing several drugs known to target such networks, they reported the combination of dasatinib and quercetin (D + Q) as a potent combination to selectively target and kill senescent cells [177]. This type of pharmacologically-active agents that selectively target and induce cell death in senescent cells were named *senolytics*. Subsequent studies revealed the effective senolytic activities of additional drugs, including navitoclax (also known as ABT-263), a BCL-2 inhibitor [178, 179], and fisetin, a flavonoid related to quercetin [180], among others.

Attempts aimed at discovering and validating novel senolytics and approaches to target senescence are on the rise, and to date, over 30 agents, inhibitors and mechanisms have been described as strategies to target, modulate and eliminate cellular senescence (**Figure 1.10**). Such approaches operate through one of four general strategies: (1) the induction of apoptosis, via the deregulation of factors that drive and maintain activated pro-survival pathways in senescent cells (such as the inhibition of BCL-2 proteins mediated by ABT-727, ABT-263 and A1331852); (2) the activation of the immune system against senescence, in order to promote senescent cell clearance (for instance, via antibody-mediated blocking of DPP4 or vimentin receptors); (3) the genetic and epigenetic manipulation of senescent cells to prompt senescence reversal or bypass (e.g. by targeting the p53 axis), and (4) the modulation of the SASP to prevent its deleterious

effects in the surrounding tissue (including mTOR and MAPK cascades blockade through modulating drugs such as rapamycin or MK2.III) (**Figure 1.10**).

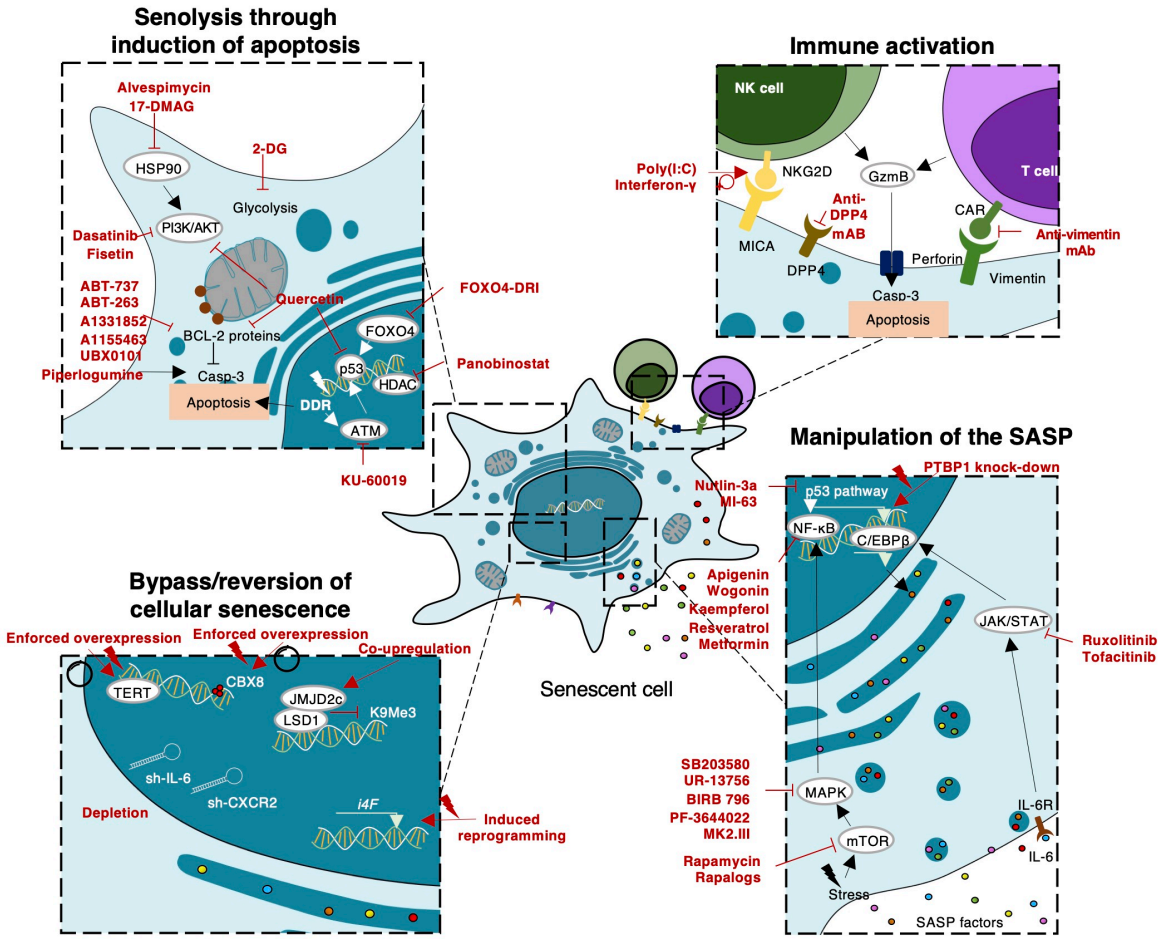

Figure 1.10. Therapeutic approaches targeting cellular senescence. To prevent the deleterious effects of cellular senescence, four different strategies can be potentially implemented. The inhibition of pro-survival pathways and apoptosis-inducing drugs is a leading approach. First and second generation of inhibitors of the BCL-2 cell death regulator family of proteins can induce selective apoptosis of senescent cells. Targeting senescence metabolism through glycolysis blockade and attenuation of ATM, HDAC, FOXO4 activities as well as the PI3K cascade have also been reported as effective approaches. A second strategy is the activation of the immune system against senescent cells to stimulate their clearance. Enhancing the cytotoxic activity of NK against senescent cells and manipulating the humoral innate immunity with the use of antibodies against receptors such as DPP4 and Vimentin are proposed attractive strategies. Thirdly, manipulation of the SASP without compromising the cell cycle arrest of senescent cells has also proven beneficial in particular settings. A large number of molecules can interfere with NF-κB and C/EBPß transcriptional activities or their upstream regulators, dampening the expression of SASP factors, such as IL-1, IL-6 and IL-8, and thus dampening the senescence-derived inflammatory milieu. Lastly, genetic and epigenetic manipulation of cells, including the induction of reprogramming, have been proposed as a means of bypassing or reverting the state of cellular

senescence, although these approaches should be taken with caution given the potential risk of cancer initiation. BCL-2, B-cell lymphoma 2; Casp-3, caspase-3; CAR, chimeric antigen receptor; GzmB, granzyme B; HDAC, histone deacetylase; HSP90, heat shock protein 90; i4F, inducible four factors; LSD1, lysine-specific histone demethylase 1A; MICA, MHC class I polypeptide-related sequence A; NK, natural killer; TERT, telomerase reverse transcriptase.

Targeting upregulated pro-survival pathways in senescent cells remains the most common senolytic approach, and a number of natural and chemical compounds have been validated as potent inducers of apoptosis in senescent cells to date. As exemplified above, these drugs include the combination of D + Q (which act as a multi-tyrosine kinase inhibitor known to interfere with ephrin B (EFNB)-dependent suppression of apoptosis, and an inhibitor of the PI3K-Akt pathway, respectively [177), navitoclax (a potent inhibitor of BCL-2, BCL-xL and BCL-W) [179], ABT-737 (an analogue of navitoclax) [181], piperlongumine (which drives the apoptotic programme through the cleavage of caspase-3) [182], panobinostat (an HDAC inhibitor) [183] and fisetin (a MAPK inhibitor) [180], among many others (**Figure 1.10**). Importantly, the use of such inhibitors has proven successful in depleting senescent cells *in vitro* and *in vivo,* and ameliorating a number of pathologies in which senescence is known to be causative, including osteoarthritis [125], premature ageing and age-related symptoms [178, 184] and Alzheimer's disease [123, 185].

In the context of cancer, pro-apoptotic compounds have demonstrated improved efficacy in combination with standard chemotherapy in mouse models of breast cancer, ovarian cancer, head and neck squamous cell carcinoma and NSCLC [182, 183, 186]. More recently, cardiac glycosides, which target Na^+/K^+-ATPase pumps on the membrane and disrupt the cellular electrochemical gradient, have emerged as a family with potent senolytic activity, and have also been reported to effectively eradicate senescent cells in living organisms in models of therapy-induced cancer senescence [187, 188].

Activation of the immune system to promote senescent cell elimination, also known as immune surveillance, is an alternative approach currently gaining attention in the field (**Figure 1.10**). Cytotoxic $CD4^+$ T lymphocytes, macrophages and NK cells are believed to be the main drivers of senescence clearance in tissues [189]. An example of such immune-promoting strategies consisted in the administration of the NK TLR3 ligand

polyI:C, which activated NK-mediated senescent cell elimination, notably ameliorating liver fibrosis [190, 191]. More recently, Amor and colleagues developed chimeric antigen receptor (CAR)-T cells targeting overexpressed uPAR on the membrane of senescent cells as a novel senolytic approach, and demonstrated effective senescent cell clearance in a model of NSCLC *in vivo* and the reversal of CCl_4- and diet-induced liver fibrosis, significantly improving clinical outcomes in both models [192]. This proof-of-principle represents an exciting approach, given the fact that the efficient development of anti-tumor CAR-T cells is known to provide long-term immunological memory, which could be beneficial to prevent further complications from persistent senescence, avoiding, for instance, future cancer relapse in the context of chemotherapy-induced senescence. However, intra-tumoral senescent cells are known to promote an immune-suppressive microenvironment, and the efficiency of such strategies in these conditions remains to be addressed. Nevertheless, given the highly pro-inflammatory profile of senescent cells, more novel interventions focused on immune activation against senescence are likely to emerge in the coming years.

As presented earlier in section 1.2.2.3, contrary to the long-standing paradigm that the senescent programme is irreversible, research has demonstrated that the reactivation of the cell cycle after senescence implementation can be achieved, at least by genetic manipulation. However, this strategy may only be beneficial in conditions where the re-establishment of cell proliferation is needed to counteract the detrimental effects of accumulated senescence. Examples of strategies to achieve reversion include the suppression of the $p16^{Ink4a}$/Rb pathway or abrogation of p53 [193], ectopic overexpression of the PcG protein CBX8 to repress the same signalling axis [194] and the induction of the so-called four Yamanaka factors (i4F) to drive the reprogramming of senescent cells and restore the cell cycle [195, 196] (**Figure 1.10**). Nevertheless, as described earlier, senescence reversion may be accompanied with a transformed cellular phenotype, including an increased aggressiveness and stem-like features, and thus this approach as a senolytic strategy should also be taken with caution.

Finally, there may be instances where blocking the adverse effects derived from the SASP while maintaining the integrity of the senescent cell cycle arrest might be relevant. In this direction, the manipulation of the SASP through the direct regulation of

key regulatory pathways, such as the NF-κB and C/EBPβ cascades, have also emerged as intriguing senomorphic approaches (**Figure 1.10**). Inhibitors of such pathways can act on different levels, and include NF-kB inhibitors apigenin, wogonin and metformin, MAPK blockers, such as SB203580, UR-13756 and MK3.II, and mTOR inhibitors including rapamycin and rapalogs, among many others (**Figure 1.10**) [197]. For instance, ginsenoside F1 and Nutlin-3a have been reported to robustly decrease the secretion of SASP factors such as IL6- and IL-8, effectively reverting SASP-activated migration of glioblastoma cells [198] and breast cancer cell invasiveness [199]. Importantly, some of these inhibitors are currently under clinical evaluation for a variety of malignancies. Although none of them have been approved for clinical use in cancer patients so far, they represent an attractive approach for cancer treatment, where the prevention of SASP-derived detrimental effects in the tumour, while keeping cancer cells arrested upon the implementation of senescence, can be a desired outcome.

1.3.2. Second-generation senotherapies and future strategies

Despite the benefits of senotherapies reported in different *in vivo* models, research demonstrates that such strategies are not risk-free and can present important associated toxicities, hampering their translation into the clinic. For instance, while navitoclax has so far been a cornerstone in the field of senolytics given its promising effects in pre-clinical studies against both liquid and solid tumours [200], it is known to cause severe thrombocytopenia and neutropenia [200, 201], as these circulating cells present increased levels of Bcl-X_L to ensure survival. In addition, it can also impact trabecular bone structure by impairing osteoblast activity, resulting in decreased bone volume *in vivo* [202]. Other strategies may also result in on- and off-target effects due to the fact that targeted pathways are generally not exclusive of the senescent phenotype and may be upregulated or overexpressed in other tissues or cell types in the body [201]. Therefore, evident issues with selectivity, universality and toxicity remain to be further addressed in pre-clinical models before attempting clinical translation of senotherapies. The above toxicities are, at least partly, caused by the heterogeneity of senescence and the absence of universal and more specific targetable biomarkers.

To this aim, a number of innovative approaches are being developed to ensure increased specificity of senolytics, and in this context, two-hit approaches remain the prevailing strategy for the proposal of tenable solutions. These either entail (1) a combinatorial drug treatment, with two compounds abrogating different senescent-specific targets, which can potentially lessen side effects by resulting in equal or improved efficacy at lower doses, or (2) the development of engineered activatable pro-drugs that remain "quenched" upon administration and become preferentially activated or released in senescent cells before exerting their senolytic functions. In this context, significant efforts are being made towards the development of second-generation drugs derived from pharmacologically active compounds that specifically target pathological senescent cells by exploiting synthetic lethal vulnerabilities. Another emerging approach focuses on enhancing specificity by modifying therapeutic agents to be activated or released by a senescent-specific ligand or enzymatic reaction, thereby increasing specificity.

Of note, the first attempts at enhanced senescent targeting were performed through the engineering of nanoparticles (NPs) encapsulating tracers and diagnostic agents. Agostini and colleagues developed silica NPs, loaded with the dye rhodamine and coated with galacto-oligosaccharides, which effectively prevented the dye from being freed. Upon cellular uptake via endocytosis, the increased levels of SA-β-gal that characterises senescence allowed the release of rhodamine in human senescent fibroblasts *ex vivo*, while rhodamine remained encapsulated within the NPs in control proliferating cancer cells [203]. Similar strategies were next employed and refined by our group, who generated the first galacto-conjugated senolytic strategy through the design of 6-mer galacto-oligosaccharide-coated NPs (GalNPs) encapsulating doxorubicin and navitoclax. Remarkably, these NPs were selectively activated in palbociclib-induced senescent cells in NSCLC xenografts *in vivo*, resulting in effective senolysis and promoting tumour regression, thereby providing proof of concept of the therapeutic potential of senescent-directed engineering compounds in cancer treatment [204]. GalNPs effectively ameliorated lung fibrosis and led to the recovery of pulmonary function in bleomycin-treated mice [204].

Subsequent approaches have since then been developed for the senescent-specific delivery of toxic compounds, including anti-CD9-lactose-wrapped NPs containing

rapamycin [205] and molecularly imprinted NPs functionalised against the senescent cell surface epitope B2M [206]. Despite the potential benefits of these innovative strategies, however, the understanding of nanotechnology-associated systemic interactions and toxicities is far from complete, which makes their clinical translation particularly challenging. Consequently, interest is expanding towards the engineering of compounds, other than NPs, that may represent safer alternatives. In this line, Lozano-Torres and colleagues reported the conjugation of an acetylated galactose to a diagnostic probe as an effective approach to increase senescence specificity [207]. This interesting approach leverages the membrane-permeable characteristics that the presence of acetyl moieties provides [208], thereby making the drug accessible to the lysosomal compartment, where it is digested by the increased β-galactosidase activity of senescent cells. The combination of this approach together with a drug that already exerts preferential activities in senescent cells with the aim of increasing specificity and decreasing associated toxicities, has not been attempted thus far. In this regard, new bio-engineering paradigms developed to ensure the clinical applicability of senolytics with improved safety profiles are likely to be pivotal in the coming years.

1.4. The TGF-β signalling pathway

Transforming Growth Factor-β (TGF-β) ligands have been reported to be secreted as part of the SASP [76, 88, 149, 209]. This family comprises more than 30 cytokines that are divided into two main branches, the first one including TGF-β1, β2 and β3, activin, nodal, lefty and myostatin, and the second one, the group of BMPs, GDFs and the anti-muellerian protein AMH, among others [210]. These ligands play a variety of crucial roles in physiology and disease, ranging from embryogenesis, morphogenesis, wound healing and neural development to regulation of the immune response and cancer.

1.4.1. The TGF-β ligands and receptors

The three known isoforms of TGF-β (TGF-β1, TGF-β2 and TGF-β3) have been extensively studied given the wide array of pleiotropic functions they exert during development and

adult tissue homeostasis [211]. The mature, bio-active form of these ligands is composed of two monomers, linked by a disulphide bridge and several hydrophobic interactions. However, they are secreted to the extracellular matrix (ECM) as biologically inactive complexes or pro-proteins [212]. These complexes are formed of the dimeric TGF-β peptide bound to a large amino-terminal domain named latency associated protein (LAP), which allows the proper folding and dimerization of the mature peptide. In the Golgi apparatus, the TGF-β dimer is cleaved from LAP, but it remains associated with it via non-covalent interactions (**Figure 1.11**) [213]. In addition, before the complex is secreted to the ECM, it is further associated with a glycoprotein named latent-TGF-β binding protein (LTBP), which aids the release of the latent complex to the ECM and regulates the bioavailability of the active dimer by preventing its interaction with target receptors (**Figure 1.11**) [214].

The activation of TGF-β is a crucial step in the regulation of its activity, and several mechanisms and molecules are known to release the active dimer from the latent complex, including fibroblast growth factor (FGF), metalloproteases such as MMP-2 and MMP-9, integrins, retinoic acid and even an acidic pH, among many others [215]. Upon cleavage, the freed bioactive TGF-β dimer will then bind to the target receptor, which will mediate the activation of downstream TGF-β signalling in the recipient cell (**Figure 1.11**). There are three types of membrane receptors that can interact with TGF-β ligands: TGF-β receptor 1 (TGF-βR1), TGF-β receptor 2 (TGF-βR2) and TGF-β receptor 3 (TGF-βR3). Out of these, TGF-βR1 and TGF-βR2, which are serine/theornine kinases, are the main mediators of signal transduction. The interaction of TGF-β ligands with TGF-βR2 induces the phosphorylation of a Gly-Ser regulatory domain in TGF-βR1, which results in the incorporation of TGF-βR1 and the generation of a multimer that consists of two pairs of TGF-βR1 and TGF-βR2. This large activated complex will then transduce the signal and prompt the activation of canonical and/or non-canonical signalling cascades in the recipient cell [215].

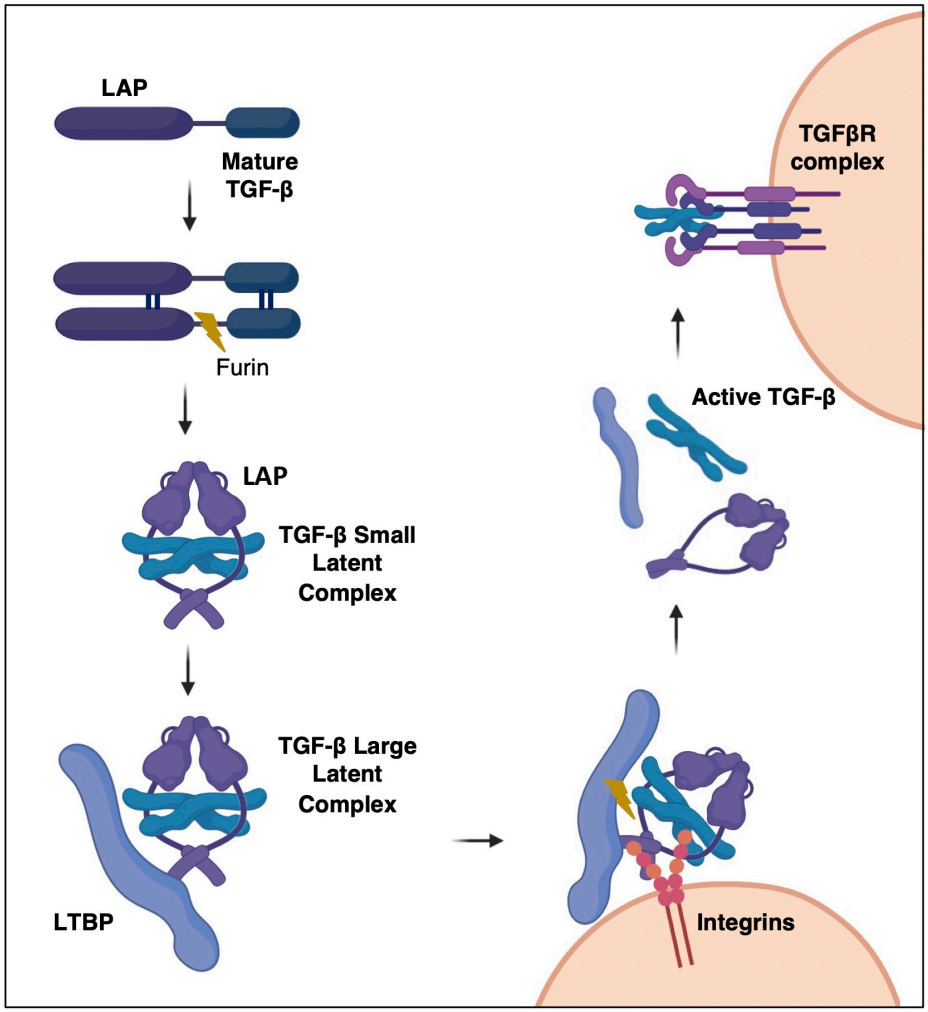

Figure 2.11. TGF-β ligands maturation and activation. TGF-β is synthesised as a pro-peptide that consists of LAP and mature TGF-β region, forming a homodimeric structure. The dimer precursor is cleaved by furin to yield the inactive small latent complex. LAP folds around TGF-β while remaining non-covalently associated, blocking access to the mature cytokine. The small latent complex can then interact with LTBP to form the secreted large latent complex, allowing associations with the extracellular matrix to anchor TGF-β outside the cell. Cell-membrane integrins or other activators, such as low pH or metalloproteases, are able to bind and dissociate the structure, leading to the release of active TGF-β. Active TGF-β subsequently triggers signalling in cells via initially binding to the TGF-β receptor complex. LAP, latency associated protein; LTBP latent- TGF-β binding protein. Figure generated with BioRender.com.

1.4.2. Canonical and non-canonical TGF-β signalling

The canonical TGF-β signalling pathway involves the activation of SMAD proteins, which are latent cytoplasmic transcription factors (TFs) and become directly mobilised upon

phosphorylation by the TGF-βR1/R2 activated complexes. R-SMAD binds to TGF-βR1 and recruits non-activated SMADs to the complex, including SMAD2 and SMAD3. When recruited SMADs become phosphorylated, they lose affinity for the receptor, dissociate from them and subsequently form a higher-order aggregate, which commonly includes the association of SMAD2/3 with SMAD4, and translocate to the nucleus. A negative feedback loop is triggered shortly after activation of the receptors, whereby R-SMADs become ubiquitinated by Smurf1 and therefore degraded, which tightly controls the duration and intensity of the SMAD signal transduction [210]. Once within the nucleus, SMAD complexes remain retained through the interaction with additional protein binding partners and DNA. Such partners can be very diverse, including FOX, E2F, AP1, RUNX and HOX, among many others, and each SMAD-partner combination is known to target the transcriptional activation or repression of a particular subset of genes, regulating numerous signalling pathways [210]. These regulatory inputs further control the transcription of inhibitory SMADs like SMAD6 and SMAD7, which initiates a second wave of negative feedback loop to halt signal transduction. The activation of the SMAD-driven canonical TGF-β signalling is known to drive the inhibitory effects of TGF-β, including cell cycle arrest and apoptosis induction (**Figure 1.12**).

Importantly, given the pleiotropic nature of TGF-β and the many (and sometimes antagonistic) functions triggered in response to TGF-β, the apparent simplicity of the SMAD-driven signalling cascade instigated a dilemma in the field. Years of research have subsequently demonstrated that the response to TGF-β signalling is determined by complex combinations of core pathway components (including TGF-β ligands and receptors, SMADs and TFs), by close interactions and cross-talks with other cascades within the target cell and by the ability of the activated receptor complexes to modulate and activate non-canonical pathways. Such non-canonical cascades include a wide range of MAP kinase (MAPK) pathways, GTPase signalling cascades and the phosphatidylinositol-3-kinase (PI3K)/Akt pathway, among many others (**Figure 1.12**).

A prominent non-SMAD cascade is triggered by the TGF-β-induced Erk activation and tyrosine phosphorylation [216]. This activation is known to occur directly within minutes of ligand exposure, or hours after TGF-β stimulation, suggesting the requirement of additional protein translation for this response to be prompted. Erk cascade can be

triggered when the non-RTK Src phosphorylates the tyrosine residue of TGF-βR2 on Y284, which recruits signal transducers such as GRB2 and Shc, thereby forming a complex that will lead to the sequential activation of Ras/Raf/Merk/Erk [216]. This pathway has been described as crucial for the induction of EMT in epithelial cells, as it drives the dissociation of cell adherens junctions and promotes cell motility through the activated transcription of genes involved in those responses (**Figure 1.12**).

Additional non-canonical signalling pathways that are known to be implicated in EMT induction upon TGF-β stimulation include the Rho-like GTPase-dependent and the JNK/p38 cascades. RhoA can be triggered via either SMAD-dependent or independent routes, and it has been reported to result in the formation of actin fibres and the dissolution of tight junctions, driving the establishment of an EMT programme. This pathway seems to be activated through the assembly and accumulation of TGF-βR complexes at tight junctions, which recruits and phosphorylates RhoA pathway transducers, including Par6, Smurf1 and Cdc42 [216]. Alternatively, activated TGF-β receptor complexes can interact with TRAF6 and induce its poly-ubiquitination, which results in the recruitment of TAK1 and subsequent stimulation of the JNK/p38 pathway. Transducers in this cascade will act in conjunction with Smads to induce TGF-β-driven apoptosis, or alternatively can activate in an Smad-independent manner the transcription of groups of genes involved in actin cytoskeleton reorganisation, mediating cellular shape changes and contributing to the EMT phenotype (**Figure 1.12**) [216].

Lastly, an intriguing alternative non-SMAD pathway is the PI3K/Akt, which has been described to result in different cellular responses in the target cell. The activation of this cascade seems to be independent of Smad phosphorylation. Despite the molecular basis of this pathway remains to be fully elucidated, it is believed that the p85 subunit of PI3K can interact with TGF-βR complexes, which results in the phosphorylation of the downstream effector Akt and the sequential activation of mTOR/S6K. Despite this pathway is described to be a crucial driver of cellular proliferation [217], its activation in the context of TGF-β has been mostly reported to drive the acquisition of EMT features in epithelial cancer cells, as well as antagonise TGF-β-induced growth arrest and apoptotic response through the inhibition of the TF FoxO and the sequestering of Smad3 in the cellular cytoplasm (**Figure 1.12**) [216].

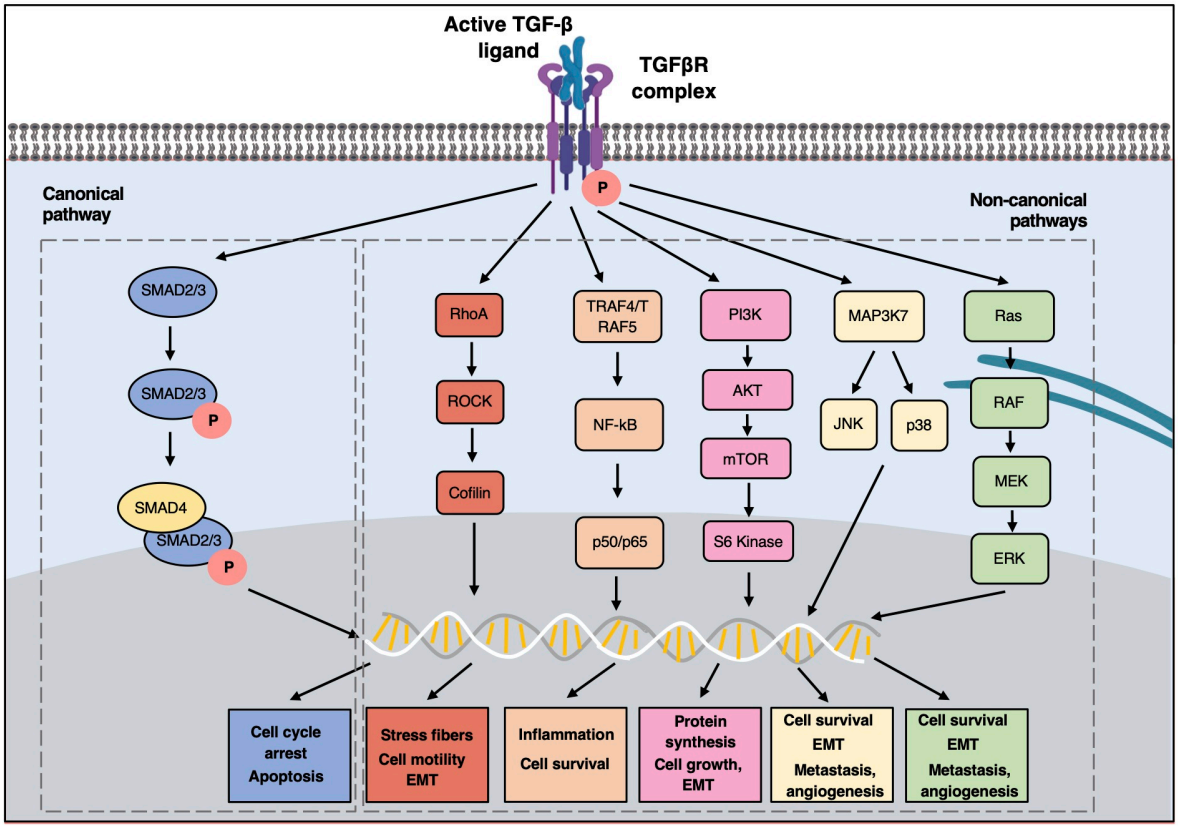

Figure 1.12. Canonical and non-canonical TGF-β signalling pathways. In the canonical cascade, biologically active TGF-β ligands bind to TGFβR2, which in turn activates TGFβR1. TGFβR1-regulated SMAD2/3 proteins are phosphorylated at their C-terminal serine residues and form complexes with SMAD4, triggering a number of biological processes through transcriptional regulation of target genes. In the non-canonical cascades, the TGF-β receptor complex transmits its signal through other factors, such MAPks, PI3K, TRAF4/6 and the Rho family of small GTPases. Activated MAPKs can exert transcriptional regulation either through direct interaction with the nuclear SMAD protein complex or via other downstream proteins. In addition, activated JNK/p38/ERK act in concert with SMADs to regulate cellular apoptosis and proliferation, whereas they mediate metastasis, angiogenesis and cellular growth through other transcription factors, such as c-JUN and ATF. RhoA/ROCK activation induces actin stress fiber formation during EMT, and PI3K and AKT activation by inducing a physical interaction between the PI3K p85 subunit and the receptor complex leads to translational responses via mTOR/S6kinase activation. TGF-β-mediated signalling of the TRAF proteins can initiate NF-κB signalling activity, which results in an inflammatory response, among other processes. MAPK, mitogen-activated protein kinases; NF-κB, nuclear factor-κB; PI3K, phosphatidylinositide 3-kinase; TRAF4/6, TNF receptor-associated factor 4/6.

1.4.3. TGF-β in cancer

As with many processes in cancer, the TGF-β ligands have been reported to play opposing roles, resulting in both tumour suppressive and tumour promoting activities. TGF-β was initially described as a repressive cytokine as it maintains tissue homeostasis by preventing incipient tumours from advancing towards malignancy through the regulation of the cell cycle, differentiation, adhesion and survival [210]. However, cancerous cells present the ability to avoid or alter the suppressive impact of the canonical TGF-β pathway, which can result in the promotion of EMT, invasion, tumour growth and even evasion of immune surveillance. Researchers have for many years tried to uncover how cancer cells are able to circumvent the inhibitory effects of TGF-β, and it is believed that malignant cells can either inactivate core components of the canonical pathway, such as SMADs or TGF-β receptors, or present downstream alterations that disable the suppressive arm of the pathway while driving the regulation of alternative cascades to their advantage. In addition, of crucial relevance to cancer progression are the effects of TGF-β on the microenvironment, given its key influence on the immune system and other stromal cells [218]. These cytokines enforce immune tolerance at high levels, as well as they can also lead to chronic inflammation and the generation of a pro-tumorigenic niche. In addition to the effects on the immune system, TGF-β ligands can also recruit other stromal cells, such as fibroblasts, which in turn further support tumour dissemination. Given the wide array of extracellular and intracellular factors that can alter or modulate the response to TGF-β, elucidating the microenvironmental context, cell type and mutational profile as well as the presence of other interfering stimuli is imperative to fully understand the effects driven by to TGF-β under particular conditions.

1.4.3.1. Tumour suppression by TGF-β

The most prominent effect of TGF-β is the suppression of cell proliferation on target cells. This growth inhibitory response is triggered through the direct inhibition of c-Myc and CDKs activities, as well as the induced expression of CDK inhibitors, such as $p15^{INK4B}$, $p21^{CIP1}$ and $p27^{KIP1}$. Of note, researchers have demonstrated that this constraining effect

on cell growth only occurs in epithelial cells in the context of tissue injury and oncogenic stress, as well as in endothelial cells, but not in mesenchymal cells or during development [210]. Various reports show that deficiencies in the canonical cascade significantly accelerate malignant progression upon oncogenic transformation, including *KRAS* overexpression and *APC* loss, in several models of oral, skin, gastrointestinal and pancreatic cancer [219-222]. Importantly, such inhibitory effect on cell cycle progression has also been reported to prompt the senescent cell programme in target cells. Mechanistically, this can be explained by the induced cytostatic response to TGF-β, as well as the increased production of mitochondrial ROS [223], the suppression of telomerase [224, 225] and the disruption of DDR through the upregulation of several miRNAs [226, 227]. Indeed, TGF-β secreted as part of the SASP has been described to result in the paracrine induction and the autocrine reinforcement of cellular senescence [228, 229]. In addition to suppressing pre-malignant progression through a cytostatic response and/or the induction of cellular senescence, TGF-β has also been reported to trigger apoptosis in target cells, despite the molecular identities governing this response are not yet fully understood. Some candidate mechanisms include the induction of the death-associated protein kinase DAPK, the death receptor FAS and the pro-apoptotic effector BIM [210].

TGF-β is regarded as a master regulator of the extracellular environment, having a prominent impact on stromal cells. However, its tumour suppressive effects are mostly reported on epithelial cells. Actually, according to the well-established paradigm regarding the opposing effects of TGF-β in cancer, it is believed that this cytokine exerts its anti-tumour response in early stages of cancer, preventing the progression of pre-malignant cells upon early transformation. As the tumour develops and cancer cells acquire increasing numbers of mutations and alterations, and the cancer niche becomes more complex, the pro-tumorigenic functions of TGF-β will overwhelm the tumour suppressive ones through what is known as the “TGF-β paradox” [230], and this signalling pathway will start acting as a tumour promoter, impacting both cancer cells and the surrounding tissue.

1.4.3.2. Tumour promotion by TGF-β

In advanced cancer stages, the role of TGF-β is prominently tumour-promoting, with effects ranging from EMT promotion to angiogenesis and immune evasion. EMT, or the transition of epithelial cells to a mesenchymal cellular phenotype, is characterised by a loss in cell polarity as well as cell-cell and cell-matrix adherence, resulting in an increased motility [231]. This process has been largely reported to orchestrate carcinoma invasion and metastatic spreading, and it is known to be one of the main responses to TGF-β stimulation in advanced tumours through the activation of the canonical pathway in combination with Smad-independent cascades, as described above. TGF-β induces the expression of TFs SNAIL, TWIST and ZEB, as well as it represses the expression of E-cadherin, thereby regulating cell polarity and cytoskeleton organisation. It further allows its remodelling by potentiating the activities of several MMPs [231]. The role of TGF-β as an EMT promoter was first reported during murine heart development, in breast cancer cell lines and in mouse models of skin carcinogenesis [232], which was subsequently followed by many other studies. In human cancer, cells with traits that are characteristic of EMT were detected in invasive areas displaying enriched levels of TGF-β together with additional cytokines known to drive EMT induction [210].

Despite the cytostatic effect elicited in response to TGF-β in pre-malignant cells, under certain conditions, the activation of TGF-βR can stimulate cell proliferation. This effect has been reported to be highly dependent on the concentration of this cytokine, and it is believed that it can drive cell growth by inducing the production of mitogens that will act in an autocrine manner when relevant effectors of the cytostatic TGF-β response, such as $p15^{INK4b}$ or RB, are non-functional [210]. Several reports in the 90s demonstrated that glioma cells elicited increased proliferation in response to TGF-β via the induction of PDGF-B and PDGF-AA [233-236]. Later on, it was demonstrated that TGF-β1 and TGF-β2 can also promote the proliferation of cells *in vitro* when in combination with other growth factors such as EGF and FGF [237]. Therefore, the final effect that TGF-β may exert on the tumour not only depends on the intrinsic characteristics of target cells, but also the

presence of additional growth factors in the microenvironment, a phenomenon that might be of particular relevance in the context of senescence and the SASP.

TGF- β receptors are believed to be universally expressed in all cell types, and as such, it is also expected to impact stromal cells within the tumour. Interestingly, inhibition of TGF-β in hepatocellular carcinoma, glioblastoma and colorectal cancer models significantly decreased VEGF levels, reduced microvessel density and inhibited the generation of new blood vessels in the tumours [238-240], indicating that this cytokine can also function as a pro-angiogenic factor. In addition, fibroblast mobilisation and recruitment is another significant component of the tumour promoting actions of TGF-β. This cytokine has been reported to facilitate the generation of myofibroblasts, which are commonly known as cancer-associated fibroblasts (CAFs) in the context of the tumour. CAFs are major producers of MMPs, cytokines and chemokines that act conjunctively to promote cancer cell proliferation and tumour invasion [210].

Further to these stromal effects, TGF-β has also been shown to play a role in cancer evasion from host immunity through the inhibition of Major Histocompatibility Complex (MHC) class II in both tumour cells and immune cells, including macrophages and NK cells [241]. This cytokine is a major inhibitor of lymphocytes, directly suppressing the functions of helper $CD4^+$ and cytotoxic $CD8^+$ T cells, and the proliferation of both T and B cells through the inhibition of c-Myc, which halts cell maturation. In humans, it has been demonstrated that high levels of TGF-β correlate with immune suppressive environments [218]. For instance, TGF-β was shown to diminish NKG2D receptor expression, which is an activator of NK and cytotoxic T cells [242].

Finally, further to the effects reported in stromal cells, an interesting study using a mouse model of SCLC showed that TGF-β can generate a marked heterogeneity in downstream signalling in the surrounding tissue, resulting in both TGF-β-responding and non-responding populations [243]. Most intriguingly, despite TGF-β-responding cells presented a decrease in proliferation rate upon exposure to cancer cell-secreted TGF-β compared to non-responders, they showed increased protection and enhanced survival following cisplatin treatment, leading to tumour relapse [243]. This importantly highlights the diversity of mechanisms whereby this complex signalling pathway may hamper cancer treatment and promote recurrence.

1.4.4. The roles of TGF-β as part of the SASP

As it has been described previously, TGF-β ligands are known to induce cellular senescence by means of their cytostatic effect on target cells. Its role as a SASP ligand is now gaining attention, particularly in the context of ageing, as its levels have been reported to be increased in the plasma of elderly individuals [244, 245], and is believed to play important roles in age-related pathologies [246]. In developmentally-programmed senescence, secreted TGF-β regulates the tissue remodelling and the formation of embryonic structures [88]. In cancer, increased levels of TGF-β in the SASP have been described in OIS and chemotherapy-induced senescence, although the effects derived from this were not addressed [247]. In addition, induction of OIS resulted in an increased upregulation of NOTCH that was subsequently linked to the production of a TGF-β-rich SASP [76]. Induced TGF-β later acted in combination with NOTCH, orchestrating a dynamic loop that regulated the SASP and induced senescence in a paracrine manner [76, 248], consistent with the tumour-suppressive effects of TGF-β in early malignant stages. However, the impact of this cytokine as part of the SASP in the context of therapy-induced senescence remains largely unexplored.

Given the tumour-promoting actions of TGF-β in advanced cancer, it is conceivable that a SASP rich in TGF-β upon therapy-induced senescence may be detrimental. In 2007, Biswas and colleagues observed an increase in the circulation of TGF-β ligands upon therapeutic irradiation in a mouse model of breast cancer, despite the implementation of cellular senescence was not assessed in this study [219]. Intriguingly, higher expression of TGF-β in mice was further associated with increased breast cancer metastatic progression *in vivo* [219]. In addition, blocking of these ligands with neutralising antibodies prevented such tumour-promoting effects, suggesting a potential link between induction of senescence upon irradiation, TGF-β1 secretion as part of the SASP and tumour promotion. To this date, however, such interplay has not been established in the context of senescence.

1.4.5. TGF-β and NSCLC

As previously stated, the role and impact of TGF-β is highly context-dependent. Importantly, a prospective analysis of a cohort of 383 NSCLC patients demonstrated a strong correlation between high expression of TGF-β in resected specimens and disease progression [249]. Elevated levels of TGF-β1 were also observed in serum samples from patients upon lung tumour resection [250]. Importantly, alterations in the downstream components of the canonical pathway seem to be crucial in NSCLC development. For example, inactivating mutations in SMAD6, which is an inhibitor of the TGF-β canonical cascade, are correlated with improved patient survival [251]. Altogether, these studies suggest that the inactivation of SMAD-mediated signalling and promotion of non-canonical pathways may play an important role in driving NSCLC progression. At the cellular level, most experimental studies demonstrate that TGF-β drives the acquisition of EMT traits in lung cancer cells *in vitro* and *in vivo*, as recently reported [252, 253], which is known to be mediated by the crosstalk with other non-Smad signalling pathways. Of relevant importance is oncogenic or constitutively active *KRAS*, which is known to be a main mediator in the shift of TGF-β signalling towards the activation of the EMT programme [254]. Besides its effects on cancer cells, this cytokine is also widely reported to orchestrate the tumour microenvironment in lung tumours. Secreted TGF-β drives the remodelling of the stroma by promoting angiogenesis, immune evasion, and the mobilisation of cancer-associated fibroblasts (CAFs), that further support tumour progression [254, 255].

Interestingly, recent evidence suggests that high levels of TGF-β contribute to treatment resistance and decreased sensitivity to chemotherapeutic treatment in NSCLC [241, 256, 257]. In addition, recent reports show that the inhibition of TGF-β may pose a promising strategy to enhance cancer NSCLC immunotherapy [258, 259]. However, the mechanisms driving the expression of TGF-β in these cases and the potential interplay between therapy-induced cellular responses in the tumour, such as senescence, and TGF-β remain largely unaddressed. As evidenced by the above, detecting and illustrating the molecular details of TGF-β in cancer is important, given the remarkable versatility, plasticity and context-dependent nature of this cytokine-signalling pathway. As evidenced

by the above, in the cases where TGF-β is found to drive lung cancer progression, the development of combinatorial therapeutic modalities aimed at circumventing its pro-tumorigenic effects can result in very attractive approaches to improve patient outcomes.

1.5. Thesis Aims and Rationale

A better understanding of the mechanisms underlying lung cancer tumorigenesis and response to current treatment paradigms are imperative to improve patient outcomes.

Early detection and prevention of NSCLC remain a formidable challenge. Several strategies have been proposed for earlier diagnosis, based on high-risk patient stratifications, liquid biopsy analyses and screenings based on low-dose CT imaging, but the benefits provided have been scarce so far. The elucidation of cellular processes and traits characteristic and exclusive of early NSCLC development can therefore result in innovative approaches that not only allow an earlier detection of cancer, but may drive the development of preventative therapies. This treatment modality still remains to be explored, but it can be of particular interest in scenarios such as the case of multifocal lung cancer. This is a complex condition, generally found incidentally, where multiple early lesions and tumours are present in the lungs, some of which will progress to malignant disease [260]. These patients therefore require close monitoring and repeated CT imaging, given the fact that there are currently no optimal strategies to target such lesions and prevent the progression to advanced stages of lung cancer. Consequently, understanding the nature of NSCLC early lesions and uncovering novel methods for their detection and abrogation can revolutionise cancer care and significantly impact patient survival.

As previously introduced, despite significant advances in targeted therapies for oncogene-addicted NSCLC cancer in advanced stages, platinum-based chemotherapies have remained the standard-of-care for adjuvant, neoadjuvant and palliative modalities for over 30 years, and survival continues to be overly poor [2]. Although some reports indicate significant flaws derived from chemotherapeutic treatment [261] and suggest a link between chemotherapy-driven induction of senescence and poorer patient survival [160], evidence of the impact of chemotherapeutic treatment and how ineffective

response to therapy may promote tumour progression remains to be addressed. For this reason, understanding the underlying mechanisms of tumour response to lung cancer standard-of-care is imperative for the identification of novel targets and the development of more effective therapeutic modalities that prevent NSCLC treatment failure and cancer relapse.

Strong evidence suggests that cellular senescence, a key player of the tumour microenvironment, may play a role in both early tumorigenesis and upon lung cancer chemotherapeutic treatment, but such interplay remains elusive. Cellular senescence was initially regarded as a cell autonomous response elicited in response to damage or stress, essentially aimed at preventing the expansion of potential malignant cells and preserve tissue homeostasis. However, as described in the previous sections, increasing evidence demonstrates that senescence can contribute to the progression and even be causative in a number of pathologies, as well as it can paradoxically contribute to tumour initiation, progression and relapse through different mechanisms. Such effects are hard to predict, as the resulting senescent phenotype greatly depends on the senescent driver, the tissue of origin, the genetic background of the cell and the chronicity of the senescent burden. Therefore, it is important to address the potential impact of senescence from a context-dependent perspective and within relevant models, which is not only crucial to advance our understanding of this cellular mechanism in other conditions like cancer, but can also provide novel insights for the prevention and improved management of NSCLC. In this context, the development of novel senescence-targeting approaches, or senotherapies, that effectively prevent the deleterious effects from unresolved senescence induction in tumours can be particularly attractive. However, existing senotherapies present worrying toxicities, such as thrombocytopenia, that can hamper their clinical translation. In addition, the potential benefits derived from the combination of senotherapies with other drugs commonly applied in the clinic, such as chemotherapy, has not been explored to date. Therefore, the development of novel, safer senolytic formulations are needed, and the potential of chemotherapeutic-senolytic modalities that may significantly improve NSCLC outcomes needs to be explored.

Taking the above observations into consideration, the main objective of this PhD work is to test the central hypothesis that **cellular senescence induced by**

chemotherapeutic conventional treatment and by oncogene activation can contribute to lung cancer progression. To obtain observational evidence that unequivocally demonstrates this, as well as provide novel therapeutic strategies to counteract such effects, the three specific aims for this work are the following (**Figure 1.13**):

Aim #1. To demonstrate the incidence and extent of cellular senescence during NSCLC tumorigenesis, evaluate its role during lung tumour progression from pre-neoplastic to malignant stages and investigate the potential of senolysis as a preventative therapy.

For this aim, the Kras-FSF^{G12V} model of NSCLC will be employed. Lung cancer will be induced in mice through the intranasal/intratrachreal administration of AdFlp viral particles, which drive the expression of the mutant Kras^{G12V} in the lungs, and markers of cellular senescence, including SA-β-gal activity, p21 and p16 will be analysed at the histological level to detect senescence in developing lesions. After assessment of senescence induction in the lesions, mice will be treated with the senolytic ABT-737 during tumorigenesis to evaluate the impact of senescent cell removal on tumour burden and animal survival. Of note, this study is performed as part of a collaboration with the group of Martínez-Barberá (University College London), who generated a novel knock-in mouse model, named *p16-FDR*, that allows the visualisation, tracing and pharmacogenetic ablation of p16-expressing cells (see **Supplementary Figure 3.1, Appendix**). Our data will be compared to those obtained from their analyses, and will help establish whether senescent cell ablation during lung tumorigenesis is an approach with the potential to deter NSCLC development.

Aim #2. To dissect the paracrine effects of senescence-inducing standard-of-care chemotherapies in the progression of NSCLC.

Despite the widely reported tumour-promoting activities of senescent cells in different conditions, the role and impact of platinum-based chemotherapy in the context of NSCLC remains to be uncovered. This is of extremely importance given the wide use of cisplatin/carboplatin as first line regimens, the documentation of senescence in lung

tumours upon neoadjuvant treatment, and the high rate of failure of such modalities. To achieve this aim, we will first evaluate the senescence-inducing capability of standard-of-

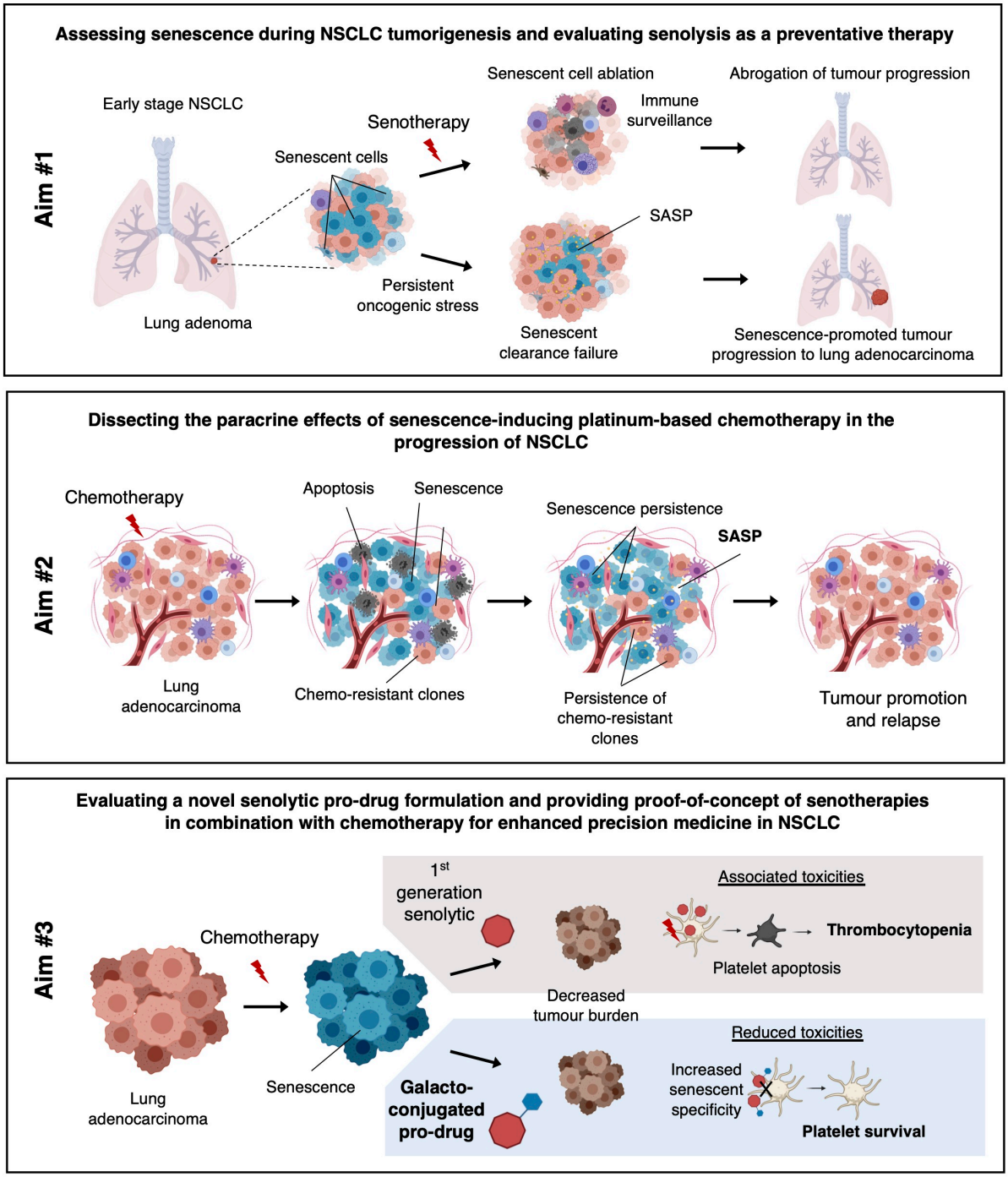

Figure 1.13. Thesis aims and rationale. Aim #1 of this work consists in demonstrating and characterising the extent and impact of cellular senescence induction during lung cancer tumorigenesis and progression. Based on published literature, lung adenomas accumulate cellular senescence. It is believed that persistent oncogenic stress leads to increased senescent burden due to a failure in immune-directed clearance. Accumulated senescent cells can subsequently contribute to tumour progression, either through the

secretion of pro-tumorigenic SASP factors, creating a favourable cancer niche, or through senescence escape and re-establishment of the cell cycle. Our working hypothesis is that senolytic elimination of senescent cells during lung cancer development prevents such tumour-promoting effects and abrogates lung cancer progression, whereby we aim to further demonstrate the benefits of senolytic-based preventative approaches for NSCLC. **Aim #2** of this work focuses on characterising the role and impact of chemotherapy-induced senescence in NSCLC progression. We hypothesise that upon chemotherapeutic insult, the majority of cancer cells may undergo different cell fates, including apoptosis and senescence. Due to tumour heterogeneity, a minority of cells may remain refractory to chemotherapeutic agent administration. If senescent cells are not effectively cleared or resected, their accumulation may contribute to the generation of a pro-inflammatory niche via the secretion of the SASP. This, together with the persistence of treatment-resistant clones and the possibility of senescence reversion, may contribute to tumour advancement. We intend to demonstrate that blocking the tumour-promoting mechanisms following chemotherapy-induced senescence can serve as an effective strategy to halt tumour progression and improve treatment outcomes. **Aim #3** of this work involves the validation of a novel, second-generation senotherapy in the context of NSCLC chemotherapy. First generation senolytics like navitoclax, despite being effective in senolysis, are associated with severe toxicities, such as thrombocytopenia, due to their on-target effect on platelets. As part of this work we will validate *in vitro* and *in vivo* a newly generated compound consisting of navitoclax conjugated to a galactose that can be cleaved upon SA-β-gal activity. The ultimate goal is to provide an innovative senolytic approach with increased specificity and decreased associated toxicities, and to propose chemotherapeutic-senolytic combinatory modalities as effective therapies for the management of NSCLC.

care chemotherapies commonly used in lung cancer management, including cisplatin, docetaxel and palbociclib, in human lung adenocarcinoma A549 cells and primary murine lung cancer cells L1475(luc), derived from a *Kras*^{G12V};*p53*^{KO} mouse model of lung adenocarcinoma (also commonly known as KP cells). Upon validation of the induction of the senescent programme, the effects from the SASP will be analysed and compared between the different chemotherapeutics to determine whether factors secreted as part of the SASP can alter the behaviour and phenotype of untreated cancer cells. We will dissect the transcriptome and secretome of senescent cells and will analyse the potential candidates driving such effects, subsequently aiming to determine the mechanism of action whereby gain of malignant properties occurs. We will also study the impact of cisplatin-induced senescence in *in vivo* systems, by using human lung cancer xenografts, an orthotopic mouse model of lung adenocarcinoma and the *Kras-FSF*^{G12V} mouse model of NSCLC. This work will help us establish whether platinum-based chemotherapy can be a contributor to treatment failure and cancer relapse in NSCLC, and determine possible

mechanisms whereby these effects take place within the tumour, so that new therapeutic approaches can be designed in order to prevent them.

Aim #3. To test novel approaches to selectively eliminate senescent tumour cells in an effort to enhance the efficacy of lung cancer therapy and provide safer drug combinatory and senolytic alternatives.

As part of this aim, we have established a collaboration with the group of Ramón Martínez-Máñez from the Polytechnic University of Valencia to develop a second-generation senolytic consisting of an acetylated-galactose covalently linked to navitoclax, a modulation that exploits the selective expression of SA-β-gal in senescent cells. We hypothesise that this novel approach may result in higher efficacy and reduced off-target effects, in particular concerning navitoclax-induced thrombocytopenia. This novel pro-drug will be systematically tested *in vitro* by performing cytotoxic assays in a variety of cancer cells and senescent inducers, including chemotherapy-induced senescent lung adenocarcinoma cells. As a first *in vivo* platform, we will use immunocompromised mice carrying subcutaneous A549 xenografts, which will be treated with the senescent-inducing drug cisplatin in combination, both simultaneously and sequentially, with our pro-drug. Phenotypic readouts from our *in vivo* analyses will help determine whether this new pro-drug efficiently eliminates senescent cells in living organisms, improving therapeutic outcomes. Finally, we will subsequently use xenograft and orthotopic models of lung adenocarcinoma, as well as *ex vivo* treatment of murine and human blood, to evaluate the impact of this second-generation senolytic on platelet survival. Our overarching goal is to obtain proof-of-principle of the therapeutic activity of senotherapies in combination with senescence-inducing chemotherapy, and propose galacto-conjugation of senolytics as a novel approach to improve specificity and reduce senolytic-associated toxicities.

CHAPTER 2:
MATERIALS AND METHODS

2.1. Human material

2.1.1. Ethical regulations

Human lung adenocarcinoma samples from independent patients upon neoadjuvant chemotherapy were obtained from the Royal Papworth Hospital Research Tissue Bank (Project Number T02722). The retrieval, acquisition, processing and analysis of human biopsies was conducted in accordance with all legal requirements and the principles of good clinical practice. Patients signed the Papworth Hospital Tissue Bank general consent and accepted the use of their biopsy for research purposes. The protocol was approved by the Research Ethics Committee.

2.1.2. Human biopsies

Human biopsies were subjected to histological analysis as described in section 2.6.9. Information about the human samples evaluated for Chapter 4 are found in **Table 1**.

Patient number	TB Number	Pathological phenotype	Stage	Location	Neoadjuvant treatment
1	TB21.0210	Lung adenocarcinoma (poorly differentiated)	T2a N2 M0	Right upper lobe	3 cycles of platinum-based chemotherapy
2	TB21.0209	Lung adenocarcinoma (acinar (70%) and micropapillary (30%) growth patterns)	T3 N0	Left upper lobe	4 cycles of cisplatin/vinorelbine
3	TB21.0208	Lung adenocarcinoma (multifocal with lepidic invasive acinar growth patterns)	T3 N3 M0	Right upper lobe	5 cycles of carboplatin/pemetrexed
4	TB14.0993	Lung adenocarcinoma (30% lepidic component)	T3 N2	Left upper lobe	Platinum-based chemotherapy

Table 1. Histological, pathological and treatment details of the human lung adenocarcinoma samples subjected to evaluation in Chapter 4.

2.2. Cell culture methods

2.2.1. Cell culture reagents

2.2.1.1. A549 cell line

A549 cells were obtained from the American Type Culture Collection (ATCC) (kindly provided by Dr Carla P Martins). The A549 cell line was developed from cells isolated from a pulmonary adenocarcinoma and specifically originated from adenocarcinoma human alveolar type II epithelial cells. These cells were authenticated during the duration of this PhD by the Biorepository and Cell Services Core Facility of the Cancer Research UK Cambridge Institute. A549 cells were maintained in DMEM medium supplemented with 10% Foetal Bovine Serum (FBS).

2.2.1.2. A549-Luc2 cell line

A549-Luc2 cells were obtained from the American Type Culture Collection (ATCC), and derived from A549 cells through the transduction with a lentiviral vector encoding for the firefly luciferase gene (luc2) under control of EF-1α promoter. The cell line was established via single cell cloning, and express high levels of luciferase enzymatic protein in a constitutive manner. These cells were maintained in DMEM medium supplemented with 10% FBS and 8 µg/mL Blasticidin (ThermoFisher Scientific).

2.2.1.3. L1475(luc) cell line

The heterozygous $Kras^{G12D/WT}$ murine L1475(luc) cell line was generated by Dr Carla P Martins from $KRas^{LSL\text{-}12D/WT}$;$p53^{-/-}$ (KP) mice. The Kras status of this cell line was confirmed by PCR and pyrosequencing, as previously described [42, 43]. For luciferase imaging purposes, L1475 cells were transduced with an MSC-luciferase-hygromycin retrovirus and

subsequently selected with 350 μg/mL hygromycin B. These cells were maintained in complete DMEM/F-12 growth medium supplemented with 10% FBS.

2.2.1.4. IMR-90 cell line

The human lung fibroblastic IMR-90 cell line was obtained from the ATCC. These cells were derived from the lungs of a 16-week female foetus and are of myofibroblastic origin with smooth muscle-like contractile properties. IMR-90 cells were grown in complete DMEM growth medium supplemented with 10% FBS.

2.2.1.5. MLg cell line

The mouse lung fibroblastic MLg cell line was obtained from the ATCC. These cells were grown in DMEM/F-12 growth medium supplemented with 2 mM GlutaMAX and 10% FBS.

2.2.1.6. SK-Mel-103 cell line

Human melanoma SK-Mel-103 cell line was obtained from the ATCC. This is a generous gift from Dr Marisol Soengas (CNIO). The cells were maintained in complete DMEM supplemented with 10% FBS.

2.2.1.7. HCT116 cell line

Human colorectal carcinoma HCT116 cell line was obtained from the ATCC. The cells were maintained in McCoy's 5A medium supplemented with 10% FBS.

2.2.1.8. HEK-293T cell line

Human Embryonic Kidney (HEK)-293T cells were obtained from ATCC and maintained in complete DMEM supplemented with 10% FBS.

2.2.1.9. Reagents and medium composition

DPBS (Gibco, 14190144)

Trypsin-EDTA (0.25%), phenol red (Gibco, 25200056)

Trypan Blue Solution, 0.4% (Sigma, 72-57-1)

Dulbecco's Modified Eagle's Medium (DMEM) (Gibco, 11965084)

DMEM, high glucose, HEPES, no phenol red (Gibco, 21063029)

DMEM/F-12 Nutrient Mixture (Gibco, 11320033)

McCoy's 5A (Modified) Medium (Gibco, 26600023)

Foetal Bovine Serum (Gibco, 12103C)

GlutaMAX® Supplement (Gibco, 35050061)

No antibiotics were routinely used unless stated otherwise for selection purposes.

2.2.2. General cell culture methods

2.2.2.1. Cell passaging

All cells were grown at 37ºC and 5% CO_2, and they were routinely tested for *Mycoplasma* contamination using the universal mycoplasma detection kit (ATCC). In general, cells were passaged when they reached 70-90% confluency. For this, medium was aspirated and DPBS was added to remove residual products and serum. DPBS was aspirated and 0.25% trypsin-EDTA was added, and cells were incubated for 3-5 min at 37ºC until detached. Next, 5 volumes of media + 10% FBS was added to neutralise the trypsin and cells were collected and transferred into a 15 mL falcon tube and/or plated in a new plate or dish at the desired cell density. For routine passaging, cells were generally split to a 1:3-1:10 ratio, depending on cell type and downstream experiments.

2.2.2.2. Cell freezing

Prior to experimental initiation, all cell lines used for this study were expanded and frozen down at low passages (<6-8) for stock generation and maintenance. For freezing, cell pellets were collected after trypsinisation as described above, and centrifuged for 5 min at 1250 rpm. Supernatant was discarded and cells were resuspended in 10% Dimethyl Sulfoxide (DMSO; Sigma-Aldrich, 276855) in FBS. Cell suspension was aliquoted into Nunc® CryoTubes cryogenic vials (Merck, V7634) in a volume of 1 mL per vial. For each flask at 70-90% confluency 2 aliquots were generated. Vials were placed into a CoolCell LX Cell Freezing Container (Merck, BCS-406) and immediately transferred to -80ºC. For long term storage, vials were transferred to a liquid N_2 tank.

2.2.2.3. Cell thawing

All experiments were performed at passages below 25. When cells reached passage limit, they were disposed of and a new vial from stock was thawed. For this, new vials were transferred from liquid N_2 to dry ice and then quickly thawed in a 37ºC water batch until most of the suspension was thawed. Cells were then transferred to a 15 mL falcon tube and resuspended with 10 mL pre-warmed medium, and then centrifuged for 5 min at 1250 rpm. Supernatant was discarded and then cell pellet was resuspended in 10-12 mL medium and plated onto a flask/plate.

2.2.2.4. Cell culture assays and procedures

2.2.2.4.1. Induction of cellular senescence and reagents

For chemotherapy-induced senescence, series of dose-ranging experiments were performed for each drug to test the optimal condition for cell senescence induction. A549 cells were treated with 15 μM cisplatin, 100 nM docetaxel and 15 μM palbociclib for 7 days and used for experimental purposes immediately after drug removal. L1475(luc) cells were treated with 3 μM cisplatin, 200 nM docetaxel and 30 μM palbociclib for 5 days.

SK-MEL-103 and 4T1 cells were treated with 5 μM palbociclib for 7 days. HCT116 cells were treated with 100 nM doxorubicin for 72 h. MLg cells were irradiated with 10 Gy and used for viability assays 10 days later. ER:Mek IMR90 cells were treated with 200 nM 4-hydroxytamoxifen for 72 h and used for viability assays 2 days later.

Cisplatin (Stratech) was reconstituted in sterile PBS and stored at 4°C for up to 6 months. Docetaxel (Sigma-Aldrich) stock solution was prepared in DMSO, aliquoted and stored at -20°C. Palbociclib (PD0332991 isethionate, Pfizer Inc.) stock solution was prepared in DMSO and stored at -20°C. Doxorubicin (Carbosynth) was resuspended in sterile PBS and stored at -20°C. The solution was filtered through a 0.22 μm Millex®GP Filter unit (Millipore) and stored at 4°C for up to 6 months. Docetaxel (Sigma-Aldrich) stock solution was prepared by dissolving 5 mg of the drug in 5 mL Dimethyl Sulfoxide (DMSO) Cell Culture Reagent (Santa Cruz Biotechnology). 4-hydroxytamoxifen (Sigma-Aldrich) was prepared in PBS, aliquoted and stored at -20°C. Solutions prepared in PBS were filtered upon preparation prior to storage.

2.2.2.4.2. *In vitro* SA-β-gal staining

After 5-7 days under treatment, cells were washed thoroughly with pre-warmed PBS twice, and then fixed and stained for Senescence Associated β-Galactosidase activity (SA-β-Gal) using the Senescence β-Galactosidase Staining Kit (Cell Signaling) as per manufacturer's instructions. Briefly, cells were fixed for 10 min at room temperature with 1x fixative solution, washed with PBS, and then incubated 6 – 8 h or overnight at 37°C with 1x staining solution containing X-gal, in N-N-dimethylformamide (pH adjusted to 6.0). After staining, cells were thoroughly washed with PBS. Cells were then imaged using an Olympus Compact Brightfield Modular Microscope (Life Technologies) at 10X magnification, and total number of SA-β-Gal-positive cells was counted to assess the proportion of senescent cells under a certain treatment.

2.2.2.4.3. Proliferation assay

To evaluate the effect of the different secreted factors or secretome on proliferation in a paracrine manner, cells that had been under chemotherapeutic treatment for at least 7 days were thoroughly washed with PBS twice, and then fresh complete medium was added. After 48 h of incubation, the conditioned medium (CM) from senescent cells was collected and transferred to a Falcon tube. CMs were centrifuged for 10 min at 750 rpm, transferred to a new Falcon tube and then centrifuged again for 10 min at 2500 rpm. CM was added on top of recipient cells previously plated at a confluency of 10% in a 24-well plate (Corning). Cells were let to grow over a period of 72 h, and pictures were taken every 2 h with an IncuCyte® S3 Live Cell Analysis System microscope (Essen Bioscience). A total number of 9 pictures covering all well were taken at 10X, and cell confluency was analysed for each time point using the IncuCyte ZOOM™ software analyser (Essen Bioscience).

For mechanistic analyses, A549 and L1475(luc) were also simultaneously treated with 50 μM galunisertib (Stratech), 1 μM rapamycin (Stratech) and 10 ng/mL rhTGF-beta1 ligand (Bio-Techne). Such treatments and concentrations were also used during clonogenic and co-culture assays.

2.2.2.4.4. Glucose analysis

Glucose levels of conditioned medium from normal-growing and senescent A549 cells was analysed using the Glucose (GO) Assay Kit (Merck). Briefly, conditioned medium was collected after 48 h of conditioning, and centrifuged at 750 rpm for 10 min. CMs were transferred to a new Falcon tube and centrifuged for 10 min at 2500 rpm. Samples were frozen and stored at -80ºC until assayed following manufacturer's instructions. Glucose levels were determined after reading optical density (OD) of samples and standards at 540 nm in an Infinite 200 PRO Plate Reader (Tecan Life Sciences).

2.2.2.4.5. Scratch-wound cell migration assay

To assess the effect of the secreted factors of the different types of cellular senescence on cell migration, a scratch wound cell migration assay was performed. A total number of 50,000 A549 cells was plated on each well in a 96-well plate (Eppendorf). On the following morning, when cells had reached 100% confluency, the WoundMaker tool (Essen Bioscience) was set on a wash boat containing 45 mL of sterile distilled water for 5 minutes. The device was then placed in 70% ethanol for 5 min. It was allowed to air-dry for 30 min. The cell plate was inserted into the plate holder of the device, and the pin block was carefully placed on top and pushed following the manufacturer's instructions to make the homogeneous wounds (700-800 μm wide) in the cell monolayers. The pin block was then washed in 0.5% Alconox (in H_2O) for 5 min. It was then immersed in 1% Virkon for 5 min. It was subsequently washed in 70% ethanol and distilled water as previously described.

CMs from senescent cells were collected and processed as previously described, and wounded cells were carefully washed once with PBS. CMs were then placed on top of monolayer cells, and the cells were allowed to migrate over a period of 36 hours. Pictures were taken every 2 h with an IncuCyte® S3 Live Cell Analysis System microscope (Essen Bioscience). A total number of 2 pictures covering all the wound were taken at 10X, and relative wound confluency was analysed for each time point using the IncuCyte ZOOM™ software analyser.

2.2.2.4.6. Clonogenic assay

A549 and L1475(luc) cells were trypsinised as usual and plated onto a 6-well plate (500 cells per well). Cells were allowed to attach, and then CM from senescent cells were collected, processed as previously described and added on top of recipient cells. Plates were allowed to grow for 14 days, and fresh CM was added every 48 h. At day 14, colonies were washed once with PBS and then fixed in 4% PFA for 10 min. They were washed once again in PBS and permeabilised in ice-cold methanol for 20 min. They were allowed to dry for 30 min and then stained with 0.2% crystal violet (ACROS organics, 548-62-9) in 20%

methanol for 30 min. The excess of crystal violet was removed by a final wash in distilled water. Colony plates were scanned, and the number of colonies were scored for each condition.

To determine the synergistic effect of the concomitant treatment of cisplatin and the senolytics used and developed in **Chapter 5** (navitoclax and Nav-Gal), we calculated the co-coefficient of drug interaction (CDI) using the normalised clonogenic potential measurements of the individual and concomitant treatments at different concentrations. CDIs were calculated as ratios following the formula CDI = (AB)/(AxB), where AB is the clonogenic potential value of the concomitant treatment with the two drugs combined at a specific concentration, and A and B are the clonogenic potential values of the individual treatments of each drug at such concentration. Following this formula, a CDI > 1 indicates that the drugs are antagonistic, a CDI = 1 indicates that the drugs are additive and a CDI < 1 indicates that the drugs are synergistic, with values closer to 0 indicating higher synergy between the drugs [262]. This effect can depend on the ratio and molarity of drugs used, and for this reason, CDIs were calculated and plotted at different molar ratios of cisplatin and Navitoclax or Nav-Gal.

2.2.2.4.7. Low-attachment sphere formation assay

As an additional assay to assess the gain of malignant properties in cells derived from their incubation with CM from senescent cells, a sphere-forming ability assay was performed. Cover glasses (size 22 x 26 mm, thickness no. 1; VWR international) were placed inside a 6-well plate and washed in 70% ethanol for 30 min. Ethanol was then removed and the covers were allowed to dry for 20 min. After that, 0.01% polylysine was added on top for 30 min, removed and let dry for 10 min.

CM from senescent cells, which had been conditioned for 48-72 h, were collected and processed as previously described. A549 cells were trypsined and counted, and a total number of 2,000 cells were centrifuged and resuspended in 2 mL of CM, supplemented with 10 ng/mL of fresh bioactive recombinant human FGF basic 146 aa (rhFGF, R&D Systems), 10 ng/mL of human recombinant epidermal growth factor (hEGF, ThermoFisher Scientific) and 1% N-2 Supplement (Life Technologies). Cells were then

placed inside the wells onto coverslips and allowed to form spheres for up to 14 days. Every 48 h, half of the volume inside each well was carefully aspirated, and fresh CM supplemented with rhFGF, hEGF and N-2 was added just before use. Cells were monitored and on day 10-14, medium was carefully aspirated, and spheres were fixed with 4% PFA for 20 min. Spheres were washed in PBS twice and kept at 4ºC until imaged with an AxioScan.Z1 microscope (Zeiss) at 10X magnification. Finally, the number of spheres for each condition was scored and sphere shape was analysed.

2.2.2.4.8. Senescent and tumour cell co-culture

As an alternative method to analyse the paracrine effects of the SASP *in vitro* with the aim of having control cancer and senescent cells in close contact, two different cell culture strategies were used.

First, control and senescent cells were thoroughly washed with DPBS and trypsinised. A total of 100,000 control cells were seeded per well at the bottom of a 6-well plate. Medium was topped up to a total of 0.5 mL per well and cells were allowed to attach for 2 h. Next, senescent cells were washed with PBS and trypsined, and a total of 100,000 senescent cells were seeded onto a Falcon® Cell Culture insert (Corning Life Sciences) in 0.5 mL fresh medium. The inserts were placed onto each 6-welll plate were control cells had previously been plated, and media was topped up to a total 2 mL per well. Cells were let to grow over a period of 72 h, and pictures were taken every 2 h with an IncuCyte® S3 Live Cell Analysis System microscope (Essen Bioscience). A total number of 9 pictures covering all well area were taken at 10X, and cell confluency was analysed for each time point using the IncuCyte ZOOM™ software analyser (Essen Bioscience).

As a second approach, in order to analyse the effect in a three-dimensional strategy, an alternative sphere-forming assay was performed. First, control cancer cells were trypsinised and a total of 5,000 cells per well were carefully resuspended in 100 µL of Matrigel® Matrix mixed with ice-cold media at a 1:1 ratio, and carefully plated drop-wise in the centre of a well in a 24-well plate. Cell-containing Matrigel drops were allowed to solidify for 20 min at 37ºC, and then senescent cells were trypsinised and plated on the

same well to a total of 15,000 cells/well. Media was topped up to a total volume of 0.5 mL, and spheres within the Matrigel were allowed to grow for 7 days. Pictures of 3D spheres formed were taken every day using an Olympus Compact Brightfield Modular Microscope (Life Technologies) at 10X and 20X magnification, and number and size of spheres were analysed for each condition.

2.2.2.4.9. Cell mitochondrial stress test

In order to assess the oxygen consumption rate (OCR) and extracellular acidification rate (ECAR) of cells after being treated with the CM from senescent cells, a total number of 40,000 cells were seeded in a XFe24 cell culture microplate in 500 µL normal DMEM. Once cells had attached, CM from senescent cells was collected and processed as previously described, and then added on top of the recipient cells. After 48 - 72 h of incubation, CM was carefully removed and cells were washed once with PBS. Then, 675 µL of bicarbonate-free DMEM (Sigma-Aldrich) supplemented with 25 mM glucose, 1 mM pyruvate, 4 mM glutamine and 40 µM phenol red was added to each well. In order to eliminate residues of carbonic acid from medium, cells were incubated for 2 – 3 h at 37ºC with atmospheric CO_2 in a non-humidified incubator. Seahorse cartridge containing the sensors for the assay were previously calibrated overnight in 1 mL of Seahorse XF Calibrant (Agilent). Around 30 minutes before performing the assay, mitochondrial stress drugs were added inside the A-C ports in the cartridge plate: 2 µM oligomycin (port A, in a total volume of 75 µL per port), 1 µM carbonyl cyanide-p-trifluoromethoxyphenylhydrazone (FCCP, port B, in a total volume of 82 µL per port), 1 µM rotenone and 1 µM antimycin A (port C, in a total volume of 83 µL per port). Cartridge previously soaked in calibrant and carrying the mitochondrial stress drugs within the ports was inserted inside the Seahorse XF-24 extracellular flux analyser for calibration. Once calibrated, the plate containing treated cells was inserted inside the flux analyser, and OCR and ECAR were assayed. Initial pH of media was also measured before drug injection. Three measurement cycles of 2 min-mix, 2 min-wait and 4-min measure were carried out at basal condition and after each drug injection. At the end of the experiment, each well was carefully washed with 800 µL PBS and protein was extracted with 50-60 µL

of RIPA lysis medium. The plates were incubated at -80ºC for 30 min and allowed to thaw at room temperature. Protein concentration in each well was measured by a Pierce™ BCA Protein Assay kit (ThermoFisher Scientific) according to manufacturer's instructions. OCR and ECAR values were normalised on total µg of protein in each well.

2.2.2.4.10. Cell viability and apoptosis analysis

For A549, SK-MEL-103, 4T1, HCT116 and ER:Mek IMR-90 cell lines, control and senescent cells were seeded in flat-bottom-clear 96-well plates at a density of 6,000–8,000 and 4,000–6,000 cells per well, respectively. The following day cells were treated with serial dilutions of Nav-Gal or navitoclax in 0.2% FBS-containing media. Viability and IC50 was assessed 48 or 72 h later after two hours of incubation at 37°C with CellTiter-Glo® Luminescent Cell Viability Assay (Promega) or CellTiter-Blue® Cell Viability Reagent (Promega). Raw data were obtained by measuring luminescence in a VICTOR Multilabel Plate Reader (Pelkin Elmer) or fluorescence at an excitation/emission wavelength of 560 nm/590 nm in an Infinite 200 PRO Multimode Spectrophotometer (TECAN).

For MLg cells, control and senescent cells were seeded in a 12-well plate at a density of 80,000 and 60,000 cells per well respectively, and cells were treated with three to five different increasing concentrations of Nav-Gal or navitoclax on the following day. After 72 h, viability was assessed with CellTiter-Blue® Cell Viability Reagent (Promega) as described above.

To determine the induction of apoptosis after the treatment with navitoclax and Nav-Gal, 4,000 senescent and 6,000 non-senescent A549 or SK-Mel-103 cells were seeded in 96-well plates. 24 h later, annexin V Fluorescent Reagent (Essen Bioscience) was added to the media, and after a first scan, the cells were treated with vehicle (DMSO), 10 µM navitoclax or 10 µM Nav-Gal for 48 h. Images were collected every 2 h with an Incucyte® S3 Live-Cell Analysis System microscope (Essen Bioscience) over time. A total of 2 pictures per well were analysed using the IncuCyte ZOOM™ software analyser, and total and annexin V-positive cells were counted using ImageJ software.

2.3. DNA procedures

2.3.1. Genotyping of mice by PCR of genomic DNA

Mice bred for experimental purposes were genotyped using an ear biopsy collected by Cambridge Biomedical Services (CBS) staff. Genomic DNA was extracted from the biopsies in 25 µL alkaline lysis solution (25 mM NaOH, 0.2 mM EDTA in H_2O) for 1 h at 95ºC. The solution was then cooled down and lysis reaction was stopped by adding 25 µL neutralising buffer (40 mM Tris-HCl). Subsequent genotyping for Kras-FSF^{G12V} mouse line was performed using 2 µL of this solution per polymerase chain reaction (PCR) amplification using the primer sets detailed in **Table 2.**

Primer name	**Primer sequence (5'-3")**	**Annealing**	**Number of cycles**	**Expected product**
Kras2F-8B2	CCACAGGGTATAGCGTACTATGCAG	30 s at 65ºC, -0.5ºC decrease per cycle (Touchdown) for 10 cycles 30 s at 72ºC for 28 next cycles	10 touchdown + 28	WT: 507 bp MUT: 358 bp
3ex1	CTCAGTCATTTTCAGCAGGC			
STOP	AGTGCCTTGACTAGAGATCA			

Table 2. Primers, amplification conditions and expected product for PCR genotyping of experimental mice.

PCR reactions mixes were prepared using 1X SYBR™ Green PCR Master Mix (ThermoFisher Scientific), 10 pmol of each primer and ddH_2O to a total volume of 20 µL per sample, and a negative control containing the lysis buffer without biopsied sample was used for each reaction. Initial strand denaturation was performed at 94ºC for 3 min (*KRas-FSF^{G12V}*). Regions of interest were amplified in cycling conditions with denaturation steps conducted at 94ºC for 30 s followed by an annealing step dependent on specific primer sets and a polymerisation extension step at 72ºC for 1 min. A final extension step

was performed after all cycles were completed at 72ºC for 5 min. Finally, PCR products were resolved by gel electrophoresis in a 1.5% agarose (Sigma-Aldrich) gel containing 1X SYBR Safe DNA Gel Stain (ThermoFisher Scientific) at a voltage of 80V. Gels were imaged using an E-gel imager (ThermoFisher Scientific).

2.3.2. Vectors and constructs

Several vectors were used during this study and obtained from different sources (**Table 3**).

Vector name	Selection	Purpose	Source
pLV-mCherry	Ampicillin	Stable expression of mCherry in A549 cells	Addgene # 36084
pCMV-GFP	Ampicillin	Stable expression of GFP in A549 cells	Addgene # 11153
pCMVDR8.91	Ampicillin	Vector encoding for packaging protein (Gag-pol driven by CMV promoter) required for lentivirus production	Nova #PVT2323
pMD2.G	Ampicillin	Vector encoding for envelope protein (VSV-G driven by CMV promoter) required for lentivirus production	Addgene #12259

Table 3. Vectors used for the fluorescent labelling of A549 cells.

2.3.3. Bacterial transformation and plasmid isolation

For vectors purchased from Addgene, bacteria containing the plasmid were picked with a sterile tip in sterile conditions (Bunsen burner) and spread onto an Agarose plate containing Ampicillin for resistance selection. The plates were left to grow overnight at 37ºC and two colonies were picked the following morning with a sterile tip and transferred into a 50 mL falcon tube containing 7 mL of LB medium + Ampicillin, and left growing overnight at 37ºC. On the following day, bacteria suspension was centrifuged for

10 min at 5,000 rpm. Half of the pellet was used for storage (resuspended in 1 mL LB + glycerol (1:1)) and stored at -80ºC. The other half was used for plasmid isolation using the GenElute™ Plasmid Miniprep as described above. Final plasmid was resuspended in 100 µL nuclease-free water, and concentration and quality was assessed with a NanoDrop N-1000 (NanoDrop Technologies) spectrophotometer. A total of 1 µg of plasmid was digested by restriction enzyme digestion to check for correct sequence by restriction enzyme digestion using two different restriction enzymes and following NEBcloner® (New England Biolabs) indications for digestion reaction conditions. In order to prevent self-ligation, digestion products were first treated with 1 µL of Alkaline Phosphatase (AP, 20 U/µL) and 10 µL of AP buffer in water to a total volume of 100 µL and then run on a 1% agarose gel at 80 V for 1.5 h. Plasmids were also sent for sequencing at the DNA Sequencing Facility, Department of Biochemistry, University of Cambridge. Once sequence was confirmed as correct, stored bacteria was thawed and grown in 100 mL LB Medium + Amp overnight (O/N), and then plasmid was purified using the GenElute™ Plasmid MidiPrep (Sigma-Aldrich, PLD35).

2.3.4. Virus construction, titration and infection

For lentivirus construction, two different plasmids encoding for the regions needed for viral particles construction were transfected into easily-transfectable HEK-293T cell line alongside the plasmid of interested. Briefly, pCMVAR8.91 (plasmid encoding for packaging), pMD2.G (plasmid encoding for envelope protein) and plasmid of interest were mixed at a 2:1:3 proportion, respectively, in Opti-MEM medium (ThermoFisher Scientific), and mixed with pre-incubated Lipofectamine 2000 (ThermoFisher Scientific) as per manufacturer's indications. Lipofectamine-DNA mix was added drop-wise on HEK-293T cells previously seeded at a confluency of around 70-80% in a 6-well plate. Cells were incubated with the mix for 6 hours and then the medium was removed and fresh medium was added. Cells were further incubated for 48 h and then supernatant containing viral particles was collected and stored at -80ºC.

Titration of the viral particles was performed following flow cytometry methodologies. Viral particles were added onto A549 cells plated in a 12-well plate

containing 1,5 x 10^5 cells per well following a 1:10 serial dilution. After 48 h, cells were washed with PBS and then detached with trypsin/EDTA. Cells were then resuspended with DMEM and transferred to a 15 mL falcon tube. Cells were centrifuged for 5 min at 1250 rpm and at 4ºC. Supernatant was removed and cells were washed twice with PBS and then centrifuged again. Supernatant was removed and 1% PFA (in PBS) was added on the cells and incubated for 5 min at room temperature for fixation and inactivation of vector particles. Cells were then washed again with PBS and resuspended in PBS for flow cytometry analysis using a Fortessa Flow Cytometer (BD Biosciences). Percentage of cells positive for infection was calculated following a gating strategy based on fluorescent reporter. For titer calculation, the viral particle dilutions yielding 1% to 20% positive cells were used. In a typical titration experiment, below 1% is not accurate enough to reliable determine the number of positive cells by flow cytometry, and above 20%, the chance for each positive target cell to be transduced more than once significantly increases, resulting in an underestimation of the number of transducing particles. The formula followed to calculate the titer was:

$$\text{Titer (transducing units/mL)} = \frac{Number\ of\ target\ cells\ (count\ at\ day\ 1)\ x\ \frac{\%\ of\ positive\ cells}{100}}{Volume\ of\ supernatant\ (mL)}$$

Once the titer was calculated, a Multiplicity of Infection (MOI) of 0.1-0.3 was used to infect a total of 250,000 A549 cells plated in a 6-well plate. Infected cells were then sorted by the Flow Cytometry Unit of the Cambridge Institute for Medical Research, pooled and collected in DMEM + 20% FBS + P/S, and then expanded.

2.4. RNA procedures

2.4.1. Transient downregulation of gene expression by siRNA technology

For transient downregulation of *GLB1* in A549 and SK-Mel-103 cells, a total of 30,000 control or 50,000 senescent cells were seeded per well in a 24-well plate. On the next morning, cells were transfected with TriFECTa® Kit DsiRNA Duplex siRNAs (Integrated DNA Technologies) hs.Ri. GLB1.13.1 (siRNA1), hs.Ri.GLB1.13.3 (siRNA2) or scrambled siRNA, using Lipotectamine RNAiMAX Reagent (Thermo Fisher Scientific) as per manufacturer's instructions. Briefly, pre-designed duplex siRNAs were resuspended in ddH_2O to a stock concentration of 2 μM, and 6 pmol of each duplex was gently mixed with 50 μL Opti-MEM® Medium (Gibco). In a different tube, 1 μL Lipofectamine RNAiMax Reagent was added to 50 μL Opti-MEM® Medium and gently mixed. The two solutions were combined and mixed and incubated for 20 min at room temperature. After incubation time, the RNAi duplex-Lipofectamine mix (100 μL) was added drop-wise onto cells bringing the total volume per well to 600 μL. After 48 hr, RNA was extracted as described below, and cells were further assayed for SA-β-gal activity and cell viability upon senolytic treatment.

2.4.2. Gene expression knockdown by shRNA technology

For *TGFBR1* and *Tgfbr1* knockdowns in A549 and L1475(luc) cells, viral particles were produced in 293T cells upon transfection with pCMVAR8.91, pMD2.G and shRNA plasmids mixed at a 1:2:3 proportion, respectively, with Lipofectamine 2000 (ThermoFisher Scientific) in Opti-MEM medium (ThermoFisher Scientific). Cells were incubated with the mix overnight and fresh medium was added the next morning. After 48 h incubation, supernatant was collected and filtered. Viral particles were added onto A549 and L1475(luc) cells, and positive selection was performed with puromycin treatment for 5 days. RNA was then extracted as described above, and lines with the highest knockdown were used for further assessment and experiments. Clone IDs, target sequence and further details of the shRNA constructs used can be found in **Table 4**.

Name	Clone ID	Vector	Clone Name	Target Sequence	Oligo Sequence (Forward)	Oligo Sequence (Reverse)
shTGFBR1	TRCN0000010443	pLKO.1	NM_004612.x-2229s1c1	CAGTAAGTGCCACTTCTGTGT	CCGGCAGTAAGTGCCACTTCTGTGTCTCGAGACACAGAAGTGGCACTTACTGTTTTTG	AATTCAAAAACAGTAAGTGCCACTTCTGTGTCTCGAGACACAGAAGTGGCACTTACTG
shTgfbr1	TRCN0000022480	pLKO.1	NM_009370.2-1394s1c1	GCCTTGAGAGTGATGGCTAAA	CCGGGCCTTGAGAGTGATGGCTAAACTCGAGTTTAGCCATCACTCTCAAGGCTTTTTG	AATTCAAAAAGCCTTGAGAGTGATGGCTAAACTCGAGTTTAGCCATCACTCTCAAGGC

Table 4. shRNA construct information and oligo sequences.

2.4.3. RNA extraction, cDNA synthesis and quantitative real-time PCR

RNA from cells was extracted using the RNeasy Mini Kit (Qiagen) and resuspended in RNase-free H_2O. For gene expression analysis, cDNA was synthesized with the High-Capacity RNA-to-cDNA™ Kit (Thermo Fisher Scientific) using a total of 500 ng of RNA per reaction. Quantitative real-time polymerase chain reaction (qRT-PCR) was performed using 2 µL of cDNA solution and 250 nM of each primer mixed with the Luna® Universal qPCR Master Mix (New England Biolabs) following manufacturer's indications. For amplification, a QuantStudio® 1 Real-Time PCR instrument (Applied Biosystems) was used with the amplification parameters detailed in **Table 5**.

Cycle step	Temperature	Time	Cycles
Initial Denaturation	95ºC	60 s	1
Denaturation	95ºC	15 s	40
Extension	60ºC	30 s (+ plate read)	
Melt curve	72ºC	5 min	1

Table 5. Amplification parameters for real-time quantitative PCR amplification.

Primers used to amplify target genes were generally pre-designed KiCqStart® SYBR® Green Primers (Sigma) and are detailed in **Table 6**.

Target gene	Forward (5' – 3')	Reverse (5' – 3')
CDKN1A	CAGCATGACAGATTTCTACC	CAGGGTATGTACATGAGGAG
IL6	GCAGAAAAGGCAAAGAATC	CTACATTTGCCGAAGAGC
IL1A	AGAGGAAGAAATCATCAAGC	TTATACTTTGATTGAGGGCG
LMNB1	GTATGAAGAGGAGATTAACGAGAC	TACTCAATTTGACGCCCAG
MMP9	TGCAACGTGAACATCTTCG	GAATCGCCAGTACTTCCCA

TGFB1	AACCCACAACGAAATCTATG	CTTTTAACTTGAGCCTCAGC
TGFB2	TTGCTTTAGAAATGTGCAGG	TCTGAACTCATAAATACGGG
TGFB3	TGTTGAGAAGAGAGTCCAAC	ATCACCTCGTGAATGTTTTC
TGFBR1	GTACCAACAATCTCCATGTG	AGACAATGGTACTTGGACTC
GLB1	GACAGTACCAGTTTTCTGAG	ATAGACTCTTTCTCTAGCAGC
ACTB	AGAAGGATTCCTATGTGGGC	TACTTCAGGGTGAGGATGC
Cdkn1a	CTAGGGGAATTGGAGTCAGG	AGAGACAACGGCACACTTTG
Cdkn2a	GGGTTTCGCCCAACGCCCCGA	TGCAGCACCACCAGCGTGTCC
Il6	CTGCAAGAGACTTCCATCCAG	AGTGGTATAGACAGGTCTGTTGG
Il1a	ATGATCTGGAAGAGACCATCC	CGAGCTTCATCAGTTTGTATCTC
Lmnb1	ATGAAGAGGAGATCAATGAGAC	CATACTCAATCTGACGCCC
Mmp9	GTCCAGACCAAGGGTACAG	ATACAGCGGGTACATGAGC
Tgfb1	ACCAAGGAGACGGAATACAG	CGTTGATTTCCACGTGGAG
Tgfb2	GAGATTTGCAGGTATTGATGG	CAACAACATTAGCAGGAGATG
Tgfb3	CTCAGTGGAGAAAAATGGAAC	GGTCGAAGTATCTGGAAGAG
Tgfbr1	CCTGAAGTTCTAGATGATTCC	CTTCATGGATTCCACCAATAG
Actb	CTTTTCCAGCCTTCCTTCTTGG	CAGCACTGTGTTGGCATAGAGG

Table 6. Sequences of oligonucleotides used for the amplification of target genes during RT-qPCR.

In order to analyse gene expression data, the Double Delta Ct Value Method (ΔΔCt) was used. Briefly, the mean of the Ct values was calculated for the housekeeping gene (H) and the gene being tested (T) in control sample (C) and experimental sample (E), returning 4 values: TE (Gene being Tested Experimental), TC (Gene being tested Control), Housekeeping Gene Experimental (HE) and Housekeeping gene Control (HC). The ΔCt values were obtained by calculating the differences between TE and HE (TE-HE) and TC and HC (TC-HC) for experimental (ΔCtE) and control conditions (ΔCtC), respectively. Next, the Double Delta Ct Values (ΔΔCt) were obtained by calculating the difference between ΔCtE and ΔCtc (ΔCtE- ΔCtC). Finally, fold change expression values were obtained by calculating logarithm base 2 of ΔΔCts (2^-ΔΔCt).

2.4.4. RNA quality control assessment for RNA sequencing analysis

For the transcriptome analysis of different chemotherapy-induced senescent cells, RNA of control, drug-treated and CM-recipient A549 cells was extracted as described above. Prior to RNA extraction and processing, all surfaces were thoroughly cleaned with 10% bleach and Ultraclean Lab Cleaner (Ultrawave) and sprayed with RNaseZap Decontamination Solution (ThermoFisher Scientific). RNA was resuspended in RNAse-free water and RNA concentration, 260/280 and 260/230 ratios were first measured using a NanoDrop Microvolume Spectrophotometer (ThermoFisher Scientific). RNA samples were diluted to a range between 200-500 ng/μL and then RNA concentration was measured again using the Qubit RNA BR Assay Kit (ThermoFisher Scientific). Diluted samples were read in a Qubit 3.9 Fluorometer 2 min after reaction time following manufacturer's indications. For RNA Integrity Number (RIN) analysis, samples were analysed using the Agilent RNA ScreenTape System (Agilent Technologies). Briefly, samples were incubated in RNA ScreenTape Sample buffer (Agilent Technologies) as per manufacturer's instructions and loaded onto an RNA ScreenTape (Agilent Technologies) along with RNA ScreenTape Ladder (Agilent Technologies) for loading control. The ScreenTape was flicked and then loaded onto the 4200 TapeStation instrument and samples were analysed.

Only samples with a RIN of 8.0 or higher were transferred to 1.5 mL Eppendorf tubes to a total quantity of 3 μg per sample, and submitted to BGI Group for DNBSeq Stranded mRNA library preparation and RNA sequencing. A total of 3 biological repeats for each experimental condition were submitted for analysis, and a minimum of 20 million reads per sample threshold was used.

2.4.5. RNA sequencing and analysis

Analysis of RNA-seq results was performed by Dr Ezequiel Martin Rodriguez (Cancer Molecular Diagnostics Laboratory, Department of Oncology, University of Cambridge). Briefly, alignment of reads and overall QC was run following a custom pipeline using STAR in double pass mode versus hg38 in alt contig aware mode, including samtools, fastqc

and custom code. Cufflinks Quantification was performed and data was normalised following a Fragments Per Kilobase (of gene length) and Million reads (FPKM) normalisation. For downstream analysis of differential expression of genes, Cummerbund package and custom code including analysis for PCA, JS Distance, Network/Overrepresentation and Unsupervised Clustering was run, assessed, analysed and represented.

2.5. Protein procedures

2.5.1. SDS-PAGE and Western blotting

2.5.1.1. Lysate production and electrophoresis

Cell plated in 100 mm dishes were lysed at different time-points in 150-350 µL of Radioimmmunoprecipitation Assay (RIPA) buffer (Sigma-Aldrich, # R0278). RIPA buffer is made of 0.5% sodium deoxycholate, 1% Tritan X-100, 20 mM Tris pH 8.0, 0.1% SDS, 150 mM NaCl and stored at 4ºC. Before use, it was supplemented with 1 mM ethylenediaminetetraacetic acid (EDTA), cOmplete™ EDTA-free *EASY*pack protease inhibitor cocktail (Roche), previously prepared as a 25X stock solution by dissolving 1 tabled in 2 mL H_2O, and PhosSTOP™ *EASYpack* phosphatase inhibitor cocktail (Roche), previously prepared as a 10X solution by dissolving 1 tablet in 1 mL H_2O. These compounds inhibit the activity of endogenous protease and phosphatase enzymes. Cells were then scrapped using a polyethylene cell lifter (Cornig) and transferred into a cold centrifuge tube, and incubated on ice for 15 min. The lysates were then centrifuged at 4ºC (15,000 g) for 15 min and the supernatant (extracted cellular proteins) was collected and transferred into a new cold Eppendorf tube for further Western blot analysis.

The protein lysate was quantified using the Pierce™ BCA Protein Assay Kit (Thermo Scientific). Diluted Bovine Serum Albumin (BSA) standards were prepared following manufacturer's instructions with a final BSA concentration of between 25 µg/mL and 2,000 µg/mL. Protein samples were mixed following a 1:8 ratio with the working solution (provided by the kit) and placed into a Thermo Scientific™ 96-well plate. The plate was

incubated for 30 min at 37ºC, and was eventually analysed in a microplate reader (Infinite 200 PRO Plate Reader (Tecan Life Sciences)) to measure protein concentration.

A total of 30 µg of protein per sample were diluted in 4x Laemmli Sample Buffer (Bio-Rad) to a total volume of 20 µL, which were loaded onto a 12% Mini-PROTEAN® TGX™ Precast Gel. The gel was resolved for 40 to 50 min at a constant voltage of 200V in SDS Running Buffer (BioRad). Following separation, the proteins were electro-transferred from the gel onto a polyvinylidene difluoride PVDF Transfer Membrane, 0.45 µm, 26.5 cm x 3.75 m (ThermoFisher) by wet tank transfer. PVDF membrane was previously activated by a 60 s incubation in 100% methanol. The gel was placed into a Trans-Blot electrophoretic transfer tank (BioRad Laboratories) containing 1 L of transfer buffer (20% methanol in SDS Transfer Buffer (BioRad)) and ran overnight at 4ºC, at a voltage of 10V.

2.5.1.2. Immunoblotting of membranes

On the following morning, the membrane was washed once with Tris Buffered Saline with Tween 20 (TBS-T) and then incubated in 5% milk (Marvel) in TBS-T for 1 h at RT. Proteins present within the milk solution bind to the PVDF membrane, minimising the non-specific binding of primary antibodies. To remove excess blocking solution, this membrane was washed three times in TBS-T for 10 min each before immunoblotting. Primary antibodies were diluted in 5% milk in TBS-T at quantities indicated in **Table 7**. The PVDF membrane was subsequently incubated in the primary antibody solutions overnight, on a rocking shaker at 4ºC.

Antibody	**Species**	**Provider**	**Catalogue Number**	**Working Dilution**
Anti-GADPH	Rabbit	Abcam	ab9485	1:2000
Anti-Rb (4H1)	Mouse	Cell Signaling	9309	1:2000
Anti-Phospho-Rb (Ser807/811)	Rabbit	Cell Signaling	9308	1:1000
Anti-p53 (CO-7)	Mouse	Santa Cruz Biotechnology	sc-47698	1:500
Anti-Phospho-p53 (Ser20)	Rabbit	Cell Signaling	9287	1:1000

Anti-p21 (F-5)	Goat	Santa Cruz Biotechnology	sc-6246	1:250
Anti-CDKN2A/p16INK4a (EPR1473)	Rabbit	Abcam	ab108349	1:2000
Anti-TGFB1	Rabbit	Abcam	ab92486	1:1000
Anti-TGFB2	Mouse	Abcam	ab36495	1:1000
Anti-TGFB3	Goat	Bio-Techne	AF-243-NA	1:1000
Anti-Pan-P70S6K	Mouse	Bio-Techne	MAB8962	1:1000
Anti-Phospho-p70S6K (T389)	Rabbit	Bio-Techne	MAB8963	1:1000
Anti-Pan-Akt	Rabbit	Cell Signaling	4691	1:1000
Anti-Phospho-Akt (S473)	Rabbit	Cell Signaling	9271	1:1000
Anti-TGFBR1	Goat	Abcam	ab121024	1:1000

Table 7. List of primary antibodies and staining conditions used for Western blotting.

Following overnight incubation, the membrane was washed three times in TBS-T for 10 min each, before incubating with the appropriate species-specific secondary antibody. Secondary antibodies were diluted in 5% milk in TBS-T at quantities indicated in **Table 8**. The membrane was subsequently washed three times in TBS-T for 5 min each to remove the excess secondary antibodies. It was then incubated with freshly made Amersham Enhanced ChemiLuminescence (ECL) detection solution (Amersham) for 1 min in the dark. The membrane was placed on X-ray cassette, a film was placed on top and exposed for 1-60 s depending on signal intensity, and the film was developed using the Xograph Compact X4 automatic processor. Alternatively, membranes were imaged using a ChemiDoc imager (Bio-Rad) at automatic exposure times. Before incubation with a new antibody, the membranes were washed in Striping Buffer (15 g glycine, 1 g SDS, 0.1% Tween 20 in 1 L ultrapure water, pH 2.2) twice for 10 min, then washed twice in PBS for 10 min each. Next the membranes were washed twice in TBS-T for 5 min each, and then finally blocked and re-probed as previously explained.

Antibody	Species	Provider	Catalogue Number	Working Dilution
HRP-conjugated AffiniPute Anti-Rabbit IgG (H+L)	Donkey	Jackson ImmunoResearch	711-035-152	1:5000
HRP-conjugated AffiniPute Anti-Mouse IgG (H+L)	Donkey	Jackson ImmunoResearch	715-035-150	1:5000
HRP-conjugated AffiniPute Anti-Goat IgG (H+L)	Donkey	Jackson ImmunoResearch	805-035-180	1:5000

Table 8. List of secondary antibodies and staining conditions used for Western blot analysis.

2.5.2. Human cytokine array

Cytokine levels in CM were analysed using the Human Cytokine Array and the Human XL Cytokine Array (ProteomeProfiler human Cytokine Array Panel A, from R&D Systems), following the manufacturer's instructions. A total volume of 700 µL of CM was mixed with 300 µL of blocking buffer provided by the kit for the Human Cytokine Array, and 500 µL with 1 mL provided blocking buffer was mixed before incubation for the Human XL Cytokine Array. Pixel density was determined using the Image J Software, after subtracting background noise.

2.5.3. Phospho-kinase array

Changes in kinase phosphorylation upon exposure to the SASP was assayed using the Proteome Profiler Human Phospho-Kinase Array (R&D Systems). Briefly, A549 cells were exposed to FBS-free CM from control and senescent cells (with either vehicle or 50 µM galunisertib (Stratech)) for 30 min at 37°C. Protein was extracted immediately after as described above and protein concentration was calculated following the Pierce™ BCA Protein Assay Kit (ThermoFisher Scientific). A total of 600 µg were immediately used for the assay following manufacturer's indications. Membranes from the kit were incubated

with ECL (Amersham) and X-ray film was exposed to 1 and 10 min. Pixel intensity was calculated using FiJi software and normalised again loading controls.

2.5.4. MicroEnvironment MicroArray (MEMA) technology

The MicroEnvironment MicroArray (MEMA) platform was used as a high-throughput technology to determine the impact of different SASP ligands on A549 cell proliferation. Reuben Hoffman, from the laboratory of James E. Korkola (Oregon Health and Science University, Portland, US) performed the experiment and the analyses. Briefly, MEMAs were blocked for 20 min with 1% non-fouling blocking agent and rinsed three times with PBS. A total of 500 A549 cells/well per seeded in DMEM medium containing 10% FBS. After 2-18 hours of adhesion, medium was aspirated and replaced with 0.1% FBS DMEM supplemented with experimental ligand. Cells were allowed to grow for up to 72 h and cells were washed and fixed with 2% PFA for 15 min. Cells were then permeabilised with 0.1% Trixon X-100 for 15 min, and washed with 0.05% Tween 20 PBS, and incubated with EdU detection reaction reagents (Click-iT™ EdU Cell Proliferation Kit (ThermoFisher Scientific) for 1 h and protected from light. Cells were then washed again with BPS and imaged on an automated imaging system. Segment cells and intensity were calculated using CellProfiler. R-environment with custom code was used to normalise, correct variations and summarise the raw Cell Profiler derived data for each condition.

2.5.5. Enzyme-linked Immunoassay (ELISA)

To determine the amount of TGF-β1 in conditioned media from control and senescent cells, cells were thoroughly washed with PBS twice and serum-free medium was added onto control and senescent cells, and conditioned for 24 h. After this, CM was collected and transferred into falcon tubes, and centrifuged for 10 min at 1250 rpm at 4ºC. Then, supernatant was carefully transferred into new falcon tubes and centrifuged for 10 min at 2500 rpm at 4ºC. Supernatant was immediately stored at -80ºC until enzyme-linked immunosorbent assay (ELISA) was performed. For this, the Human TGF-beta 1 Quantikine ELISA Kit (R&D Systems), Human TGF-beta 2 Quantikine ELISA Kit (R&D Systems) and the

Human TGF-beta 3 DuoSet ELISA Kit (R&D Systems) were used following manufacturer's instructions. First, in order to activate TGF-β ligands to their immunoreactive form, 100 µL of each conditioned medium was mixed with 20 µL of 1 N HCl, mixed and incubated at room temperature for 10 min. Next, reaction was neutralised with 20 µL 1.2 N NaOH/0.5 M HEPES. Assay was continued following steps as described in the kit, and each sample was assayed in duplicates. Optical density was measured using an Infinite 200 PRO Plate Reader (Tecan Life Sciences) at 450 nm, after applying a wavelength correction set to 540 nm. To calculate concentration in each of the samples, a standard curve was first constructed by plotting the mean absorbance for each standard used during the assay on the y-axis against its concentration on the x-axis, and a best fit curve through the points was drawn. Final concentration was calculated by subtracting the data from the fitted curve, and by multiplying by the final dilution factor performed during the assay (1:1.4 dilution).

2.5.6. Recombinant proteins

2.5.6.1. Proteins used *in vitro*

Name of Ligand	Manufacturer	Catalogue number	Uniprot ID	Concentration used (µg/mL)
ANG	R&D Systems	265-AN	P03950	0.05
AREG	R&D Systems	262-AR-100	P15514	0.02
CCL1	R&D Systems	272-I/CF	P22362	0.005
CCL11	R&D Systems	320-EO/CF	P51671	0.005
CCL13	R&D Systems	327-P4	Q99616	0.06
CCL16	R&D Systems	802-HC	O15467	0.125
CCL2	R&D Systems	279-MC	P13500	0.03
CCL20|1	R&D Systems	360-MP	P78556|1	0.002
CCL25|1	R&D Systems	9046-TK/CF	O15444|1	0.15
CCL26	R&D Systems	653-E3/CF	Q9Y258	0.5
CCL3	R&D Systems	270-LD	P10147	0.01
CCL8	R&D Systems	281-CP	P80075	0.09

CSF1|1	R&D Systems	216-MC	P09603|1	0.0015
CSF2	R&D Systems	215-GM-010	P04141	0.02
CSF3|Short	R&D Systems	214-CS/CF	P09919|2	0.000006
CXCL1	R&D Systems	275-GR/CF	P09341	0.004
CXCL10	R&D Systems	266-IP/CF	P02778	0.15
CXCL11	R&D Systems	672-IT/CF	O14625	0.02
CXCL12|Alpha	R&D Systems	350-NS-010	P48061|2	0.01
CXCL12|Beta	R&D Systems	351-FS	P48061|1	0.03
CXCL13	R&D Systems	801-CX/CF	O43927	0.02
CXCL5	R&D Systems	254-XB/CF	P42830	0.015
CXCL8|1	R&D Systems	208-IL/CF	P10145|1	0.0025
EGF|1	R&D Systems	236-EG-200	P01133|1	0.01
EREG	R&D Systems	1195-EP/CF	O14944	0.000125
FAS|1	R&D Systems	7398-FS	P25445|1	0.036
FGF2|3	R&D Systems	SRP4037-50UG	P09038|2	0.01
FGF7|1	R&D Systems	251-KG	P21781|1	0.06
HGF|1	R&D Systems	294-HG	P14210|1	0.04
ICAM1	R&D Systems	720-IC	P05362	2
ICAM3	R&D Systems	715-IC	P32942	2.25
IFNG	R&D Systems	285-IF	P01579	0.00075
IGFBP1	R&D Systems	871-B1	P08833	0.5
IGFBP2	R&D Systems	674-B2-025	P18065	0.05
IGFBP3|1	R&D Systems	675-B3-025	P17936|1	0.1
IGFBP4|1	R&D Systems	804-GB	P22692|1	0.09
IGFBP6	R&D Systems	876-B6	P24592	0.15
IL13	R&D Systems	213-ILB-005	P35225	0.01
IL15|IL15S48AA	R&D Systems	247-IL	P40933|1	0.01
IL1A	R&D Systems	200-LA/CF	P01583	0.000006
IL1B	R&D Systems	201-LB-005	P01584	0.001
IL6	R&D Systems	206-IL-010	P05231	0.01
IL7|1	R&D Systems	207-IL-005	P13232|1	0.01
JAG1|1	R&D Systems	1277-JG	P78504|1	0.5
KITLG|1	R&D Systems	255-SC	P21583|1	0.05

MIF	R&D Systems	289-MF	P14174	0.0001
NGF	R&D Systems	256-GF/CF	P01138	0.002
NRG1|1	R&D Systems	296-HR-050	Q02297|1	0.05
OSTP|A	R&D Systems	264-PGB/CF	Q07326|1	0.0009
PIGF|1	R&D Systems	9489-PS	P07225	0.9
PROS1	R&D Systems	1433-OP	P10451|1	0.1
rhTGF-beta1	Bio-Techne	240-B	P01137	0.01
TGFB1||Cterminus	R&D Systems	240-B-010	P01137	0.01
TGFB2|A	R&D Systems	302-B2-010	P61812|1	0.01
TNFRSF10C	R&D Systems	630-TR	O14798	0.06
TNFRSF11B	R&D Systems	185-OS	O00300	0.02
TNFRSF1A|1	R&D Systems	726-R2	P20333	0.016
TNFRSF1B|1	R&D Systems	636-R1	P20333|1	0.09
VEGFA|VEGF206	R&D Systems	293-VE-010	P15692|1	0.01
WNT10A	R&D Systems	90009	Q9GZT5	0.1
WNT3A|1	R&D Systems	5036-WNP	P56704|1	0.0075
Wnt5a|1	R&D Systems	645-WN/CF	P22725|1	0.1
WNT7A	R&D Systems	3008-WN	O00755	1
WNT7B	Abnova	H00007477-P01	P56706	0.1

Table 9. List of recombinant protein ligands used in cell culture experiments.

2.5.7. Immunohistochemistry (IHC)

Tissue samples were fixed in 4% PFA, embedded in paraffin and cut in 3 µm sections, and then mounted in Superfrost® plus slides. Slides were deparaffinised in xylene and re-hydrated through a series of graded ethanol until water. Masson's trichrome staining was used to assess the presence of fibrotic areas in the lung. For immunohistochemistry, an automated immunostaining platform (Ventana discovery XT, Roche) was used. Antigen retrieval was first performed with high pH buffer (CC1m, Roche), endogenous peroxidase was blocked, and slides were then incubated with the appropriate primary antibodies as detailed in **Table 10**.

Antibody	Provider	Target Species	Catalogue Number	Clonal (Clone)
Ki-67	Dako	Human	IR626	Mouse monoclonal (MIB-1)
Ki-67	Cell Signaling	Mouse	12202	Rabbit monoclonal (D3B5)
p21	Dako	Human	M7202	Mouse monoclonal (CO-7)
p16	Abcam	Human	ab81278	Rabbit monoclonal (EP435Y-129R)
Phospho-Histone H2A.X (Ser139)	Millipore	Mouse	05-636	Mouse monoclonal (JBW301)
Cleaved Caspase-3	Cell Signaling	Mouse	9661	Rabbit Polyclonal (Asp175)
Phospho-AKT (Ser473)	Cell Signaling	Human	4060	Rabbit Monoclonal (D9E)
Phospho-p70 S6 Kinase	Cell Signaling	Human	9206	Mouse Monoclonal (1A5)

Table 10. List of antibodies used for immunohistochemistry staining.

After primary antibody incubation, slides were incubated with the corresponding secondary antibodies and visualization systems (OmniRabbit, Ventana, Roche) conjugated with horseradish peroxidase (Chromomap, Ventana, Roche). Immunohistochemical reactions were developed by using 3,3'-diaminobenzidine tetrahydrochloride (DAB) as a chromogen, and nuclei were counterstained with hematoxylin. Finally, the slides were dehydrated and mounted with a permanent mounting medium. Whole slides were digitalised with a slide scanner (AxioScan, Zeiss) using polarised light, and Zen 2.3 (Zeiss) software was used for image acquisition.

2.5.8. Immunofluorescence (IF)

For the evaluation of apoptosis in the lungs upon *in vivo* senolytic treatment, frozen tissue samples were processed for TUNEL staining using the DeadEnd™ fluorometric TUNEL System (Promega) as per manufacturer's instructions. Briefly, slides were immersed in 4% PFA for 25 min at 4ºC and subsequently washed with PBS twice. Sections were then permeabilised in 0.2% Triton X-100 for 5 min, and washed again with PBS twice. They were then incubated for 10 min in Equilibration Buffer (from the kit) and labelled with the addition of 50 µL TdT reaction mix. Reaction was stopped and slides were washed three times with PBS. Vectashield® Antiface Mounting Medium plus DAPI (Vector Laboratories) was used to mount the slides and counterstain cell nuclei. Whole slides were digitalised with a slide scanner (AxioScan, Zeiss), and Zen 2.3 (Zeiss) software was used for image acquisition.

2.6. Mouse models and *in vivo*/*ex vivo* procedures

2.6.1. Maintenance of mouse colonies

All animal procedures were approved for Ethical Conduct by the Home Office England and Central Biomedical Services (CBS) of the University of Cambridge, regulated under the Animals (Scientific Procedures) Act 1986 (ASPA), as stated in The International Guiding Principles for Biomedical Research involving Animals, which are fully compliant with the current Home Office legislation.

2.6.2. Mouse strains

2.6.2.1. Kras-FSF^{G12V} mouse line

The *Kras-G12V* or *Kras*$^{FSF\text{-}G12V/+}$ mouse line has previously been described [40], available at The Jackson Laboratory (B6.129-*Krastm3Bbd*/J). It was kindly gifted by Prof Mariano Barbacid (CNIO). In this line, the expression of the Kras^{G12V} oncogenic protein is activated

following Flippase-mediated recombination, driven by the administration of FLP Recombinase (FLPo) Adenovirus (Vector Biolabs, #1775) particles. This line was maintained on a C57BL/6 background and bred in house, and heterozygous animals were used for experimentation.

2.6.2.2. C57BL/6 mouse line

For lung orthotopic transplantation experiments, the C57BL/6 mouse line was used. Although this strain is refractory to many tumours, it is a permissive background for maximal expression of most mutations, and therefore it used for the development of the $Kras^{G12D}$;$p53^{-/-}$ model and the generation of the cell line L1475(luc) for orthotopic transplant experimentation as described earlier. These mice were not bred in house and were obtained from Charles Rivers Laboratories.

2.6.2.3. SCID mouse line

For xenograft transplantation experiments, the Severe Combined Immunodeficiency Disease (SCID) mouse line was used. These mice contain the *Pkrdc*^{scid} autosomal recessive mutation, which impairs the functionality of both B and T lymphocites, which prevents the rejection of transplanted tissue from human origin. These mice were not bred in house and were obtained from Charles Rivers Laboratories.

2.6.3. Induction of murine lung tumours

Lung tumours were generated in *Kras-G12V* mice through intranasal or intratracheal administration with FLPo-expressing adenovirus (Vector Biolabs, #1775). For virus solution preparation, viral particles (stored at -80ºC at a $6x10^7$ PFU/µL titration) were thawed in ice, diluted in ice-cold DMEM, precipitated with 10 mM $CaCl_2$ and incubated for 20 min prior to nasal inhalation or intratracheal administration. In order to prevent titer

decrease over time, fresh virus solution was prepared every hour during intranasal and intratracheal administration procedures.

For intratracheal administration of FLP-expressing adenovirus, mice were anaesthetised by an intraperitoneal injection of ketamine (Vetalar, Ketaset, Ketalar) (100 mg/kg) and xylazine (Rompun) (16 mg/kg). Mice were transferred to an incubation platform, an optic fibre light source was placed onto the trachea for illumination, and a polyethylene tube (PE10) was inserted into the trachea. To confirm this, a 1 mL syringe containing bubbles was inserted into the tube, and correct placement was confirmed by the evidence of air flow passing through the syringe and moving the bubbles. Next, a total of 62.5 µL containing $5x10^8$ pfu/mouse of virus of Adeno-FLIP particles was carefully inserted into the tube, and the tube was carefully held until the totality of the solution was aspirated by respiration. After this, mice were finally placed onto a pile of bedding in an upright position to prevent airway obstruction while still under anaesthesia, and the cage was placed inside a heat rack until full recovery.

2.6.4. Administration of substances and treatments

2.6.4.1. ABT-737 treatment

To assess the effect of cellular senescence during lung cancer early tumorigenesis, $Kras^{G12V}$ mice that had been infected with Ad-FlpO particles via intratracheal administration were treated twice a month on two consecutive days with 25 mg/kg body weight of ABT-737 or vehicle (via i.p. injection) from month 5 to month 9 post-Ad infection.

To evaluate the senolytic effect of ABT-737 in combination with cisplatin treatment in the Kras-FSFG12V mouse model, mice were treated twice weekly on two consecutive days with 25 mg/kg body weight for two weeks (starting the day after cisplatin administration) via i.p.

To determine the impact of depleting senescent cells during xenograft development, mice bearing A549 xenografts co-transplanted with cisplatin-induced senescent cells were also treated with ABT-737 at the same dosing following the experimental timing detailed in Chapter 3.

ABT-737 stock solution was prepared by dissolving ABT-737 (MedChemExpress) in DMSO at a concentration of 100 mg/mL, and stored at -20ºC in 100 µL-aliquots. Immediately before administration on each day of the treatment, aliquots were thawed and diluted in 1.9 mL vehicle, which was made of 30% propylene glycol (Fisher Scientific), 5% TWEEN® 80 (Sigma-Aldrich) and 3.3% dextrose (D-glucose, Sigma-Aldrich) in water, and the pH was adjusted to 4-5 (final concentration of the solution: 5 mg/mL)).

2.6.4.2. Cisplatin treatment

Mice bearing A549-derived xenografts as well as $Kras^{G12V}$ animals were treated at the specified time-points with cisplatin. Generally, animals were treated with 1.5 mg/kg body weight of cisplatin or vehicle (via i.p. injection) 2 to 3 times a week during 2 weeks, unless stated otherwise.

Cisplatin (Sigma-Aldrich) was dissolved fresh in sterile 0.85% saline solution to a final concentration of 150 mg/mL.

2.6.4.3. Galunisertib treatment

To evaluate the effect of TGFβR1 inhibition during lung tumour progression, A549 xenograft- and L1475(luc)-orthotopically transplanted tumour-bearing mice were treated with 150 mg/kg body weight Galunisertib (LY2157299) or vehicle daily by oral gavage for 5 consecutive days or as described in the respective figures in subsequent chapters.

Galunisertib solution was prepared fresh daily. Galunisertib was first dissolved in DMSO and subsequently diluted in sterile 0.85% saline solution to the desired final concentration immediately prior to administration.

2.6.4.4. Navitoclax and Nav-Gal treatments

To evaluate the therapeutic efficacy of senolytics in combination with chemotherapeutic treatment *in vivo*, mice bearing A549-derived xenografts as well as L1475(luc)-orthotopically transplanted tumours were treated with 100 mg/kg body weight navitoclax

(via oral gavage), with 85 mg/kg body weight navitoclax (via i.p. injection) or with 85 mg/kg body weight Nav-Gal as described in subsequent chapters.

Navitoclax was dissolved and prepared in freshly made vehicle dilution weekly, and stored at -4ºC. The vehicle was made of 10% ethanol, 30% PEG 400 (Sigma-Aldrich) and 60% PhosalPG:Phosphatidylcholine. To prepare Phosal PG: Phosphatidylcholine solution, soybean lecithin (ThermoFisher Scientific) was dissolved in 10% w/w propylene glycol (Fisher Scientific) to a concentration of 1.04 g/cm^3.

Nav-Gal was prepared fresh daily by dissolving in DMSO and further diluted in sterile 0.85% saline solution to the desired final concentration.

2.6.5. Xenograft subcutaneous transplantation

A549 cells were treated with 15 μM cisplatin for 10 days, then thoroughly washed twice with PBS and trypsinised. Control and senescent A549 cells were then centrifuged at 1250 rpm for 5 min and resuspended to a concentration of 1-4x10^6 cells/75 μL in DMEM. Matrigel was added 1:1 and the cell suspension was mixed and kept on ice. A total of 1-4x10^6 senescent and/or control A549 cells were injected subcutaneously in the flank of SCID mice using a 22G syringe. Xenograft formation and growth was recorded using a digital calliper twice a week, and imaged using an IVIS Spectrum Zenogen machine (Calliper Life Sciences; small binning) as described below. Tumour volume was calculated as Volume = (D x d^2)/2, where D and d refer to the long and short tumour diameters, respectively. Experiments were terminated at either pre-established time endpoints or when tumours reached an average diameter of 1.2 cm. At specified end-points or when tumours reached an average diameter of 1.2 cm, mice were culled and tumours were collected in 10% formalin for histological analyses.

2.6.6. Lung cancer cell orthotopic transplantation in the lung

Luciferase-expressing Kras$^{G12D/WT}$;p53$^{-/-}$ murine lung tumour L1575(luc) cells were treated with 3 μM cisplatin, 20 nM docetaxel or 30 μM palbociclib. When cells became senescent, they were thoroughly washed and fresh DMEM-F12 media (supplemented with 10% FBS)

was added for medium conditioning. Conditioned medium (CM) was collected every 24 h, centrifuged for 10 min at 2500 rpm, and transferred onto normal luciferase-expressing L1575(luc) cells for 10 days. After this, cells exposed to the different CM were trypsinised, centrifuged for 5 min at 1250 rpm, washed three times with PBS and resuspended in PBS to a final concentration of $1x10^6$ cells/mL.

C57BL/6J female mice were sublethally irradiated at 4 Gy using a Caesium source irradiator 6 h before a total of $2x10^5$ cells in 200 µL were injected via tail-vein. Baseline luminescence values were recorded 24 h after transplantation, and tumour growth was monitored twice a week by bioluminescence imaging after intraperitoneal injection with D-luciferin (150 mg/kg body weight, PerkinElmer) using an IVIS Spectrum Zenogen machine (Calliper Life Sciences). Relative luciferase activity corresponds to change from baseline at indicated time points, normalised to a blank control (luciferase-negative animal). Tumour survival represent the onset of moderate signs of disease. At this point, lungs were removed and fixed in 10% formalin overnight, and then transferred to 70% ethanol until paraffin embedding for further histological analyses. For tumour load analysis, lungs were collected 17 days after transplantation.

2.6.7. *In vivo* bioluminescence imaging and analysis

To monitor tumour burden in the orthotopic lung cancer model, luminescence intensity was recorded 24 h post-L1475(luc) cell transplantation for baseline luminescence values and at later time-points twice a week until experimental end-point was reached. To monitor A549-luc xenografts, luminescence intensity was recorded 7 days post-transplantation for baseline luminescence values and then once a week until end of experiment.

For this, animals were anaesthetised by isoflurane inhalation and injected with D-luciferin (150 mg/kg body weight, PerkinElmer). After 10 min, mice were places within visualizer and luminescence was measured with an IVIS Spectrum Zenogen machine (Calliper Life Sciences; small binning). For analysis, images were analysed using Living Image Software (PerkinElmer). A ROI was drawn covering the lung area and total flux of radiance was subtracted (Total Flux [p/s]). Relative luciferase activity was then calculated,

and it corresponds to change from baseline at indicated time points, normalised to a blank control (luciferase-negative animal).

2.6.8. Micro-Computed Tomography (micro-CT) imaging and analysis

For tumour burden analysis, mice were anaesthetised by isoflurane inhalation and scanned using a microPET-CT scanner (Mediso Medical) using the parameters described in **Table 11**.

Scan parameters	**XRay energy**	**35 kVp**
	Exposure time	450 ms
	Number of projections	720
	Projections per step	1
	Scan method	Semi-circular single field of view
Reconstruction parameters	Voxel size	Small
	Slice thickness	Thin
	Filter type	Butterworth
X-Ray Dose	Volume size (mm)	40 x 40 x 22
	Voxel size (µm)	40 x 40 x 40
	Voxels	972 x 972 x 538

Table 11. Scanning and reconstruction parameters used for the micro-CT imaging of murine lungs.

Scans were analysed and 3D reconstructions generated using Slicer 4.10.2 software (3D Slicer) by Dr Guillermo Medrano, Dr Guillermo Garaulet and Dr Francisca Mulero (Molecular Imaging Unit, CNIO). To determine tumour size, the length (longest diameter, L) and width (diameter perpendicular to the length, W) were measured and the following ellipsoid formula was applied: $(4/3)xPIx(W/2)^2x(L/2)$. Results were plotted as individual tumour volume or as tumour burden/mouse, where volumes of total number

of tumours in each experimental mouse were added. Statistical differences were calculated with GraphPad following two-tailed Mann Whitney tests.

2.6.9. Sample collection and processing

2.6.9.1. Blood collection and platelet analysis

In order to analyse platelet count in mice to assess the cytotoxic effect of *in vivo* senolytic treatment, blood was collected by cardiac puncture during isoflurane anaesthesia in xenograft experimental mice, and by superficial vessel puncture in wild-type C57BL/6J experimental mice. Blood was collected into anticoagulating Microvette® tubes (Sarstedt), and platelet levels were immediately measured using a Scil Vet abc Plus haematology analyser (Horiba).

For *ex vivo* platelet apoptosis analysis, blood from five wild-type C57BL/6J mice was collected by cardiac puncture in accordance with the University of Cambridge ethical committee and the UK Home Office guidelines. Samples were collected in non-vacuum citrate tubes (DH medical material), and blood in control tubes was diluted in Tyrode's Buffer (Sigma-Aldrich). Blood in treated samples was mixed with 2X drug solution (either Navitoclax or Nav-Gal) in RPMI supplemented with 10% FBS at the concentrations specified in Chapter 5. Control and treated specimens were incubated for 5 h in 20% O_2 and 5% CO_2 at 37°C. Treated samples were diluted in Tyrode's Buffer (Sigma-Aldrich), and then all specimens were mixed with Annexin Binding Buffer (Thermo Fisher Scientific) and incubated for 10 min with Annexin V-FITC (Immunostep) and CD-41-PE (Immunostep) conjugated antibodies. A23187 (Sigma), a calcium ionophore, was also added in parallel control samples to induce cell death and be used as a positive control. Samples were finally diluted in Annexin Binding Buffer (Thermo Fisher Scientific), and data were acquired using an FC500 MPL Flow Cytometer (Beckman-Coulter) for human samples and an LSR Fortessa cell analyser running the FACSDiva software (BD Biosciences) for mouse samples. FlowJo 10.3 software was used to analyse the results.

2.6.9.2. Lung and tumour collection for histology

Tissue of interest from experimental mice were collected and processed through different methodologies. In the case of lungs, mice were generally injected with an overdose of Dolethal (20% pentobarbital; Vetoquinol). Blood from lungs was carefully flushed by an intracardiac injection of 2 mL PBS and then processed differently depending on subsequent histological analysis objective as described below. In the case of xenografts, mice were culled by cervical dislocation and tumours were collected, washed once with PBS and fixed in 10% formalin overnight, or processed for flow cytometry analysis as described below.

2.6.9.3. Lung vibratome-sectioning and fresh SA-β-gal staining

Lungs were inflated with 1mL of 4% UltraPure™ Low Melting Point Agarose (ThermoFisher) (dissolved in PBS) previously warmed at 42ºC via intratracheal injection, and then allowed to set until agarose solidified. Lungs were removed, and placed on ice-cold PBS, and immediately sectioned using a VT100S vibratome (Leica Biosystems) in 500 µm-thick sections, at a vibration amplitude of 1.20 and a speed of 0.26 mm/s, submerged in ice-cold PBS. Fresh sections were then fixed in 1X SA-β-Gal Staining Kit (Cell Signaling) fixative buffer for 20 min at room temperature, washed twice with saline solution and stained for SA-β-gal activity using the same kit for 6 h at 37ºC. Sections were washed thoroughly with PBS, immersed in 70% ethanol and subsequently embedded in paraffin for further histological processing. Some of the vibratome-sections were not stained for SA-β-gal. In this case, they were fixed with 10% formalin for 40 min, washed thoroughly with PBS, immersed in 70% ethanol and subsequently embedded in paraffin for further histological processing.

2.6.9.4. Whole-mount staining

Lungs were inflated with 1 mL of PBS or saline solution via intratracheal injection, and a knot was made around the trachea with a thread before removing the needle to prevent

deflation of the lungs. Lungs were then submerged in PBS once to wash them, and then fixed in 1X SA-β-Gal Staining Kit (Cell Signaling) fixative buffer for 40 min at room temperature. Lungs were washed twice with saline solution and stained for SA-β-gal activity using the same kit at 37ºC overnight. On the next day, lungs were thoroughly washed with PBS, immersed in 70% ethanol and subsequently embedded in paraffin for further histological processing.

2.6.9.5. OCT embedding and snap-freezing

Lungs were inflated with 1 mL of 5% sucrose (dissolved in 1:1 PBS:OCT) via intratracheal injection, and a knot was made around the trachea with a thread before removing the needle, to prevent deflation of the lungs. They were then removed, washed once with PBS and carefully dried up to prevent the formation of crystals during freezing process. They were then embedded in OCT cryoembedding matrix (ThermoFisher Scientific, #12678646) and snap-frozen onto dry ice before storage at -80ºC. Lungs were sectioned using a cryostat in 10 µm-thick sections, which were mounted on Superfrost® plus slides. For SA-β-gal staining, sections were then fixed in 4% PFA for 4 min, washed with PBS, and stained using the SA-β-Gal Staining Kit (Cell Signaling) for 6 h at 37ºC. Slides were then immersed in PBS for several minutes to remove excess of staining solution. They were then placed on a tank with Haematoxylin Solution (Sigma-Aldrich) until stained as desired and subsequently washed in H_2O. They were then transferred to a new tank containing Eosin Solution (Sigma-Aldrich) until stained as desired. Slides were transferred to 70% ethanol to wash out excess of staining, and then washed three times with 70% ethanol. Slides were washed twice in ethanol 100% for 5 min, then placed on Histoclear™ Tissue Clearing Agent (National Diagnostics) twice for 10 min for dehydration) and then covered in Eukitt mounting media (Sigma-Aldrich), covered with a coverslip and kept at room temperature in the dark. For TUNEL staining, sections were fixed and stained as described previously.

2.7. Cell and tissue imaging and microscopy

2.7.1.1. Image acquisition and analysis

Slides were digitalised using with a slide scanner (AxioScan, Zeiss) with polarised and fluorescent light at 10X magnification, and Zen 2.3 (Zeiss) software was used for image acquisition. The scale of the image was then calculated from graticuled images at the same magnification and Zen 2.3 (Zeiss) or Fiji/ImageJ was used to measure tissue sizes. Cell counting from microscope images was conducted manually using Fiji/ImageJ and the cell counter plugin.

2.7.1.2. Cell quantification

For quantification of p16+, p21+ and Ki67+ cells for the study of the accumulation of senescent cells during lung adenocarcinoma in Chapter 3, cell counting was performed in histological sections from at least 3 independent mice per experimental condition. For quantification of Caspase-3+, p16+, F4/80+, CD31+ and Ki67+ cells upon vehicle or ABT-737 treatment in Chapter 3, 15 total tumours from at least 3 different experimental mice were analysed. Quantification of p21+, Ki67+ and TUNEL+ cells in A549 xenografts upon cisplatin, cisplatin + navitoclax and cisplatin + Nav-Gal treatment, a total of 4 representative fields per tumour was analysed (total of 10-12 tumours per treatment condition). Populations were determined by taking the proportion of positive cells relative to total nuclei as marked with haematoxylin staining, except for CD31 staining, for which total pixel positive for the staining area was normalised to total nuclei, and TUNEL, where proportion of positive cells was calculated to total DAPI+ nuclei.

2.8. Statistical methods

R studio was used for statistical assessment of RNA-seq data and GraphPad Prism (GraphPad, CA, USA) software was used for statistical analysis of all other experiments. One-way ANOVA tests were performed to compare multiple experimental conditions,

followed by Tukey's Multiple comparison test. Two sample Student's t-tests were performed to calculate the statistical significance of all the results when comparing two independent groups. Where data did not follow a normal distribution or did not present equal variances between the groups, Welch's correction was applied. Mann Whitney tests were performed to calculate the significance for tumour burden analysis. Statistical significance of survival analyses was calculated following a Log-rank (Mantel-Doc) test. A p-value below 0.05 was considered significant and indicated with an asterisk: *p, 0.05; **p, 0.01; ***p, 0.005. The asterisk is sometimes replaced by other symbols in the figures to indicate significant differences compared to a certain group, as detailed in the figure or figure legend.

CHAPTER 3:
THE ROLE OF CELLULAR SENESCENCE DURING LUNG ADENOCARCINOMA TUMORIGENESIS

3.1. Introduction

Carcinogenesis involves a multi-stage process through which normal tissue is morphologically altered and eventually becomes cancerous. Pre-neoplastic or pre-malignant lesions are defined as the first step in the process and are comprised of genetically and phenotypically transformed cells that present a higher risk of malignant evolution [263]. These lesions therefore represent a crucial stage of tumour formation and understanding their cellular heterogeneity, features and gene expression profiles and how they relate to the early tumour microenvirontment is vital for improved diagnostic, preventative and therapeutic strategies to enhance patient prognosis.

In the context of lung cancer, Auerbach and Saccomano were the first researchers to detect the presence of early morphological alterations in bronchial cells found in the sputum of high-risk individuals [264]. Subsequently, research on the different steps of cancer initiation has for many years focused on centrally arising tumours, such as squamous carcinomas of the lung, given the higher accessibility of the airways, compared to lesions commonly developing in the distal lung, including lung adenocarcinoma, neuroendocrine tumours and small-cell lung cancer (SCLC) [13, 264]. In the last years, the development of new approaches and animal models to study genome-wide and phenotypic alterations in human lung premalignancy has provided insights into the cellular processes preceding malignant stages. The current consensus sequence of the development of lung adenocarcinoma consists of three pre-malignant stages: atypical adenomatous hyperplasia (AAH), adenocarcinoma in situ (AIS) and minimally invasive adenocarcinoma (MIA) [15]. Importantly, these can be histologically recapitulated in *Kras*-

driven lung cancer mouse models commonly used in research, where the development of tumours includes hyperplasia (correlating to AAH), low- and high-grade adenoma (corresponding to AIS or MIA) and adenocarcinoma (human lung ADC). In addition, these models have also been described to closely mirror human NSCLC gene expression profiles and phenotypes [14]. However, despite advances in genomic and molecular characterisations, the particular cellular processes driving each of the stages remain to be fully elucidated.

Accumulation of cellular senescence has been reported in several premalignant lesions, including prostatic intraepithelial neoplasia, melanoma and colon adenoma [132-136], among others [265]. Of note, Collado and colleagues demonstrated that senescence is a defining feature of lung adenomas in a *Kras*^{G12V} mouse model of NSCLC, suggesting that it may contribute to tumour suppression during early lung carcinogenesis in a cell-intrinsic manner, by preventing the expansion of potential malignant cells upon oncogenic stimulation [135]. Paradoxically, as the understanding of this mechanism has expanded over the past few years, mounting evidence demonstrates that the cell extrinsic effects of cellular senescence can also alter the local milieu, promoting cancer progression via the SASP [266, 267], suggesting that the beneficial effects of senescence induction may be short-lived. Despite the impact this might have on cancer initiation, a full understanding of the prevalence and role of cellular senescence during the early stages of cancer development is far from complete. Insights into the interplay between senescence and lung cancer initiation are therefore needed and may be critical for novel interventions aimed at improving diagnosis and preventing tumour development.

Following the elucidation of the detrimental consequences of cellular senescence, senolytic therapies have surged as a growing area of active investigation for cancer treatment. Several drugs have been identified and designed to preferentially ablate senescent cells, including Bcl2 anti-apoptotic inhibitors (such as ABT-263, or navitoclax, and second-generation ABT-737), dasatinib and quercetin, and a FOXO4-derived peptide, among others [268, 269]. Senolytics have been reported to enhance healthspan and effectively treat, prevent and even reverse a variety of chronic conditions and age-related complications [270]. However, to our knowledge, the use of senolytic therapies in the context of cancer prevention has not been evaluated thus far.

In this chapter, we investigate and assess the incidence and extent of senescent cells during the development of lung adenocarcinoma by using a Kras-FSF^{G12V} mouse model of lung cancer, and demonstrate an increased senescent burden in lung adenomas compared to hyperplasias and adenocarcinomas. Of note, we performed this work in collaboration with Dr Martínez-Barberá's group, who developed a novel engineered mouse model, named P16-FDR, in which p16-positive cells can be detected, traced, isolated and eliminated (**Supplementary Figure 3.1, Appendix**). Importantly, our collaborators generated a p16-FDR-Kras^{G12D} mouse model of NSCLC and also observed an accumulation of p16-positive cells during early stages of lung cancer progression, which further validates our observations in an alternative model. Next in this chapter, we explore the expression of senescent markers in some stromal populations following observations by our collaborators, and determine a predominant expression of p16 in the macrophage compartment. Finally, we evaluate the impact of selectively eliminating senescent cells during lung cancer development with ABT-737, and demonstrate that senolytic treatment effectively abrogates tumour progression and improves survival in lung tumour-bearing mice.

3.2. Results

3.2.1. Senescent cells accumulate during lung adenoma development in the Kras-FSF$^{G12V/+}$ mouse model

Initially, we sought to investigate and evaluate the potential burden of senescence during lung tumorigenesis by employing the Kras-FSF^{G12V} mouse model of lung adenocarcinoma, in which the intratracheal administration of Adeno-FLP viral particles induces the expression of a Flp recombinase that in turn allows the expression of oncogenic mutant *Kras^{G12V}* in the lungs of mice. In this model, the aberrant expression of the oncogene results in the development of malignant lesions that evolve from epithelial hyperplasia to lung adenomas and, eventually, adenocarcinomas, closely recapitulating human lung adenocarcinoma progression [14]. Lung tumorigenesis was induced in Kras-FSF^{G12V} mice at 6-8 weeks of age, and then lungs were harvested and collected for histological analysis

at months 4, 5 and 6 post-induction of tumours. Of note, this is a p53 WT model in a pure C57BL/6 background, meaning that tumorigenesis is significantly slower than in other models and early lesions are only detected from month 4 post-induction of tumours. In addition, preneoplasia and neoplasia development occurs asynchronically, and lungs usually present with several lesions at different stages of tumour progression at a given time-point.

Evaluation of senescence and proliferation markers in tumour-bearing $Kras^{G12V}$ lungs revealed that a higher proportion of cells in lung adenomas were immunoreactive for proliferative arrest-related $p16^{INK4a}$ marker, compared to hyperplasia and lung adenocarcinomas (**Figure 3.1a**). Quantitative analysis showed that hyperplasias presented a mean average of 12.84% ± 6.45 of $p16^{Ink4a}$-positive cells per lesion, while adenomas and adenocarcinomas showed a mean average of 18.37% ± 6.46 and 7.00% ± 5.11, respectively. Posthoc multiple comparisons revealed that the difference between adenoma and adenocarcinoma was statistically significant (**Figure 3.1b**, top). In a similar fashion, p21 expression was also increased in adenoma lesions compared to the other two stages (mean average of p21-positive cells per lesion: hyperplasia, 6.64% ± 3.81; adenoma, 18.33% ± 11.29; adenocarcinoma, 4.32% ± 1.72), despite the differences did not reach statistical significance (**Figure 3.1b,** middle). Inversely, the proportion of Ki67-positive cells was significantly lower in adenomas compared to adenocarcinomas (4.98% ± 3.06 Ki67-positive cells/lesion vs. 33.78% ± 13.08, respectively). Hyperplasias presented an increased proportion of cells immunoreactive for Ki67 compared to adenomas (17.28% ± 10.10), but the difference was not significant (**Figure 3.1b**, bottom). Of note, SA-β-gal staining was more extensive in adenoma lesions compared to hyperplasia and adenocarcinomas, further suggesting the accumulation of senescent cells in these pre-malignant lesions (**Figure 3.1a**).

Together, these results indicate that cells undergoing cell arrest (expressing cell cycle inhibitors) and presenting increased SA-β-gal activity (two major hallmarks of cellular senescence) accrue during lung tumorigenesis and particularly accumulate in adenoma lesions of the lung.

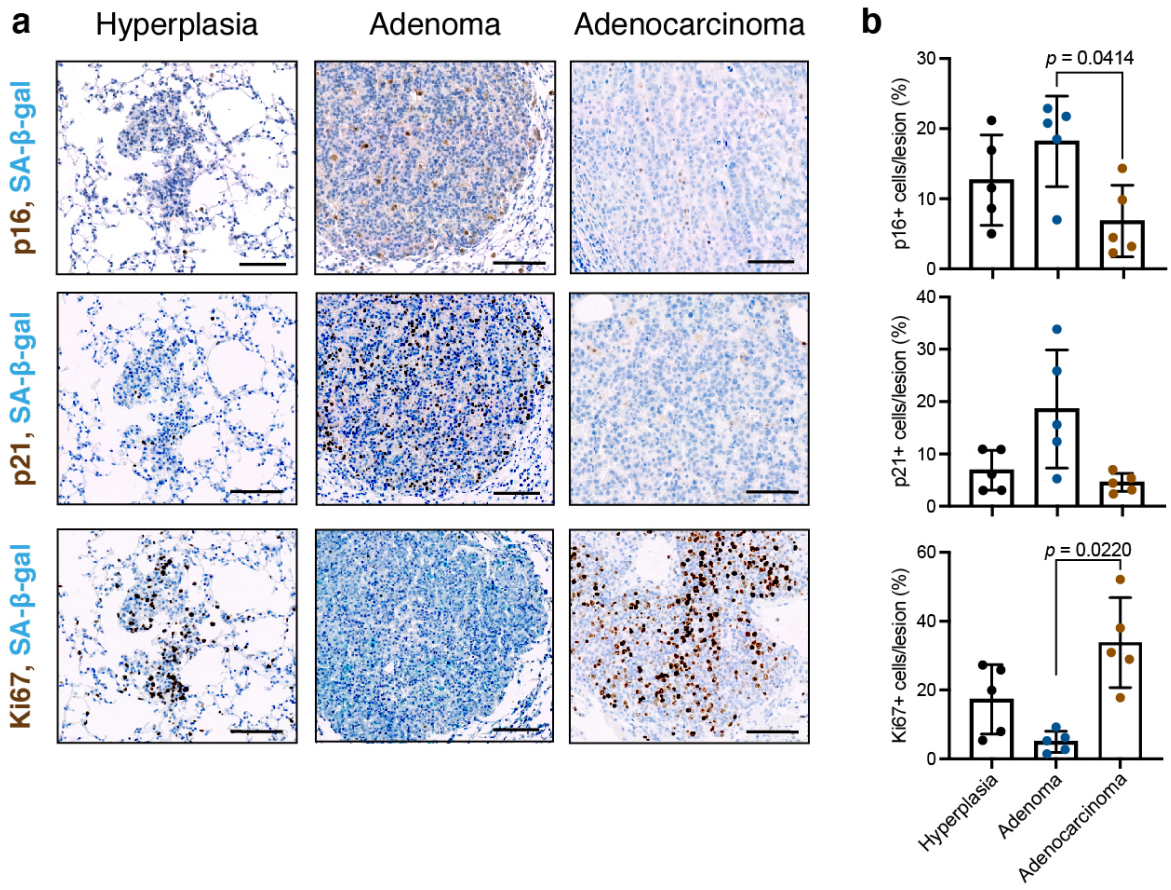

Figure 3.1. Senescent cells accumulate in lung adenomas in Kras-FSF^{G12V} mouse model of lung cancer. **a.** Representative histological images of tumour-bearing lung sections stained for p16, p21 and Ki67 marker expression, from lungs harvested 5 to 6 months post-induction of tumours. Lungs were also subjected to whole-mount SA-β-gal staining prior to histological processing. Scale bar = 100 μm. **b.** Quantification of p16-, p21- and ki67-positive cells per total cells in each lesion. Data is shown as mean ± SD (n = 5). One-way ANOVA followed by Tukey's multiple comparisons test were performed to determine statistical significance of the result. Only statistically significant p-values (<0.05) are shown in the graphs.

3.2.2. P16 expression predominantly co-localises with macrophage cell identity markers

The results obtained from a transcriptomic analysis of isolated p16^{Ink4a}-expressing cells performed by our collaborators indicated that a significant proportion of endothelial cells and macrophages activate the expression of p16 during Kras^{G12D}-mediated lung tumorigenesis (see Discussion below). To validate these findings and as part of our interest in understanding the cellular identity of putative senescent cells in our model, we next set out to analyse the co-localisation of macrophage and endothelial cell markers

in tumour-bearing lungs. Our examinations revealed a noteworthy recruitment of F4/80-positive cells in the lesions and a high degree of co-localisation between p16 and F4/80 expression (**Figure 3.2a**). Of note, an average of 36.88% ± 16.00 of all macrophages were immunoreactive for p16. Conversely, the proportion of p16-positive cells that expressed the F4/80 macrophage marker totalled to an average of 45.14% ± 25.59 in the lesions (**Figure 3.2b**). We continued our investigations with the aim of detecting co-localising CD31 and p16 double-positive staining, but given the nature of the technique, the shape of endothelial cells and the distribution of CD31 in the cell membrane, we were unable to distinguish the two stainings separately, thereby making difficult a quantification. However, and although most p16-positive cells resembled monocyte and epithelial cell morphologies, we observed scattered p16-positive cells in close association with endothelial cells (**Figure 3.2a**, right).

These data indicate a particularly predominant expression of the senescent marker p16 in the macrophage compartment, and warrants future validations of CD31 and p16 co-expression using alternative techniques, such as confocal fluorescence imaging.

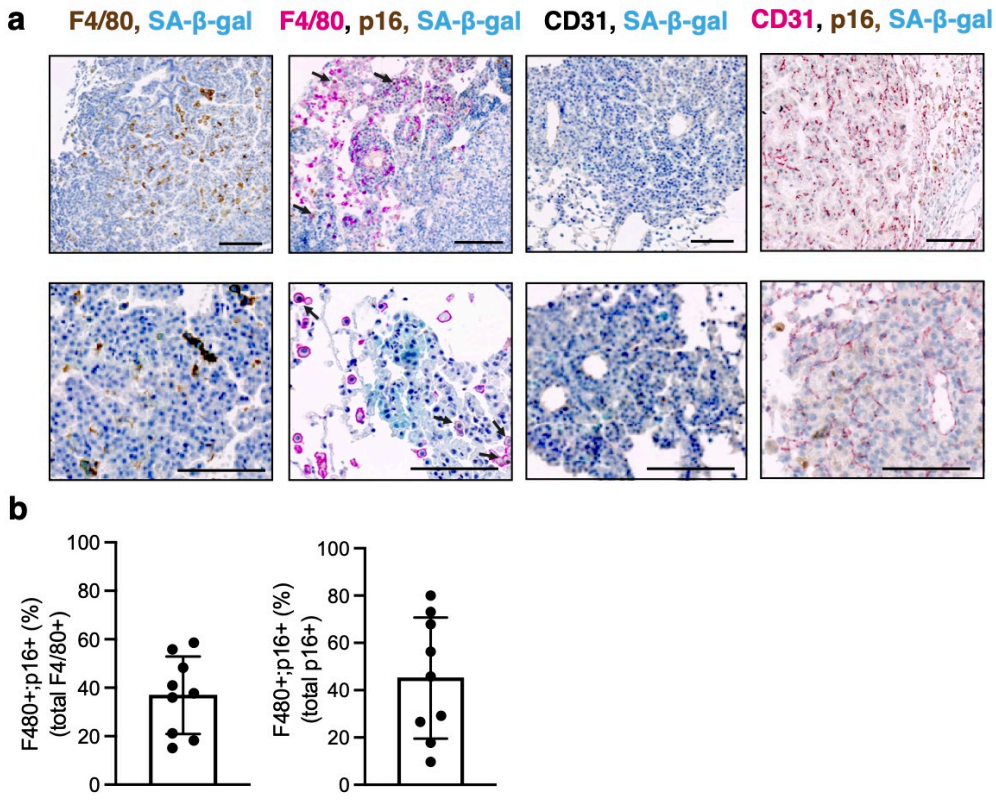

Figure 3.2. p16 expression co-localises with macrophage markers in Kras-FSF^{G12V} tumour-bearing lungs during tumorigenesis. a. Representative histological images of tumour-bearing lung sections stained for p16, F4/80 and CD31 marker expression, from lungs harvested 6 months post-induction of tumours. Lungs were also subjected to whole-mount SA-β-gal staining prior to histological processing. Scale bar = 100 μm. **b.** Left, quantification of p16- and F4/80-double positive cells out of all F4/80- and p16-positive cells in the lesions. Data is shown as mean ± SD (*n* = 9 lesions).

3.2.3. Pharmacologic ablation of putative senescent cells through senolytic treatment ameliorates tumour burden and increases survival

With the aim of evaluating the impact and efficiency of senolysis during lung tumorigenesis, we next tested if senolytic treatment could be used to ablate putative senescent cells in our model. Bcl-2 inhibitors, which are one of the most promising senolytics being used in pre-clinical models, like navitoclax, effectively target multiple types of cells (including lung adenocarcinoma and fibroblastic cells) undergoing chemotherapy- and oncogene-induced senescence (see Chapter 5, **Figure 5.3** and **Figure 5.4**). We therefore opted to use ABT-737, a second-generation Bcl-2 inhibitor [181] that has shown potent senolytic capabilities in different models *in vivo* [271, 272]. ABT-737 was injected intraperitoneally on two consecutive days once a month, from month 5 to month 8 post-induction of tumours (**Figure 3.3a**). Lungs were harvested immediately upon treatment completion and subjected to histological evaluation to assess the effect of senolytic treatment in the lesions. Representative histological images are shown in **Figure 3.3b**. Quantitative analyses revealed that specimens subjected to senolytic treatment showed a significant increase in cleaved-caspase 3 levels compared to vehicle-treated animals (vehicle, 0.29% ± 0.25; ABT-737, 12.17% ± 9.13 of total cells in the lesion), confirming that pan-Bcl-2 inhibitor treatment induces apoptosis in the lesions (**Figure 3.3c**). In addition, we observed that senolytic treatment also resulted in a significant reduction in cells immunoreactive for p16, which further indicates the preferential cytotoxic effect in senescent cells (vehicle, 2.49% ± 1.05; ABT-737, 1.19% ± 0.61 of total

cells in the lesion). Because we previously observed that p16 expression is predominant in the macrophage compartment, we analysed the effect of senolytic treatment on F4/80 and detected a significant reduction compared to lungs from vehicle-treated individuals (mean F4/80-positive cells per total cells in lesion: vehicle, 11.05% ± 3.62; ABT-737, 5.469 ± 3.30). Despite we were not able to validate a predominant expression of p16 in endothelial cells, we still evaluated the effect on CD31-expressing cells in our lesions, given the fact that our collaborators have observed this enrichment. Interestingly, CD31 expression in the lesions was also significantly reduced compared to vehicle-treated lungs (mean CD31-positive area/lesion: vehicle, 87.04% ± 73.28; ABT-737, 40.92% ± 23.37). Finally, ABT-737 treatment also significantly led to a reduction in the proportion of cells immunoreactive for the proliferation marker Ki67 (vehicle, 5.24 ± 3.14; ABT-737, 2.67 ± 2.87). These data confirm that the intraperitoneal administration of ABT-737 effectively induces cell death, reducing the number of p16- and associated senescence markers-expressing cells in the lesions.

Next, in order to uncover the potential role of senescent burden during lung tumorigenesis, we subjected KRas-FSF^{G12V} lung tumour-bearing mice to ABT-737 or vehicle treatment as described above (**Figure 3.3a**) and evaluated tumour burden by micro-computed tomography (micro-CT) imaging at 10.5 months post-induction of tumours. Strikingly, senolytic treatment led to a significant reduction in tumour burden compared to vehicle-treated mice (vehicle, 66.09 mm^3 ± 33.1 average tumour burden per mouse; ABT-737, 22.53 mm^3 ± 10.38) (**Figure 3.3d**). Representative micro-CT images and 3D reconstructions of the lungs from vehicle- and ABT-737-treated animals are shown in **Figure 3.3e**. Remarkably, chemical ablation of senescent cells resulted in a significant prolonged survival of the mice (vehicle, average survival of 289 days ± 46.5 post-AdFlp administration; ABT-747, 384 days ± 138.4) (**Figure 3.3f**).

Together, our data indicates that ablation of senescent cells with the senolytic ABT-737 significantly reduces tumour burden and enhances survival in a *Kras^{G12V}* mouse model of NSCLC.

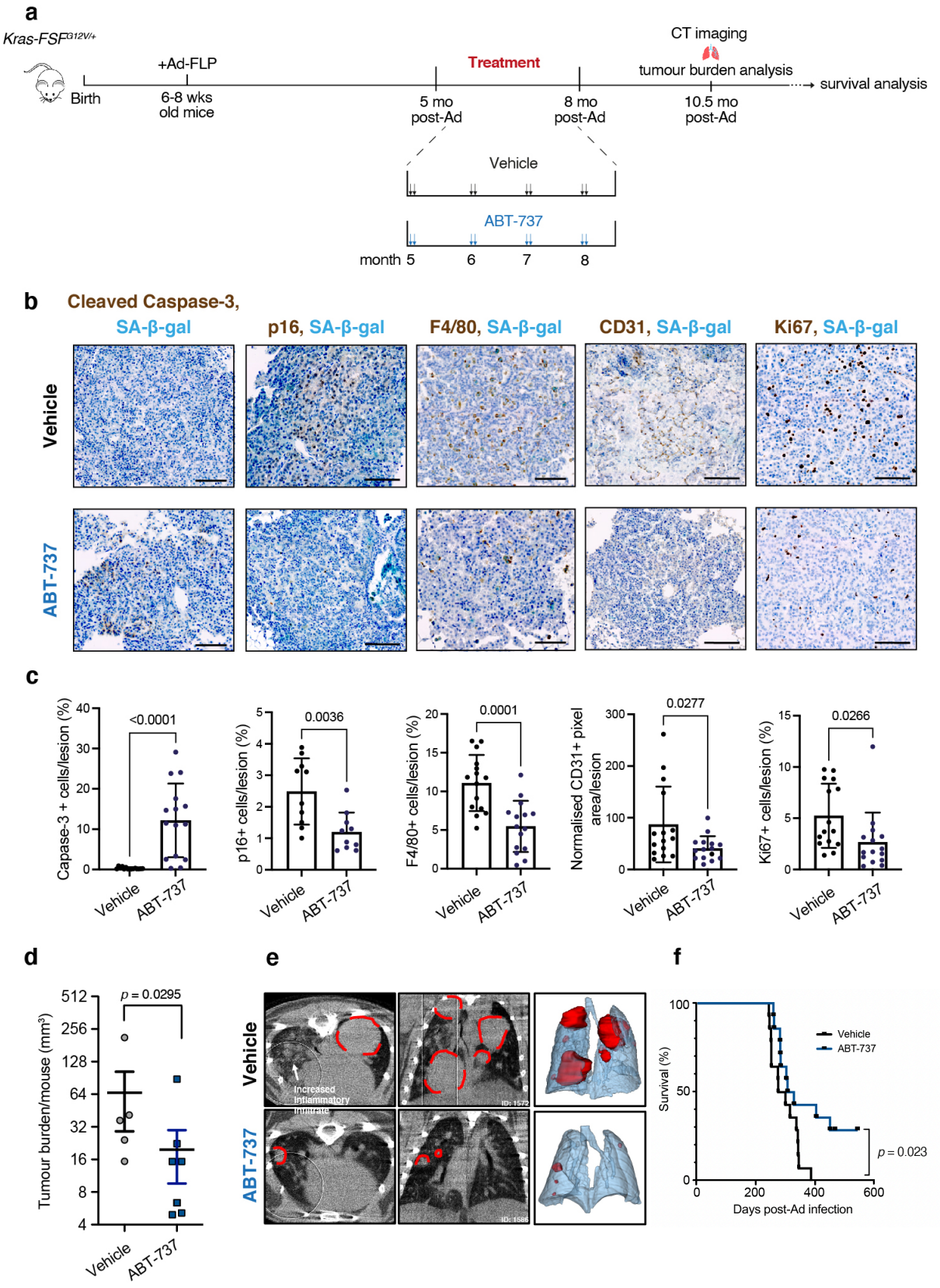

Figure 3.3. Pharmacologic ablation of senescent cells with ABT-737 treatment in *Kras*^{G12V} mice during lung cancer tumorigenesis reduces tumour burden and prolongs survival. a. Schematic representation of experimental layout. Briefly, *Kras*^{G12V} mice were infected with AdFlp viral particles at 6-8 weeks post-birth.

Animals were treated with 25 mg/kg ABT-737 or vehicle on two consecutive days once every 4 weeks from month 5 to 8 post-induction of tumours. Tumour burden was analysed at month 10.5 post-AdFlp by micro-CT imaging, and survival was evaluated. **b**. Representative histological images of tumour-bearing lung sections stained for cleaved Capase-3, p16, F4/80, CD31 and Ki67 marker expression, from lungs harvested immediately after treatment completion at month 8 post-induction of tumours. Lungs were also subjected to SA-β-gal staining prior to histological processing. Scale bar = 100 μm. **c.** Quantification of cleaved Caspase-3-, p16-, F4/80-, CD31- and ki67-positive cells or area per total cells in each lesion. Data is shown as mean ± SD (n = 15 tumours). Two-tailed Student's t tests were performed to determine statistical significance of the results. **d.** Tumour burden in $Kras^{G12V}$ mice at month 10.5 post-tumour induction, plotted as the total volume occupied by tumours in the lungs per mouse. Data represents mean ± SEM (vehicle, n = 5; ABT-737, n = 7) and statistical significance was assessed by Welch's t test. **e**. Transversal and sagittal micro-CT scan images and 3D reconstruction of representative lungs scanned at month 10.5 post-AdFlp. Tumours are delineated and reconstructed in red colour. **f.** Survival curve of $Kras^{G12V}$ mice (vehicle, n = 13; ABT-737, n = 14). Statistical significance was assessed by log-rank test.

3.3. Discussion

The role and impact of cellular senescence during NSCLC initiation and progression remains largely unexplored. While extensive research has expanded our knowledge on the benefits and disadvantages of senescence induction in cancer therapy and age-related and chronic disorders, where senescence's causative connection has been reported to a greater extent, the involvement of oncogene-induced senescence in tumorigenesis has not been extensively addressed and remains a formidable challenge. In lung cancer, senescent cells were described as a defining feature of adenomas but not adenocarcinomas [135], and it was therefore considered to act as a barrier to tumour progression by preventing the expansion of potential malignant cells. However, the lung microenvironment has been reported to be a crucial regulator of tumour initiation, progression and metastasis [273] and, in this context, the potential impact of accumulated senescence and its associated SASP has been omitted for years.

In this chapter, we have captured supporting evidence of the accumulation of senescent cells in lung adenoma premalignant lesions in contrast to hyperplasia and adenocarcinomas. As introduced earlier, this work was performed as part of a collaboration led by Dr Scott Haston from Martínez-Barberá group (University College

London), and findings were compared and assessed in parallel. Our collaborators generated a novel knock-in mouse model named *p16-FDR* in which the endogenous *Cdkn2a* promoter drives the expression of a cassette encoding the flippase-recombinase (FLPo) and a diphtheria toxin receptor (DTR)/mCherry fusion protein (**Supplementary Figure 3.1a, b, Appendix**). This remarkably allows the visualisation, isolation, genetic lineage tracing and pharmacogenetic ablation of $p16^{INK4a}$-expressing cells *in vivo*. Following the subsequent generation of *p16-FDR-YFP-Kras*$^{G12D/+}$ heterozygous mice (**Supplementary Figure 3.1b, Appendix**), our collaborators were able to isolate p16/mCherry-positive cells from lungs post-induction of tumours, and perform RNA sequencing to explore the phenotype of these cells during $Kras^{G12D}$-driven lung tumorigenesis. Gene set enrichment analysis (GSEA) demonstrated that mCherry-expressing cells were positively enriched for signatures of senescence, SASP and lysosomal pathways, and negatively enriched for proliferation pathways, confirming the induction of senescence in early lesions in this alternative model of NSCLC (**Supplementary Figure 3.1c, Appendix**). It is worth noting, however, that the two models are inherently different in the timing and development of lung cancer lesions. Despite the correlation of the findings between the two studies, it would be interesting to generate *p16-FDR-Kras-FSF*^{G12V} heterozygous mice and perform transcriptomic analyses of p16/mCherry-positive cells at the different time-points evaluated as part of this chapter, in order to further understand the dynamics of senescence induction and accumulation, and determine the extent of transcriptional similarities between the two models.

Further, as part of our interest in uncovering the predominant senescent cell type during lung tumorigenesis, cell type identity deconvolution of RNAseq data performed by our collaborators suggested that $p16^{Ink4a}$-expressing cells in the *p16-FDR-Kras*$^{G12D/+}$ model predominantly featured a macrophage and endothelial cell identity (**Supplementary Figure 3.1d, Appendix**). To validate these findings, immunofluorescence analysis of early lesions was performed using antibodies against macrophages (CD68) and endothelial cells (Pecam), among others (**Supplementary Figure 3.1e, Appendix**), and Haston and colleagues demonstrated that the majority of mCherry/$p16^{Ink4a}$-expressing cells appeared to be macrophages (63% ± 17.8%) and endothelial cells (24% ± 10.7%) (**Supplementary**

Figure 3.1f, Appendix). In this chapter we therefore aimed to validate these observations using the *Kras-FSF*^{G12V} model, and confirmed a significant co-localisation between F4/80 and p16 markers in early lesions, although to a slightly lower extent (proportion of p16 cells immunoreactive for F4/80, 45.14% ± 25.59). However, we could not validate the findings in the endothelial cell compartment, given the nature of the histological stainings performed for such analysis. In any manner, our results indicate that a large proportion of p16-expressing cells during lung tumorigenesis in both the *Kras*^{G12D} and *Kras*^{G12V} models of NSCLC fall outside the tumour cell lineage. To our knowledge, this is the first time that senescence is reported predominantly in non-epithelial cells in the context of pre-neoplastic lesions. Previous studies have demonstrated that AdCre and AdFlp intratracheal administration largely results in the infection and subsequent aberrant *Kras* expression in epithelial cells [23], and therefore oncogene-induced senescence (OIS) would be expected to occur in this cell compartment. While we cannot discard that epithelial cell OIS is induced in our model, the most prominent senescent response in our models seems to occur in stromal cells. Of note, a recent study reported that adenoviral vectors can actually transduce alveolar macrophages in NSCLC mouse models and activate *Kras*^{G12D} expression in the cells, despite a senescent phenotype was not investigated [274]. However, RNA sequencing data from our collaborators demonstrates that *Kras*^{G12D}-expressing cells largely present an epithelial cell identity signature (**Supplementary Figure 3.1d, Appendix**), and thus it is conceivable that senescence in macrophage and vascular cells is implemented in an extrinsic, paracrine fashion, and not as a result of oncogene insult. Indeed, a senescent-like phenotype has been reported in macrophages upon exposure to pro-inflammatory microenvironments [275, 276], and endothelial cells have also been described to undergo senescence *in vivo* in inflammatory conditions, including diabetes, atherosclerosis and ageing [277, 278]. Importantly, these observations open up the possibility of a crosstalk between oncogene-induced senescent pre-cancerous cells and the induction of senescence in macrophages and endothelial cells, an intriguing potential phenomenon that warrants further investigations. In future analyses, we will continue our validations of the senescent phenotype and p16-expression in vascular cells using alternative immunofluorescence techniques, and will

also explore the extent of senescent markers expression in the epithelial cell compartment during the development of early lung cancer lesions.

Remarkably, we demonstrate that pharmacologic ablation of senescent cells during lung tumorigenesis with ABT-737 senolytic treatment results in a significant reduction in tumour burden and prolonged survival in *Kras^{G12V}* mice. A limitation of this approach includes the possibility of non-specific ablation of non-senescent cells, since ABT-737 particularly targets cells that exhibit apoptosis resistance, a trait that is also detected in some tumour cells [279]. Indeed, despite the obvious impact in the senescent cell compartment, observed through the significant reduction of p16-expressing cells upon senolytic treatment, we cannot exclude potential off-target effects of ABT-737 in our model. Importantly, however, our collaborators reproduced these findings using an alternative approach that reduced the possibility of non-specific killing by ablating senescent cells in a pharmacogenetic fashion. For this, Haston and colleagues made use of the newly generated *Kras$^{G12D/+}$;p16$^{FDR/+}$;Rosa26$^{loxP\text{-}STOP\text{-}loxP\text{-}YFP/+}$ (KY-FDR)* model, where the administration of diphtheria toxin (DT) results in the induction of cell death in p16-expressing cells, and tumour cells can be detected through the induced expression of YFP (**Supplementary Figure 3.1b, Appendix**). Animals were treated with either DT or vehicle via subcutaneous injection twice a week from week 2 to week 8 post-induction of tumours, and tumour burden was analysed by immunofluorescence staining and FACS analysis at the different time-points (**Supplementary Figure 3.1g, Appendix**). In line with our observations, Haston and colleagues detected that pharmacogenetic ablation of p16-expressing cells during early lung tumorigenesis in this model resulted in a remarkable decrease in tumour burden, with up to a 74.4% reduction in the proportion of YFP-positive tumour cells, depending on the time-point assessed (2 weeks, 74.4% reduction; 4 weeks, 33.2% reduction, 8 weeks, 47.6% reduction) **Supplementary Figure 3.1h, Appendix**. Likewise, the number of YFP-positive tumour lesions decreased significantly in the DT treated group compared with the control, by an 85.42%, 76.32% and 52.55% reduction at weeks 2, 4 and 8, respectively (**Supplementary Figure 3.1i, Appendix)**. These data further validate the outcome of eliminating senescent cells during lung tumorigenesis using an alternative approach and a different Kras-driven model of lung

adenocarcinoma, and together with our results, indicate that senescence exerts tumour-promoting effects in early NSCLC lesions.

Based on evidence reported in the literature in the past years, cellular senescence can promote tumour progression through two main mechanisms: (1) by escaping the proliferative arrest and re-entering the cell cycle, which has also been associated with increased plasticity, stemness and malignant properties in senescence-escaping cells [86, 164, 280, 281], and (2) by secreting pro-inflammatory, immune-suppressive and tumour-promoting factors via the implementation of the SASP [167]. It is believed that premalignant lesions in which senescent cells accumulate upon oncogenic stimulation may progress through the reversion of senescence, driven by the acquisition of mutations or alterations that disrupt critical senescence maintenance pathways. Although compelling evidence of senescence reversion *in vivo* is still lacking, several studies have demonstrated that the modulation of key senescence drivers, including p53, Rb, DDR components and the SAHFs, can abrogate an established senescent state *in vitro* and reinstate DNA replication and cell cycle progression [282]. However, it is more plausible that a combination of a primary bypass of senescence (whereby transformed pre-malignant cells acquire a proliferative advantage and are unable to undergo senescence upon oncogenic stimulation in the first place) together with senescence reversion take place simultaneously during neoplasia. In this context, the potential role of the SASP might be even more impactful, as its tumour-promoting effects could be boosting the progression of both senescence *bypassers* and *escapers*.

The pro-tumorigenic nature of the SASP has been extensively reported, particularly in the context of therapy-induced senescence. Some of the factors reported to play a tumour-progressive role include IL6, IL-8, IL-1 α, AREG, CCL5, CXCL12 and several metalloproteases, which can increase cancer cell proliferation, invasion and migration in a paracrine manner [167]. In the context of tumour initiation, senescent fibroblasts were reported to directly promote the proliferation of pre-neoplastic ovarian epithelial cells [283], partially transformed epithelial keratynocytes [168, 284] and transformed breast, prostatic and hepatic cancer cells [129]. Of note, however, the paracrine impact derived from other senescent stromal cells remains largely unexplored. In this chapter, we demonstrate that the ablation of senescent cells, which largely present macrophage cell

identities in our model, and both macrophage and endothelial cell phenotypes in our collaborator's studies, abrogates lung cancer tumorigenesis. The role of macrophages in cancer has been addressed extensively, and, in the context of NSCLC, recent research demonstrates that they provide a pro-tumorigenic niche in early stages of lung tumorigenesis [285]. On the other hand, endothelial cells have been described as key drivers of angiogenesis, immune recruitment and tumour cell proliferation and invasion [286]. However, how the implementation of senescence in these cells alters their phenotype and impacts tumour initiation and progression remains to be elucidated. Further work is therefore required to determine how p16-expressing macrophages and endothelial cells in our models drive lung adenoma-adenocarcinoma progression. The use of lineage tracing approaches where p16-expressing cells and neighbouring cells impacted by the SASP can be tracked, isolated and assessed can be very important to fully uncover the cell of origin in NSCLC and how senescence lends itself to the process of cell malignant transformation. This might not only be crucial to uncover tumour-initiating mechanisms during lung tumorigenesis, but can also shed light on potential markers that could be utilised for early detection purposes.

As shown in this chapter, the use of senolytics provide a means to elucidate the role of senescent cells. Our results indicate that senolytic treatment may serve as a novel and effective treatment against *Kras*-driven NSCLC, a modality that, to our knowledge, has not been proposed in the context of early lung tumorigenesis thus far. Senolytics are emerging as a class of drugs with the potential to revolutionise cancer treatment, particularly in combination with senescence-inducing treatments such as chemotherapy and radiation, where multiple studies have been generated in support of the detrimental effect of therapy-induced senescence [268]. We here demonstrate the potential benefit of senolytic drug treatment as a preventative cancer therapy, an approach that could be of particular importance in populations with an increased susceptibility for lung cancer, such as emphysema, pulmonary fibrosis and COPD patients [287], which have interestingly also been strongly associated with senescence accumulation [288-290]. However, it is important to take into consideration that the use of senolytics in other settings requires a detailed understanding of the context in which senescence is implemented and its connection with the disease.

Overall, the findings reported in this chapter demonstrate that senolytic therapies might provide a novel therapeutic strategy to control early-stage lung adenomas and manage NSCLC progression effectively. Finally, our observations can also serve as the basis for the development of novel tools aimed at detecting senescence burden in lung adenocarcinoma patients for diagnostic purposes.

CHAPTER 4:
THE PARACRINE ROLE OF CELLULAR SENESCENCE UPON CHEMOTHERAPY IN LUNG ADENOCARCINOMA

4.1. Introduction

Lung cancer accounts for the highest proportion of cancer-related deaths in our society. The most common histological subtype is Non-Small Cell Lung Cancer (NSCLC), which constitutes around 85% of all lung cancer diagnoses. Significant advances over the last two decades have been made towards improving lung cancer treatment, including the development of targeted therapies for some subsets of patients with advanced disease. However, the overall survival and cure rates for NSCLC remain very low. Platinum-based doublet therapy, based on cisplatin or carboplatin administration in combination with another cytotoxic drug, remains the standard first-line therapy for early stage and non-oncogene-addicted late-stage tumours. Despite favourable initial response rates, most patients relapse shortly after treatment completion, and around 84% of patients die within 5 years of first diagnosis [291]. Therefore, continued research into the mechanisms underlying treatment response and failure as well as enhanced therapeutic regimens are imperative to improve outcomes in NSCLC.

Platinum-based compounds are cytotoxic agents that create crosslinks in the DNA, interfering with replication and cell division. In 2005, research demonstrated for the first time that this type of chemotherapy results in increased levels of intratumoral Senescence Associated β-galactosidase (SA-β-gal) activity, a marker that is strongly associated with cellular senescence [292]. Additional studies have further demonstrated the accumulation of senescent cells in different human tumour types upon neoadjuvant chemotherapy, including breast cancer, mesothelioma, prostate cancer, renal cell carcinoma and rectal cancer [137], suggesting that it is a common response to anti-cancer

therapies. Senescence can be elicited in response to a variety of stimuli, including DNA damage and oncogenic stress, and its implementation includes an irreversible cell cycle arrest, as well as the acquisition of a series of structural and metabolic changes that impacts tissue homeostasis. As presented in previous chapters, a key hallmark of this cellular state is the implementation of a strong paracrine secretion of cytokines, growth factors, proteases and other mediators, known as Senescence-Associated Secretory Phenotype (SASP), that creates a local inflammatory milieu and affects the surrounding tissue. Senescence is therefore a well-established tumour suppressive mechanism as it prevents the propagation of damaged cells, but compiling evidence indicates that it can also drive tumorigenesis through the promotion of cellular proliferation, invasion, angiogenesis and even metastasis in a paracrine manner [167, 293]. Recent investigations have primarily focused on the therapeutic benefits of therapy-induced senescence in tumour cells [294], but given the detrimental effects largely attributed to the SASP [167], it is conceivable that unresolved and persistent senescence upon chemotherapy may represent a barrier to effective lung cancer treatment.

Despite a general list of factors is commonly described to constitute the SASP, including IL-6, IL-1α, CXCL2, MMP-3 and VEGF, among many others, its composition is known to be highly dependent on the inducer, the tissue of origin or cell type and even the duration and chronicity of the senescent burden [167]. Transforming Growth Factor-β (TGF-β) is a pleiotropic cytokine that governs a wide array of cellular mechanisms in physiological and pathological processes, and it has also been reported to be secreted by senescent cells, contributing to paracrine-induced senescence, fibrosis and immunomodulation [295-297]. In the context of cancer, TGF-β has been described to play a dual role, the result of which largely depends on the surrounding microenvironment and the genetic background and phenotype of the recipient cell [231]. Paradoxically, this cytokine functions as a tumour suppressor in pre-malignant cells by inducing cell cycle arrest and apoptosis, but it can also drive tumorigenic and pro-metastatic responses in overtly malignant cells through the promotion of EMT, tumour invasion, proliferation and immune suppression [231, 298]. The complexity of the contextual nature of TGF-β as part of the SASP and its potential connection with chemotherapy-induced senescence remains unexplored and warrants further investigations.

In this chapter, we demonstrate that cisplatin treatment results in the induction and accumulation of senescent cells in human and murine lung adenocarcinomas. Comprehensive phenotypic assessment reveals that the SASP derived from human and murine cisplatin-induced senescent lung cancer cells drives the acquisition of pro-tumorigenic traits in a paracrine manner, which can be recapitulated in human xenografts and orthotopic mouse models of lung cancer. Mechanistically, we show that exposure to cisplatin-derived SASP orchestrates the TGFβR1-driven activation of Akt/mTOR signalling, which is responsible for the induction of increased proliferation in SASP-exposed cells. In agreement with this, we determine that pharmacological inhibition of TGFβR1 with galunisertib treatment reverts the tumour promoting effects of cisplatin-induced senescence both *in vitro* and *in vivo*. Finally, we propose a novel therapeutic modality combining chemotherapeutic cisplatin treatment together with TGFβR1 inhibition, which demonstrates improved treatment outcomes and enhanced survival in lung tumour-bearing mice.

4.2. Results

4.2.1. Platinum treatment induces expression of cellular senescence markers in *Kras-FSF*$^{G12V/+}$ murine and human NSCLC tumours

Anticancer therapeutics, including cytotoxic and genotoxic agents such as cisplatin, have been widely reported to induce senescence in experimental conditions [66, 299]. However, evidence of therapy-induced senescence in clinical settings remains limited. In the context of lung cancer, Roberson and colleagues demonstrated for the first time that lung tumours resected from patients upon neoadjuvant platinum-based therapy accumulated SA-β-gal-positive cells, a marker widely used to detect senescent cells *in vitro* and in tissues, compared to untreated specimens [292].

To better define the physiological response to commonly used chemotherapeutics in lung adenocarcinoma, we first subjected lung-tumour bearing Kras-FSF$^{G12V/+}$ mice to two cycles of cisplatin treatment. Histological analyses revealed a reduction in Ki67+ cells and an enhanced expression of p21+ in tumours compared to vehicle-treated individuals

(**Figure 4.1**), suggesting the induction of cell cycle arrest in the lesions. In addition, we observed increased reactivity against γH2AX, a particular phosphorylation of H2A histone that occurs upon the formation of double DNA strand breaks, confirming the genotoxic effect of cisplatin administration in the tumours (**Figure 4.1**). Next, we evaluated the effect of ABT-737 administration alone or in combination with cisplatin treatment. ABT-737 is a second-generation senolytic agent that preferentially kills senescent cells through the induction apoptosis, and we hypothesised that its administration would result in increased apoptosis in tumours that had been treated with cisplatin compared to vehicle-treated tumours, due to the induction of cellular senescence upon cisplatin treatment. As observed in **Figure 4.1**, as an internal control, we did not observe a general decrease in the expression of the proliferative marker Ki67 with ABT-737 single treatment, and levels of cleaved caspase-3 (a marker of apoptosis used to confirm the mechanism of action of the drug) remained similar to those in tumours from mice treated with vehicle or cisplatin alone, with some sporadic cleaved caspase-3-positive cells in the tumours. On the other hand, combined treatment of cisplatin and ABT-737 resulted in a marked decrease in Ki67 expression in the tumours and an enhanced expression of senescence and DNA damage markers p21 and γH2AX, as observed in cisplatin-only-treated specimens. Of note, in contrast to ABT-737 single administration, combinatory treatment resulted in an enhanced expression of cleaved caspase-3 in the tumours, thereby suggesting the induction of cell death in putative cisplatin-induced senescent cells (**Figure 4.1**).

Importantly, these analyses indicate that cisplatin *in vivo* treatment of lung adenocarcinoma-bearing mice results in increased expression of DNA-damage and senescence-related markers, combined with a decrease in proliferation in the tumours. Of note, levels of apoptosis evaluated through cleaved caspase-3 upon cisplatin treatment were negligible, overall suggesting that the decrease in proliferation derives from the induction of cellular senescence in the tumours. Notably, histological assessments indicate that senolytic treatment may result in increased cell death in the tumours when combined with cisplatin treatment compared to ABT-737-single administration, which may also be an indication of the increased senescent burden

following cisplatin treatment, and highlights the potential of this combinatory modality in arresting tumour progression.

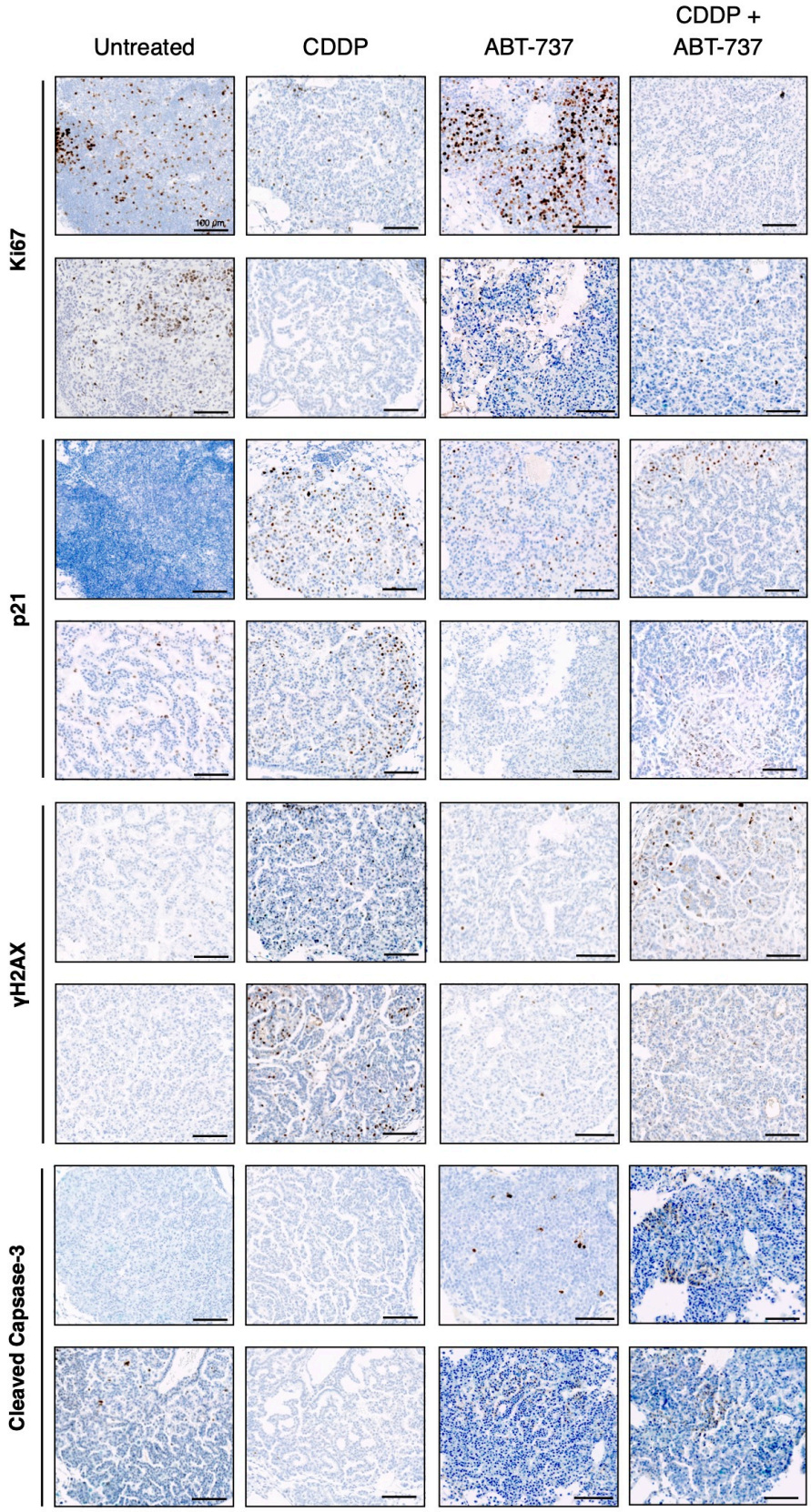

Figure 4.1. Cisplatin treatment of lung tumour-bearing KrasG12V mice is associated with increased expression of p21 and γH2AX, and concomitant cisplatin + ABT-737 treatment results in higher cleaved caspase-3 signal in tumours. Representative histological images of lung tumours resected from mice at month 11-12 post-induction of tumours in the Kras-FSF^{G12V} mouse model. Mice were treated with two cycles of cisplatin (1.5 mg/kg body weight i.p., once weekly) or vehicle, and/or ABT-737 (25 mg/kg body weight, i.p. twice weekly on two consecutive days after cisplatin administration) or vehicle. Lung sections were stained for Ki67, p21, γH2AX and cleaved caspase-3, and images depict representative regions from two independent mice per condition. Scale bar = 100 μm.

Interestingly, a study reported that high levels of SA-β-gal in tumours following neoadjuvant therapy correlated with a significantly poorer prognosis in a small cohort of locally advanced NSCLC patients [161], suggesting a link between senescence induction and cancer relapse. We therefore set out to determine the impact of selectively eliminating senescent cells upon cisplatin treatment in lung cancer progression. *Kras-FSF$^{G12V/+}$* mice bearing lung adenocarcinomas were subjected to 4 cycles of chemotherapy plus vehicle or ABT-737, and micro-CT imaging was used to assess tumour burden before and immediately after regimen completion, as well as 2 months after treatment (**Figure 4.2a**). CT analysis showed that while the number of tumours in the lungs per mouse increased over time in animals treated with cisplatin only, it remained largely unchanged in animals treated with a combination of both drugs (**Figure 4.2b**). In addition, co-treatment with cisplatin and ABT-737 resulted in a significantly decreased mean tumour volume compared to cisplatin-only treatment, relative to the volume before the start of chemotherapy (**Figure 4.2c**). While we cannot conclude the effect on tumour progression derived from the induction of senescence in the tumours, these results demonstrate that the combination of platinum-based chemotherapy induces senescence, and that its combination with senolysis is an effective and superior approach to abrogate lung adenocarcinoma growth *in vivo* compared to chemotherapy only.

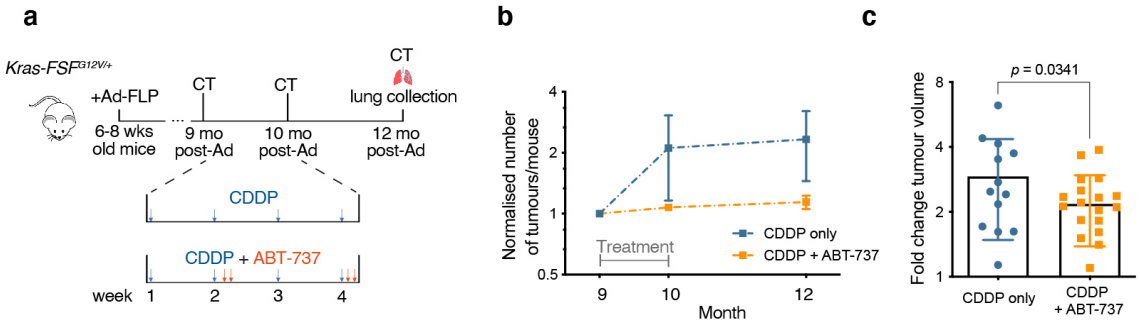

Figure 4.2. Combination of senolytic treatment with platinum-based chemotherapy significantly decreases tumour burden in the KrasFSF$^{G12V/+}$ mouse model of NSCLC. a. Schematic representation of experimental timeline used to determine effect of chemotherapy ± senolytic treatment in lung adenocarcinoma in KrasFSF$^{G12V/+}$ animals. **c.** Number of tumours per mouse upon chemotherapeutic/senolytic treatment, as assessed by micro-CT imaging and analysis, normalised to the initial number of tumours in each animal pre-treatment (n = 3 per group). Data is shown as mean ± SEM. **d.** Fold change tumour volume at month 12 post-AdFLP administration, relative to tumour volume at pre-treatment time-point (month 9). Data is shown as mean ± SD. Statistical significance was assessed by two-tailed unpaired Student's t-test.

While the histological assessment performed by Roberson and colleagues was relevant, the detection of SA-β-gal in tumour specimens is insufficient to fully confirm a senescent phenotype *in vivo*. In order to further explore the potential of a senescent response upon platinum-based chemotherapy in human clinical settings, we analysed the expression of different proliferation and senescence-related markers in stage II-III human lung adenocarcinoma samples resected from individuals within one month of chemotherapeutic regiment completion (for more clinical and pathological information regarding the patients, see **Table 1**). Histological analysis showed that Ki-67 detection is heterogeneous and scattered throughout the tumours (**Figure 4.3**). Tumours were also immunoreactive for p21 and p16 cell cycle arrest markers, generally accumulating in the outer regions of the lesions and presenting a more dispersed pattern in the inner areas. Importantly, the sections where positive signal was observed for these two senescence-related markers substantially overlapped, revealing an association between the expression of the two cell cycle inhibitors (**Figure 4.3**). Despite no treatment-naïve tumour samples were assessed and, therefore, we cannot conclude an accumulation of these markers upon chemotherapeutic treatment, the regional association between the

two cell cycle-dependent kinase inhibitors is compatible with the accumulation of a senescent response in different tumour areas.

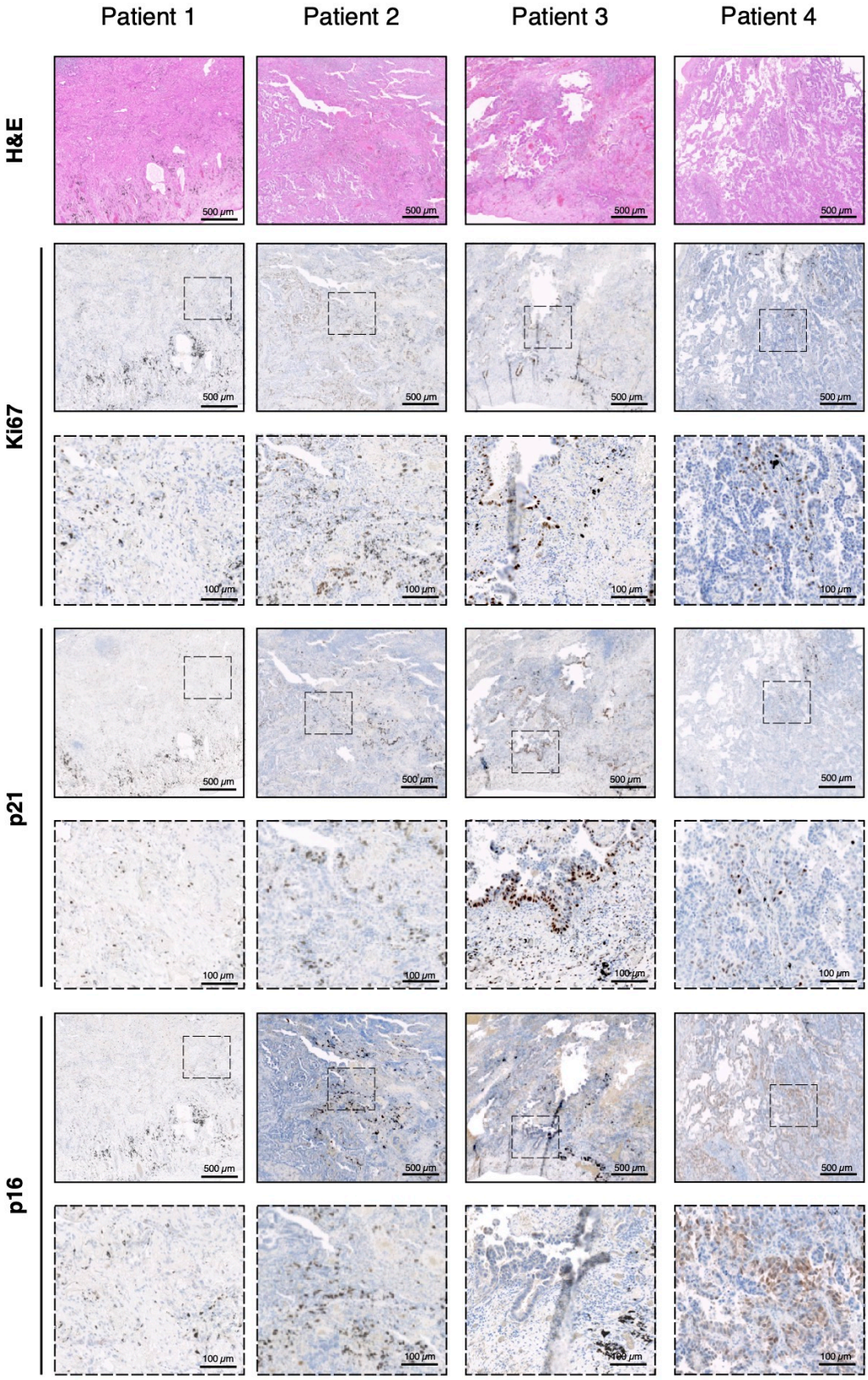

Figure 4.3. Human lung adenocarcinomas from patients subjected to neoadjuvant platinum-based chemotherapy express senescence-related markers suggesting the induction of cellular senescence in the tumours. Representative histological images of lung adenomas resected from patients within 1 month of completing neoadjuvant platinum-based chemotherapeutic treatment (**Table 1**). Lung tumour sections were stained for H&E, Ki67, p16 and p21, and images depict a representative region from each patient. Scale bar = 500 or 100 μm as shown in picture.

Taken together, our analyses with patient samples and genetically-engineered mouse models of KRas-driven NSCLCL are compatible with the induction of cellular senescence in lung adenocarcinomas upon platinum-based drug treatment. Intriguingly, we further demonstrate that senolytic treatment combined with cisplatin administration improves therapeutic outcomes, suggesting that the removal of senescent cells abrogates tumour growth, and therefore the accumulation of senescent cells might interfere with therapeutic effectiveness and contribute to tumour progression.

4.2.2. Chemotherapeutic agents induce a senescent response in human and murine lung adenocarcinoma cells

After exploring and having evidence of the induction of senescence in murine and human tumours upon cisplatin treatment *in vivo* and in clinical settings, we next evaluated the response to cisplatin and other common chemotherapeutics in the A549 human lung adenocarcinoma cell line and the primary *Kras*$^{G12D/+}$;*p53*$^{-/-}$ L1475(luc) cell line (also commonly known as KP cells [300]), in order to establish an *in vitro* model to investigate and compare the effects of cisplatin-induced senescence. Cells were subjected to increasing concentrations and treatment durations of each of the chemotherapeutic drugs until the optimal concentrations for senescence inductions were determined.

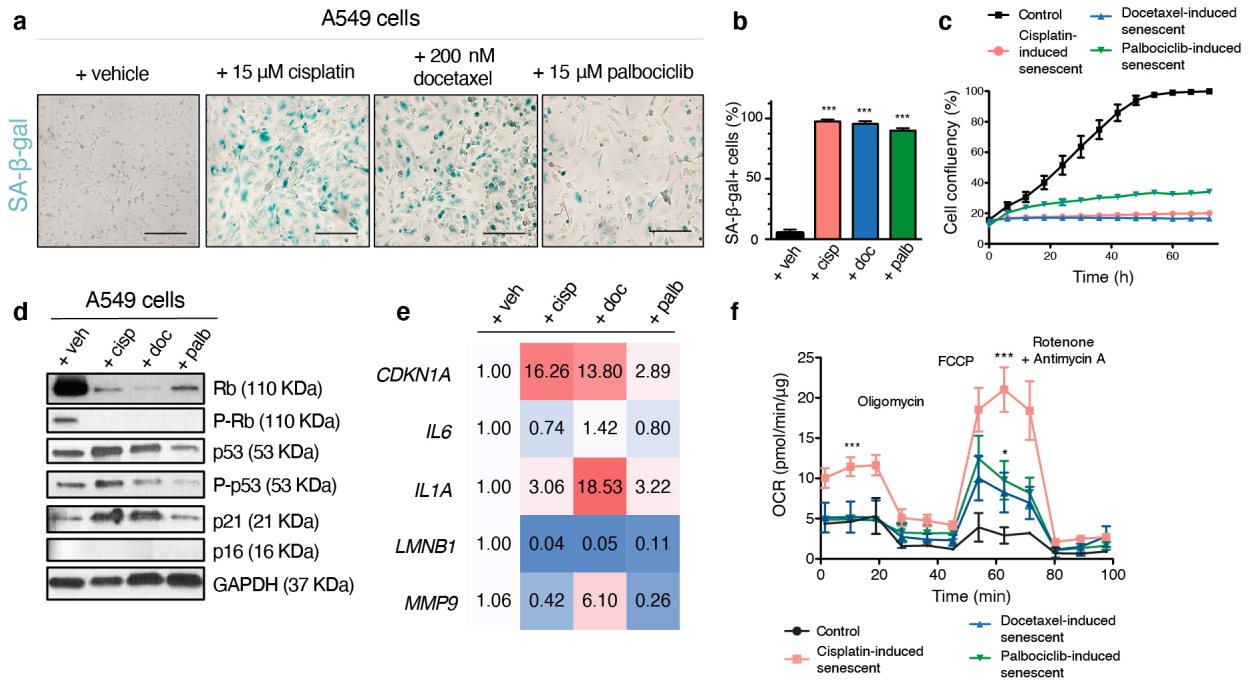

Figure 4.4. A549 cells undergo cellular senescence upon treatment with cisplatin, docetaxel and palbociclib *in vitro.* **a.** Representative images of control and chemotherapy-treated A549 cells fixed and stained for SA-β-gal activity after 7 days of treatment. Scale bar = 100 μm. **b.** Proportion of SA-β-gal+ A549 cells for each treatment. **c.** Cell confluency over time of control and senescent A549 cells after 7 days of treatment ($n = 3$). **d.** Western blot analysis for the expression of relevant senescence markers in control and senescent A549 cells upon 7 days of treatment. Note that A549 cells bear a deletion of the *INK4/ARF* locus and hence do not express p16**. e.** Fold change gene expression levels of different senescence markers in senescent A549 cells relative to vehicle-treated cells. **f.** Oxygen-consumption rate (OCR) of control and cisplatin-, docetaxel- and palbociclib-induced senescent A549 in basal conditions and upon injection of oligomycin, FCCP, rotenone and antimycin A. Statistical significance was assessed by one-way or two-way ANOVA, followed by Tukey's multiple comparisons test, $*p < 0.05$, $**p < 0.01$, $***p < 0.005$.

As observed in **Figure 4.4a**, A549 cells increased the expression of senescence marker SA-β-gal upon treatment with 15 μM cisplatin, 200 nM docetaxel and 15 μM palbociclib for 7 days. Quantification analysis confirmed a significant increase in SA-β-gal-positive cells for all chemotherapeutic-treated cells compared to control (**Figure 4.4b**). In addition, cell growth evaluation over a 72 h period after completing the 7 days of treatment confirmed the cell cycle arrest that characterises cellular senescence for all three chemotherapeutics compared to control A549 cells (**Figure 4.4c**). We further validated the upregulation of several senescence-related markers at the protein level, including the decrease in phosphorylated Rb (**Figure 4.4d**). Of note, A549 cells are null

for the cell cycle inhibitor p16 (encoded by the *CDKN2A* gene). RT-qPCR analyses confirmed increased levels of expression of *CDKN1A*, *IL6*, *IL1A* and *MMP9*, and the downregulation of *LMNB1* (**Figure 4.4e**). Finally, as part of our interests in understanding the metabolic and respiratory changes in the cells, we analysed the bioenergectic profile of control and senescent cells, and observed that cisplatin-induced senescent cells present a significantly higher basal respiration rate compared to control cells (**Figure 4.4f**). Of note, all senescent cells presented a significantly increased maximal respiration rate upon FCCP injection, with cisplatin-induced senescent cells displaying the highest rate among the three chemotherapeutics (**Figure 4.4f**).

We next continued our senescence assessment in the murine L1475(luc) line, and confirmed that after treatment with 3 μM cisplatin, 100 nM docetaxel and 20 μM palbociclib for 5 days, cells displayed relevant features of senescence. As observed in **Figure 4.5a**, SA-β-gal staining was not as prominent in these cells compared to A549, but quantification analysis confirmed a significant increase in SA-β-gal-positive cells for all chemotherapeutic-treated cells compared to control (**Figure 4.5b**). Further, cell growth evaluation over a 72 h period after the 5 days of treatment confirmed the cell cycle arrest that characterises cellular senescence for all three chemotherapeutics compared to control L1475(luc) cells (**Figure 4.5c**). Of note, Western blot analyses were not successful with these cell line, as they are null for *TP53* gene, encoding for tumour suppressor p53, and therefore no changes were observed. In addition, antibodies against phospho-Rb and $p16^{Ink4a}$ did not result in positive reactivity. However, when we assessed changes at the transcription level, we observed a marked increase in the expression of cell cycle inhibitors *Cdkn1a* and *Cdkn2a* (encoding for p21 and p16, respectively), as well as for SASP factors *Il6, Il1a* and *Mmp9*. We next observed a marked downregulation of *Lmnb1*, further confirming a phenotype consistent with senescence in the cells (**Figure 4.5d**). Finally, mitochondrial respiration analysis of the cells confirmed the same trend as observed with A549 cells, with the exception of docetaxel-induced senescent L1475(luc) cells, which did not present an increased maximal respiration rate compared to control cells (**Figure 4.5e**).

These analyses confirmed that A549 and L1475(luc) cells can effectively undergo a stable cell cycle arrest and enter a robust senescent programme upon treatment with

cisplatin, docetaxel and palbociclib *in vitro*, allowing for the further assessment of our working hypothesis.

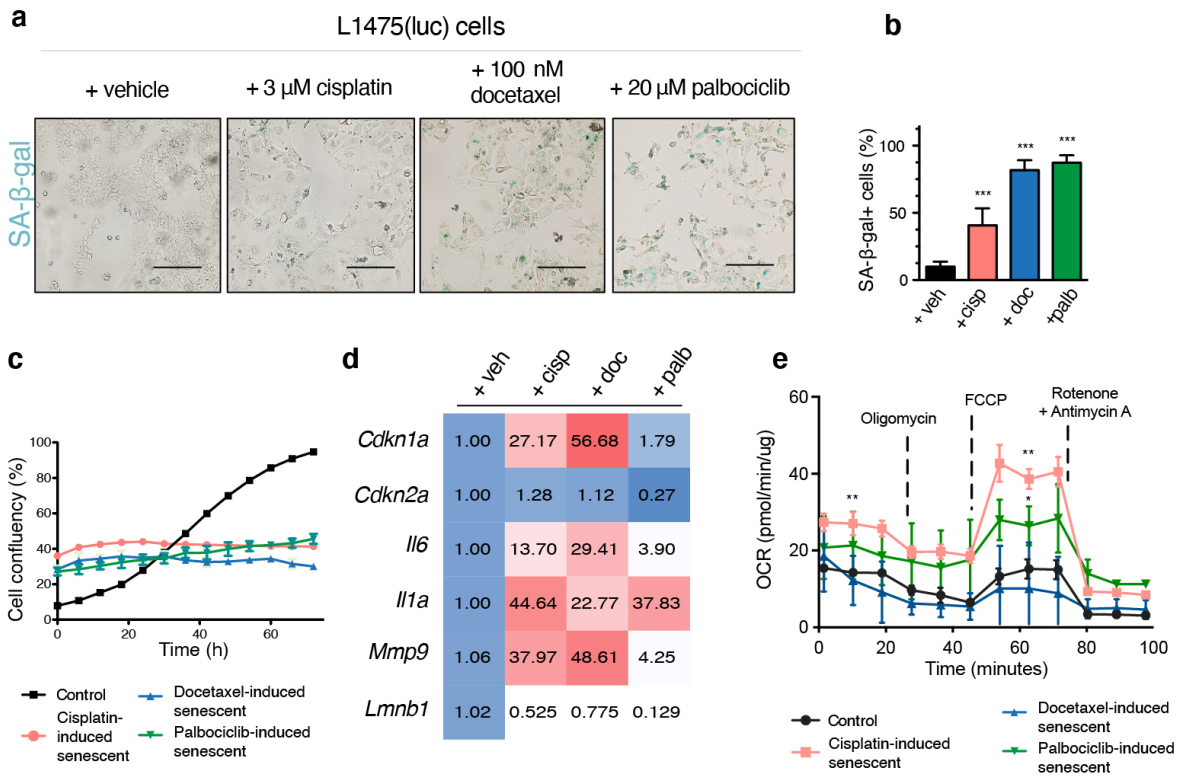

Figure 4.5. L1475(luc) cells undergo cellular senescence upon treatment with cisplatin, docetaxel and palbociclib *in vitro*. **a.** Representative images of control and chemotherapy-treated L1475(luc) cells fixed and stained for SA-β-gal activity after 5 days of treatment. Scale bar = 100 µm. **b.** Proportion of SA-β-gal+ L1475(luc) cells for each treatment. **c.** Cell confluency over time of control and senescent L1475(luc) cells after 5 days of treatment (n = 3). **d.** Fold change gene expression levels of different senescence markers in senescent L1475(luc) cells relative to vehicle-treated cells. **e.** Oxygen-consumption rate (OCR) of control and cisplatin-, docetaxel- and palbociclib-induced senescent L1475(luc) in basal conditions and upon injection of oligomycin, FCCP, rotenone and antimycin A. Statistical significance was assessed by one-way or two-way ANOVA, followed by Tukey's multiple comparisons test, $*p < 0.05$, $**p < 0.01$, $***p < 0.005$.

4.2.3. Cisplatin-induced senescence of lung cancer cells promotes the acquisition of malignant properties in non-senescent untreated cells *in vitro* through the SASP

Mounting evidence has demonstrated that therapy-induced senescence can promote a chronic inflammatory niche in the tumour, which in turn has been reported to modulate

tumorigenesis and drive tumour progression via the SASP [167, 301]. To investigate the effects of chemotherapy-derived SASP, we used A549 cells and *Kras*$^{G12D/+}$*;p53*$^{-/-}$ L1475(luc) cells subjected to cisplatin, docetaxel and palbociclib treatments, which effectively undergo cellular senescence (**Figures 4.4** and **4.5**, respectively). First, medium was conditioned for 48 h with each type of senescent cells upon drug removal, and untreated A549 cells were exposed to each type of drug-free conditioned medium (CM) (**Figure 4.6a**). Our analyses revealed that exposure to cisplatin-derived SASP resulted in increased cell proliferation, compared to control CM and docetaxel- and palbociclib-derived SASPs, with exposed cells achieving an average 85.4% confluency at 42 h in the presence of cisplatin-induced senescent CM versus 53.2% in control conditions (**Figure 4.6b**). Cell tracking during wound-healing scratch assay showed that exposure to cisplatin-SASP also significantly increased A549 cells migration, compared to all other conditions (**Figure 4.6c**).

We next detected that exposure to cisplatin-induced senescent CM for 10 days led to a 3.4-fold increase in the number of colonies formed compared to control CM, while palbociclib-induced senescent CM had no effect and docetaxel-derived SASP resulted in a significantly lower number of colonies (**Figure 4.6d, top**). The number of spheres formed in low-attachment conditions was also significantly higher in the presence of cisplatin-derived SASP compared to all other conditions. Notably, these spheres also exhibited irregular morphologies as well as the formation of protrusions (**Figure 4.6d, bottom**), which, together with enhanced migration properties observed in our wound-healing analyses, interestingly suggested the acquisition of an invasive phenotype consistent with an Epithelial-to-Mesenchymal Transition (EMT). To study the effect of the direct interaction between senescent and untreated tumour cells instead of exposure to CM, we cultured A549 cells in a three-dimensional (3D) spheroid system alone or co-cultured with chemotherapy-induced senescent cells. Notably, 3D co-culture with cisplatin-induced senescent A549 cells resulted in the development of significantly bigger spheres compared to all other conditions (**Figure 4.6e**).

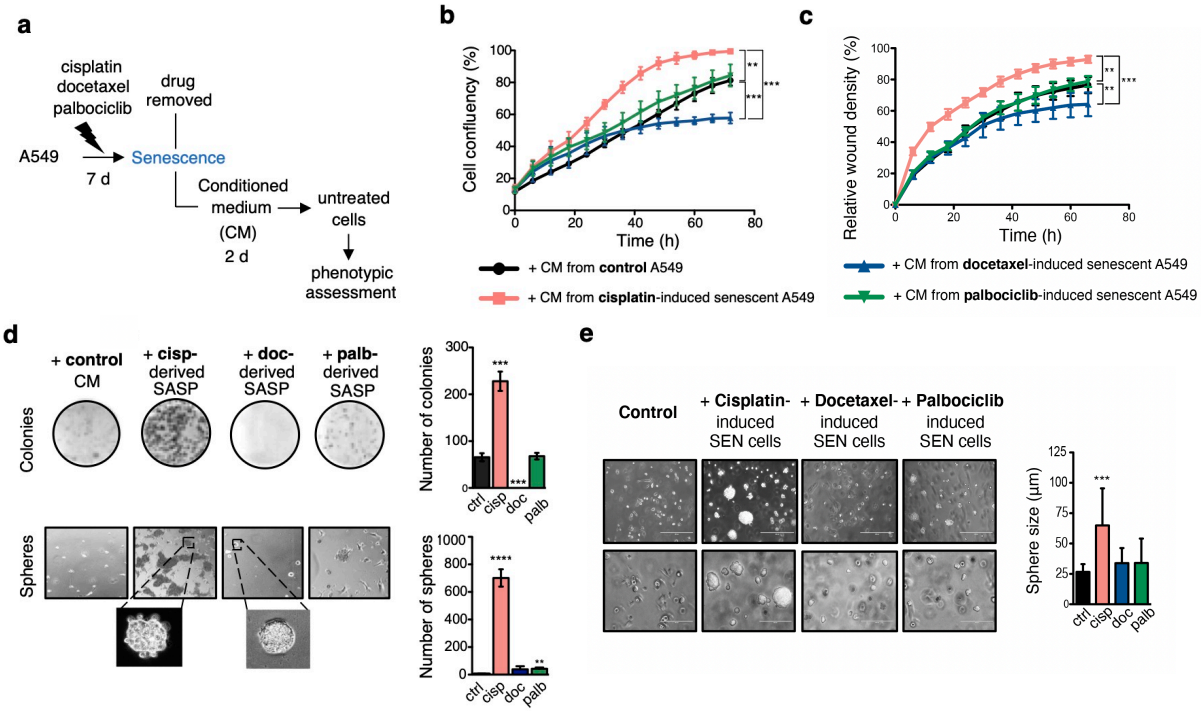

Figure 4.6. Cisplatin-induced senescence promotes malignant traits on non-senescent A549 cancer cells through the secretion of SASP factors. a. Schematic representation of experimental layout to test the effect of chemotherapy-derived SASP on non-senescent cells. A549 cells were treated with 15 µM CDDP, 150 nM docetaxel or 15 µM Palbociclib for 7 days for senescence induction. Senescent cells were subsequently washed and fresh medium was added and conditioned for 48 h. Conditioned Media (CM) were collected, centrifuged and added onto non-senescent A549 cells, which were subsequently assayed for phenotypic assessment. **b**. A549 cell confluency (%) over a 72 h incubation-period exposed to CM from control or chemotherapy-induced senescent cells. **c**. Relative wound density of migrating A549 cells after scratching over a 66 h period exposed to CM from control or chemotherapy-induced senescent cells. **d**. Left, representative images of A549 colonies (top) and spheres (bottom) formed after 10 days upon the exposure to the different CMs from non-senescent and chemotherapy-induced senescent cells. Right, quantification of the number of colonies (top) and the number of spheres (bottom) for each experimental condition. **e.** Left, representative images of A549 3D tumour spheres formed after 7 days of two-phase co-culture with control or chemotherapy-induced senescent cells. Right, quantification of sphere size in each experimental condition. Data are shown as mean ± SD (n = 3). Statistical significance was assessed using two-tailed one-way or two-way ANOVA, followed by Tukey's multiple comparisons test, **p < 0.01, ***p < 0.005, ****p < 0.001.

As part of our interest in understanding the changes occurring in cells upon exposure to cisplatin-derived SASP, we subjected A549 cells to a mitochondrial stress metabolic assay after the incubation with CM for 48 h. Oxygen Consumption Rate (OCR)

analysis upon injection of drugs targeting different complexes of the mitochondrial respiratory chain revealed a significantly increased maximal respiration in cells exposed to cisplatin-derived SASP compared to control (**Figure 4.7a**), suggesting a metabolic rewiring characterised by an increased ability to appropriately respond to high demands of ATP, and therefore a higher endurance during stress periods. No changes in respiratory ability were detected after the incubation of A549 cells with docetaxel- or palbociclib-induced senescent CM (**Figure 4.7b, c**).

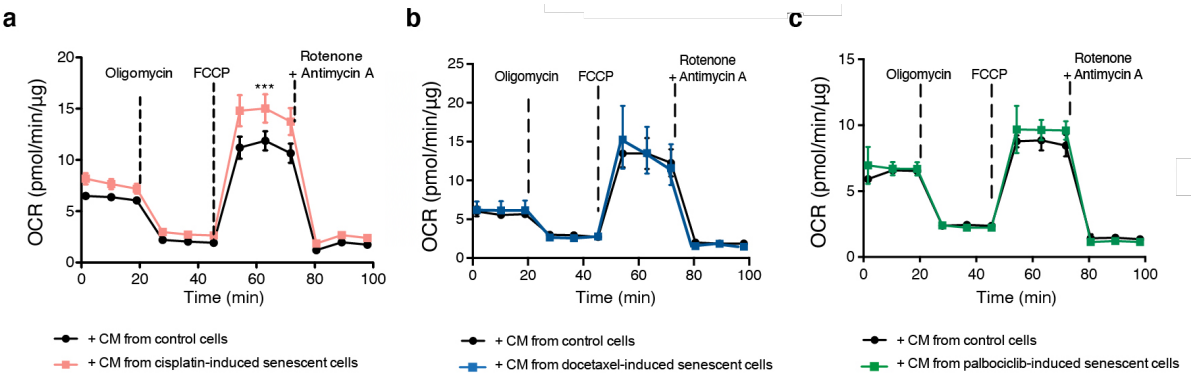

Figure 4.7. Bioenergetic profiling reveals that exposure of untreated A549 cells to cisplatin-induced senescence CM significantly increases basal and maximal respiratory rate, as opposed to other chemotherapies-derived SASPs. OCR of untreated A549 cells exposed to control and (**a**) cisplatin-induced senescent CM, (**b**) docetaxel-induced senescent cell CM and (**c**) palbociclib-induced senescent cell CM, in basal conditions and upon the injection of mitochondria-targeting drugs. Graphs show one representative biological repeat out of three independently performed (n = 3). Statistical significance was assessed using two-tailed one-way or two-way ANOVA, followed by Tukey's multiple comparisons test, **p < 0.01, ***p < 0.005, ****p < 0.001.

To determine whether acidification or lower nutrient levels in CMs could be having an effect, we analysed the pH and glucose concentration and observed no changes between the different CMs (**Figure 4.8 a, b**), indicating that factors secreted by the cells to the CM, rather than biochemical changes or difference in nutrients, are the drivers of the paracrine effects detected.

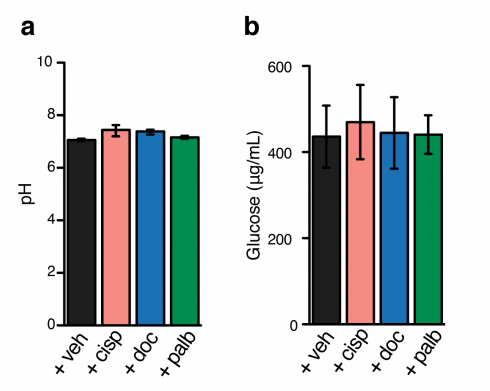

Figure 4.8. Glucose and pH levels of the different CMs from control- and senescent A549 cells remain unaltered. a. Average pH measurements of the conditioned media (CM) collected from control and senescent A549 conditioned for 48 h post-removal of drug. **b.** Glucose levels of CM from control and senescent A549 cells conditioned for 48 h pot-removal of drug.

We next aimed to validate our findings using the primary KRas$^{G12D/WT}$;p53$^{-/-}$ murine L1475(luc) cell line, which also effectively underwent cellular senescence upon cisplatin, docetaxel and palbociclib treatments (**Figure 4.5**). Of note, these cells grow in clusters and become smaller as the clusters increase in size, and therefore cell confluency analysis did not fully recapitulate change in cell number. For this reason, we opted to assess cell growth by flow cytometry-based quantification. Relative cell count upon 48 h of exposure to CMs demonstrated that cisplatin-induced senescent CM also increased proliferation in untreated L1475(luc) cells compared to all other conditions, with a striking average fold cell count of 4.65 versus control (**Figure 4.9a**). In addition, culture of L1475(luc) with cisplatin-induced senescent CM for 10 days resulted in a significantly higher number of colonies formed, following the same trend observed for human A549 cells (**Figure 4.9b**). In addition, respiratory profiling of cells exposed to cisplatin-derived CM revealed a significantly enhanced maximal respiration, in line with our findings in human cells (**Figure 4.9c**). In contrast with these cells, L1475(luc) cells exposed to docetaxel- and palbociclib-induced senescent CM also presented increased OCR levels, despite to a lower extent compared to cisplatin-derived SASP exposure (**Figure 4.9d, e**).

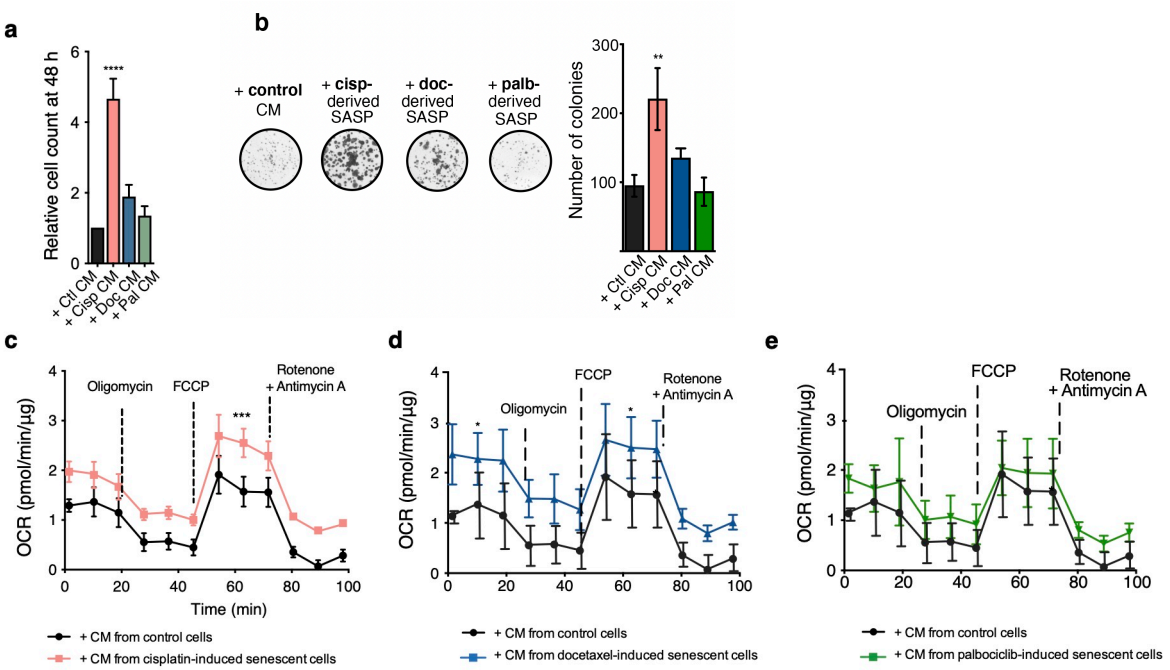

Figure 4.9. Cisplatin-induced senescence promotes malignant traits on non-senescent murine L1475(luc) cancer cells through the secretion of SASP factors. a. Left, L1475(luc) cell count relative to control condition of cells exposed to control- or chemotherapy-induced senescent CM for 48 h. **b.** Left, representative images of L1475(luc) colonies formed upon exposure to control- or chemotherapy-induced senescent CM for 10 days. Right, quantification of the number of colonies formed in each experimental condition. **c, d, e.** OCR of untreated L1475(luc) cells exposed to control and (**c**) cisplatin-induced senescent CM, (**d**) docetaxel-induced senescent cell CM and (**e**) palbociclib-induced senescent cell CM, n basal conditions and upon the injection of mitochondria-targeting drugs. Graphs show one representative biological repeat out of three independently performed ($n = 3$). Statistical significance was assessed using two-tailed one-way or two-way ANOVA, followed by Tukey's multiple comparisons test, **p < 0.01, ***p < 0.005, ****p < 0.001.

Altogether, our *in vitro* assessments on both human and murine lung adenocarcinoma cells indicate that cisplatin treatment results in a particular type of senescence that can drive the acquisition of malignant properties in untreated cells through the SASP, promoting tumour cell proliferation, migration and enhanced respiratory endurance.

4.2.4. Cisplatin-induced senescent SASP promotes tumour proliferation *in vivo*

With the aim to validate the ability of cisplatin-induced senescence to drive increased tumour cell proliferation in physiological models, we first co-transplanted subcutaneously cisplatin-induced senescent A549-GFP$^+$ cells together with untreated A549-mCherry$^+$ cells and analysed the growth of the xenografts formed over time (**Figure 4.10a**). As observed in **Figure 4.10b**, relative tumour volume was significantly higher when tumour cells were co-transplanted with senescent cells, as compared to untreated cells transplanted alone. Strikingly, by day 21, co-transplanted tumours (untreated + senescent cells) were 2.18 times the volume of control tumours (co-transplanted, 325.44 mm^3 average tumour volume; control, 149.00 mm^3) (**Figure 4.10b**). Importantly, transplantation of senescent cells alone resulted in xenograft recession, confirming the effect in co-transplanted tumours was likely driven through paracrine support from senescent cells and not because of senescence escape and cell cycle re-entry. Mean tumour weight of co-transplanted xenografts was also significantly higher than untreated tumours and senescent tumours (co-transplanted tumours, 251.11 mg mean tumour weight; control, 156.67 mg; senescent-only, 37.22 mg) (**Figure 4.10c**). Of note, histological analyses of the tumours confirmed decreased levels of the proliferative marker Ki67 and increased expression of p21 in senescent xenografts compared to untreated and co-transplanted tumours (**Figure 4.10d**). Representative pictures of the resected tumours at experiment completion are shown in **Figure 4.10e**. Despite fluorescent signal imaging confirmed senescent tumours were uniquely GFP$^+$ and control tumours were positive for mCherry signal, we did not observe GFP signal in co-transplanted tumours, as expected. Of note, the number of senescent cells transplanted in mixed tumours was 4 times lower than in senescent-only tumours, and thus it is possible that the outgrowth of untreated co-transplanted mCherry+ cells in these tumours might have masked any GFP signal remaining from senescent cells. Another possibility is that the co-transplantation with untreated tumour cells drives an increase in senescent cell clearance in the tumours. Despite cells were transplanted in an immunodeficient mouse model (SCID) that lacks both B and T lymphocytes, these mice have normal NK, macrophages and granulocytes,

and therefore senescent clearance could also explain the lack of GFP signal in co-transplanted tumours (**Figure 4.10e**).

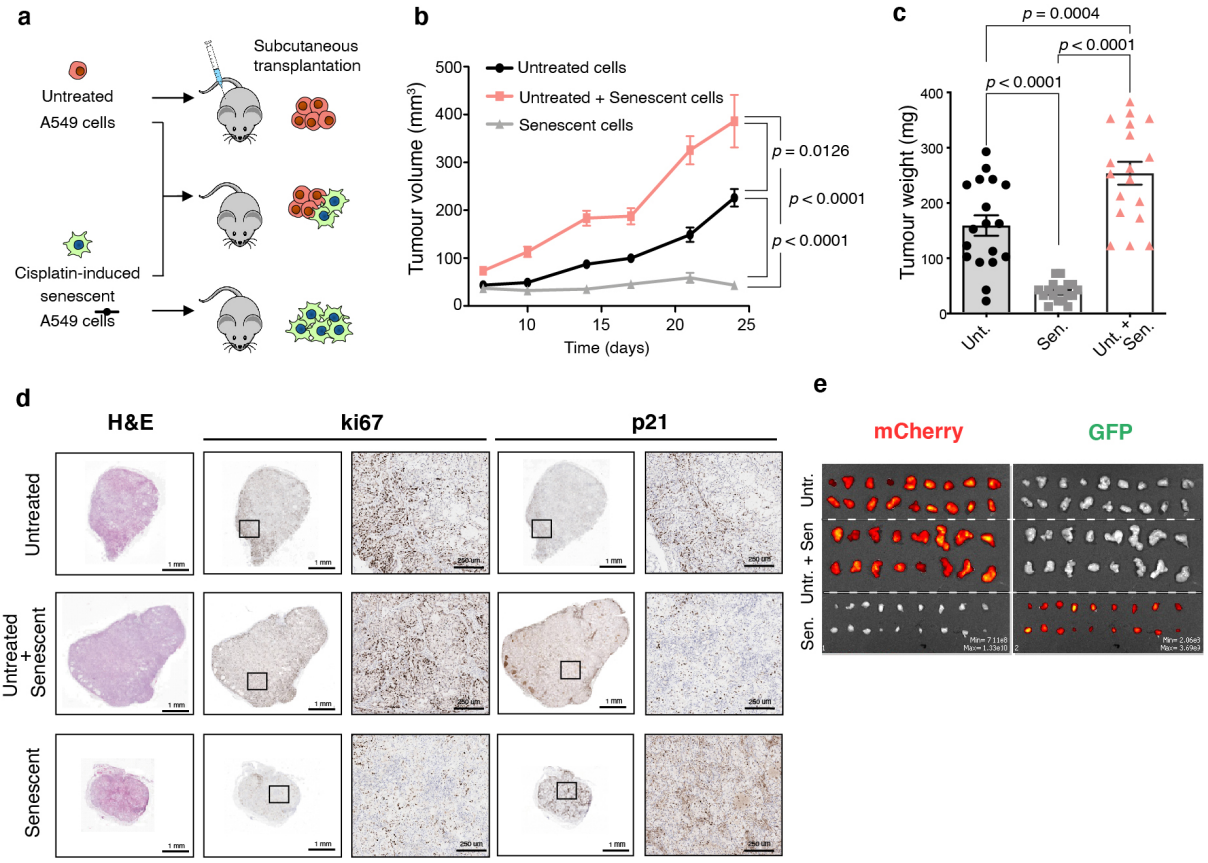

Figure 4.10. Cisplatin-induced senescent A549 cells drive increased xenograft growth *in vivo*. **a.** Schematic representation of experimental layout using the subcutaneous xenograft model. Briefly, animals were transplanted with either $4x10^6$ untreated A549-mCherry+ cells, $4x10^6$ untreated A549-mCherry+ cells and $1x10^6$ cisplatin-induced senescent A549-GFP+ cells, or $4x10^6$ cisplatin-induced senescent A549-GFP+ cells alone in the flank. **b.** Tumour volume of xenografts over time. Data is shown as mean ± SEM (n = 18 tumours per group). **c.** Mean tumour weight at experimental endpoint resected from mice transplanted with untreated A549 cells, a combination of untreated and cisplatin-induced senescent A549 cells or senescent-cells only (n = 18 tumours per group). **d.** Representative histological images of resected xenograft from each experimental group, stained for H&E, Ki67 and p21 expression. **e.** Fluorescent images of resected tumours at the end of the experiment. Data in **b** and **c** are shown as mean ± SEM. Statistical significance for tumour volume was assessed using two-way ANOVA, followed by Tukey's multiple comparisons test.

We next investigated the paracrine effects of cisplatin-induced senescence using a $KRas^{G12D/WT};p53^{-/-}$ orthotopic murine model. L1475(luc) cells were continuously exposed to control or cisplatin-induced senescent CM for 10 days and were subsequently

transplanted in the lungs of C57BL/6 mice via tail-vein injection (**Figure 4.11a**). The expression of luciferase in these cells allowed the analysis of tumour burden over time via D-luciferin administration and longitudinal bioluminescence imaging. We observed that the transplantation of cells that had been exposed to cisplatin-derived SASP resulted in a significantly greater luciferase activity in the lungs, relative to day 1 post-injection (**Figure 4.11b**). Representative images of luciferase signal at 17 days post-transplantation are shown in **Figure 4.11c**, and higher number and size of tumour foci in lungs transplanted with cells exposed to cisplatin-derived SASP at the same time-point can be observed in **Figure 4.11e**, stained with haematoxylin and eosin. Notably, the transplantation of tumours previously exposed to cisplatin-induced senescent CM resulted in a significant decrease in survival by 30 %, with an average median survival of 23 days compared to 32.5 in mice transplanted with tumours pre-conditioned with control CM (**Figure 4.11d**).

To test whether sustained increased proliferation after exposure to cisplatin-derived SASP could explain the accelerated tumour growth in animals, we analysed cell proliferation of cells pre-conditioned in parallel to transplantation. As previously observed, during CM exposure, cells under cisplatin-SASP conditions proliferated faster than those exposed to control CM (**Figure 4.11f**). However, upon removal of CM and culture of pre-conditioned cells in normal media conditions, we observed that the paracrine effect of cisplatin-derived SASP on cell proliferation decreased after 48 h and was neglectable after 10 days (**Figure 4.11g**), suggesting that the increased tumour growth in animals transplanted with cells pre-exposed to cisplatin-induced senescent CM is likely due to an initial accelerated expansion driven by the recent exposure to the SASP, rather than a higher proliferation rate sustained in time.

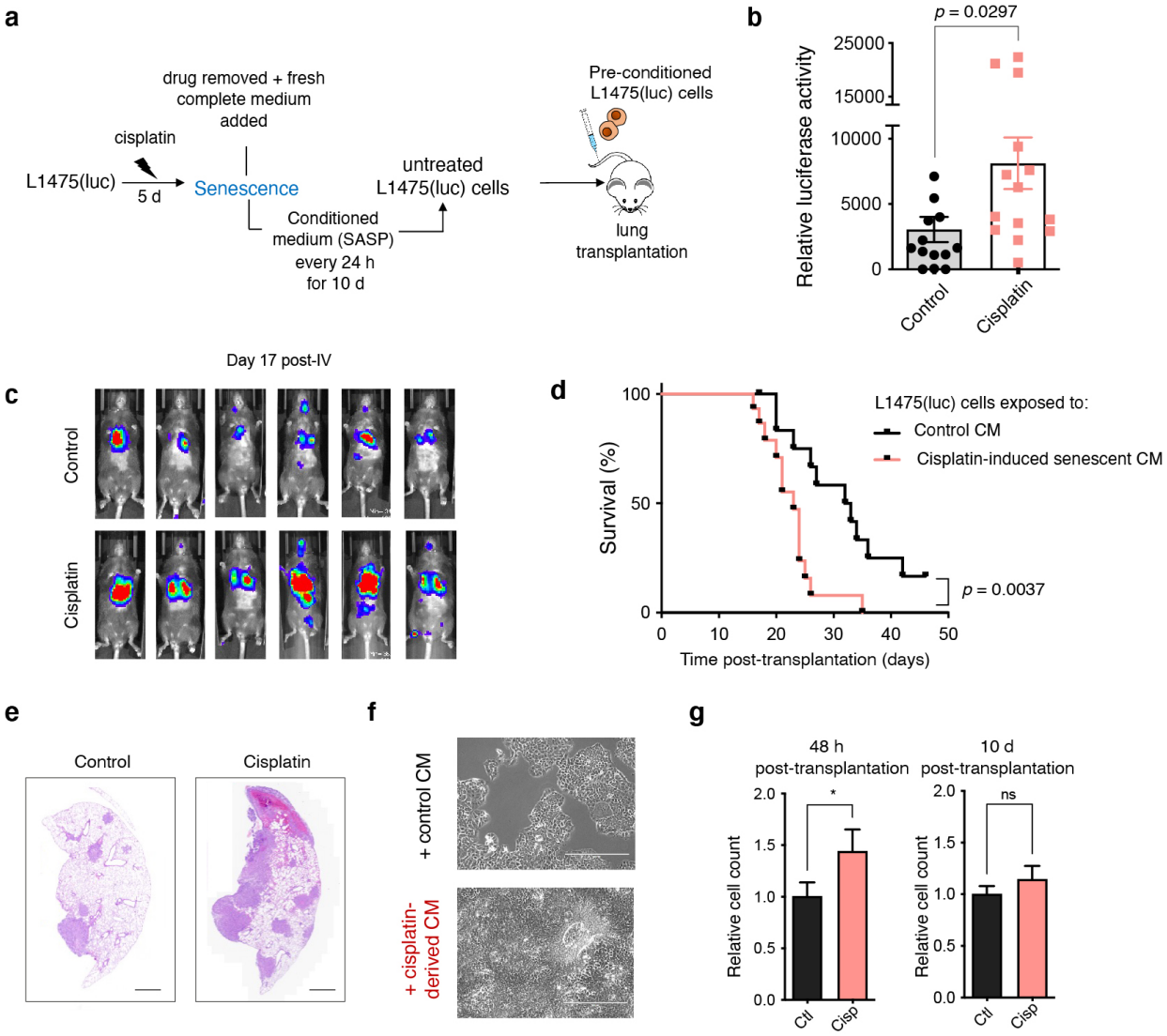

Figure 4.11. Transplantation of L1475(luc) cells previously exposed to cisplatin-induced senescent cell CM drives increased lung cancer growth compared to unexposed cells in an orthotopic model of NSCLC. a. Schematic representation of experimental layout. Briefly, untreated L1475(luc) cells were continuously exposed to the CM from control- or cisplatin-induced senescent cells for 10 days prior to lung transplantation via tail-vein injection. **b.** Quantification of luciferase activity at day 17 post-transplantation, relative to activity recorded on day 1 after cell transplantation (n = 14 per group). **c.** Representative images of luciferase activity in mice 17 days after transplantation with lung cancer cells exposed to control- or cisplatin-induced senescent cell CM. **d.** Survival curve of mice in each experimental group (n = 14 per group). **e.** Representative images of histological sections from lungs resected at 17 days post-transplantation of lung cancer cells in each experimental condition. Scale bar = 1 mm. **f.** Representative images of L1475(luc) cells exposed to control- and cisplatin-induced senescent CM prior to transplantation. Scale bar = 400 µm. **g.** Statistical significance for tumour volume and difference in relative cell count was assessed using two-tailed Student's t-tests. Data are shown as mean ± SEM in b and as mean ± SD. Survival analysis was performed using the Kaplan-Meier method and a two-sided log-rank test was conducted to determine statistical

significance. Orthotopic model data represents three independent experiments. *p < 0.05, n.s. = not significant.

As part of our interest in better understanding the impact of platinum-based chemotherapy at the systemic level, we next investigated the effects of cisplatin treatment prior to lung cancer transplantation in our orthotopic model. Anti-cancer treatments that are administered intravenously, like platinum-based chemotherapy, have been reported to induce senescence in noncancerous tissues as well [302]. This has not only been linked to the worsening of chemotherapy-derived side effects, but it can also promote cancer progression and metastasis effects [130]. In addition, consistent with the known increase of senescence burden (and cancer incidence) with age [303], and considering that the average age of lung cancer patients at diagnosis is 70 years, we decided to investigate the interplay between systemic senescence induction, ageing and tumour progression. To this aim, we subjected young and aged mice to two cycles of cisplatin treatment and then transplanted L1475(luc) cells orthotopically in the lungs (**Figure 4.12a**). Tumour burden analysis by bioluminescence imaging at 7 days post-transplantation revealed a trend for increased tumour volume in aged mice, despite the difference was not significant at this time-point (**Figure 4.12b**). However, analysis at day 14 after tumour transplantation showed a significantly higher relative luciferase activity in aged animals compared to young individuals (**Figure 4.12c**). Representative images of luciferase signal at day 7 and 14 post-injection of cells are shown in **Figure 4.12b** and **c**, respectively. Strikingly, survival in aged animals was decreased by 31%, with a median survival time of 14.5 days compared to 21 days in young animals (**Figure 4.12d**). Finally, in order to gain further insights on the impact of systemic therapy, we analysed body weight over time as an indirect measure of chemotherapy-related adverse effects, and observed no major differences between the groups during cisplatin administration. However, aged individuals suffered a marked weight loss shortly after tumour transplantation, while young mice recovered the weight lost upon the second dose of administration during that same time frame (**Figure 4.12e**). These results suggest that young individuals present higher tolerability towards cisplatin treatment, and that ageing exacerbates tumour progression.

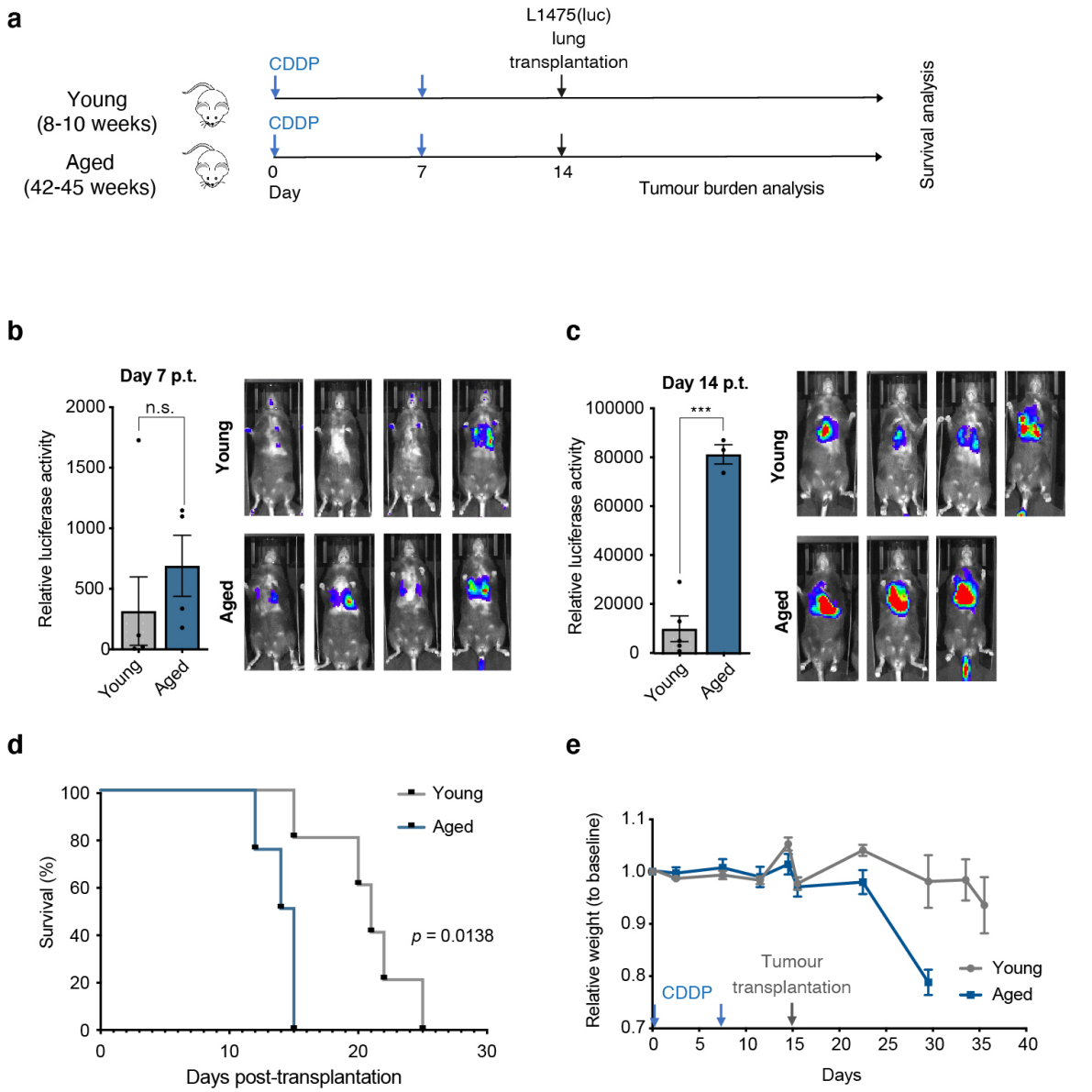

Figure 4.12. Cisplatin treatment in aged mice prior to orthotopic transplantation supports increased lung cancer growth compared to young mice. a. Schematic representation of experimental layout. Young (8-10-week old) and aged (42-45-week old) animals were subjected to two cycles of 1.5 mg/kg body weight CDDP treatment. Mice were then transplanted with L1475(luc) in the lungs via tail-vein injection; tumour burden was assessed twice a week by bioluminescence imaging and survival was determined as the time from tumour transplantation until the onset of moderate signs of disease. **b**. Left, quantification of luciferase activity at day 7 post-transplantation, relative to activity recorded on day 1 after cell transplantation (n = 4 per group). Right, representative images of luciferase activity in mice at the same time-point. **c**. Left, quantification of luciferase activity at day 14 post-transplantation, relative to activity recorded on day 1 after cell transplantation (young, n = 5; aged, n = 3). Right, representative images of luciferase activity in mice at the same time-point. **d**. Survival curve of mice in the in each experimental group. **e**. Weight relative to baseline over time. Two-tailed Student's t test was applied to assess significance relative luciferase activity. Survival

analysis was performed using the Kaplan-Meier method and a two-sided log-rank test was conducted to determine statistical significance. *p < 0.05, **p < 0.01, ***p < 0.005, *n.s.* = not significant.

Taken together, our findings confirm that the induction of senescence with cisplatin treatment in living organisms exerts detrimental effects in a paracrine fashion, boosting lung cancer progression and shortening lifespan.

4.2.5. Transcriptomic and proteomics analyses reveal differences in SASP signatures and highlight TGFβ ligands as potential factors driving pro-tumorigenic effects in cisplatin-derived SASP

To gain a deeper understanding of the changes that take place upon cisplatin-induced senescence, including those with a potential role in driving pro-tumorigenic properties, we next performed RNA-seq analyses of control, cisplatin-, docetaxel- and palbociclib-induced senescent A549 cells. Gene-set enrichment analysis (GSEA) showed the upregulation of several senescence-related pathways, including the *Fridman Senescence Up* and the *KEGG Cell Cycle* ranked signatures, in all chemotherapeutic-treated A549 cells compared to vehicle-treated cells, confirming the induction of the programme (**Figure 4.13b**). Scaled expression profile of the top differentially expressed genes are shown in the heatmap in **Figure 4.13a**. As expected, a much higher expression of mismatch repair and DNA repair-related genes were detected in cisplatin-treated cells. Notably, palbociclib-induced senescent cells presented the most distinct transcriptional profile compared to cisplatin- and docetaxel-induced senescent A549 cells. We next sought to uncover the genes exclusively upregulated in each type of chemotherapy-driven senescence, and observed that docetaxel-induced senescent cells present the highest number of uniquely upregulated genes (1961, including the significant representation of KEGG pathways such as *Hippo signalling*, *N-Glycan biosynthesis* and *Phyrimidine metabolism*, for instance), versus 751 in cisplatin-induced senescence (which were significantly overrepresented in *Proteoglycans in cancer*, *Pentose Phosphate metabolic pathway* and *TGF-β signalling* according to the KEGG database, among others) and 363

in palbociclib-induced senescent cells (**Figure 4.13d**) (overrepresented in *FoxO signalling*, *TNF signalling* and *Autophagy* KEGG pathways).

In order to characterise the changes in the secretory phenotype of each type of senescence, we next investigated the expression of known SASP factors in vehicle- and chemotherapy-treated A549 cells (**Figure 4.13c**). As expected, we observed a general increase in the transcription of inflammatory ligands and proteases in senescent cells, with the exception of cluster 9, which included the expression of factors such as CSF3, PLAUR, ANXA2 and EGFR, which were found generally expressed at a higher level in vehicle-treated A549 cells. Cluster 8, on the other hand, appeared particularly enriched in cisplatin-induced senescent cells versus docetaxel- and palbociclib-induced senescent and control A549 cells, which included genes encoding for CSF2RB, PDGFA and LIF.

To further understand the most significant changes at the signalling level upon senescence induction in A549 cells, we performed pathway enrichment analyses of significantly differentially expressed genes in each type of chemotherapy-induced senescent cells against pre-defined sets from the Molecular signatures database (MSigDB). This revealed a significant enrichment in metabolic pathways across the three types of senescence, including fatty acid metabolism, oxidative phosphorylation, and ROS-related pathways (**Figure 4.13e**). Importantly, biologically relevant pathways including IL-2/STAT5 and TGF-β pathways were found to be uniquely enriched in cisplatin-induced senescent cells, posing potential signalling cascades driving the paracrine effects observed for this type of senescence.

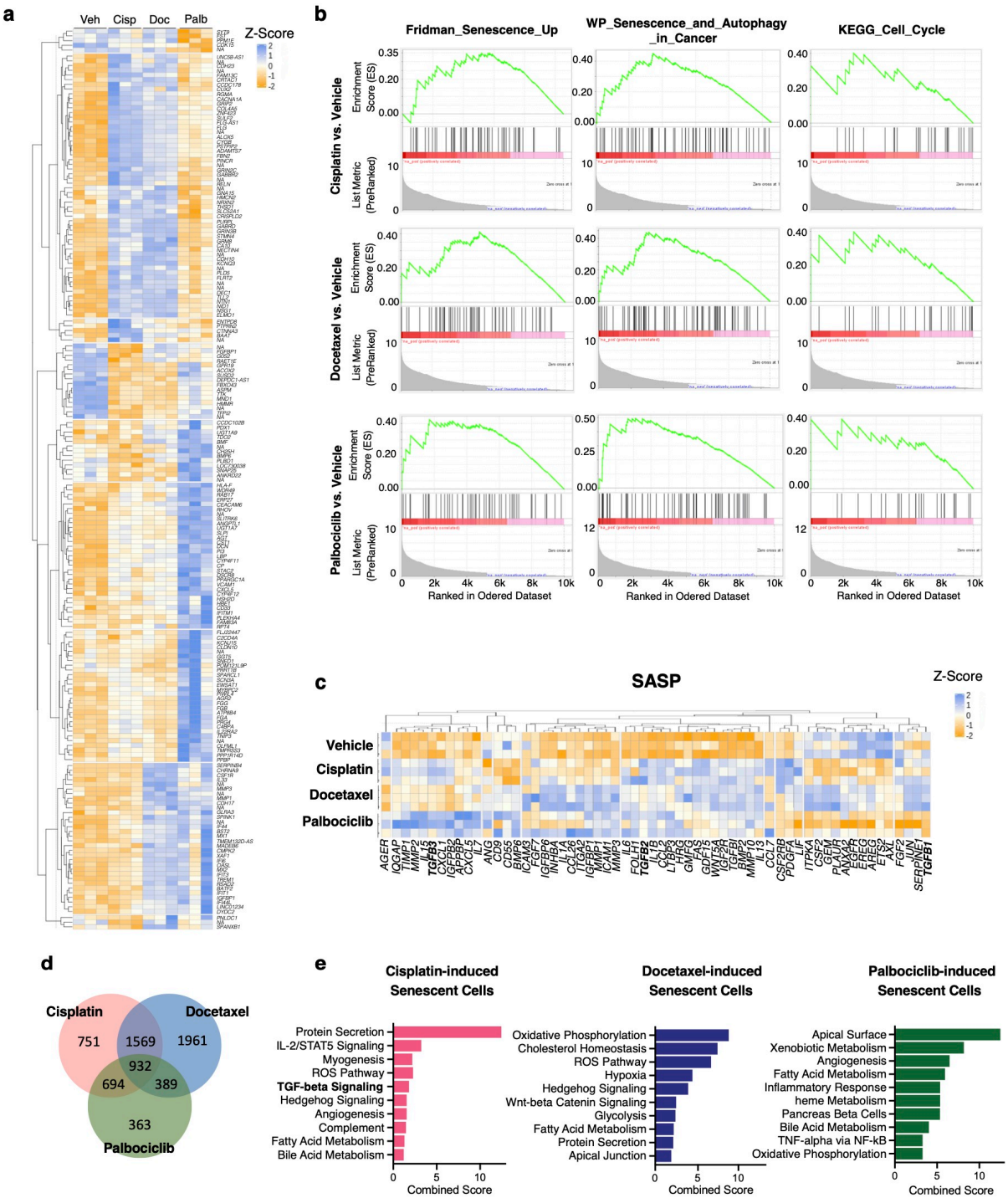

Figure 4.13. **Transcriptomic analysis reveals different transcriptional and SASP signatures of chemotherapy-induced senescent A549 cells. a.** Heatmap displaying expression z-scores of most significantly altered top gene expression changes and their hierarchical clustering in control and cisplatin-, docetaxel- and palbociclib-induced senescent A549 cells. **b**. GSEA of Fridman Senescence Up, WP Senescence and Autophagy in Cancer and KEGG Cell Cycle sets in cisplatin-, docetaxel- and palbociclib-induced senescent A549 cells versus untreated A549 cells. **c.** Heatmap of expression z-scores of selected SASP genes in control and cisplatin-, docetaxel- and palbociclib-induced senescent A549 cells. **d.** Venn diagram of the number of genes significantly upregulated in cisplatin-, docetaxel- and palbociclib-induced senescent A549 cells vs

control. **e.** Top differentially enriched pathways in MSigDB Hallmark 2020 collection, sorted by combined score ranking, in cisplatin-, docetaxel- and palbociclib-induced A549 senescent cells vs control.

In order to narrow down the factors likely driving increased proliferation in A549 cells, we decided to collaborate with the group of James Korkola at the Oregon Health & Science University (OHSU) to make use of a recently developed microenvironment microarray (MEMA) platform. This technology allows the screening of the effects of multiple combinations of individual factors and cytokines in a high-throughput manner and the subsequent analysis of treated cells read-outs through advanced imaging [304]. Remarkably, analysis of the proportion of high-EdU+ A549 cells upon 72 h treatment with an array of SASP-related ligands performed by our collaborators revealed that exposure to TGFβ-2 and TGFβ-1 led to the highest proliferation rate of all factors tested in the array (**Figure 4.14a**). Representative immunofluorescence images of the wells stained for DAPI, EdU and KRT5 (as a marker of tumour cells) can be seen in **Figure 4.14b**, highlighting the increased number of EdU-positive cells upon exposure to TGFβ-1 and TGFβ-2. We therefore hypothesized that increased secretion of TGF-β ligands could be mediating the pro-tumorigenic effects observed in cells that are exposed to cisplatin-derived SASP. Thus, we confirmed that cisplatin-induced senescent cells present an increased expression of *TGFB1*, *TGFB2* and *TGFB3* ligands in our RNA-seq data (**Figure 14.4c**), which was further validated by RT-qPCR analysis in both A549 and L1475(luc) cells (**Figure 4.14d**). Western blot investigation of control and senescent A549 cell extracts revealed increased protein levels of inactive and active TGFβ-1 in cisplatin-induced senescent cells versus control A549 cells, while free TGFβ-2 and TGFβ-3 expression was decreased (**Figure 4.14e**).

Biologically active TGF-β ligands are closely regulated in producing cells, where they are normally stored in a latent form, and the efficient secretion, folding and extracellular deposition requires tight regulation of multiple steps [218]. To determine whether the lower intracellular levels of the ligands observed by Western blot were due to an increased secretion to the extracellular compartment compared to control cells, we analysed the levels of the active form in the SASP by ELISA. Importantly, this confirmed that the CM of cisplatin-induced senescent cells is significantly enriched in active TGFβ-1,

TGFβ-2 and TGFβ-3 compared to control and docetaxel- and palbociclib-induced senescent cells (**Figure 4.14f**).

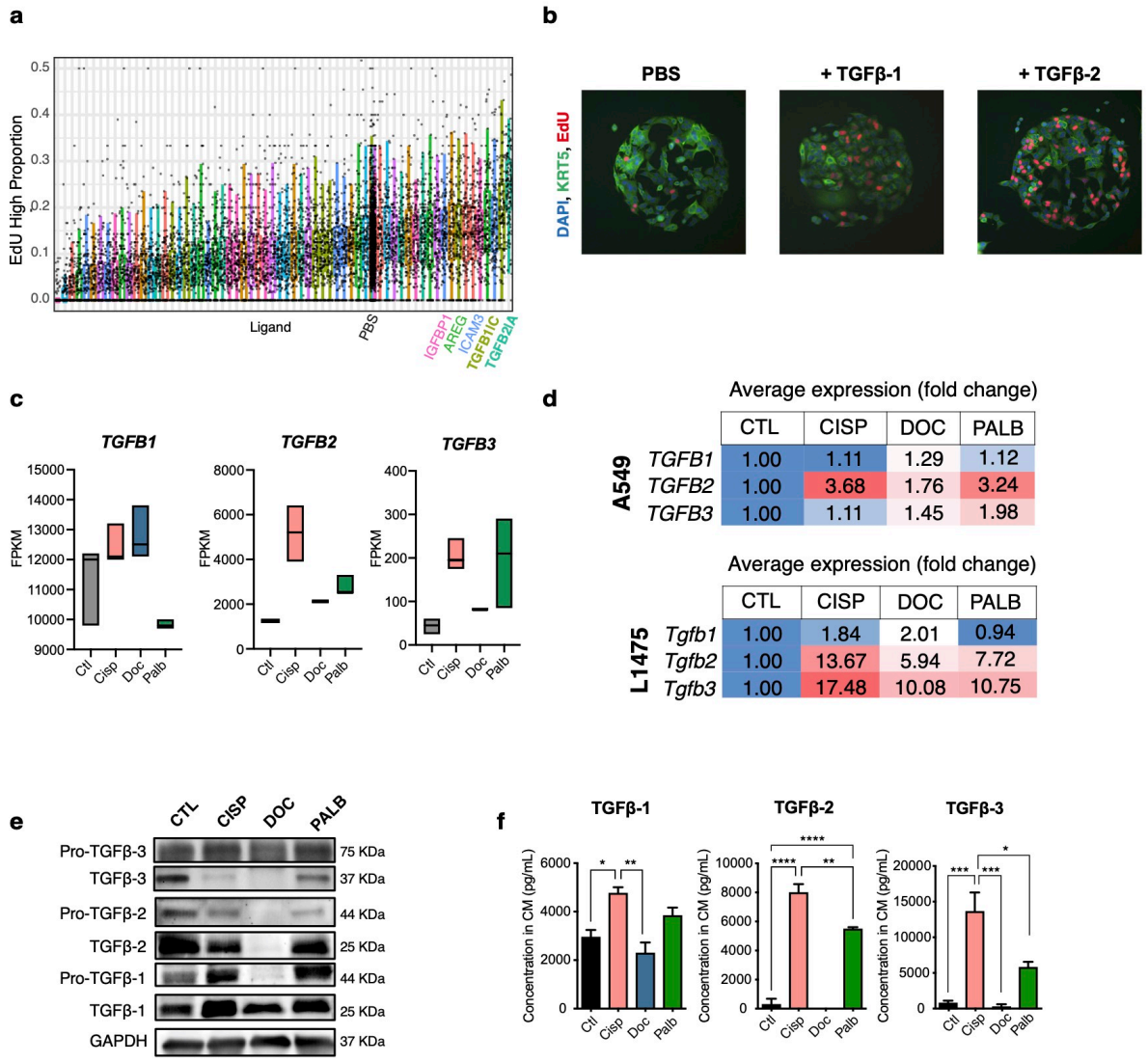

Figure 4.14. High through-put and transcriptomic data highlight TGFβ ligands as potential candidate drivers of malignant traits in cisplatin-derived SASP. a. Proportion of EdU High intensity A549 cells upon 72 h of exposure to different SASP ligands using the MEMA technology, ranked left to right form lowest induced proportion to highest. For the full list of factors assessed please refer to Table 9. **b.** Representative immunofluorescence images of MEMA wells containing A549 cells upon exposure to PBS, TGFβ-1 and TGFβ-2 recombinant ligands, depicting DAPI and KRT5 staining and EdU incorporation. **c.** Fragments per Kilobase of transcript per Million mapped reads (FPKM) of *TGFB1*, *TGFB2* and *TGFB3* ligands in control and cisplatin-, docetaxel- and palbociclib-induced senescent A549 cells. **d.** Fold change *TGFB1/Tgfb1*, *TGFB2/Tgfb2* and *TGFB3/Tgfb3* gene expression levels in control and chemotherapy-treated A549 and L1475(luc) cells. **e.** Western blot analysis of whole cell extracts of control and cisplatin-, docetaxel- and palbociclib-induced senescent A549 cells. **f.** Average concentration in CM of TGFβ1, TGFβ2 and TGFβ3 free ligands (activated) in each experimental condition measured by ELISA. Data are shown as mean ± SD ($n = 3$). Statistical significance

was assessed by one-way ANOVA, followed by Tukey's multiple comparisons test, $*p < 0.05$, $**p < 0.01$, $***p < 0.005$, $****p < 0.001$.

Together, these data indicate that chemotherapeutic treatment results in markedly distinct senescent transcriptional phenotypes, and suggest the secretion of TGF-β ligands in cisplatin-induced senescent A549 SASP as potential candidates promoting distinctive cisplatin-derived SASP pro-tumorigenic phenotypes on tumour growth.

4.2.6. TGFβR1-driven activation of Akt/mTOR pathway orchestrates the induction of increased proliferation upon exposure to cisplatin-derived SASP

Bioactive TGF-β cytokines secreted to the extracellular space activate downstream signalling responses in recipient cells by driving the dimerisation of TGFβR1 and TGFβR2, two pairs of receptor serine and threonine kinases, respectively. To test whether blocking of TGFβR1 was sufficient to reverse the pro-tumorigenic effects derived from the exposure to cisplatin-induced senescent SASP, A549 and L1475(luc) cells were grown in the presence of control- and cisplatin-derived CMs and treated with galunisertib (LY2157299), a TGFβR1 inhibitor. Cell confluency and relative cell count analysis at 48 h revealed that TGFβR1 inhibition significantly hindered increased proliferation of cells exposed to cisplatin-derived SASPs (**Figure 4.15a**). We next observed that galunisertib treatment also resulted in a significant reduction in the number of colonies formed after exposure to cisplatin-induced senescent A549 and L1475(luc) CM for 10 days, compared to cisplatin-derived SASP exposure alone, while no differences were observed in cells treated with control CM (**Figure 4.15b**). In addition, TGFβR1 inhibition prevented the increase in the number of spheres and sphere size observed in 3D co-cultures of A549 and L1475(luc) cells with cisplatin-induced senescent cells (**Figure 4.15c**). To ascertain the effects observed with galunisertib treatment were specific to the inhibition of TGFβR1, we silenced the expression of *TGFβR1* and *Tgfbr1* through the generation of A549 and L1475(luc) cell lines constitutively knocked down for these genes, respectively (**Figure**

4.15e). In agreement with the effects observed with galunisertib, reduced expression of *TGFβR1* and *Tgfbr1* resulted in a decreased impact on enhanced proliferation when A549 and L1475(luc) cells were exposed to cisplatin-derived CM, compared to parental and scrambled-transduced cells (**Figure 4.15f**). In addition, we also observed that treatment of A549 cells with recombinant human TGFβ1 ligand significantly increased cell growth (**Figure 4.15d**), further validating our observations with the high-throughput MEMA platform. These results therefore confirm that the activation of TGFβR1 in recipient cells, likely through TGFβ ligands secreted by cisplatin-induced senescent cells, is responsible for the increased tumour growth driven by this particular secretome.

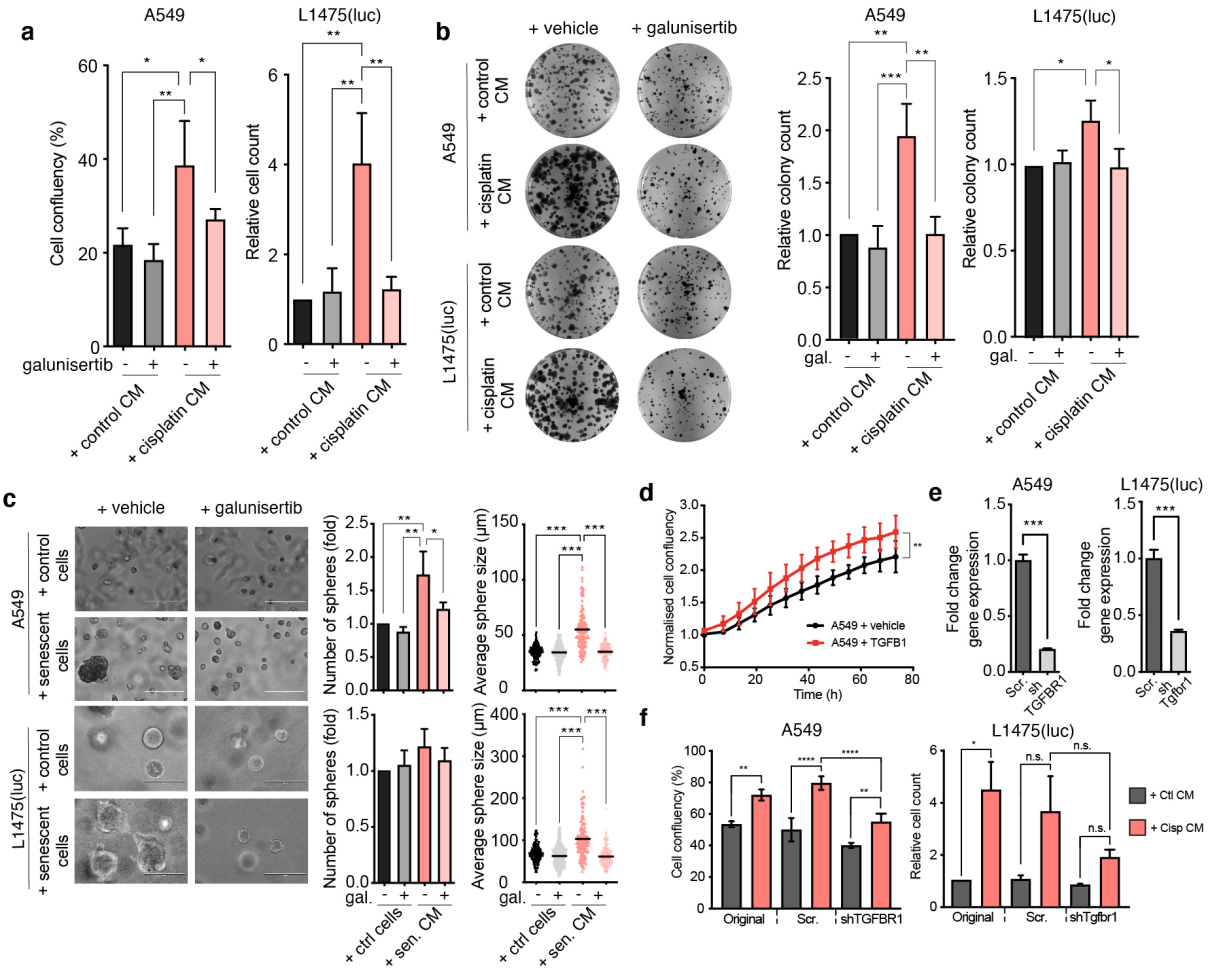

Figure 4.15. Pharmacologic inhibition and silencing of TGFβR1 abrogates enhanced proliferation, colony- and sphere-forming abilities derived from exposure to cisplatin-induced senescent A549 and L1475(luc) CM. a. Cell confluency and relative cell count of A549 and L1475(luc) cells exposed to control and cisplatin-induced senescent CM with and without 50 µM galunisertib treatment for 48 h. **b.** Left, representative images of A549 and L1475(luc) colonies formed upon exposure to control and cisplatin-

induced senescent CM for 10 days with and without 50 μM galunisertib treatment Right, quantification of the number of colonies formed relative to control condition treated with vehicle. **c.** Left, representative images of A549 and L1475(luc) tumour spheres formed after 7 days of two-phase co-culture with control or chemotherapy-induced senescent cells with and without 50 μM galunisertib treatment. Middle, number of spheres formed in each condition, relative to co-culture with control cells treated with vehicle. Right, average sphere size in each condition. For average sphere size, a total of 150 spheres from 3 independent biological repeats were measured. **d.** Normalised cell confluency over time of A549 cells treated with human recombinant TGFβ-1 ligand. **e.** Fold change *TGFBR1/Tgfbr1* gene expression of scrambled- and shTGFβR1-A549 cells (left) and scrambled- and shTgfbr1-L1475(luc) cells (right). **f.** Cell confluency and relative cell count of A549 (left) and L1475(luc) (right) original, scrambled and shTGFB1/shTgfb1 cells upon exposure to control- and cisplatin-induced senescent CM for 48 h. Data represent mean ± SD ($n = 3$). Statistical significance was determined by one- or two-way ANOVA followed by Tukey's multiple comparisons test, and by two-tailed Student's t-test. *$p < 0.05$, **$p < 0.01$, ***$p < 0.005$, ****$p < 0.0001$, *n.s.* = not significant. gal. = galunisertib.

Intriguingly, TGF-β cytokines can signal through the activation of several different pathways in recipient cells, which, paradoxically, can result in both tumour-suppressive and tumour-promoting effects [210]. In order to uncover the mechanism involved in the transduction of TGFβR1 activation upon exposure to cisplatin-induced senescent CM, we explored protein phosphorylation changes in A549 recipient cells exposed to control and cisplatin-induced senescent CM with and without galunisertib treatment. Phospho-kinase array analysis revealed increased phosphorylation of Akt1/2/3 at residue S473, one of the activating sites of this kinase, upon exposure of cells to cisplatin-induced senescent CM, and TGFβR1 inhibition through galunisertib treatment markedly prevented the phosphorylation of the same kinase (**Figure 4.16a, b**). This suggested that binding to and activation of TGFβR1 upon exposure to cisplatin-derived SASP mediates the downstream activation of the kinase Akt by a non-canonical mechanism. Because the Akt/mTOR/p70S6K is a cascade known to promote cell proliferation, we furthered our investigations into this signalling pathway. As observed in our phospho-kinase arrays, we detected an increase in phospho-Akt S473 in both A549 and L1475(luc) cells exposed to cisplatin-induced CM by Western blotting, which was substantially diminished upon galunisertib treatment (**Figure 4.16c**). Importantly, we observed the same trend in the phosphorylation of P70S6K in its activating site at Thr389, suggesting that phosphorylation of Akt results in the activation of P70S6K, a kinase downstream of mTOR

that induces protein synthesis and cell cycle progression (**Figure 4.16c**). To determine the implication of mTOR and this kinase, we treated CM recipient cells with rapamycin, a well-known mTOR inhibitor. While increased phosphorylation of Akt at S473 remained unchanged in cells exposed to cisplatin-derived SASP and treated with rapamycin simultaneously, phosphorylation of P70S6K was reduced, confirming the connection of mTOR in the cascade stimulated upon TGFβR1 and Tgfbr1 activation in cells exposed to the CM from cisplatin-induced senescent cells (**Figure 4.16c**). To further validate the effect of this pathway on the phenotypic response observed upon exposure to the SASP, we conditioned A549 and L1475(luc) cells with control and cisplatin-induced senescent CM and observed that mTOR inhibition through rapamycin treatment also hampered the effect on proliferation driven by cisplatin-derived SASP in both human and murine cells (**Figure 4.16d**). Representative images of A549 cell confluency under each CM condition and upon galunisertib and rapamycin treatments are shown in **Figure 4.16e**.

Together, our investigations demonstrate that the exposure of lung cancer A549 and L1475(luc) cells to the SASP derived from cisplatin-induced senescent cells results in the TGFβR1-mediated activation of the Akt/mTOR/P70S6K pathway, which in turn ensues increased proliferation in the cells.

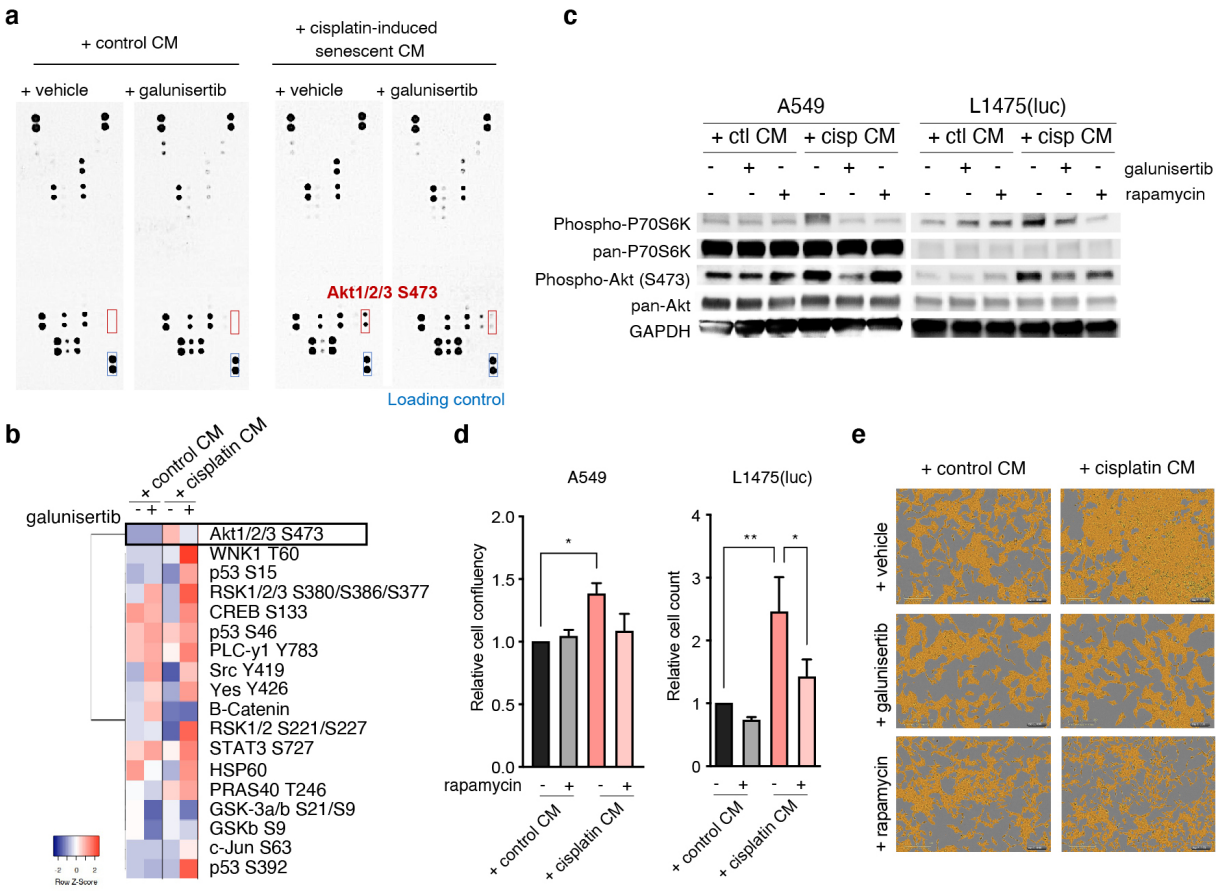

Figure 4.16. TGFβR1-driven activation of Akt/mTOR pathway orchestrates the induction of malignant traits upon exposure to cisplatin-derived SASP. a. Representative pictures of human phospho-kinase array panels of whole-protein extracts from A549 cells exposed for 30 min to either control- or cisplatin-induced senescent CM with and without 50 μM galunisertib treatment. **b.** Heatmap of pixel intensity z-score of each kinase phosphorylation listed upon 30 min exposure to control and cisplatin-induced senescent CM in A549 cells. **c**. Western blot analysis of whole extracts of A549 and L1475(luc) cells exposed to control and cisplatin-induced senescent CM for 30 min with and without 50 μM galunisertib and 1 μM rapamycin. **d.** Cell confluency and cell count of A549 and L1475(luc) cells exposed to control and cisplatin-induced senescent CM for 48 h upon 1 μM rapamycin treatment, relative to cells exposed to control CM with vehicle. **e.** Representative images depicting cell confluency from cells exposed to control- or cisplatin-induced senescent CM for 48 h treated with either vehicle, 50 μM galunisertib or 1 μM rapamycin. Data represent mean ± SD (n = 3). Statistical significance was determined by one-way ANOVA followed by Tukey's multiple comparisons tests. *$p < 0.05$, **$p < 0.01$.

4.2.7. Histological assessment of human lung adenocarcinoma specimens subjected to platinum-based chemotherapy reveals association between senescent markers and activation of the Akt/mTOR pathway

A major goal of this chapter was to obtain clinical supporting evidence of the effects and phenotypes observed through our *in vitro* and *in vivo* analyses. Towards this aim, we retrieved valuable samples resected from patients that had recently undergone neoadjuvant platinum-based treatment (for pathological, clinical and treatment details see **Table 1**). As described earlier, we detected areas enriched in p16 and p21 senescence markers in lung tumours subjected to platinum-based neoadjuvant chemotherapy in all four patients analysed. Further analyses showed a marked reactivity against phospho-AKT and phospho-P70S6K in the tumours, which intriguingly correlated with the regions of accumulated p16- and p21-positive expression within the lesions (**Figure 4.17**). While further analyses are needed to determine the exact expression patterns, these findings importantly indicate an association between the induction of senescence in the tumours and the activation of the mTOR/Akt pathway in human lung adenocarcinoma following platinum-based chemotherapy.

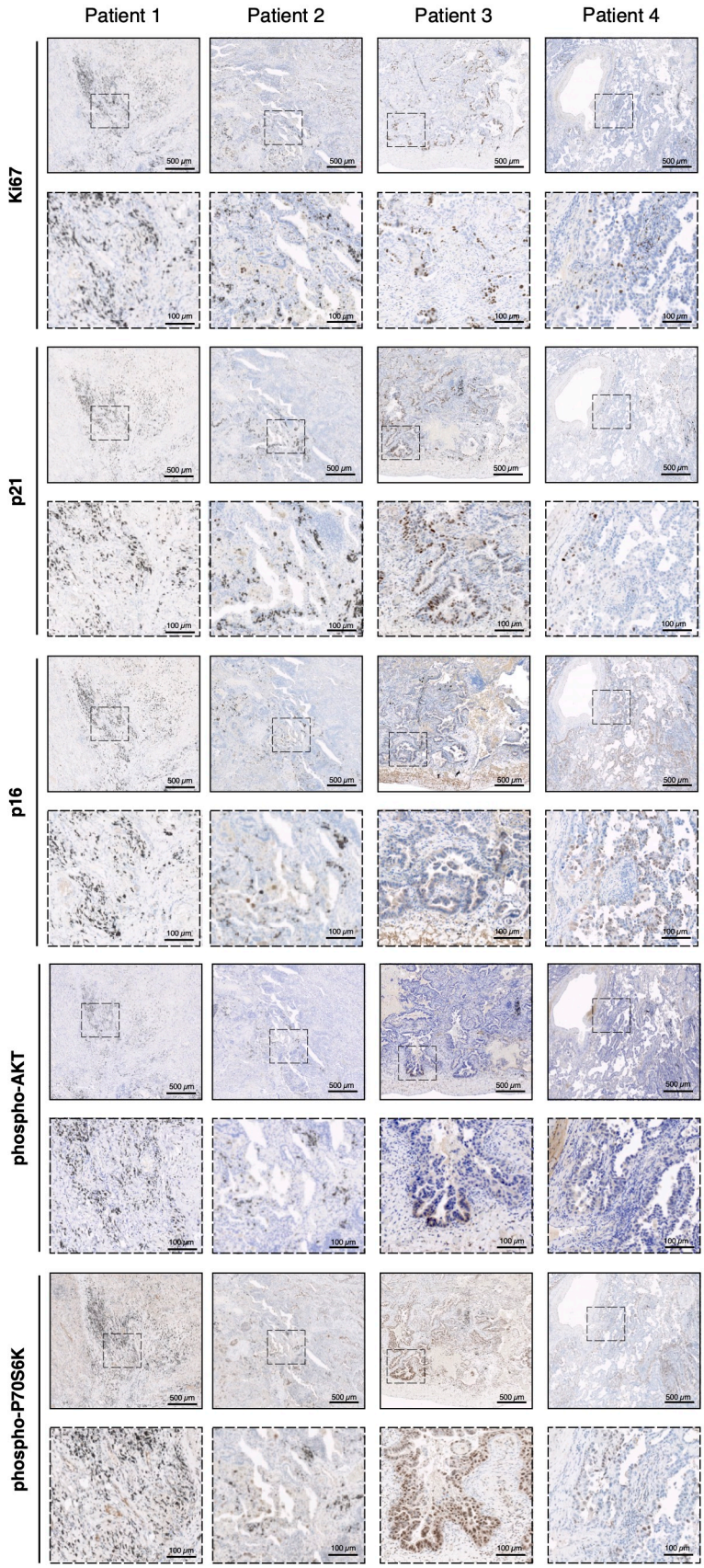

Figure 4.17. Histological analysis of neoadjuvant chemotherapy-treated lung adenocarcinoma specimens shows association between p16, p21 markers and activation of the Akt/mTOR pathway

effectors. Representative histological images of lung adenomas resected from patients within 1 month of completing neoadjuvant platinum-based chemotherapeutic treatment (**Table 1**). Lung tumour sections were stained for Ki67, p21, p16, phosphor-AKT and phosphor-P70S6K, and images depict a representative region from each patient. Scale bar = 500 or 100 μm as shown in picture.

4.2.8. Pharmacologic TGFβR1 inhibition effectively blocks pro-tumorigenic effects derived from exposure to cisplatin-induced senescence *in vivo*

With the aim of validating our mechanistic findings in *in vivo* settings, we transplanted subcutaneously cisplatin-induced senescent A549 cells together with untreated A549 cells, and subjected mice to galunisertib and senolytic treatment with ABT-737 during tumour development (**Figure 4.18a**). As expected, ablation of senescent cells in the tumours through senolytic treatment prevented the increase in tumour growth in co-transplanted xenografts, compared to co-transplanted tumours treated with vehicle only (**Figure 4.18b, c**). In addition, galunisertib treatment in mice also significantly blocked the tumour-promoting effect derived from co-transplantation with senescent cells in the xenografts, while it had no effects in control A549-transplanted mice (**Figure 4.18b, c**). This confirmed the efficiency of inhibiting TGFβR1 as a means to prevent the deleterious effects derived from cisplatin-induced senescent SASP *in vivo*.

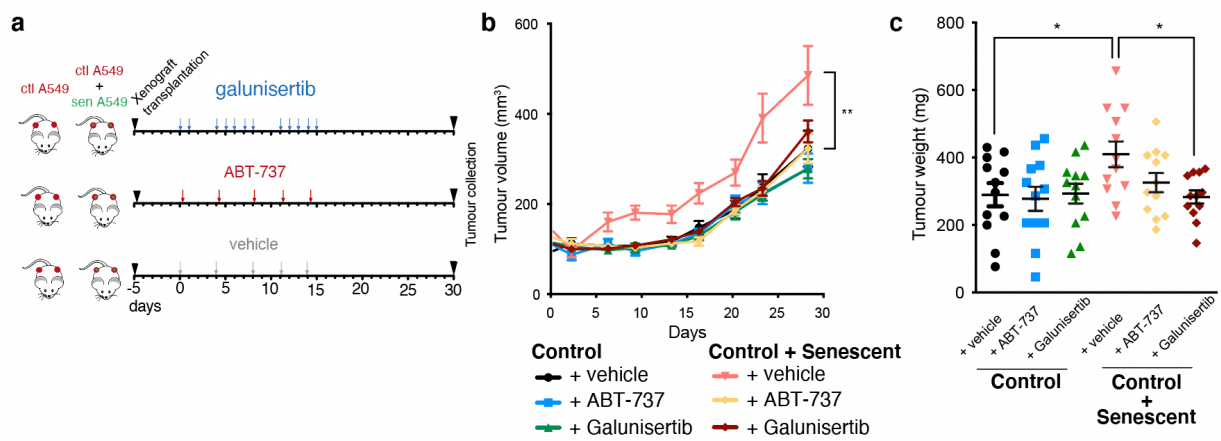

Figure 4.18. TGFβR1 inhibition and senolytic treatment markedly prevent cisplatin-induced senescent-driven increased tumour growth in A549 xenografts. a. Schematic representation of experimental layout. Briefly, animals were transplanted subcutaneously with either $4x10^6$ untreated A549 cells or $4x10^6$ untreated A549 combined with $1x10^6$ cisplatin-induced senescent A549 cells. 5 days post-transplantation, animals were subjected to 150 mg/kg body weight galunisertib treatment, 25mg/kg body

weight ABT-737 or vehicle at timings depicted. Tumour volume was measured twice a week and tumours were resected at day 30 post-initiation of treatment. **b.** Tumour volume over time for each experimental condition (n = 12 tumours per group). **c.** Tumour weight of each experimental group upon resection of tumours at day 30. Data are shown as mean ± SD. Statistical significance was determined by one- or two-way ANOVA followed by Tukey's multiple comparisons test. $*p < 0.05$, $**p < 0.01$.

We next investigated the effects of Tgfbr1 inhibition simultaneous to cisplatin-induced senescence CM exposure using the $KRas^{G12D/WT}$ orthotopic murine model. L1475(luc) cells were exposed to cisplatin-induced senescent CM with or without galunisertib for 10 days and were subsequently transplanted in the lungs of C57BL/6 mice via tail-vein injection (**Figure 4.19a**). Analysis of relative luciferase signal in mice at day 16 post-transplantation revealed a significantly decreased tumour burden in those animals transplanted with cells simultaneously exposed to cisplatin-derived SASP and galunisertib (**Figure 4.19b**). Representative images of luciferase activity are shown in **Figure 4.19c**. Finally, we observed a clear trend for an increased survival in mice transplanted with tumours that had been pre-treated with the TGFβR1 inhibitor during exposure to cisplatin-induced senescent CM (**Figure 4.19d**).

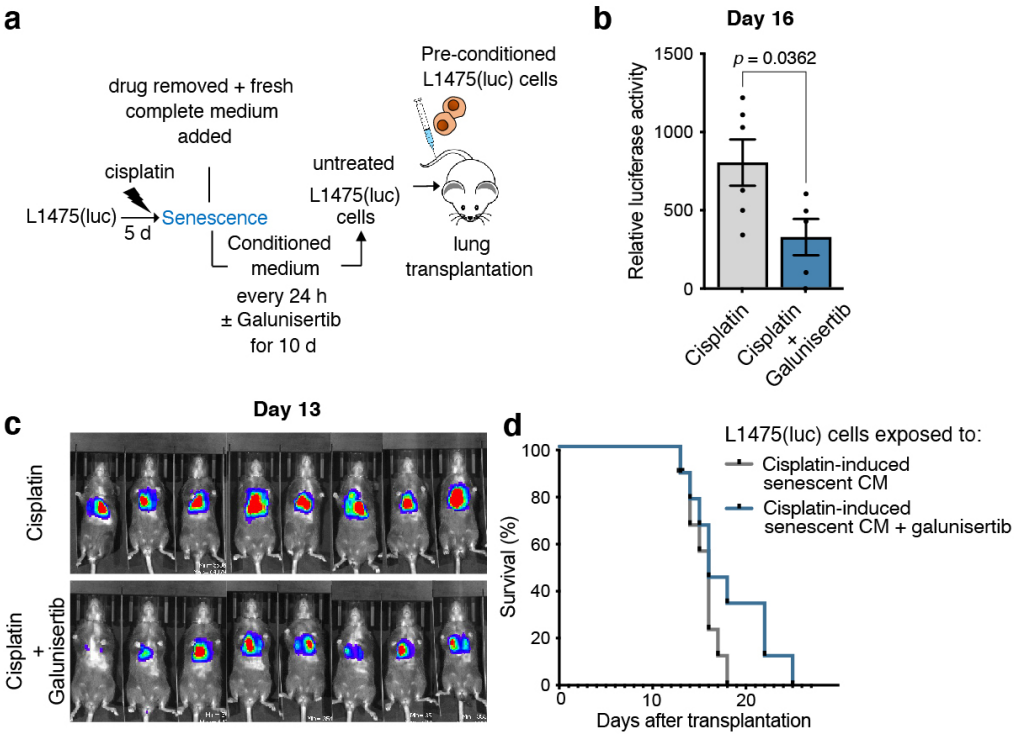

Figure 4.19. **Galunisertib treatment during cisplatin-derived SASP exposure prevents increased tumour burden in orthotopic model of NSCLC. a.** Schematic representation of experimental layout.

L1475(luc) cells were exposed to cisplatin-induced senescent CM continuously for 10 days and treated with either vehicle or 50 μM galunisertib. Pre-conditioned cells were subsequently transplanted in the lungs of mice via tail-vein injection. Tumour burden was then assessed twice a week by bioluminescence imaging and survival was determined as the time from tumour transplantation until the onset of moderate signs of disease. **b.** Relative luciferase activity at day 16 of mice transplanted with cells pre-conditioned to cisplatin-derived CM with and without galuniseritb (*n* = 6). **c.** Representative images of luciferase activity at day 13 post-transplantation from each experimental group. **d.** Survival curve of mice from each experimental group. Statistical significance was determined by two-tailed Student's t-test. Survival analysis was performed using the Kaplan-Meier method and a two-sided log-rank test was conducted to determine statistical significance.

Altogether, these results provide mechanistic evidence *in vitro* and *in vivo* of the implication of the TGFβR1/Akt/mTOR/P70S6K pathway in driving cancer progression through cisplatin-induced senescent paracrine effects in human and murine lung cancer models, including subcutaneous and orthotopic transplantation models.

4.2.9. Cisplatin and galunisertib concomitant treatment reduces tumour burden and improves survival

Given the evidence in this study demonstrating the detrimental paracrine impact of cisplatin-induced senescent lung cancer cells on tumour progression, we next aimed to determine whether combinatory treatments that can prevent the deleterious non-autonomous effects of senescence accumulation in the tumours could serve as novel and more efficient strategies to improve lung cancer treatment. To this aim, we used the KRas$^{G12D/WT}$;p53$^{-/-}$ orthotopic murine model and first analysed the expression of senescence-related markers and Tgf-β ligands in the lungs of mice subjected to vehicle, cisplatin and galunisertib treatment or a combination of both drugs as described in **Figure 4.20a**. As we have previously reported using this model, cisplatin treatment of L1475(luc)-transplanted mice results in the increased expression of the of SA-β-gal in tumour-bearing lungs [305]. Importantly, RT-qPCR analysis of RNA extracted form whole lungs upon 7 days of treatment revealed a trend for increased gene expression levels of senescence marker *Cdkn1a* as well as *Tgfb1* and *Tgfb2* in cisplatin-treated animals compared to the vehicle group (**Figure 4.20b**).

Having confirmed the increased expression of such factors, we subjected lung tumour-bearing mice to either single treatment with cisplatin or galunisertib or a regimen combining the two pharmacologic drugs, and analysed tumour burden over time (**Figure 4.20c**). Analysis of luciferase activity revealed that while single-drug treatments did not decrease luciferase activity signal compared to vehicle treatment, animals treated with the combined regimen presented a trend for decreased tumour burden as compared to the other experimental groups, despite this did not reach statistical significance (**Figure 4.20d**, **e**). Of note, cisplatin and galunisertib co-treatment significantly improved survival of individuals by 33%, with a mean average survival of 20 days compared to 15 in vehicle-treated mice (**Figure 4.20f**). Finally, as an indirect measure of chemotherapy side-effects, we studied the impact of the addition of galunisertib to cisplatin treatment on body weight throughout the therapeutic regimen, and observed that animals receiving the combination of the two drugs displayed improved tolerability and decreased weight loss and fluctuation, compared to cisplatin-only-treated animals (**Figure 4.20e**). Importantly, these results demonstrate the potential of modulating the detrimental effects of the SASP in combination with platinum-based chemotherapy to improve treatment outcomes in lung cancer.

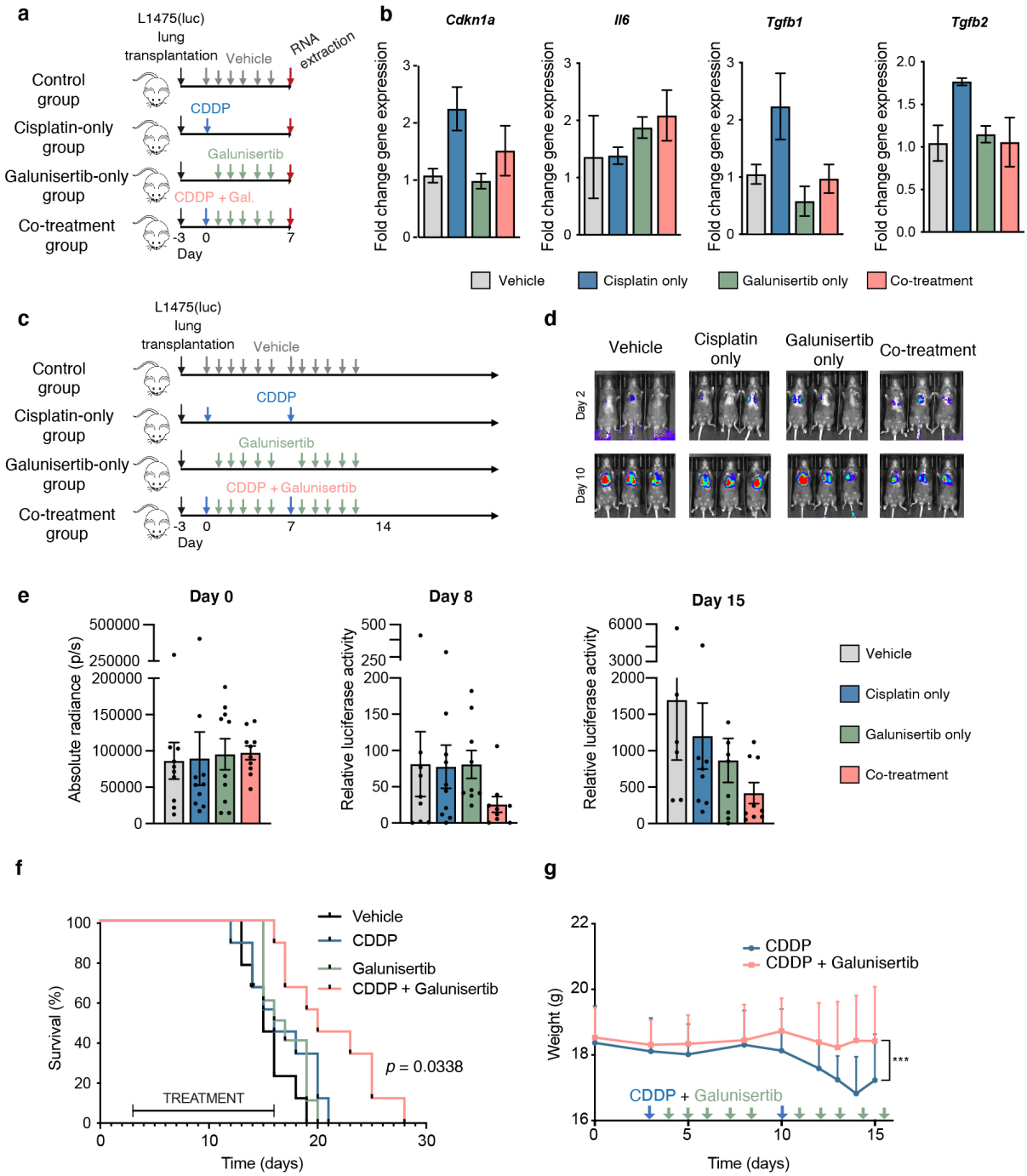

Figure 4.20. Cisplatin and galunisertib concomitant treatment reduces tumour burden and significantly enhances survival in orthotopic model of lung cancer. a. Animals were transplanted with L1475(luc) cells in the lung via tail-vein injection, and after 3 days, they were subjected to 1.5 mg/kg body CDDP, 150 mg/kg body weight, a combination of both or vehicle as shown in the timeline. Lungs were resected at day 7 post-transplantation and RNA was extracted from whole lungs. **b.** Fold change gene expression of *Cdkn1a*, *Il6*, *Tgfb1* and *Tgfb2* in samples from each experimental condition ($n = 3$). **c.** Schematic representation of experimental layout. Animals were transplanted with L1475(luc) in the lungs via tail-vein injection, and after 3 days, they were subjected to 1.5 mg/kg body CDDP, 150 mg/kg body weight, a combination of both or vehicle as shown in the timeline. Tumour burden was assessed twice a week by

bioluminescence imaging and survival was determined as the time from tumour transplantation until the onset of moderate signs of disease. **d.** Representative images of luciferase activity in mice at day 2 and 10 post-initiation of treatment. **e.** Absolute radiance and relative luciferase activity recorded in each experimental group at day 0, 8 and 15 post-initiation of treatment ($n = 9$ per group). **f.** Survival curve of mice in each experimental condition. **g.** Weight of mice subjected to CDDP and CDDP + Galunisertib treatment over time. Data are shown as mean ± SEM. Statistical significance in luciferase activity measurements was assessed by ANOVA test using Welch's correction for unequal variances. Survival analysis was performed using the Kaplan-Meier method and a two-sided log-rank test. Statistical significance in weight differences were assessed by one-way ANOVA, followed by Tukey's comparisons test, $***p < 0.005$.

4.3. Discussion

The treatment of NSCLC has experienced significant changes over the past decades. Targeted therapies have evolved as an important strategy providing remarkable improvements in survival, but their benefit is limited to a subset of advanced patients, since only about 20% of all metastatic NSCLC tumours are oncogene-addicted [306]. In addition, lasting responses to these treatments are infrequent, and emergence of secondary clones and treatment resistance are still a concern [291]. Thus, cytotoxic chemotherapies are likely to remain the mainstay option as neoadjuvant, adjuvant and second-line therapies, as well as first-line regimens for the treatment of earlier stages of NSCLC tumours with curative intent. It is for this reason that an enhanced perception of the tumour biology upon chemotherapeutic treatment is imperative to overcome complications derived from ineffective tumour response and improve outcomes further.

Platinum-based chemotherapeutic regimens were introduced in 1979 with the approval of cisplatin for cancer treatment, followed by carboplatin and oxaliplatin in the coming decades [306]. The mechanisms whereby platinum compounds exert their anti-tumorigenic effects and the processes driving treatment resistance have been studied extensively *in vitro*, but the clinical relevance of tumour response in animals and humans is not entirely clear. DNA-damage-driven apoptosis has historically been believed to be the main cell response to these genotoxic agents, but mounting evidence suggests that cellular senescence can be a major therapeutic outcome, particularly with the adoption of lower doses schedules to increase treatment tolerability [137, 157]. In this work, we demonstrate that cisplatin treatment results in decreased proliferation and higher

expression of markers of cell cycle arrest, accompanied by low levels of apoptosis, in murine lung adenocarcinomas. Further, we show that cisplatin and senolytic co-treatment results in enhanced expression of apoptotic marker cleaved caspase-3, which further indicates the accumulation of putative senescent cells in the tumours. With the aim of finding supporting clinical evidence, we show that human lung adenocarcinoma samples resected from patients that had recently received platinum-based neoadjuvant therapy present a marked expression of p16 and p21 senescence markers, further expanding the observations reported by Roberson and colleagues in human lung NSCLC specimens upon platinum-based chemotherapy, who assessed senescence based on SA-β-gal staining only [292]. The expression of senescence-related markers has also been reported to be upregulated following chemotherapeutic treatment in breast cancer, malignant pleural mesothelioma, prostate cancer, renal cell carcinoma, breast cancer and rectal cancer [137], among other cancer types, providing solid evidence of a senescent response in clinical settings.

It is important to note that the utility of inducing cellular senescence as a therapeutic endpoint remains a subject for discussion, as it can paradoxically result in both tumour-suppressive and tumour-promoting effects, in particular when senescent cells are not cleared and persist post-treatment. Its cytostatic response through the implementation of the cell cycle arrest is by nature a powerful barrier against cancer progression and has proven beneficial. For instance, doxorubicin-induced senescence was reported to inhibit tumour relapse in T cell acute lymphoblastic leukaemia by stably halting cancer cell replication [307]. In addition, the implementation of the SASP has also been reported to recruit a tumour-suppressive immune microenvironment following therapy in melanoma patient-derived xenografts, promoting tumour cell killing by tumour-infiltrating lymphocytes [308]. On the other hand, however, increasing evidence demonstrates that senescence and the SASP implemented upon chemotherapy can also yield opposing outcomes, driving tumour relapse, resistance to therapy, metastasis and chemotherapy-related adverse effects [167]. Nevertheless, most studies have focused their investigations on the effect derived from senescent stromal cells, such as fibroblasts, rather than chemotherapy-induced senescent cancer cells [62, 129, 130, 309, 310]. Despite the importance of the local and systemic effect from senescent stromal cells

upon chemotherapy, senescence in cancer cells is likely to be a major determinant in treatment response and efficacy due to their predominance in the tumour and their inherent genetic and phenotypic complexities. Here, we examined the effect of the SASP from different chemotherapy-induced senescent lung cancer cells in both human and murine lung models, and we demonstrate that the SASP derived from cisplatin treatment of lung adenocarcinoma cells drives enhanced proliferation, migration, EMT and maximal respiratory abilities in recipient lung cancer cells, as opposed to docetaxel and palbociclib. Cisplatin is a genotoxic agent that induces a robust DNA damage response, while docetaxel blocks microtubular depolymerisation, and palbociclib directly inhibits Cdk4/6. It has been postulated that persistent DNA damage prompts an enhanced and more inflammatory SASP [309], and therefore it is likely that the divergent responses to the different SASPs from these three chemotherapeutics are explained by the interplay between the cascades activated in response to the drug in particular and the different regulatory pathways of the SASP.

In this chapter, we show that cisplatin-induced senescence supports increased tumour growth in xenograft and orthotopic models of lung cancer through paracrine effects on recipient cancer cells. Of note, previous reports have reported similar effects derived from doxorubicin treatment in breast cancer and melanoma cells [130, 311, 312], and have even explored the effect of cisplatin on A549 lung adenocarcinoma cells, but the treatment conditions used by the authors in this study were suboptimal for the effective induction of cellular senescence [311]. Further, we also demonstrate that the concomitant treatment with cisplatin and the senolytic ABT-737 of lung cancer in the *KrasFSF*$^{G12V/+}$ NSCLC mouse model effectively decreases tumour burden and blocks progression compared to cisplatin treatment alone. Of note, these observations are in accordance with early findings showing that induction of cisplatin-based chemotherapy in a small cohort of NSCLC patients actually resulted in increased tumour progression during the waiting time for radiotherapy compared to untreated patients [261]. This importantly highlights the potential detrimental impact of unresolved senescence driven by cisplatin administration, and the clinical dimension of the mechanistic outcomes and proposed therapeutic strategy of our study.

Importantly, systemic administration of chemotherapeutics targets not only cancer cells but healthy tissue as well, resulting in the induction of senescence in non-transformed cells, mirroring the effects of ageing [313]. Despite we did not evaluate the changes occurring in the mice upon cisplatin treatment, such as the analysis of circulating SASP factors in the plasma that could confirm the induction of this cell response, chemotherapeutic treatment is known to result in senescence in non-cancerous tissues, which has in turn been demonstrated to contribute to organismal toxicity, including frailty, physical decline, cardiac dysfunction and even bone loss [130, 294, 314]. Taking into consideration that most cancer patients are 65 years of age or older at diagnosis, the potential interplay between ageing and the systemic effect of chemotherapy is intriguing. While research has extensively demonstrated that senescent cells accumulate with age [303, 315], it remains unknown to what extent the ability to implement a senescent response upon chemotherapy is affected in aged individuals or whether the already existent senescent burden plays a role in chemotherapy-derived effects. In this chapter, we show that cisplatin treatment prior to lung cancer orthotopic transplantation may boost cancer progression in aged individuals compared to young mice, resulting in decreased survival. While further analyses are needed in our model to better understand the systemic impact of chemotherapy in the different age groups, this effect could be explained by an increased systemic inflammation (*inflamm-ageing*) supporting tumour progression, due to either the already existent senescent burden, or the induction of a particular type of chemotherapy-induced senescence with a more pro-tumorigenic profile. Of note, the comparison between chemotherapy- and non-treated aged individuals should help clarify the differences observed. Understanding the crosslink between ageing and systemic chemotherapy-induced senescence may be crucial for improved, less toxic strategies in cancer management.

Mechanistically, we establish that the SASP derived from cisplatin treatment of lung adenocarcinoma cells is enriched in TGF-β ligands, which bind to TGFβ-R1 in untreated cells, resulting in the activation of the mTOR/Akt/P70S6K pathway, thereby driving an enhanced proliferation in the cells. TGF-β is a highly pleiotropic cytokine that has multiple and dual effects in cancer, highly dependent on the extracellular context and the phenotype of the recipient cell [298]. Given the multifaceted nature of this ligand and

the complexity of the senescent phenotype, the relationship between the two remain largely elusive. Recent findings suggest that senescent-derived secretion of TGF-β exacerbates age-related disorders including Alzheimer's disease, muscular atrophy and obesity [246]. In the context of cancer, the most prominent function of TGF-β is its cytostatic effect. In fact, TGF-β has been reported to induce cellular senescence and reinforce the proliferative arrest in an autocrine fashion, mainly through the Smad-driven activation of CDK inhibitors [228, 297, 316]. The exact molecular mechanisms underlying TGF-β-mediated promotion of cell proliferation and survival remain unclear, but it is believed that they rely on the balance of all signalling inputs received by the cell, the insensitivity to the TGF-β-induced anti-proliferative cascade and the abundance or activity of TGF-β in the extracellular matrix and the tumour microenvironment. Intriguingly, early reports demonstrate that the presence of additional growth factors in the environment, such as EGF and FGF, supports the switch towards TGF-β-driven pro-proliferative effects [237]. An additional study demonstrated that TGF-β treatment of glioma cells resulted in the autocrine induced expression of mitogens, including PDGF-B and PDGF-AA, eliciting an increased proliferation in the cells. The complex combination of factors present in the SASP is therefore likely to play a role in the pro-tumorigenic effects derived from TGF-β in our experiments, but further investigations are needed in order to elucidate this potential crosstalk. Actually, our data show that TGF-β cytokines are also present in docetaxel- and palbociclib-induced senescence, although to a lower extent compared to cisplatin-derived SASP, which further suggests that an interplay between different factors might be taking place. Intriguingly, preliminary cytokine array analyses showed that cisplatin-derived SASP is enriched in factors such as PDGF-A and HGF compared to docetaxel- and palbociclib-SASPs (data not shown), but the impact of these cytokines and their potential interplay with TGF-β has not been evaluated thus far. In any manner, to our knowledge, here we report for the first time the connection between senescence, TGF-β and mTOR/Akt-driven increased proliferation upon chemotherapeutic treatment. This non-Smad TGF-β signalling was first reported in 2007 [317], and several studies have since then demonstrated that the interplay between TGF-β and mTOR/Akt pathways is a strong promoter of EMT and metastasis in malignant cells [318]. Indeed, the increased migratory properties and formation of protuberances during sphere development of

A549 cells observed in our analyses suggest the acquisition of an EMT phenotype in response to cisplatin-derived SASP, which interestingly warrants further investigations. Supporting these mechanistic insights detected *in vitro*, in this chapter we importantly demonstrate an association between the accumulation of cellular senescence markers and the activation of the mTOR/AKT pathway in human lung adenocarcinoma samples obtained from patients that had recently received platinum-based neoadjuvant therapy. While further analyses are needed, including the evaluation of such markers in treatment-naïve specimens, these encouraging observations indicate the potential relevance of our findings in human clinical settings.

We further report that the pharmacologic inhibition of TGFβ-R1 through galunisertib treatment, as well as senescent cell depletion with senolytic ABT-737, effectively prevent the detrimental effects derived from cisplatin-induced senescent cells, both *in vitro* and *in vivo*. Galunisertib is a promising oral small molecule inhibitor currently under extensive clinical investigation both as a monotherapy and in combination with standard anti-cancer regimens for the treatment of various cancer types, including hepatocellular carcinoma, glioblastoma, ovarian cancer and NSCLC, among many others, and it renders great potential in suppressing tumour progression and promoting immune-surveillance [319]. Of note, TGF-β is a potent immune regulator, and its circulation as part of the SASP resulted in immunosuppression via the recruitment of M2 macrophages following irradiation-induced senescence in murine kidneys [320]. In addition, tumour-promoting paracrine effects of senescent cells establishing an immunosuppressive microenvironment have been shown to apply not only to senescent cancer cells but also to stromal senescence [314]. Despite the effects on immunomodulation have not been explored in this chapter, it is tempting to speculate that a TGF-β-rich cisplatin-derived SASP may also contribute to additional adverse effects through the promotion of immunosuppression in tumours.

Finally, as evidenced by recent advances in cancer management, novel treatment modalities are urgently needed in the context of chemotherapy to prevent treatment failure and relapse and maximize beneficial outcomes. We here propose the concomitant administration of platinum-based chemotherapy with galunisertib for the treatment of NSCLC tumours in which cisplatin results in the increased secretion of TGF-β ligands as a

strategy to prevent the paracrine promotion of malignant properties and prevent potential cancer relapse.

Despite our focus on the paracrine effects of chemotherapy-induced senescence, it is important to note that the SASP may not be the only contributor to treatment failure following the induction of senescence. Contrary to the long-standing belief that senescence is an irreversible state, recent research demonstrates that a fraction of chemotherapy-induced senescent cells can escape the senescent phenotype and start proliferating again with enhanced malignancy [280, 281] and increased stemness properties [164], driving cancer recurrence. Notably, chemotherapeutic treatment has recently been reported to induce very heterogenous responses across lesions and within tumours [30, 31], and thus it is likely that a combination of different cellular processes occurs simultaneously in response to the treatment, including senescent, apoptotic and resistant cells as well as senescence-escapers. Indeed, high mutational burden has been linked to greater heterogeneity in tumours and poorer prognosis after first-line chemotherapy [30]. In this scenario, it is conceivable that the detrimental effects of the SASP are exacerbated, and therefore a complete and thorough dissection of tumour response in patients undergoing chemotherapy might be imperative for optimal personalised anti-cancer regimens.

Taken together, our data demonstrate that cisplatin treatment in human and murine lung adenocarcinoma cells results in the implementation of a senescent phenotype that drives the acquisition of pro-tumorigenic phenotypes in a paracrine manner through the implementation of a SASP enriched in TGF-β ligands. We demonstrate that the detrimental effects of cisplatin-induced senescent can be effectively prevented through TGFβ-R1 inhibition and senolytic treatment. Finally, we present the combination of cisplatin chemotherapy and TGFβ-R1 pharmacological inhibition as a novel therapeutic approach for the treatment of NSCLC in order to prevent the detrimental effects from unresolved bystander senescence in tumours.

CHAPTER 5:
A NOVEL APPROACH TO TARGET CHEMOTHERAPY-INDUCED SENESCENCE IN LUNG CANCER

5.1. Introduction

Growing evidence demonstrates that therapy-induced senescent cells from both cancerous and stromal origins can drive tumorigenesis, either by releasing complex pro-inflammatory and tumour-promoting SASP cocktails [127, 321], or by the reversion of the cell cycle arrest and the acquisition of stemness and aggressive clonogenic growth potentials [322]. Remarkably, it has been shown that chemotherapy-induced senescent breast cancer cells can promote tumour relapse in the lung [169], and senescent stromal cells create a niche that promotes metastasis in the bone [314]. In the case of NSCLC, neoadjuvant platinum-based chemotherapy results in the accumulation of senescent cancer cells in patients, and evidence has been found of the escape of replicative arrest in humans (therapy-induced) senescent lung cancer cells [146]. In line with these reports, we have demonstrated in previous chapters the detrimental effects of unresolved cellular senescence during the early development and therapeutic management of NSCLC. Accumulated senescent cells in adenomas contribute to tumour progression, and senolytic-driven clearance resulted in improved survival and decreased tumour burden in a *Kras*^{G12V} mouse model of lung cancer (Chapter 3). In addition, findings in Chapter 4 indicate that platinum-based chemotherapy induces a particular senescent phenotype that promotes the acquisition of malignant traits in untreated lung cancer cells through the SASP. We further show that senolytic ABT-737 treatment effectively prevents enhanced tumour growth driven by the co-transplantation of untreated and cisplatin-induced senescent A549 cells compared to untreated cells only. Therefore, treatment modalities that specifically eliminate senescent cells may be critical for tumour

eradication, and thus senolytics, which preferentially kill senescent cells by different mechanisms [197, 323], represent an exciting avenue for cancer management.

Senolytic drugs have been described and developed in the recent years through the identification of targetable vulnerabilities in senescent cells. These compounds include the BCL-2 family inhibitors navitoclax (ABT-263) [178] and ABT-737 [181], which have been used in throughout this PhD work, the flavonoid fisetin [324], combinations of tyrosine kinase inhibitors and flavonoids (such as dasatinib and quercetin, which are used in combination [177]), FOXO4-p53 interfering peptides [325], HSP90 chaperone inhibitors [326], piperlongumine [182] and cardiac glycosides [187, 188]. Senolytics have emerged as promising agents for the treatment of pulmonary fibrosis, atherosclerosis, osteoarthritis, type 1 and 2 diabetes mellitus, and neurocognitive decline, among other diseases, and they can also rejuvenate aged hematopoietic and muscle stem cells and extend the lifespan of naturally aged mice [197]. However, less research has focused on their application as part of cancer management and preventative modalities.

Despite successful pre-clinical *proofs-of-concept* for this class of drugs, their potential translatability is hampered by their associated toxicities, which warrants the development of more specific and less toxic second-generation senolytics. Navitoclax has been validated in a variety of pre-clinical models showing a prominent ability in killing senescent cells. However, it also results in significant on-target haematological toxicities, including thrombocytopenia [327]. This importantly narrows its therapeutic window and can preclude concomitant treatment with other agents with haematological toxicities. While targetable vulnerabilities of senescence have been discovered, these are often also present in some non-senescent tissues, leading to problems with specifically targeting senescent cells. As described in Chapter 1, a prominent feature of senescent cells is their enrichment in lysosomes and lysosomal proteins, including senescence-associated β-galactosidase (SA-β-gal), which is widely used as a marker of senescence [328] and can be readily detected in these cells [59]. Interestingly, researchers have utilised these traits as a means to enhance the targeting of senescent cells. Recent reports from our group and collaborators (Prof Manuel Serrano (IRB, Barcelona) and Prof Martínez-Máñez, (Polytechnic University of Valencia)) showed that the encapsulation of nanoparticles with galacto-oligosaccharides (GalNPs) is an efficient method to preferentially deliver cytotoxic

drugs and tracers to the lysosomes of senescent cells, where SA-β-gal activity digests the galacto-oligosaccharides, thereby releasing the cargo [203, 204]. This work demonstrated that galacto-encapsulated doxorubicin is preferentially released into fibrotic tissues and tumours accumulating senescent cells, and its concomitant administration with the senescence-inducing anti-cancer treatment palbociclib effectively halts tumour growth in xenograft models of melanoma and NSCLC [204]. Authors also showed that a fluorescent probe covalently linked to multi-acetylated galactose is preferentially digested by senescent cells, releasing the free fluorophore [207]. The presence of multiple acetyl moieties in the galactose residue is thought to render it membrane-permeable and therefore accessible to the lysosomal compartment [208]. Consequently, engineering approaches that modify the structure of senolytics by leveraging senescence biochemistry to increase their specificity have the potential to accelerate their translation into the clinic.

As part of this chapter, we collaborated with the group of Ramón Martínez-Máñez (Polytechnic University of Valencia) with the aim of developing a novel senolytic to enhance senescence specificity and reduce potential on-target or off-target toxicities for improved cancer therapeutic management. To this aim, and in order to exploit the enriched SA-β-gal activity of senescent cells, Dr Beatriz Lozano-Torres (Polytechnic University of Valencia) and colleagues generated an engineered and activatable version of navitoclax by modifying its molecular structure with an acetylated galactose, which we named Nav-Gal (**Figure 5.1a**).

To do so, navitoclax was reacted with 2,3,4,6-tetra-O-acetyl-α-D-galactopyranosyl bromide (Gal) through bimolecular nucleophilic substitution (S_{N2}) in the presence of potassium carbonate, yielding the Nav-Gal prodrug (**Figure 5.1a**). This was comprehensively characterised by several nuclear magnetic resonance techniques (NMR), including ^{1}H-NMR, ^{13}C-NMR and correlated spectroscopy (COSY) NMR, as well as by attenuated total reflectance (ATR) and high-resolution mass spectrometry (HRMS) (**Supplementary Figure 5.1, Appendix**). The ^{1}H NMR signal centred at 5.6 ppm (**Supplementary Figure 5.1b, Appendix**) corresponds to the anomeric proton of the attached galactose and indicates the successful covalent linkage of the monosaccharide to navitoclax. In addition, the appearance of a signal centred at 1,749 cm^{-1} in the ATR

spectra (**Supplementary Figure 5.1e, Appendix)** indicates that galactose remains acetylated after purification. Correct functionalisation to the nitrogen atom of bis(sulfonyl)aniline is further corroborated through the fragmentation peaks observed in the mass spectrum (**Supplementary Figure 5.1f, Appendix**). After extensive structural characterisation, Lozano-Torres and colleagues examined the ability of Nav-Gal to be enzymatically hydrolysed to navitoclax. GLB1 is the human lysosomal β-galactosidase responsible for the SA-β-gal activity [59]. Our collaborators used high performance liquid chromatography (HPLC) to examine the time-dependent hydrolysis reaction of PBS (pH 7)-DMSO (0.01%) solutions containing Nav-Gal in the presence of recombinant GLB1 and compared the peaks with those of navitoclax (**Figure 5.1b**). The obtained chromatograms showed the Nav-Gal peak with the subsequent appearance of free navitoclax signal in the presence of the human β-galactosidase activity of the lysosomal enzyme and confirmed that Nav-Gal was completely hydrolysed. No significant spontaneous Nav-Gal hydrolysis was observed (data not shown).

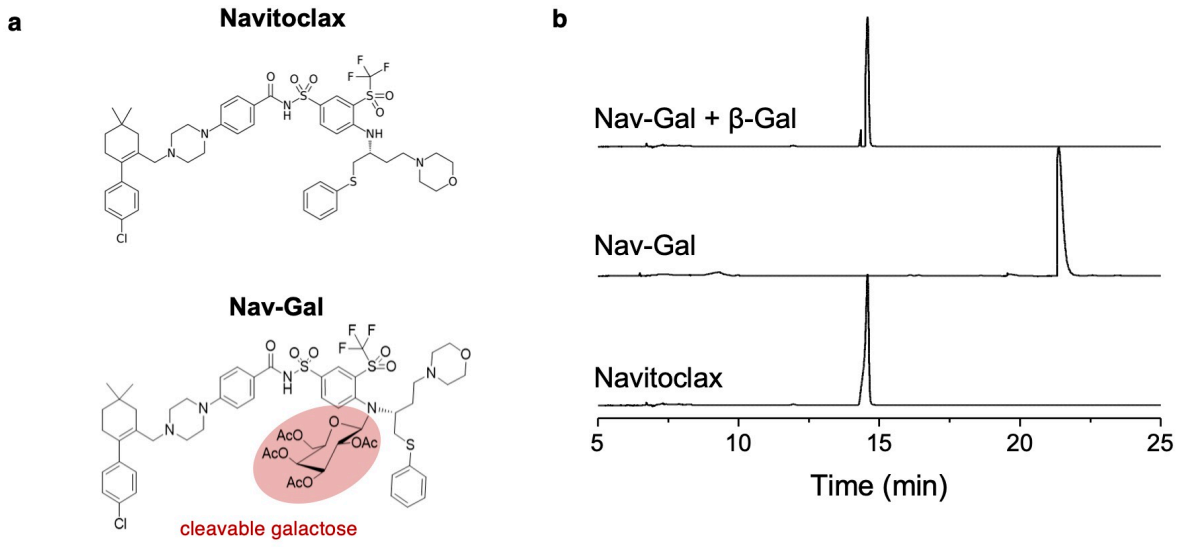

Figure 5.1. Galacto-conjugation of the senolytic navitoclax into a new generation senolytic prodrug, namely Nav-Gal. a. Chemical structures of Nav-Gal prodrug and navitoclax. The presence of galactopyranoside, covalently linked to the N of bis(sulfonyl)aniline as synthesised in this prodrug, hinders two key interactions: (i) π-π interaction between the phenylthioether moiety and the bis(sulfonyl)aniline ring; and (ii) the hydrogen bond between morpholine with Tyr-199 [329], thereby preventing the inhibitory effect of the molecule. This moiety, the galactopyranoside, can be hydrolysed in the presence of human β-galactosidase (cleavable galactose). **b**. Chromatograms depicting hydrolysis reaction of Nav-Gal aqueous solutions in the presence of human β-galactosidase followed by HPLC-UV as described in the text.

Following synthesis, characterisation and hydrolysis reaction studies performed by our colleagues at the Polytechnic University of Valencia, we proceeded with the *in vitro* and *in vivo* assessment and validations of the new pro-drug. In this chapter, using a variety of model systems, we show that galacto-conjugation of navitoclax, namely Nav-Gal, results in a prodrug with selective, pro-apoptotic senolytic activity released in senescent cells that is dependent on GLB1 activity. Concomitant treatment of Nav-Gal with the senescence-inducing chemotherapy cisplatin (CDDP) efficiently arrests tumour progression in models of orthotopically transplanted murine lung adenocarcinoma cells and in a tumour xenograft model of human NSCLC. Importantly, galacto-conjugation of navitoclax reduces thrombocytopenia in treated mice at therapeutically effective doses, as well as apoptosis of platelets in human blood samples treated *ex vivo*.

5.2. Results

5.2.1. Nav-Gal shows efficient senolytic activity and an increased senolytic index compared to navitoclax

Senescent cells commonly display high lysosomal SA-β-gal activity, thus we hypothesised that galacto-conjugated navitoclax would be preferentially processed and activated in senescent cells and hence could function as a pro-drug with more selective senolytic activity. To investigate this, we performed cell viability assays using a model of therapy-induced senescence. The lung carcinoma cell line A549 was treated with cisplatin (CDDP) for 10 days, resulting in elevated SA-β-gal activity and expression of markers of senescence (**Figure 5.2a-c**). Cisplatin-treated A549 cells were then subjected to increasing doses of either navitoclax or newly developed Nav-Gal for 72 h. As shown in **Figure 5.3a**, after 72 h of treatment, the concentration of navitoclax required to induce death in 50% of the cells, termed half maximal inhibitory concentration (IC50), was 1.926 μM for non-senescent and 0.122 μM for cisplatin-induced senescent A549 cells, while the IC50 for Nav-Gal was 9.758 μM for non-senescent and 0.275 μM for senescent A549 cells (**Figure 5.3b**). Indeed, the senolytic index of Nav-Gal was substantially higher than navitoclax

(35.52 vs. 15.85, respectively; **Figure 5.3a,b**), indicating an increased senescent specificity in Nav-Gal.

Lozano-Torres further validated the same effects in a model of palbociclib-induced senescence with the human melanoma cell line SK-Mel-103, which according to our experiments is generally more sensitive to senolytic treatment (**Figure 5.2a-c** and **Figure 5.3c,d**). In this case, the concentration of navitoclax required to kill 50% of the cells was 28 nM non-senescent cells and 0.1 nM for palbociclib-induced senescent SK-Mel-103 cells (**Figure 5.3c**). On the other hand, Nav-Gal IC50 was 125.2 nM in non-senescent cells, and 0.16 nM in palbociclib-induced senescent cells (**Figure 5.3d**). Consequently, the senolytic index for Nav-Gal in SK-Mel-103 cells was also substantially higher than navitoclax (78.45 vs. 25.68, respectively) (**Figure 5.3c,d**), indicating the increased protection of non-senescent cells

Taken together, these results show in two different models of chemotherapy-induced senescence that Nav-Gal has an improved senolytic index over navitoclax and indicates that this effect is mainly mediated by a higher degree of protection of non-senescent cells from cytotoxic activity.

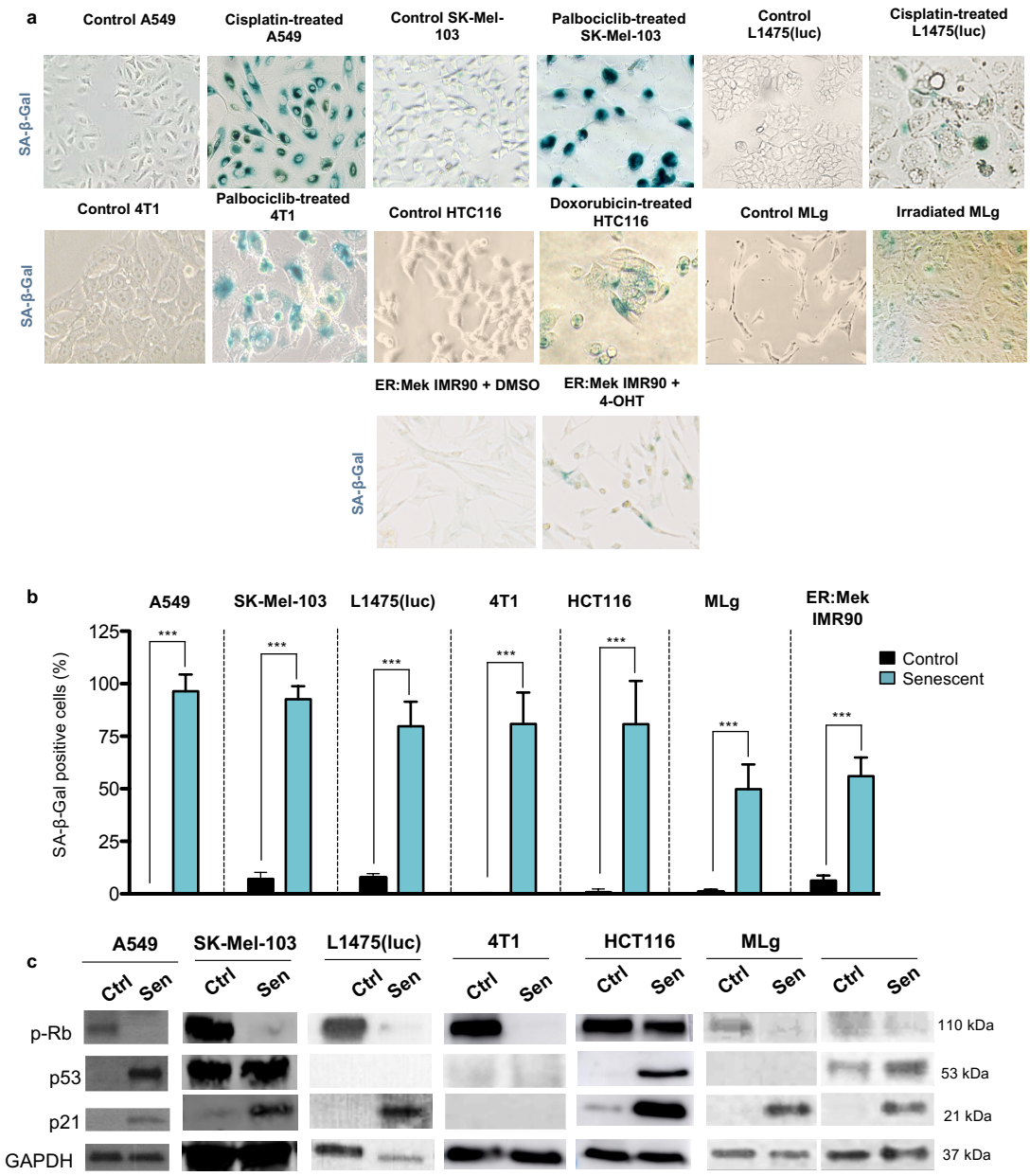

Figure 5.2. Assessment of the induction of cellular senescence in cell lines used for *in vitro* **experiments. a.** Representative images of SA-β-gal staining of control and cisplatin-induced senescent A549 cells, palbociclib-induced senescent SK-Mel-103 cells, cisplatin-induced senescent KRas$^{G12D/WT}$;p53$^{-/-}$ lung cancer cells (L1475(luc)), palbociclib-induced 4T1 senescent cells, doxorubicin-induced senescent HTC116 cells, irradiation-induced MLg fibroblastic cells and hydroxy-tamoxifen-treated ER:Mek IMR90 cells. **b.** Quantification of SA-β-gal positive cells of control and senescent cells. **C.** Western blot analysis of the expression of phospho-retinoblastoma (p-Rb), p53 and p21 in control and senescent cells.

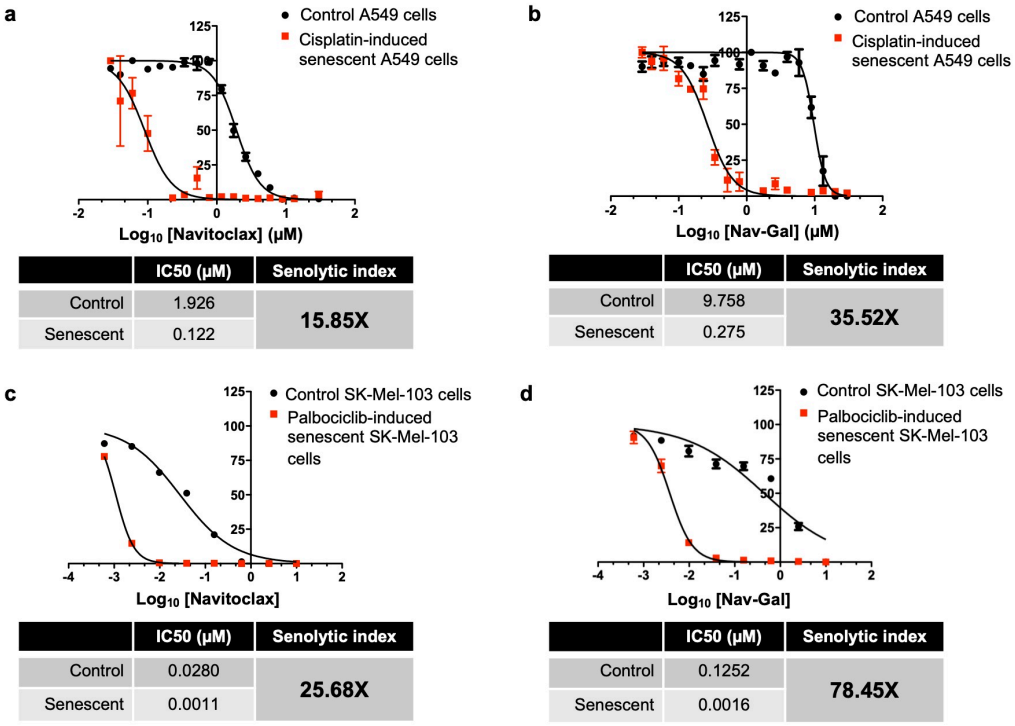

	IC50 (μM)	Senolytic index
Control	1.926	15.85X
Senescent	0.122	

	IC50 (μM)	Senolytic index
Control	9.758	35.52X
Senescent	0.275	

	IC50 (μM)	Senolytic index
Control	0.0280	25.68X
Senescent	0.0011	

	IC50 (μM)	Senolytic index
Control	0.1252	78.45X
Senescent	0.0016	

Figure 5.3. The prodrug Nav-Gal shows efficient senolytic activity and an increased senolytic index, conferring a protective effect on non-senescent cells. a, b. Quantification of viability and half maximal inhibitory concentration (IC50) of **(a)** navitoclax and **(b)** Nav-Gal on control and cisplatin-induced senescent A549 cells. Senolytic indices for each drug are shown in the tables below. Viability assay on A549 cells was performed as $n = 5$, and graphs depict one representative repeat. **c, d.** Quantification of viability and maximal inhibitory concentration (IC50) of **(c)** navitoclax and **(d)** Nav-Gal on control and palbociclib-induced senescent SK-Mel-103 cells. Senolytic indices of each drug are shown in the tables below. Viability assay on SK-Mel-103 cells was performed as $n = 3$, and graphs depict one representative repeat.

In an attempt to determine whether senolytic activity and non-senescent cell protection by Nav-Gal were more widely observed, we then performed cell viability assays using a variety of cell lines and diverse triggers of cellular senescence. **Figure 5.4a-e** shows the effects on cell viability of both navitoclax and Nav-Gal at different concentrations in cisplatin-induced senescent mouse lung adenocarcinoma (*Kras*$^{G12D/+}$;*p53*$^{-/-}$ (KP)) L1475(luc) cells [300], which have been used in previous chapters, palbociclib-induced senescent mouse breast cancer 4T1 cells, doxorubicin-induced senescent human colorectal carcinoma HCT116 cells, irradiation-induced senescent mouse lung fibroblasts MLg and oncogene-induced senescent human lung IMR90 fibroblasts, versus their non-senescent counterparts. Efficient implementation of cellular

senescence using these triggers was confirmed by SA-β-gal staining and Western blotting for senescence markers (**Figure 5.2a-c**). In L1475(luc) cells, Nav-Gal treatment resulted in 76.8% viability of non-senescent cells at the highest dose tested (20 μM), while non-senescent cell viability upon 20 μM navitoclax treatment was just 53.1%, a difference that was statistically significant (**Figure 5.4a**). Significantly higher cell viability of non-senescent cells remained consistent in all the additional human and murine cell lines at the highest doses of navitoclax and Nav-Gal tested, while senolytic activity of Nav-Gal was generally as effective as that of navitoclax, independently of the senescence-inducing trigger used. This confirmed that Nav-Gal exerts effective senolysis and presents a significantly higher degree of protection of non-senescent cells when compared to navitoclax.

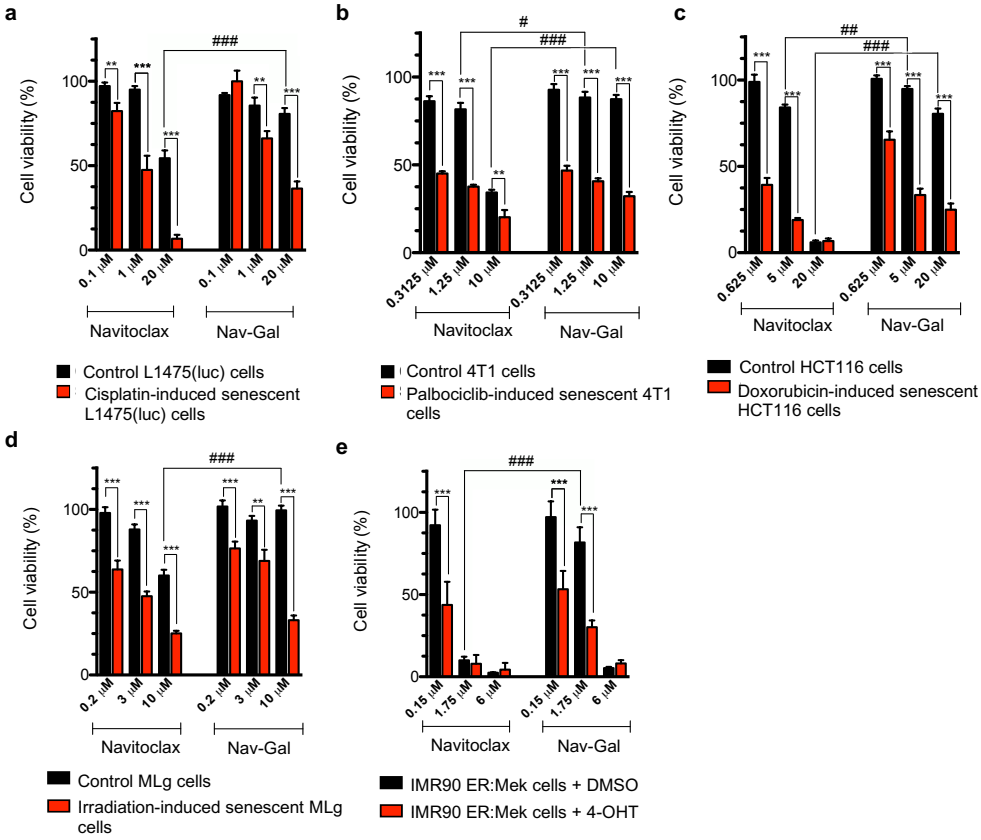

Figure 5.4. The prodrug Nav-Gal shows efficient, broad range, senolytic activity in different cell lines and models of cellular senescence. a-e. Quantification of cell viability upon Navitoclax and Nav-Gal treatment of control and **(a)** cisplatin-induced senescent KRas$^{G12D/WT}$;p53$^{-/-}$ lung adenocarcinoma tumour cells L1475(luc) (n = 4), **(b)** palbociclib-induced senescent 4T1 cells (n = 3), **(c)** doxorubicin-induced senescent HCTT116 cells (n = 3), **(d)** irradiation-induced senescent MLg cells (n = 3) and **(e)** oncogene-induced senescent

IMR90 cells (previously treated for 72 h with 200 nM 4-hydroxytamoxifen (4-OHT)) (*n* = 3). Data represent mean ± SD of all replicates, and statistical significance was calculated using two-way ANOVA ; *p < 0.05, **p < 0.01, ***p < 0.001; #p < 0.05, ##p < 0.01, ###p < 0.001.

5.2.2. *GLB1* transient downregulation prevents the senolytic activity of Nav-Gal

To ascertain whether the senolytic effect of the prodrug Nav-Gal depends on the increased lysosomal β-galactosidase activity of senescent cells, siRNAs were used to transiently knock-down the expression of *GLB1* in A549 and SK-Mel-103 cells. Of note, A549 cell transduction with siRNA2 resulted in a significantly decreased number of SA-β-galactosidase-positive cells (**Figure 5.5a,b**) and efficiently downregulated the transcription of *GLB1* after 48 h (**Figure 5.5c**), when compared to scrambled siRNA and siRNA1, which was deemed non-functional. The same trends were observed in SK-Mel1-3 cells, where siRNA2 resulted in a more efficient downregulation of *GLB1* and SA-β-gal staining, compared to A549 cells (**Figure 5.5d-f**).

We next compared the senolytic effects of navitoclax and Nav-Gal treatment in both cell lines, and observed that, as expected, the killing efficiency of navitoclax was maintained in the senescent cells knocked-down for the enzymatic expression, compared to scrambled and siRNA1-transfected cells (**Figure 5.5g**). Of note, a slight decrease in cell viability was observed in siRNA1-transfected A549 cells, which we assume is caused by an off-target effect of such transfection. Markedly, transient downregulation of *GLB1* with siRNA2 significantly prevented the senolytic activity of Nav-Gal. Average cell viability of senescent scrambled and siRNA1-trasnfected A549 cells upon 48 h treatment with Nav-Gal was 49.1% and 47.3%, respectively, while *GLB1* downregulation with siRNA2 resulted in an increased viability of 82.7% (**Figure 5.5h**, left). On the other hand, average cell viability of senescent scrambled and siRNA1-trasnfected SK-Mel-103 cells upon 48 h treatment with Nav-Gal was 38.0% and 41.1%, respectively, while *GLB1* downregulation with siRNA2 resulted in a significantly increased viability of 67.9% (**Figure 5.5h**, right). Importantly, these results indicate that the selective senolysis of the prodrug is at least partially driven by the increased *GLB1* expression of senescent cells.

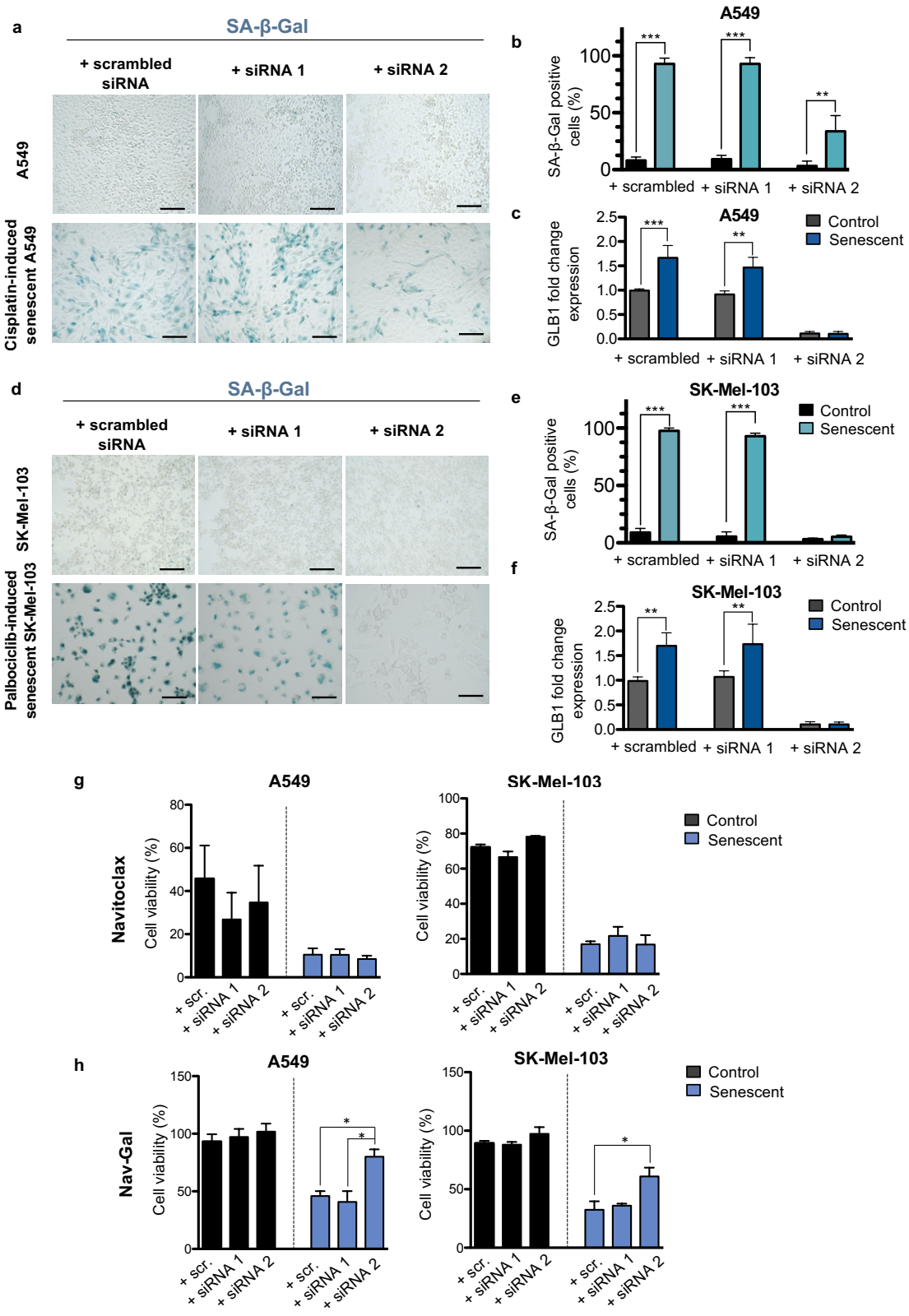

Figure 5.5. *GLB1* **transient downregulation prevents the senolytic activity of Nav-Gal. a**. Representative images of SA-β-gal staining of control and cisplatin-induced senescent A549 cells 48 hr after transfection with scrambled siRNA, siRNA 1 and siRNA 2. Scale bar = 200 µm. **b.** Percentage of SA-β-gal-positive cells in conditions presented in (a). Bars represent mean ± SD (*n* = 3). **c.** *GLB1* fold change gene expression in control and senescent A549 cells 48 h post-transfection with different siRNAs. **d.** Representative images of SA-β-gal

staining of control and palbociclib-induced senescent SK-Mel-103 cells 48 h after transfection with scrambled siRNA, siRNA 1 and siRNA 2. Scale bar = 200 μm. **e**. Percentage of SA-β-gal-positive cells in conditions presented in (d). Bars represent mean ± SD (*n* = 3). **f**. *GLB1* fold change gene expression in control and senescent SK-Mel-103 cells 48 hr post-transfection with different siRNAs. **g**. Quantification of cell viability upon 48 hr Navitoclax treatment of control and cisplatin-induced senescent A549 cells (10 μM navitoclax) (left) and control and palbociclib-induced senescent SK-Mel103 cells (7.5 μM navitoclax) (right) previously transfected with different experimental siRNAs against GLB1 transcript. **h.** Quantification of cell viability upon 48 hr Nav-Gal treatment of control and cisplatin-induced senescent A549 cells (10 μM Nav-Gal) (left) and control and palbociclib-induced senescent SK-Mel103 cells (7.5 μM Nav-Gal) (right) previously transfected with different experimental siRNAs against *GLB1* transcript. Note that siRNA 1 was not functional in all the experiments and hence used as an internal negative control. All bars represent mean ± SEM (*n* = 3). One-way ANOVA followed by Tukey's post-tests were performed to calculate the significance of the results; *p < 0.05, **p < 0.01, ***p < 0.001.

5.2.3. Nav-Gal induces cell death through apoptosis in senescent cells, while it maintains viability of non-senescent cells

The use of navitoclax has been described to induce apoptosis preferentially in senescent cells through inhibition of the BCL-2-regulated pathway [178]. To assess whether Nav-Gal and navitoclax killed senescent cells by the same end mechanism, cisplatin-induced senescent lung cancer A549 cells and palbociclib-induced senescent melanoma SK-Mel-103 cells were treated with navitoclax or Nav-Gal (or vehicle) in parallel, with automated real-time measurement of apoptosis study using a live-cell analysis system. **Figure 5.6a,b** and **Figure 5.7a-d** show that treatment with either navitoclax or Nav-Gal induced apoptosis preferentially in chemotherapy-induced senescent cells (as inferred from an increased annexin V signal). Importantly, and consistent with the results described previously, the induction of apoptosis was lower in control non-senescent cells treated with Nav-Gal compared with navitoclax (both at a high dose; 10 μM), particularly at later time points. While over 70% of non-senescent A549 cells presented a strong signal for annexin V after 36 hr of treatment with navitoclax, this was true for only ~30% of the cells after treatment with the same dose of Nav-Gal (**Figure 5.6a,b** and **Figure 5.7a**). Consistent effects were observed with the melanoma cell line SK-Mel-103 (**Figure 5.7b-**

d). These results indicate that Nav-Gal kills senescent cells by inducing apoptosis and that it protects against non-senescent cell death to a higher extent than navitoclax.

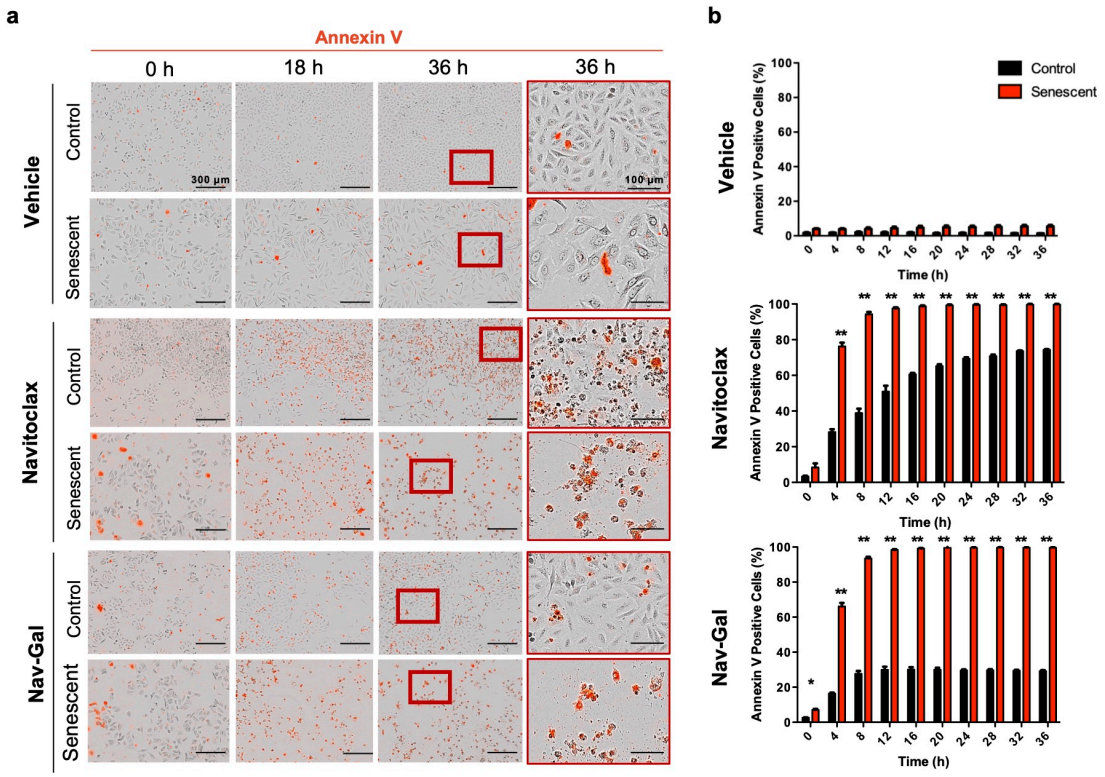

Figure 5.6. The galacto-conjugated prodrug Nav-Gal demonstrates a lower induction of apoptosis of non-senescent cells. a. Representative images of cell viability showing staining for annexin V (red) of control or cisplatin-induced senescent A549 cells, exposed to vehicle, navitoclax (10 µM) or Nav-Gal (10 µM) treatment over time. Red scale bar = 300 µm; black scale bar = 100 µm. **b.** Average percentage of annexin V-positive cells in control and cisplatin-induced senescent A549 cells exposed to vehicle (top), navitoclax (10 µM; middle) or Nav-Gal (10 µM; bottom) treatment over time. Data represent mean ± SD (n = 3), where for each biological repeat the percentage of annexin V-positive cells was calculated in 3 independent technical repeats per experimental condition. Statistical significance was calculated using two-tailed Student's t tests; *p < 0.05, **p < 0.001.

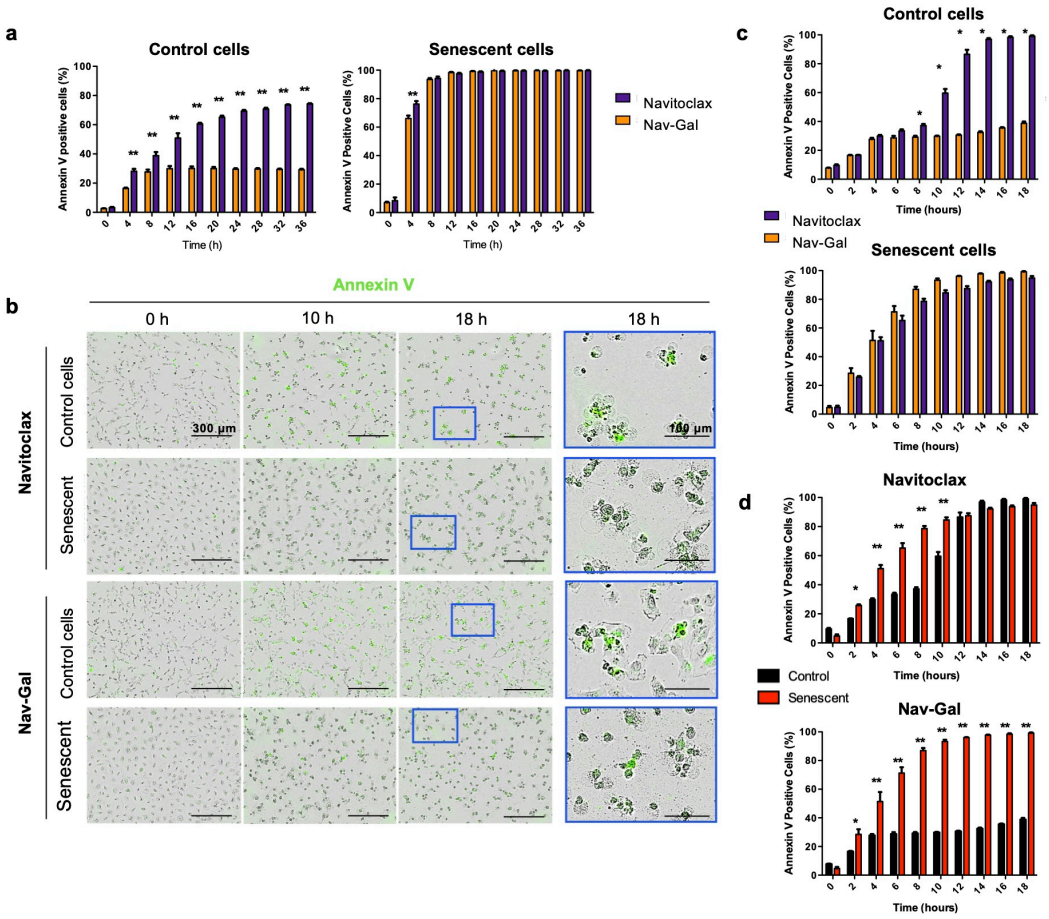

Figure 5.7. The galacto-conjugated pro-drug Nav-Gal shows a lower induction of apoptosis of non-senescent melanoma SK-Mel-103 cells and lung cancer A549 cells. a. Average percentage of Annexin V-positive cells in control (left) or cisplatin (CDDP)-induced senescent A549 cells (right) exposed to navitoclax (10 µM) or Nav-Gal (10 µM) treatment over time. **b.** Representative images of cell viability depicting staining for Annexin V (green) of control or palbociclib-induced senescent SK-Mel-103 cells, exposed to navitoclax (10 µM) or Nav-Gal (10 µM) treatment over time. Scale bar at lower magnification = 300 µm. Scale bar at higher magnification = 100 µm**. c.** Average percentage of Annexin V-positive cells in control (top) or palbociclib-induced senescent SK-Mel-103 cells (bottom) exposed to navitoclax (10 µM) or Nav-Gal (10 µM) treatment overtime. **d.** Same as in (c) but directly comparing the effect in control and senescent cells of navitoclax (top) or Nav-Gal (bottom) treatment. Data represent mean ± SD (n = 3), where for each biological repeat the percentage of Annexin V-positive cells was calculated in 3 independent technical repeats per experimental condition. Statistical significance was calculated using two-tailed Student's t-tests; *p < 0.05, **p < 0.001.

5.2.4. Cisplatin and Nav-Gal have additive anti-tumour effects *in vitro*

Effective anti-cancer treatments have enhanced clinically beneficial effects when given in combination, including in NSCLC. We therefore next sought to ascertain the efficacy of

concurrent cisplatin and Nav-Gal treatment *in vitro*. We first used clonogenic assays to determine the efficacy of the combination of senescence-inducing cisplatin and navitoclax, Nav-Gal or vehicle, administered concomitantly to A549 cells. Compared with monotherapies, the combination of cisplatin and a senolytic drug was substantially more effective at inhibiting cell proliferation (**Figure 5.8a-d**). From 0 to 2 μM cisplatin, as the concentration of both navitoclax and Nav-Gal increases, additional impairment of cell growth was observed. There was also a significant reduction in the concentration of Nav-Gal required to produce growth inhibition in 1 μM cisplatin versus 0.5 μM cisplatin (**Figure 5.8e**). Similar to the IC50 experiments (**Figure 5.3a, b**), a higher dose of Nav-Gal than Navitoclax was required to achieve the same effect, likely due to the sequential requirement for Nav-Gal processing and activation by lysosomal β-galactosidase activity. While both senolytic drugs showed an additive effect in combination with cisplatin, increasing doses of Nav-Gal exhibited coefficients of drug interactions (CDIs) <1 and closer to 0 in combination with 1 μM cisplatin (**Figure 5.8e**), which suggests that the combination of drugs may be synergistic [262]. Of note, these observations were also validated in the context of a sequential treatment, where colonies were first exposed to increasing concentrations of cisplatin for 7 days, followed by 7 days of senotherapy (**Figure 5.9a,b**).

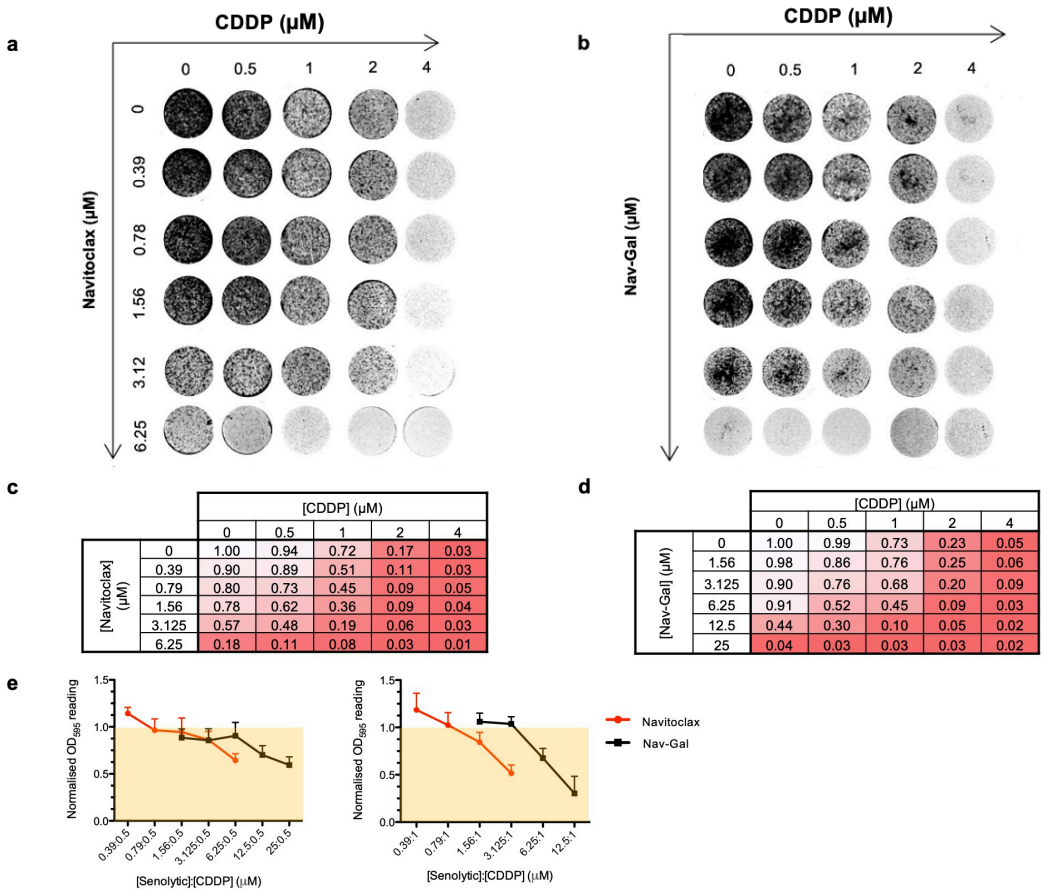

Figure 5.8. The galacto-conjugated prodrug Nav-Gal shows an enhanced effect when combined to senescence-inducing cisplatin treatment. a, b. Representative images of clonogenic survival of A549 cells exposed to increasing concomitant concentrations of cisplatin (CDDP) and **c** navitoclax or **d** Nav-Gal as specified in axis. **c, d.** Numerical heat map representation of normalised mean clonogenic potential after 10 days of increasing concomitant treatment with CDDP and **d** navitoclax or **d** Nav-Gal, where 1 = maximum clonogenic potential corresponding to untreated condition ($n = 3$). **e.** Co-coefficient of drug interaction (CDI) value trend of navitoclax and Nav-Gal across 0.5 μM cisplatin treatment (left) and 1 μM cisplatin treatment (right). CDI < 1 (yellow area) indicates a synergistic effect, where CDI values closer to 0 correlate to higher synergy between the drugs concomitantly used. Data represent mean ± SD ($n = 3$).

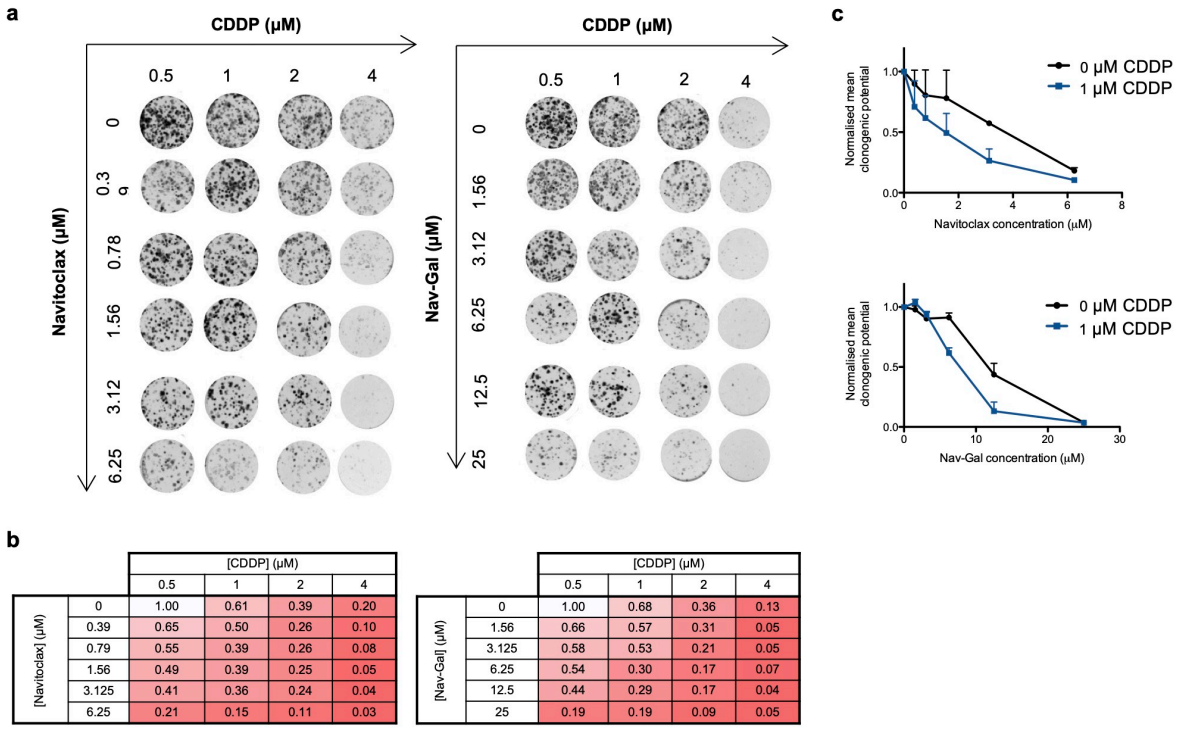

b

[Navitoclax] (μM)	[CDDP] (μM) 0.5	1	2	4
0	1.00	0.61	0.39	0.20
0.39	0.65	0.50	0.26	0.10
0.79	0.55	0.39	0.26	0.08
1.56	0.49	0.39	0.25	0.05
3.125	0.41	0.36	0.24	0.04
6.25	0.21	0.15	0.11	0.03

[Nav-Gal] (μM)	[CDDP] (μM) 0.5	1	2	4
0	1.00	0.68	0.36	0.13
1.56	0.66	0.57	0.31	0.05
3.125	0.58	0.53	0.21	0.05
6.25	0.54	0.30	0.17	0.07
12.5	0.44	0.29	0.17	0.04
25	0.19	0.19	0.09	0.05

Figure 5.9. The galacto-conjugated pro-drug Nav-Gal significantly decreases clonogenic potential in combination with cisplatin. a. Representative images of clonogenic survival of A549 cells exposed to increasing concentrations of CDDP for 7 days followed by the treatment of navitoclax (left) or Nav-Gal (right) as specified in axis for 7 days. **b.** Numerical heat-map representation of normalised mean clonogenic potential after 7 days of CDDP treatment followed by 7 days of senotherapy treatment navitoclax (left) or Nav-Gal (right), where 1 = maximum clonogenic potential corresponding to untreated condition (*n* = 2). **c.** Normalised mean clonogenic potential of A549 cells upon increasing concentrations of navitoclax (left) or Nav-Gal (right) as a single or combined treatment with CDDP.

5.2.5. Nav-Gal demonstrates therapeutic effect in combination with cisplatin treatment *in vivo*

In order to validate the efficiency of the prodrug Nav-Gal in combination with senescence-inducing chemotherapy *in vivo*, we used a model whereby A549 cells were transplanted subcutaneously into the flanks of severe combined immunodeficient (SCID) mice. In a first approach, we aimed to assess the induction of senescence in tumour-bearing mice treated with cisplatin. Histological analyses of the tumours collected after treatment showed evidence of senescence induction upon cisplatin administration (as inferred from SA-β-gal positivity) (**Figure 5.10a**). The effects of concomitant treatment with cisplatin and

each senolytic were then investigated. Once tumours reached an average volume of 100 mm^3, mice were treated with cisplatin and daily doses of navitoclax or Nav-Gal, alone or in combination, for 17 days (as shown in **Figure 5.10b**). Importantly, both drugs significantly improved the tumour growth inhibition of cisplatin (**Figure 5.10c**). The combination of cisplatin with either navitoclax or Nav-Gal had comparable effects on tumour growth inhibition, but both showed statistically significant differences with control and monotherapy groups. In contrast, navitoclax and Nav-Gal had no appreciable effect on tumour growth when administered in the absence of cisplatin, indicating that their therapeutic activities require concomitant induction of senescence by cisplatin in this model system. Consistently, histological analyses of the tumours revealed that cisplatin treatment results in increased p21 positivity (correlating with Western blot analyses of cisplatin-treated cells *in vitro*, **Figure 5.2c**) and decreased Ki67 positivity, which together constitute a hallmark of senescent cells (**Figure 5.10d,e**). Treatment with cisplatin and either navitoclax or Nav-Gal exhibited reduced levels of p21 and Ki67 positivity, alongside a strong TUNEL signal, strongly suggesting that apoptosis of senescent cells facilitates the anti-tumour effect. Additionally, a therapeutic effect of both navitoclax and Nav-Gal in tumour growth was observed in a sequential treatment after one week of cisplatin administration, suggesting a potential application as adjuvant therapy for clearing senescent cells (**Figure 5.11a,b**).

To obtain further evidence of the therapeutic potential of Nav-Gal in combination with senescence-inducing chemotherapy in a more physiological context, we used an orthotopic model of NSCLC. Here, wild-type C57BL/6J mice were transplanted (via tail vein injection) with a syngeneic luciferase-expressing KP lung adenocarcinoma cell line (L1475luc) [300]. Once tumours were established in the lungs, baseline luciferase signals were obtained and mice were then treated for 10 days with cisplatin alone, cisplatin and Nav-Gal in combination, or their vehicles in combination, using the experimental scheme shown in **Figure 5.12a**. Representative images of the luciferase signal at initial- and end-points are shown in **Figure 5.12b**. Luciferase signal monitoring demonstrated that concomitant treatment of the mice with cisplatin and Nav-Gal significantly decreased tumour burden (**Figure 5.12c**) compared with cisplatin monotherapy. Histological analysis of the lungs showed high burden of senescent cells only in cisplatin-treated mice

(as evidenced by increased SA-β-gal and p21 levels), and decreased SA-β-gal and p21 levels and higher TUNEL staining in mice concomitantly treated with cisplatin and Nav-Gal, indicating enhanced apoptosis of senescent cells (representative areas are shown in **Figure 5.12d**).

Taken together, these results demonstrate that the combination of senescence-inducing therapy with senotherapy is highly effective in inhibiting tumour growth *in vivo*, providing preclinical *proof-of-principle* of the therapeutic benefits of using Nav-Gal as a potent activatable prodrug with senolytic activity.

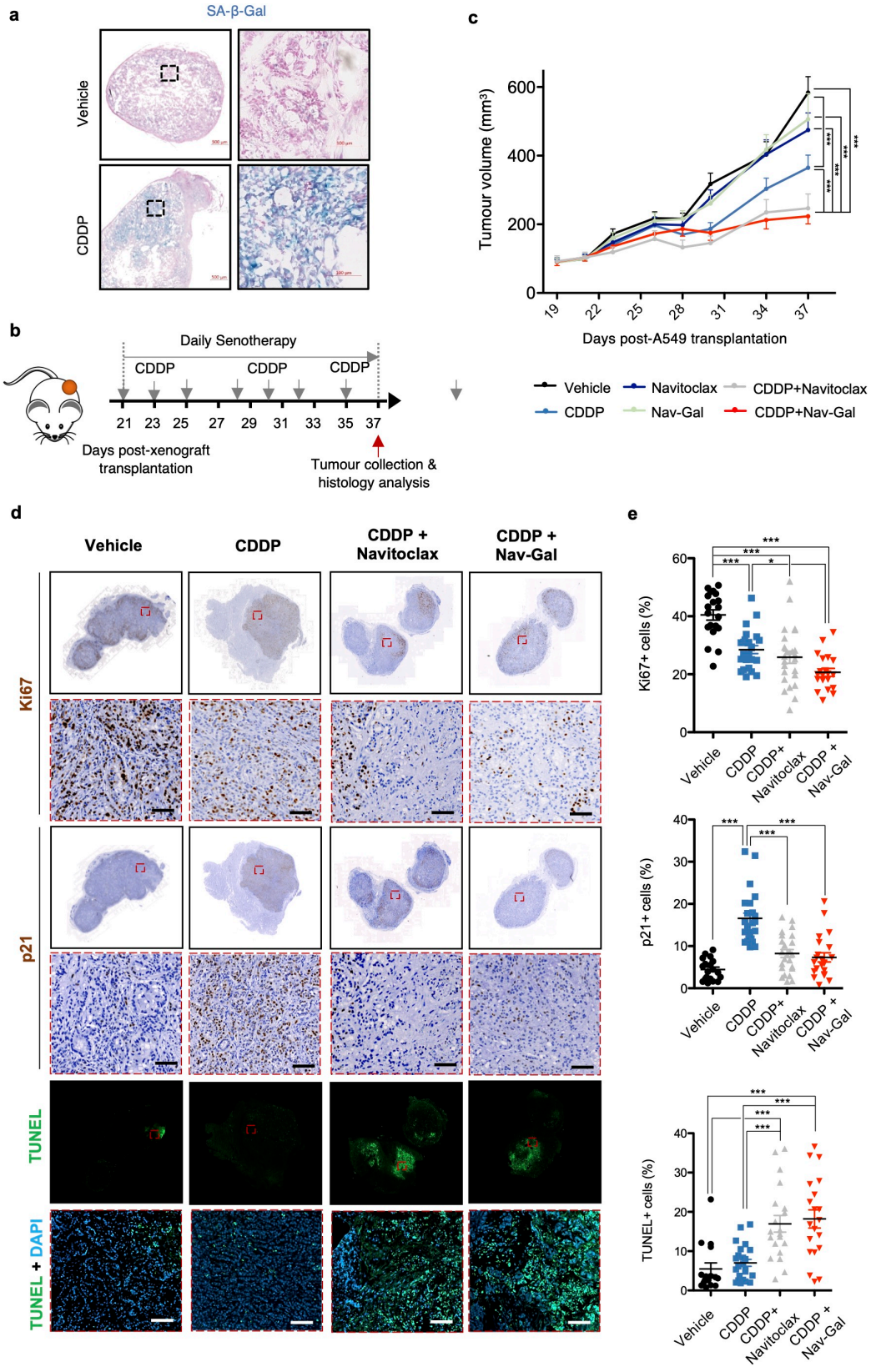

Figure 5.10. Concomitant treatment with the prodrug Nav-Gal and cisplatin significantly inhibits tumour growth in a human lung cancer xenograft mouse model. a. Representative images of A549 xenografts stained for SA-β-Gal activity (in blue) after treatment with cisplatin or vehicle. **b.** Schematic representation of concomitant treatment on A549 xenograft-bearing mice. **c.** Tumour volume of A549

xenografts in mice concomitantly treated with cisplatin and navitoclax or Nav-Gal (as described in b; $n \geq 10$ tumours per group. Data represent mean ± SEM. **d.** Representative histological images of tumours at the end of concomitant treatment, stained for Ki67 and p21 expression, and labelled using TUNEL staining. Scale bar = 100 µm. **e.** Percentage of Ki67- (top), p21- (middle) and TUNEL-positive (bottom) cells in tumours from animals treated with vehicle, cisplatin, or cisplatin and navitoclax or Nav-Gal concomitantly ($n \geq 5$ tumours per group). For quantification, a total of 4 fields per tumour was analysed, covering most of the total tumour area. Two-way ANOVA followed by Bonferroni post-tests was performed to calculate the significance of the results; *p < 0.05; **p < 0.01; ***p < 0.001.

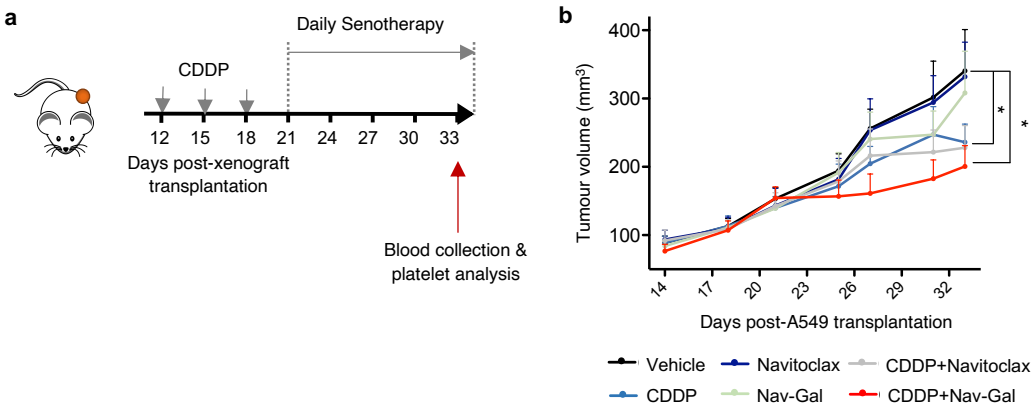

Figure 5.11. Sequential Nav-Gal treatment after chemotherapy decreases tumour volume compared to navitoclax. a. A549-xenograft-bearing mice were first treated for a week with cisplatin (CDDP, 1.5 mg/kg three times a week) and then treated daily with navitoclax (100 mg/kg body weight) or Nav-Gal (85 mg/kg body weight) or their vehicles until end-point. **b**. Tumour volume of A549 xenografts in mice treated as described in (a) over time. Data represent mean ± SEM. Two-way ANOVA followed by Bonferroni post-tests or one-tailed t-tests were performed to calculate the significance of the results; *$p < 0.05$; ***$p < 0.001$; ****$p < 0.0001$.

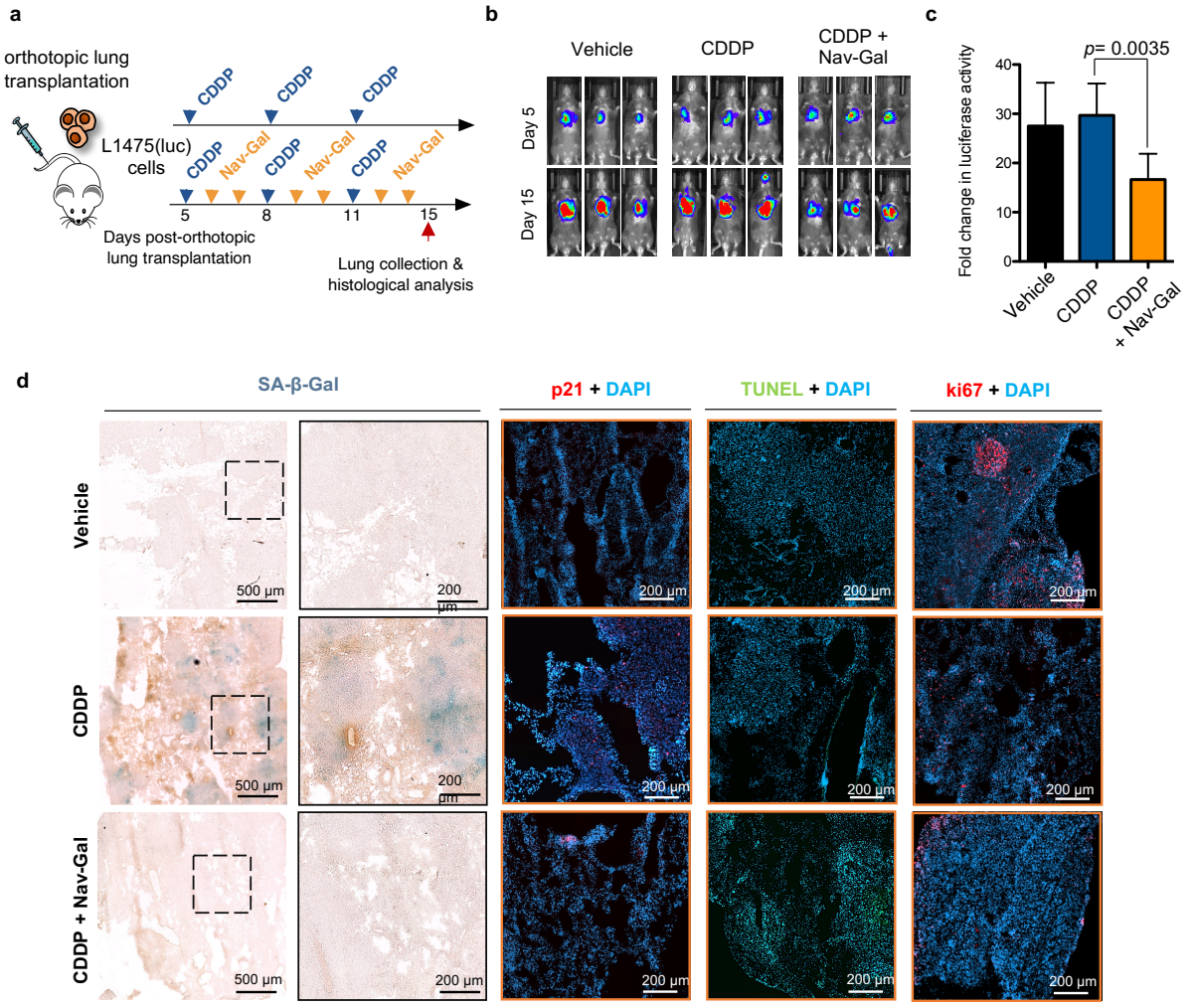

Figure 5.12. Concomitant treatment of lung tumours with pro-drug Nav-Gal and cisplatin significantly decreases tumour burden in lung orthotopic mouse model. a. Transformed primary luciferase-expressing KRas$^{G12D/WT}$;p53$^{-/-}$ lung cancer cells (L1475(luc)) were orthotopically transplanted in the lungs of C57BL/6J mice via tail-vein injection. After 5 days, animals were imaged and randomised into different groups following luciferase signal analysis, and subsequently treated with either vehicle (n = 4), cisplatin (1 mg/kg body weight; n = 5) or cisplatin and Nav-Gal (85 mg/kg body weight; n = 6) as shown in schematic representation. Mice were imaged at day 10 and 15 post-transplantation and lungs were collected at end-point for histological analysis. **b.** Representative images of luciferase activity signal at day 5 (start of treatment) and 15 (end of treatment) of each experimental group. **c.** Fold-change of relative luciferase activity of each group over-time. **d.** Representative histological images of lung sections of each experimental group stained for SA-β-gal activity (left, in blue) and TUNEL (right, in green). Data in (c) represents mean ± SEM, and statistical significance was calculated by one-way ANOVA followed by Bonferroni post-tests.

5.2.6. Nav-Gal presents reduced platelet toxicity *ex vivo* and prevents thrombocytopenia in mice upon chemotherapeutic and Nav-Gal co-treatment

Thrombocytopenia is a major dose-limiting, and clinically important, toxicity that is produced by navitoclax in human patients [327, 330]. A potential benefit for galacto-conjugation of senolytic drugs is the reduction of their associated toxicities, and the potential widening of their therapeutic windows. To determine whether galacto-conjugation affected platelet toxicity, Dr David Macías and Dr Beatriz Lozano-Torres continued with this work performing *ex vivo* experiments with both human and murine blood samples, where whole blood was exposed to increasing concentrations of either navitoclax or Nav-Gal, using fluorescein-labelled annexin V to identify apoptotic platelets by flow cytometry ([331]; **Figure 5.13e, f**). As observed in **Figure 5.13a, b** for human blood and in **Figure 5.13c, d** for mouse blood, when samples were exposed to the same concentrations of navitoclax and Nav-Gal, the proportion of platelets with annexin V signal was significantly higher after exposure to navitoclax than with Nav-Gal. This effect persists in both models, despite a significant difference in platelet sensitivity to BCL-2 family inhibition between each model.

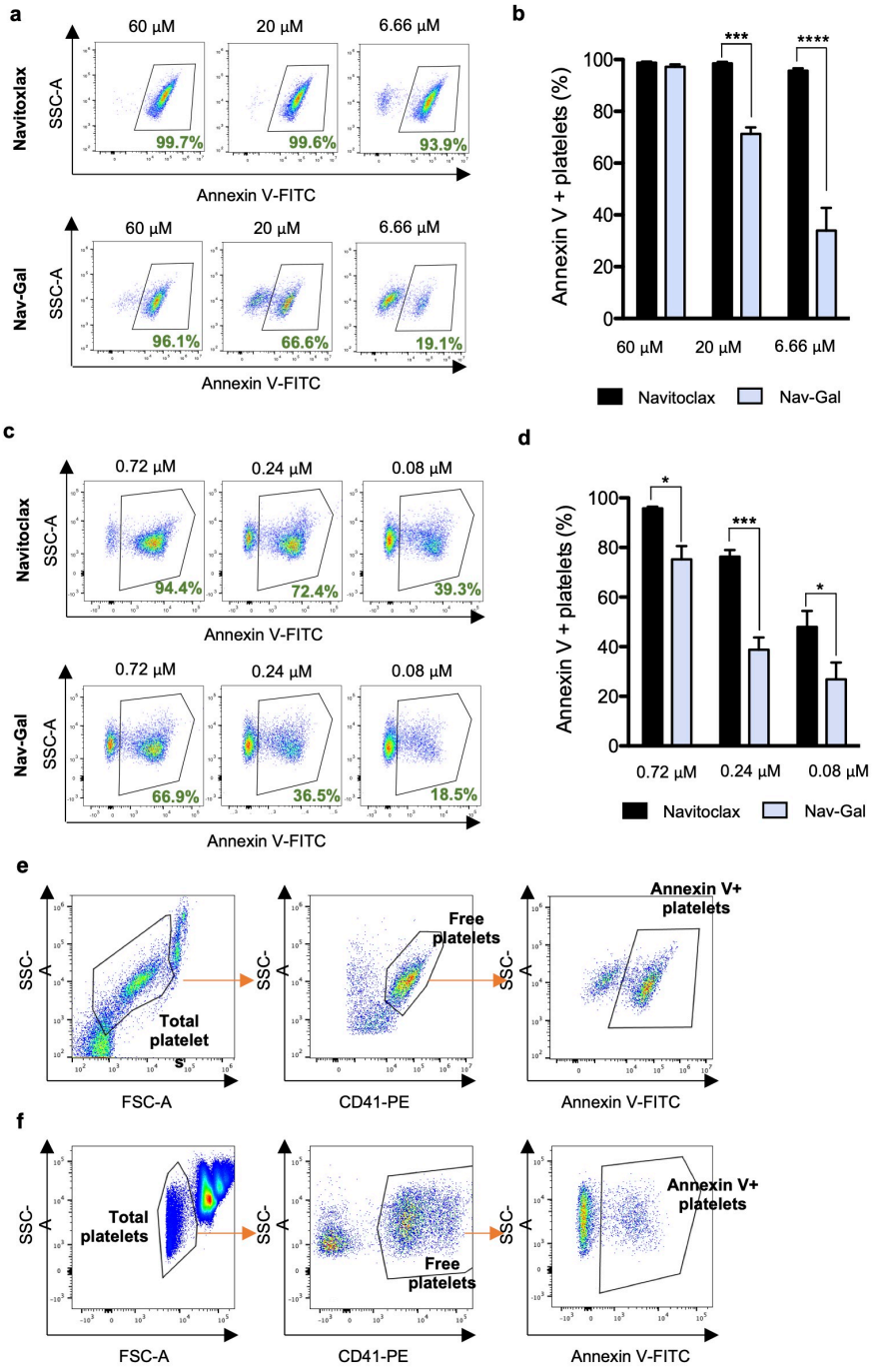

Figure 5.13. Nav-Gal reduces platelet apoptosis in human and mouse blood *ex vivo*. **a.** Blood from healthy human volunteers was collected and treated *ex vivo* with 60, 20 and 6.66 µM navitoclax or Nav-Gal as described. Apoptosis was analysed after annexin V-FITC antibody incubation by flow cytometry. Graphs show proportion of apoptotic platelets upon each treatment based on scatter signals and annexin V expression signal after gating for CD41-positive cells. **b.** Percentage of annexin V-positive platelets in human blood after treatment with 60, 20 and 6.66 µM navitoclax or Nav-Gal. Bars represent mean ± *SD* (*n* = 3). **c.** Blood from wild-type C57BL/6J mice was collected and treated *ex vivo* with 0.72, 0.24 and 0.08 µM navitoclax or Nav-Gal as described. Apoptosis was analysed after annexin V-FITC antibody incubation by flow cytometry. Graphs show proportion of apoptotic platelets upon each treatment based on scatter signals and annexin V

expression signal after gating for CD41-positive cells. **d.** Percentage of annexin V-positive platelets in mouse blood after treatment with 0.72, 0.24 and 0.08 μM navitoclax or Nav-Gal. Bars represent mean ± *SD* (*n* = 5). **e, f.** Gating strategy for the analysis of Annexin V-positive platelets (apoptotic platelets) in samples from **(e)** human and **(f)** mouse blood. Total platelet events were gated based on scatter signals (SSC-A vs FSC-A) and then free platelets were gated through CD41 expression. The percentage of apoptotic platelet was determined by analysing Annexin V-positive population. Two-way ANOVA followed by Bonferroni post-tests or one-tailed *t* tests was performed to calculate the significance of the results; * $p < 0.05$; *** $p < 0.001$; **** $p < 0.0001$.

To determine whether Nav-Gal also protected platelet levels at therapeutic doses i*n vivo*, we first examined the platelet count of wild-type C57BL/6J treated daily with senotherapy for a total of 10 days (**Figure 5.14a**). As shown in **Figure 5.14b**, daily administration of navitoclax resulted in severe thrombocytopenia after only 5 days of treatment, independently of the route of administration. Remarkably, Nav-Gal treatment did not cause thrombocytopenia in the mice and led to platelet count levels comparable to those of vehicle-treated individuals, showing reduced platelet toxicity compared to navitoclax. In order to validate our findings in the context of an *in vivo* cancer model, the platelet count was also assessed at end-points of the concomitant treatment of xenograft-bearing mice described in **Figure 5.10b-d**. Notably, as shown in **Figure 5.14d**, no significant additional thrombocytopenia was observed in the group treated with cisplatin and Nav-Gal (cf. navitoclax). We also found that Nav-Gal reduced platelet toxicity, either in combination with cisplatin or as monotherapy, when administered in a sequential manner (**Figure 5.14e,f**), providing further evidence of platelet protection *in vivo*.

These results confirm that the galacto-conjugation of navitoclax to produce the Nav-Gal activatable pro-drug serves as an effective strategy to decrease navitoclax-driven thrombocytopenia at physiologically relevant concentrations capable of halting cancer growth. Altogether, we conclude that galacto-conjugated navitoclax is effective in clearing senescent cells *in vivo* and can reduce its associated toxicities.

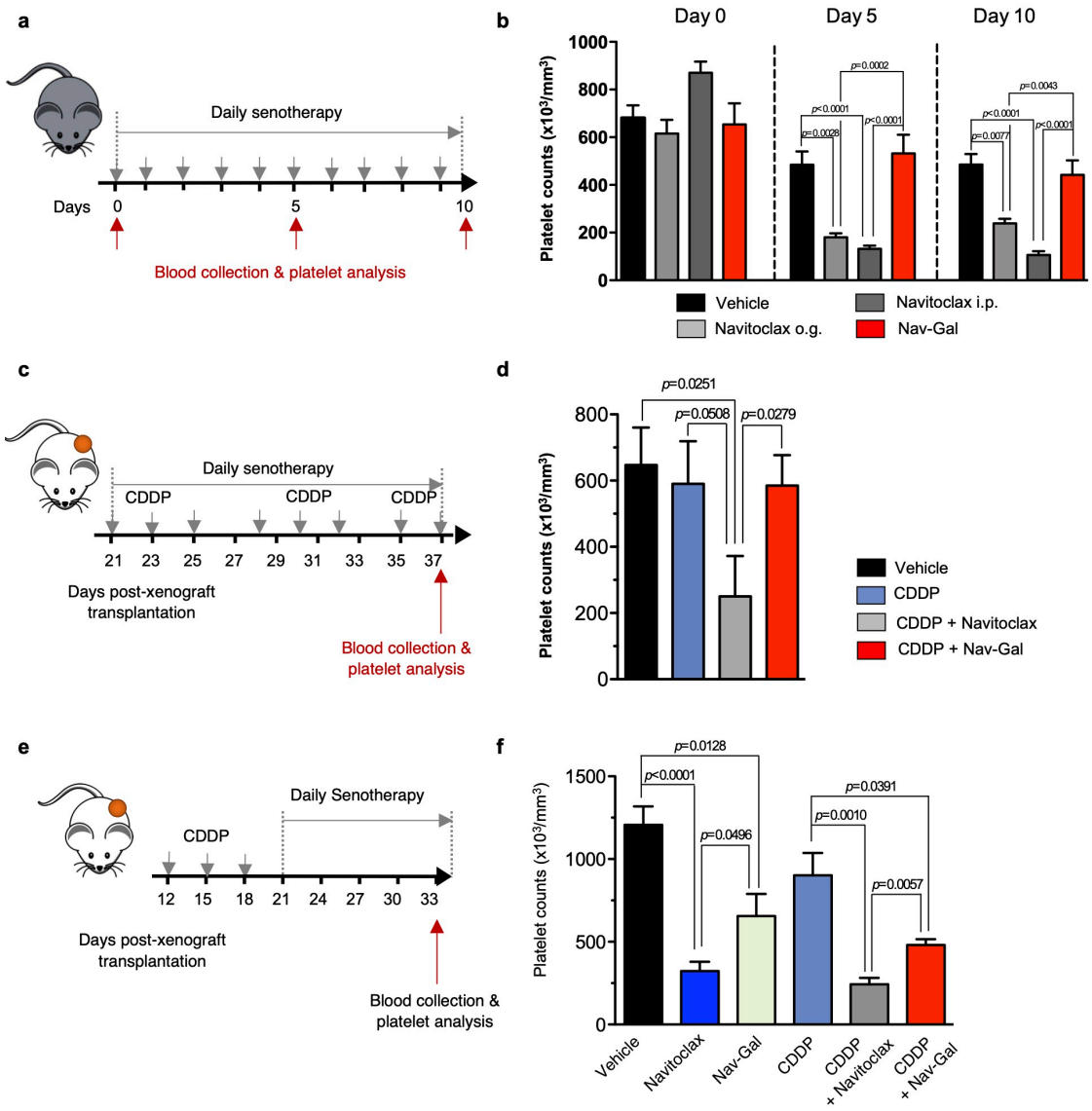

Figure 5.14. Nav-Gal reduces prevents thrombocytopenia in mice treated concomitantly and sequentially with chemotherapy, compared to navitoclax. a. Wild-type C57BL/6J mice were treated daily with navitoclax by oral gavage (o.g.) (100 mg/kg body weight), with navitoclax administered by i.p. injection (85 mg/kg body weight) or with Nav-Gal by o.g administration (85 mg/kg body weight) for 10 consecutive days. Blood was collected on day 0, 5 and 10 by superficial vessel puncture and platelet counts were analysed. **b.** Platelet count on day 0, 5 and 10 during the treatment of wild-type C57BL/6J mice in each experimental condition as described in (e) (vehicle, $n = 4$; navitoclax o.g., $n = 9$; navitoclax i.p., $n = 8$; Nav-Gal o.g., $n = 8$). Bars represent mean ± *SEM*. **c.** SCID mice bearing A549-derived xenografts were treated with cisplatin (CDDP, 1.5 mg/kg body weight three times a week) and concomitant daily senotherapy (navitoclax [100 mg/kg body weight] or Nav-Gal [85 mg/kg body weight]) as shown in this schematic representation. Blood was collected after treatment by cardiac puncture and, platelet counts were analysed. **d.** Platelet count in each experimental condition described in (g) upon end of treatment *in vivo* (vehicle and CDDP, $n = 5$; CDDP + navitoclax, $n = 4$; CDDP + Nav-Gal, $n = 6$). **e.** A549-xenograft-bearing mice were first treated for a week with cisplatin (CDDP, 1.5 mg/kg three times a week) and then treated daily with navitoclax (100 mg/kg

body weight) or Nav-Gal (85 mg/kg body weight) or their vehicles until end-point. Blood was then collected by cardiac puncture and platelet counts in each group were analysed. **f.** Platelet count normalised to vehicle (left) or cisplatin-only treatment (right) in each experimental condition upon end of treatment *in vivo* (vehicle, navitoclax, Nav-Gal and CDDP + navitoclax, n = 5; CDDP and CDDP + Nav-Gal, n = 3). Data represent mean ± *SEM*. Two-way ANOVA followed by Bonferroni post-tests or one-tailed *t* tests was performed to calculate the significance of the results; * $p < 0.05$; *** $p < 0.001$; **** $p < 0.0001$.

5.3. Discussion

In the past years, the development and use of novel genetically engineered mouse models has demonstrated that the selective abrogation of senescent cells attenuates a variety of age-related pathologies and promotes both the lifespan and healthspan of mice [332]. These observations led to the development of senotherapies, treatment modalities aimed at interfering with cellular senescence, either by killing senescent cells (senolytics) or by inhibiting its associated SASP (senomorphics or senostatics) [197]. However, specifically targeting senescent cells still remains a considerable challenge in most cases, and senotherapies are not exempt from both on- and off-target toxicities, due to the activity of these agents in non-senescent cells, such as platelets. In this chapter, we report a versatile methodology for the generation of pro-drugs that increases the selectivity of senolytic activity. We show that galacto-conjugation of the BCL-2 family inhibitor navitoclax allows therapeutically relevant activity in subcutaneous tumour xenografts and orthotopic mouse models of chemotherapy-induced senescence in the context of lung carcinoma. In addition, this strategy reduces navitoclax-associated thrombocytopenia in treated mice, and platelet apoptosis in human and murine blood samples.

Galacto-conjugation as a strategy to target cellular senescence relies on the high levels of lysosomal β-galactosidase (SA-β-gal) activity present in senescent cells. Although SA-β-gal is an imperfect marker of senescence, diseased tissues are often positive for this marker, particularly when senescent cells accumulate and persist in damaged areas [328, 333]. In order to exploit the accumulated pathological SA-β-gal activity, a previous study from our laboratory in collaboration with the same group from the Polytechnic University of Valencia used beads with a mesoporous silica core that were functionally capped with

a homogeneous coating of galacto-oligosaccharides, thereby allowing the encapsulation of cytotoxic drugs, including doxorubicin and navitoclax, as well as fluorescent tracers for the detection of senescent cells. This nanotechnology allowed the preferential cargo release within senescent cells, and the efficacy of this approach was validated in models of bleomycin-induced pulmonary fibrosis and palbociclib-treated melanoma and NSCLC tumours [204]. However, despite the emergent interest in the development of nanomedicine and the considerable technical success of an increasing number of nanotechnologies in preclinical models, only a small number of formulations have reached clinical translation. The current limitations stem from an incomplete understanding of nano-bio interactions, potential toxicities, and challenges regarding biodistribution, such as systemic trafficking, presence of physiological barriers (such as the phagocytic reticuloendothelial system (RES)), mechanisms of cellular uptake, pharmacokinetics/pharmacodynamics (PK/PD), and routes and timelines of elimination [334]. In order to simplify the delivery of tracers to the lysosome of senescent cells, our group created an OFF-ON two-photon fluorescent probe conjugated with an acetylated galactose for tracking cellular senescence *in vivo* [207]. Acetylation is a widely used technique to markedly increase cellular permeabilisation and uptake of N-acetylated amino sugars [208], and represented an attractive approach to generate a novel senolytic pro-drug with increased senescence specificity.

In this chapter, we demonstrate that conjugation of navitoclax with a β-galactosidase activity-driven, cleavable acetylated galactose results in an effective pro-drug that enhances its selective senolytic activity over the parent agent in a variety of cell types and senescent phenotypes, suggesting a potentially universal approach for senescence targeting. This includes cisplatin-induced senescence in human (A549) and mouse (KP) lung cancer lines; human melanoma (SK-Mel-103) and mouse mammary gland (4T1) cancer cell lines responsive to palbociclib; doxorubicin-induced senescent colorectal carcinoma cells (HCT116); mouse lung fibroblasts (MLg cells) subjected to X-ray radiation and human lung fibroblasts undergoing oncogene-induced senescence (ER:Mek IMR90 cells). Since navitoclax is a potent small-molecule inhibitor of BCL-2, BCL-X_L, and BCL-$_W$ proteins that exerts its killing activity by inducing apoptosis [335], we also tested whether this underlying mechanism of cell death is conserved for Nav-Gal. Following the

action of navitoclax, we observed that Nav-Gal induces the appearance of annexin V-positive cells in two models of chemotherapy-induced senescence (cisplatin-induced senescent A549 lung cancer cells and palbociclib-induced senescent SK-Mel-103 melanoma cells), thereby indicating that senolysis by Nav-Gal is driven by the implementation of the apoptotic programme.

After validating the use of Nav-Gal with senescent cancer cells in culture, we focused on two *in vivo* models of lung carcinogenesis subjected to senescence-inducing chemotherapy. Data presented in this chapter showed that simultaneous administration of Nav-Gal with the *standard-of-care* senescence-inducing cisplatin treatment (widely used in the management of NSCLC patients, as presented in previous chapters) resulted in reduced tumour burden in SCID mice bearing subcutaneous human A549 lung tumour xenografts. Concomitant treatment with cisplatin and Nav-Gal also reduced tumour burden in an orthotopic transplantation model using murine KP lung adenocarcinoma cells. Nav-Gal administration showed a strong effect in reducing tumour growth during both sequential and concomitant treatment with cisplatin. Combination treatment suggests an additive/synergistic effect between cisplatin and Nav-Gal, as observed in our clonogenic assays and further confirmed by the calculated coefficient of drug interaction (CDI). It is important to note that neither navitoclax nor Nav-Gal had any relevant impact on tumour burden in the absence of cisplatin in our murine models, strongly suggesting a therapeutic activity restricted to the induction of senescence or whenever tumours contain senescent areas, but not in fully proliferative tumours. These observations reinforce the concept of Nav-Gal as a senolytic pro-drug and, more generally, open up the possibility of using senotherapies as promising adjuncts to treat cancer in combination with senescence-inducing chemotherapies. The eradication of senescent cancer cells by Nav-Gal may also prevent tumour progression by mitigating the senescent secretome (SASP) and its broad range of potential pro-tumorigenic effects [167], which have also been reported in our models in Chapter 4. In this regard, cancer therapies can induce senescence not only in cancer cells but also in stromal cells, and this is also the case in lung cancer patients subjected to platinum- and taxane-based chemotherapy regimens [146]. Stromal senescence appears to establish an immunosuppressive microenvironment that influences and promotes tumorigenesis [128] and can also be a

fundamental driver of the metastatic niche [314]. Future studies will examine the impact of Nav-Gal on stromal senescence. Taken together, our data reinforce the concept that combination treatments comprised of senescence-inducing radio/chemotherapy and senolytics might result in potent approaches for precision cancer management in the near future.

As with many targeted agents, navitoclax presents clinically important and dose-limiting haematological toxicities in clinical trials, including thrombocytopenia [327], presenting particular challenges when given in combination with cytotoxic chemotherapies which also have dose-limiting haematological toxicities. For navitoclax, this occurs because of the importance of BCL-X_L in platelet survival, and the gradual reduction of its levels by navitoclax promotes a change in the molecular clock that determines platelet lifespan leading to the pro-apoptotic activity of BAK [336]. In addition to thrombocytopenia, the first trial to evaluate navitoclax in lymphoid malignancies resulted in grade III transaminitis and gastrointestinal bleed in a proportion of patients subjected to a continuous dosing schedule [330]. The modification of navitoclax with an acetylated galactose may prevent the exposure of healthy (non-senescent) cells to the inhibitory activity of BCL-2 family protein members and, thereby, reduce unwanted side effects. In support of this, our IC_{50} experiments with A549 cells treated with cisplatin indicated that the enhanced senolytic index of Nav-Gal when compared to navitoclax is mainly due to reduced cytotoxicity in the absence of senescence induction, suggesting that the pro-drug is not efficiently activated in non-senescent A549 cells. Also, we noted that although the percentage of annexin V-positive senescent cancer cells at a high concentration of both navitoclax and Nav-Gal is similar and results in the complete eradication of these cells, non-senescent cancer cells were substantially more protected from the induction of apoptosis when exposed to Nav-Gal, indicating enhanced selective sensitivity for Nav-Gal for senescent cells. Importantly, we have observed that Nav-Gal results in less thrombocytopenia (compared with navitoclax) in daily-treated mice. We also show that Nav-Gal reduces apoptosis in platelets, using both human and mouse blood samples. A recent study has shown that another navitoclax derivative, namely DT2216, exerts anti-tumour activity by targeting BCL-X_L to the VHL E3 ligase for proteolytic degradation [337]. However, distinctly to Nav-Gal, DT2216 has not been designed for

targeting senescent cells, but for reducing thrombocytopenia (as platelets are characterized by poor VHL E3 ligase expression) while maintaining anti-cancer properties. In addition, DT2216 specifically targets BCL-X_L, but not BCL-2 or BCL-W, and its potential senolytic activity was not explored. Shortly after the publication of our work [305], He and colleagues made use of the same PROTAC strategy to develop PZ15227 [338]. Despite it is also designed to target BCL-X_L specifically, the authors demonstrated a decrease in platelet toxicity, while equal senolytic *in vitro* effectiveness compared to navitoclax upon treatment of irradiation-induced senescent human lung fibroblasts. This new senolytic, however, was only tested *in vivo* to evaluate its effect in rejuvenating aged mice, and its potential therapeutic benefits were not explored in the context of cancer treatment.

In summary, this chapter presents the synthesis of a potent senolytic prodrug that can be used to kill multiple types of senescent cells. We propose galacto-conjugation as a versatile strategy that might be expanded to other cytotoxic agents and senolytic drugs to develop more specific, next-generation senolytics. As a *proof-of-principle*, we show that galacto-conjugated navitoclax (Nav-Gal) selectively kills a variety of human and murine cell types undergoing senescence by different stressors *in vitro* and that it has therapeutic efficacy in combination with cisplatin in murine NSCLC models. Importantly, we also demonstrate that galacto-conjugation of senolytics can reduce potential toxicities of the conjugated drug. The development of galacto-conjugated prodrugs has considerable promise for improving cancer treatment, as well as other human senescence-related disorders.

CHAPTER 6:
GENERAL DISCUSSION AND FUTURE DIRECTIONS

Lung cancer remains the leading cause of cancer-related deaths worldwide, with more than 1.6 million deceases every year. Despite notable declines in lung cancer incidence and the development of novel and effective targeted therapies, most of the cases are detected incidentally and at late stages, at which point therapeutic options are limited, which results in poor survival. Consequently, the postulated approach to tackle this disease is two-fold nowadays: first, by improving our understanding of early lung cancer development in order to generate efficient early detection and screening strategies and identify more specific targetable biomarkers, and second, by elucidating the physiological, cellular and molecular mechanisms that occur upon standard-of-care treatment, for the development of more efficient treatment modalities aimed at preventing failure and relapse. This thesis provides evidence of the incidence and role that cellular senescence exerts in promoting the progression of early and advanced NSCLC, and demonstrates that platinum-based chemotherapy drives the acquisition of malignant phenotypes in a paracrine fashion. It presents senolytic and TGFβR1 inhibitory treatments as effective management approaches with the potential to prevent such tumour-promoting effects. Lastly, it introduces a novel therapeutic strategy, based on the galacto-conjugation of navitoclax, to mitigate senolytic-associated toxicities and enhance senescence targeting in the context of lung cancer treatment.

6.1. Understanding the role of senescence during NSCLC tumorigenesis

Efforts in the last decades have focused on uncovering the molecular drivers of lung cancer with the aim to identify high-risk populations and biomarkers, and develop effective prediction tools largely based on genomic technologies [339]. Indeed, emergent

evidence highlights the benefits of lung cancer screening [340]. Despite the high rate of false positives, low-dose computed tomography (CT) screening of high-risk populations has shown to be valuable, leading to a reduction in lung cancer mortality by more than 20% compared to chest radiography screening [340, 341]. In addition, recent clinical trials have evaluated liquid biopsy and plasma analysis coupled with CT scanning, which has been shown to effectively reduce the rate of false positives [342, 343]. In spite of these advances, the implementation of a national screening programme based on such approaches still remains controversial, mostly due to cost-effectiveness concerns. Novel strategies to detect NSCLC earlier are needed, but a comprehensive understanding of how this cancer type initiates and develops during early stages is still lacking. Therefore, uncovering new vulnerabilities and defining features that could be leveraged for the development of effective diagnostic approaches is imperative to improve lung cancer patient prognosis.

Cellular senescence is an intriguing cell response known to be causative in a wide array of conditions and pathologies [64], and several studies have demonstrated its accumulation in early cancer lesions [265], including lung adenomas [135]. In Chapter 3, we present further evidence of a marked senescent burden in lung adenomas in comparison with hyperplasias and lung adenocarcinomas. Importantly, the detection and monitoring of this accumulation in clinical settings may represent an attractive approach for diagnostic purposes. In this context, several probes have been developed aimed at monitoring senescence in living organisms, most of which are generated through technologies that leverage the increased lysosomal SA-β-gal activity of senescent cells, providing fluorescent or chromogenic labelling upon catalytic activity [197]. Although these so-called senoprobes are still in pre-clinical phases and further characterisation, optimisation and safety studies are needed before they can be tested in humans, they hold the potential to enhance screening strategies if integrated in combination with CT or X-ray scanning, as the use of contrast materials that can distinguish particular phenotypes in the lesions is known to significantly improve diagnostic confidence [344]. Moving forward, a next step in this study will involve the validation of increased senescent burden in early NSCLC human lesions, which is particularly challenging given the scarcity of available specimens at such stages. In an effort to find supportive clinical evidence of

the incidence and extent of cellular senescence in NSCLC, our group has recently obtained several human lung samples through our collaboration with Dr Robert Rintoul and Dr Doris Rassl (Papwoth Hospital), consisting of a wide histological representation of early lesions, including atypical adenomatous hyperplasia (AAH), minimally invasive adenocarcinoma (MIA), adenocarcinoma *in situ* (AIS) as well as treatment-naïve lung adenocarcinoma (ADC). Immediate future work will therefore focus on performing immunohistochemical analyses in order to detect and determine the extent of senescent markers in each type of lesion. If a significant increase in early lesions (AAH, MIA, AIS) is uncovered in comparison with untreated ADC, our analyses will present, for the first time, evidence of a senescent accrual in the context of human lung tumorigenesis, providing crucial clinical insights and allowing the evaluation of senescence-targeted approaches as potential early detection strategies.

Despite the validation of its accumulation can be of significant clinical value *per se*, understanding the processes whereby senescence may contribute to tumour progression in the early lesions can also be essential for the development of monitoring or preventative approaches. From a cell-intrinsic perspective, the net effect of senescent induction is a robust suppression of tumour progression. It is for this reason that early reports describing senescence as a defining feature of early cancer lesions deemed OIS as a barrier to tumour development [132, 133, 135, 154, 155]. However, in the context of complex biological systems, senescence fostering tumour progression through paracrine signalling or escape from the senescent programme is a possibility. Nevertheless, spontaneous senescence escape upon OIS in living organisms has not been demonstrated so far. In addition, probably owing to the challenging nature of evaluating this *in vivo*, the cell extrinsic role of senescence in the context of early cancerous lesions remains largely elusive. Intriguingly, a recent study demonstrated that accumulated senescent cells in pre-malignant lesions in a *Kras*-driven mouse model of pancreatic cancer support tumour progression through the secretion of pro-inflammatory factors, including Cox2 [345], thereby proposing OIS as an actual driver of tumorigenesis. In line with this, our analyses indicate that senescence accrual in lung adenomas in a $Kras^{G12V}$-driven NSCLC mouse model may promote lung cancer advancement, since senescent

eradication through senolytic treatment abrogates tumour growth and enhances mouse survival.

Importantly, histological evaluation and transcriptomic analyses performed by our collaborators have shed light onto the most prominent cell types exhibiting a senescent phenotype, but further work is needed to uncover the mechanisms through which they exert pro-tumorigenic effects in the pre-malignant niche, and how such effects eventually result in the initiation or progression of the disease. In this context, it would be interesting to determine whether a link between senescent and tumour-initiating cells in the lung exists. To this date, the identification of the cell of origin NSCLC is still controversial and challenging [346], but recent studies have concluded that the cell of origin may be a differentiated cell that upon oncogenic damage, including the activation of oncogenes and/or the loss of tumour suppressors, undergoes de-differentiation and acquires an aberrant or hyperplastic plastic state, initiating cancer (reviewed in [347, 348]). Accordingly, AT2 progenitors with stem-cell activity have been reported as adenocarcinoma initiating cells [22-24]. The concept of cell damage creating a microenvironment that favours cell de-differentiation and plasticity places cellular senescence as an intriguing key process, given the fact that the SASP is known to promote reprogramming-like processes during tissue regeneration, including the secretion of factors like IL-6 [85, 173, 349]. It is therefore tempting to speculate that the accumulation of senescence in adenomas may promote a maladaptive gain of plasticity in nearby cells, favouring lung cancer initiation. In the future, we will explore the expression of reprogramming, stemness and proliferation markers in cells located in close vicinity to senescent cells in early lesions, to further elucidate the interaction between the two and the particular phenotypic changes elicited in response to the SASP. We also plan to generate *in vivo* tracing approaches that allow us to detect, monitor and isolate both senescent and SASP-exposed cells in the early pre-malignant niche, in order to characterise by single-cell RNAseq the transcriptional changes and the cell identity of the cells involved in these potential interactions.

In this work, we further demonstrate that senolytic treatment of lung cancer developing lesions can serve as an efficient strategy to hamper NSCLC progression. Senolytic modalities are currently entering clinical trial stages for the management of

several age-related diseases [197], and their potential benefits in the context of cancer care are only beginning to be explored. Although a promising approach, the use of senolytics should be considered with caution, especially considering that targeting senescence at the systemic level may compromise patient health. For instance, targeting senescence holds the risk of abrogating particular subsets of macrophages [275, 276], megakaryocytes [90] and osteoblast progenitors in long bones [350]. In addition, senescent elimination in the case of ageing or age-related disorders can result in problems of structural integrity. As an example, Grosse and colleagues demonstrated that abrogation of p16-high cells in aged mice led to severe bleeding due to the accumulation of senescent endothelial cells and hepatic fibrosis [351].

In addition to systemic senescence, it is worth noting that, as evident from our analyses, different subtypes of senescent cells co-exist in early lung pre-malignant lesions. Consistent with our data, Kolodkin-Gal and colleagues also demonstrate distinct subsets of senescent cells in pancreatic pre-malignant lesions, identified in both the epithelial and stromal cell compartments [345]. Given the fact that the resulting senescent phenotype and exerted SASP largely depend on the cell type, it is important to understand the role of the different types of senescent cells in pre-malignant lesions. Can different senescent subsets be exerting opposing roles in the niche? Could *Kras*-driven epithelial senescent cells be acting as a barrier to tumour progression, while senescent stromal cells (such as macrophages) promote tumour progression in a paracrine manner? In such scenario, the resulting overall net effect of senescence induction could also depend on the proportion of each subset of senescent population. Consequently, it is imperative to explicitly characterise both the phenotype and proportion of each senescent population to ensure maximum benefit from senolytic strategies.

In this thesis, we demonstrate that senolytic treatment has the potential to serve as a preventative therapy in the context of NSCLC. This is of particular relevance in the case of multifocal lung primary lesions or neoplasms, a complex condition in which multiple precancerous early lesions are present in the lungs, with a minority of them, if any, eventually progressing to malignant disease [260]. These multifocal primary pre-invasive NSCLC patients are usually patients with a smoking history, and their numbers are dramatically increasing the set-up of screening programmes in many countries,

including the UK. Since they accumulate high numbers of premalignant neoplasms, patients are not suitable for lung tissue resection and require frequent monitoring by CT, given that no effective pharmacological strategies are currently available in order to prevent the potential progression of the lesions (i.e. chemotherapies do not usually work in precancerous tumours that hardly progress or develop slowly). Approaches as the one we propose in Chapter 3 could therefore be considered as effective preventative courses for the progression of pre-cancerous NSCLC lesions, and may even be extended to other pre-malignant diseases where senescence accrual has been reported as a key player of the tumour niche [265]. Despite chemoprevention currently remains limited to very few circumstances (such as tamoxifen and raloxifene for high-risk of breast cancer individuals [352]), with further research and clinical support, we believe that senolytic preventive strategies hold the potential to revolutionise cancer care in the future.

In closing, future work will uncover the potential existence of cellular senescence in human early lung pre-malignant specimens. Planned studies should also provide a more detailed elucidation of the identity and characteristics of the different senescent cell subtypes that exert pro-tumorigenic effects in lung adenomas, as well as the mechanism of action whereby tumour promotion or initiation takes place. In addition, future analyses will address the potential effects of the senolytic treatment on other cell populations for a complete picture of the benefits and risks of these modalities in early cancer management. The elucidation of such elements will be crucial for the understanding of NSCLC initiation and progression, and will open up the dialogue for the potential implementation of senescence-targeting strategies as diagnostic and preventative approaches in the context of lung and other cancers.

6.2. The impact of chemotherapy-induced senescence in lung cancer management

As the evidence of therapy-induced senescence and tumour-promoting effects accumulates, the impact of senescence in cancer care has become an increasing concern. Therapy-induced senescence substantially contributes to the efficacy of anti-cancer treatments, but unresolved senescence has been reported to drive tumour relapse,

metastasis and even chemotherapy-derived toxicities and complications [294]. Consequently, the growth arrest observed by imaging techniques during chemotherapy monitoring should not always be interpreted as a favourable response.

In the context of NSCLC, the first clinical evidence of a potential detrimental effect from cisplatin administration was reported in a study published in 2003, where authors observed that NSCLC patients who received platinum-based chemotherapy presented increased tumour progression while waiting for radiotherapy, compared to untreated patients [261], contrary to the general cytostatic perception of chemotherapy to date. Later studies demonstrated that platinum-based treatment results in increased SA-β-gal levels in lung adenocarcinoma tumours, and that higher levels of this senescent marker correlated with poorer patient outcomes [160, 292]. However, the role of senescence or the mechanisms whereby these pro-tumorigenic effects take place upon chemotherapy in NSCLC have not been addressed to date. In this thesis, we present evidence of the induction of cellular senescence upon cisplatin treatment in both human and murine lung adenocarcinoma cells, and we demonstrate that the SASP implemented by these cells, enriched in TGF-β ligands, drives the acquisition of malignant traits in untreated or nearby lung cancer cells.

Evidence of the role of TGF-β as a promoter of proliferation is scarce. While this cytokine has been widely reported to play a dual role in cancer, the pro-tumorigenic effects are largely related to the promotion of EMT phenotypes in advanced tumours and metastasis [210]. However, a limited number of reports demonstrate that, in certain circumstances, exposure to TGF-β can also result in increased proliferation. Intriguingly, these studies indicate that growth promotion is greatly dependent on the concentration levels of this cytokine in the conditioned media, and that subtle changes can lead to opposing effects in proliferation [298]. Other reports, on the other hand, highlight the interplay between TGF-β and other factors, including PDGF-B, PDGF-AA and HGF, in driving cell growth [233-235, 237]. Intriguingly, we have actually found PDGF-AA and HGF particularly enriched in cisplatin-derived SASP in preliminary cytokine array analyses. Considering the complexity of TGF-β extracellular regulation and interplay with other factors, it is likely that additional mechanisms underlying TGF-β-derived pro-proliferative effects in our experiments are also taking place. Such scenarios may include not only the

parallel secretion of other factors as part of cisplatin-derived SASP, but also the existence of particular co-receptors or membrane-bound activating molecules already present in untreated cells, their *de novo* expression upon exposure to TGF-β, or the induced secretion of mitogens in recipient cells that promote cell proliferation in an autocrine manner. While we cannot exclude these additional mechanisms, especially considering that TGF-β ligands also appear upregulated in docetaxel- and palbociclib-induced senescent cells (although to a lower extent compared to cisplatin-induced senescent cells), the effects observed are likely to be driven by these cytokines, given the fact that both genetic downregulation and pharmacologic inhibition of TGFβR1 reverts the observed phenotype. In addition, we also demonstrate that exposure of A549 cells to TGF-β1 and TGF-β2 is sufficient to increase cell proliferation. In the future, further experiments will be performed in order to validate the specific TGF-β factor(s) responsible for the promotion of malignant traits in untreated cells, including antibody-mediated inhibition assays and the generation of A549 and L1475(luc) lines deficient for each of the ligands.

As part of our on-going interest in elucidating the impact of TGF-β-rich SASP in the tumour microenvironment, we will also aim to investigate the immune landscape and dynamics during cisplatin-induced senescence in mice, since TGF-β is known to be a strong immune modulator. For this, we have recently generated a new cell line derived from L1475(luc) mouse adenocarcinoma cells that secretes a cell-penetrating fluorescent protein that can be taken up by surrounding cells *in vivo*, allowing their labelling and identification [353]. We plan to transplant senescent and non-senescent L1475(luc)-labelling cells orthotopically, characterise the phenotype of labelled (recruited) immune cells in the tumour niche, and investigate whether the effects or phenotypes detected are dependent on SASP-derived TGF-β signalling, via galunisertib treatment.

Elucidating an impact not only on the direct support of cancer cell growth but also the promotion of an immune suppressive environment would place TGF-β as an intriguing target in NSCLC management. Indeed, several clinical trials are currently evaluating anti-TGF-β therapies for the treatment of lung cancer. For instance, a phase 1/2 trial is investigating the effect of galunisertib (TGFβ-R1 inhibitor) in combination with the anti-PD1 antibody Nivolumab for the treatment of recurrent or refractory NSCLC

(NCT02423343). In addition, the safety and efficacy of Fresolimumab, a human clonal monoclonal antibody directed against TGFβ-1, -2 and -3, is being tested on Stage IA and IB NSCLC patients as a way of inhibiting steoreotactive ablative radiotherapy (SABR)-derived side effects on tumour growth (NCT02581787). Finally, a bifunctional fusion protein named M7824 that targets TGF-β ligands is being evaluated in comparison with pembrolizumab in patients with advanced NSCLC presenting high PD-L1 tumour expression (NCT03631706). If proven safe and successful, these trials may encourage the clinical evaluation of novel treatment modalities that have the ability to enhance standard-of-care chemotherapy by modulating TGF-β, such as the combination of cisplatin and galunisertib treatment proposed in this thesis, which has demonstrated potential in reducing tumour burden compared to cisplatin treatment alone.

Signalling pathway investigations in Chapter 4 indicate that the promotion of malignant traits occurs through the activation of the Akt/mTOR/P70S6K cascade, since the pharmacological inhibition of both TGFβ-R1 and mTOR (through galunisertib and rapamycin treatment, respectively) results in decreased activating phosphorylation levels and hinders the promotion of cell growth. Of note, the increased tumour burden observed in the orthotopic model when L1475(luc) cells previously exposed to cisplatin-derived SASP were transplanted in the lungs of mice made us consider that the enhanced proliferation could be sustained in time, and therefore the cells had undergone epigenetic modifications and had been reprogrammed to proliferate faster indefinitely. Indeed, the activation of PI3K/Akt pathway in response to drug treatment, including cisplatin, has been reported to induce epigenetic changes that perpetuates a metabolic reprogramming in cancer cells, leading to treatment resistance [354]. However, our analyses determined that the effect on proliferation wore off with time and disappeared 10 days after the exposure to cisplatin-derived SASP, suggesting that the promotion of proliferation is likely driven by a direct and transient response to the activation of the Akt/mTOR cascade. It is worth noting, however, that despite the stimulation of this pathway is only transient, the response *in vivo* can be chronic, as observed in our experiments, if senescent cells are not eliminated. In order to better understand the particular changes that occur in cells exposed to cisplatin-derived SASP, we plan to perform RNAseq analysis of A549 and L1475(luc) cells upon incubation with the CM at

different time-points and elucidate the transcriptional dynamics that can explain the acquisition of a more malignant phenotype in the cells.

An important aim of Chapter 4 included the validation of our findings in human clinical settings. We aimed to analyse NSCLC data from The Cancer Genome Atlas (TCGA) in order to find evidence of a senescent transcriptomic signature in patients receiving platinum-based chemotherapy, but the available datasets only gather data from specimens resected prior to treatment or at the time of relapse, meaning that the evaluation of tumour response immediately after or close to chemotherapy administration was not possible. Future alternatives can include the analysis of additional datasets recently published in studies where the mutational burden of different chemotherapies has been studied in large sets of patients, including NSCLC [355]. Importantly, however, in Chapter 4 we show a marked expression of senescent markers, including p21 and p16, in samples resected from stage II and III NSCLC patients that underwent platinum-based neoadjuvant treatment. Next analyses will evaluate the expression of these markers in treatment-naïve human lung adenocarcinomas, and we will perform quantifications to determine the increased senescent burden compared to untreated specimens. Further, in support of our mechanistic insights upon exposure to cisplatin-derived SASP, we were able to identify an intriguing association between the expression of senescent markers in these samples and the activation of the mTOR/AKT pathway. In the future, we will perform co-stainings in order to evaluate the expression of these markers at the cellular level and validate a close vicinity between putative senescent cells and other tumour cells where this cascade is activated, together with more detailed histological analyses. The reported connection in our histological analyses, however, are promising and indicate the potential relevance of our findings in human clinical settings.

The evidence presented in this thesis strongly highlights the importance of elucidating the impact of chemotherapy-induced senescence in cancer care. In this context, it is crucial not only to understand the senescent phenotype (and its associated SASP) elicited in response to a particular treatment, but also to uncover how senescent cells prevail, adapt and evolve under the pressure of persistent genotoxic stress, something that has not been explored as part of this work, and that is likely to impact the

already well-established genetic instability of tumours. In addition, it remains unknown to what extent the cancer type, the molecular drivers of the tumour, the existent mutational burden before treatment and the chemotherapeutic agent itself can determine the phenotype of the senescent programme that is implemented during therapy. Of note, recent reports demonstrate that increased intra-tumoral heterogeneity in treatment-naïve tumours is linked to treatment resistance, and that platinum-based chemotherapy results in significant transcriptional and phenotypic diversity within the tumour [30, 31]. Intriguingly, this might indicate a significant heterogenic response in the tumour upon platinum treatment, including apoptotic, senescent and treatment-resistant populations, setting a particular situation where the detrimental effects from unresolved senescence might be exacerbated. We thus believe that strategies for the detection of such unfavourable responses are needed, and in this context, the monitoring of relevant SASP factors, including TGF-β, could potentially help predict patient prognosis, contribute to patient stratification and motivate the administration of treatment modalities aimed at preventing tumour relapse and ensuring maximum benefit from chemotherapy. Understanding the different heterogenic responses within the tumour upon chemotherapeutic treatment and how these are implicated in treatment resistance and tumour relapse is therefore an essential goal for the future of chemotherapy.

In summary, we here demonstrate that cisplatin treatment results in the robust induction of cellular senescence in lung adenocarcinoma cells. Comprehensive phenotypic assessment reveals that the SASP derived from human and murine cisplatin-induced senescent lung cancer cells drives the acquisition of pro-tumorigenic traits in a paracrine manner, which can be recapitulated in human xenografts and orthotopic mouse models of lung cancer. Mechanistically, we show that exposure to cisplatin-derived SASP orchestrates the TGFβR1-driven activation of Akt/mTOR signalling, which is responsible for the induction of increased proliferation in SASP-exposed cells. In agreement with this, we determine that pharmacological inhibition of TGFβR1 with galunisertib treatment reverts the tumour-promoting effects of cisplatin-induced senescence both *in vitro* and *in vivo*. Finally, we propose a novel therapeutic modality combining chemotherapeutic cisplatin treatment together with TGFβR1 inhibition, which demonstrates improved treatment outcomes and enhanced survival in lung tumour-

bearing mice. Future work will involve furthering the exploration of senescence and the mechanistic evaluation of our findings in clinical samples and patient-derived xenografts, as well as the analysis of SASP factors, including TGF-β, in peripheral blood collected from patients undergoing platinum-based treatment. We will also characterise the transcriptional changes elicited in response to the exposure of cisplatin-derived SASP with the aim of further understanding the mechanisms whereby acquisition of malignant traits take place in the cells. These insights can result not only in senolytic but in more refined senomorphic concomitant modalities with senescence-inducing therapies. In addition, we plan to explore the impact of cisplatin treatment in other cancer types where platinum chemotherapy largely remains the standard-of-cancer, such as ovarian cancer. Finally, in the long-term, we plan to explore if our observations can be expanded to other relevant cancer treatments, such as TKI and hormonal therapies. These further insights will not only strengthen our observations upon platinum-based chemotherapeutic treatment of NSCLC, but they can also help position the manipulation and targeting of cellular senescence as a relevant therapeutic proxy for improved cancer management and prioritise the most efficient preclinical strategies to early phase clinical trials.

6.3. Second-generation senolytics with reduced toxicities and improved efficiency as novel modalities for cancer treatment

Combinatory therapies for cancer management were first postulated in 1965 for the treatment of leukaemia [356], and represent today a cornerstone of cancer management. Finding additional tumour vulnerabilities or the mechanisms whereby the efficacy of single agent therapies may be compromised has proven crucial for new treatment paradigms. Indeed, the combination of chemotherapeutics and additional inhibitors that target different pathways can provide a synergistic or potentiation effects, yielding significant anti-tumour results [357]. The data generated in Chapter 4 indicates that unresolved platinum-based chemotherapy drives tumour progression through the implementation of a TGF-β-rich SASP, which poses the possibility of targeting either senescence, the SASP or TGF-β for improved treatment outcomes as an intriguing approach. Importantly, our investigations provide evidence of the therapeutic benefit

obtained through senolytic-driven ablation of senescent cells in the context of cisplatin treatment in NSCLC, which supports the potential of combining senolytics and chemotherapeutic regimens as promising two-hit strategies to increase cancer cell killing, eliminate residual disease and prevent unwanted tumour-promoting effects.

In response to the identification of the deleterious consequences of senescence in cancer, ageing and other conditions, the field of senolytics and senomorphics has rapidly expanded. A number of novel small molecules that preferentially target, kill or modulate senescent cells have been identified and developed, providing a solid springboard for the evaluation of novel modalities in cancer care. Out of these, navitoclax, which is a synthetic small molecule that acts as a BH3 mimetic, has been the most successful in preclinical models of cancer to date. It has demonstrated a remarkable ability in eliminating cancer cells induced to senesce through varying therapeutic agents, including lung cancer cells treated with etoposide, kinase inhibitors and irradiation [358, 359], ovarian and prostate cancer cells treated with PARP inhibitors [360, 361] and breast cancer cells exposed to doxorubicin, radiation or BET inhibitory treatments [359, 362, 363], among many others. Despite its success, a major drawback of navitoclax treatment derives from its systemic toxicity, which appears to be a consequence of on-target BCL-X_L inhibition in platelets [364]. This results in severe thrombocytopenia and neutropenia in patients, which regrettably precludes its utilisation in the clinic [364]. Therefore, the development of advanced strategies with increased senescence specificity that leverage its senolytic potential while preventing such hematologic adverse reactions can be promising candidates for cancer treatment.

In Chapter 5, we present the formulation of a novel pro-drug, named Nav-Gal, developed through the conjugation of a cleavable galactose to navitoclax, with the aim to increase specificity and reduce navitoclax-associated toxicities. Through a variety of model systems, our data shows that Nav-Gal is effectively activated in senescent cells in a GLB1-mediated manner, resulting in selective, pro-apoptotic senolytic activity. Concomitant treatment of Nav-Gal with the senescence-inducing chemotherapy cisplatin efficiently arrests tumour progression in models of orthotopically transplanted murine lung adenocarcinoma cells and in a tumour xenograft model of human NSCLC.

Importantly, recent studies have applied novel technologies for the development of new senolytics. Galacto-conjugation has recently been used by Guerrero and colleagues to generate a pro-drug through the combination of a galactose residue to the cytotoxic drug duocarmycin [365]. The authors demonstrate that the resulting agent preferentially kills a variety of senescent cells *in vitro* and reduces the number of precancerous senescent cells in an *in vivo* model of craniopharyngioma [365]. However, duocarmycin is not a senolytic *per se*, and the authors did not assess any potential associated toxicities derived from systemic off-target or on-target effects. Shortly after the publication of this study, He and colleagues made use of the proteolysis-targeting chimera technology [305] to develop a new drug, named PZ15227, with the aim of reducing platelet toxicity of navitoclax. PROTAC are small molecules that contain a ligand able to recognise a target protein (in this case, Bcl-xl) and a second region that is able to recruit the E3 ubiquitin kinase [337]. The induced proximity of the target (Bcl-xl) and the ubiquitin kinase drives the ubiquitination of the first one, and its subsequent degradation by proteasomes [338]. The application of this intriguing approach by the authors demonstrated a decrease in platelet toxicity, while equal senolytic *in vitro* effectiveness compared to navitoclax upon treatment of irradiation-induced senescent human lung fibroblasts [338]. This new drug, however, has been generated *de novo* and not derived form an existing and already well-studied senolytic, like Nav-Gal. In addition, it was only tested *in vivo* to evaluate its effect in rejuvenating aged mice, and its potential therapeutic benefits were not explored in the context of cancer treatment. Consequently, to our knowledge, our approach is the only one that has provided an actual second-generation senolytic, as we use galacto-conjugation as a means to increase the specificity of an *existing* first-generation senolytic, and tested in the context of cancer treatment. By applying this two-level functionalisation approach (targeting both the increased SA-β-gal and resistance to apoptosis of senescent cells), on-target effects on platelets are efficiently reduced, resulting in a marked decrease of thrombocytopenia in mice treated at therapeutically effective doses, as well as a reduction in apoptotic platelets in human blood samples treated *ex vivo*. In addition, we believe that using navitoclax as the backbone of our new pro-drug places Nav-Gal at a particular advantage for rapid clinical translation. Indeed, navitoclax is already being evaluated in several clinical trials in

combination with different chemotherapies to treat solid tumours, including EGFR-positive advanced NSCLC (NCT02520778), SCLC (NCT00878449) and metastatic melanoma (NCT01989585), among many others [197], highlighting the potential impact that Nav-Gal presents as a combinatory approach for cancer treatment.

Of note, we did not evaluate the potential uptake and effects of galacto-conjugation of navitoclax in tissues and cells known to have increased GLB1 activity in living organisms, such as macrophages and osteoclasts. Despite we hypothesise Nav-Gal will not result in detrimental effects in these cells, given the underlying working mechanism of the active drug, the assessment of potential side effects in these populations should be carried out in the future. In addition, although no obvious side effects derived from Nav-Gal administration were detected in any of the *in vivo* models tested, further safety and toxicity studies that elucidate the pharmacodynamics and pharmacokinetics processes will be imperative to confirm the favourable safety profile of Nav-Gal and allow its further evaluation and assessment in clinical settings.

Finally, it is worth noting that navitoclax treatment has been reported to provide additional benefits derived from the removal of non-malignant therapy-induced senescent cells. Strikingly, this has been shown to result in less severe bone-marrow suppression and a decrease in cardiac dysfunction following doxorubicin treatment in an orthotopic model of breast cancer [130], as well as it alleviated symptoms of cisplatin-induced peripheral neuropathy [367] and hampered cortical bone loss, also upon doxorubicin treatment [368]. In the future, it would therefore be interesting to investigate whether Nav-Gal preserves such therapeutic benefits while maintaining the efficiency in senescent cell removal in the tumours and preserving platelet survival. Future investigations will also evaluate the therapeutic benefit in additional conditions where senescence accumulation is known to be detrimental, such as pulmonary fibrosis [204].

Altogether, our results from Chapter 5 provide the proof-of-concept of a novel potent formulation that has the potential to increase senolytic specificity, improving chemotherapeutic treatment outcomes in NSCLC models, and providing a safer alternative that precludes haematologic toxicities.

6.4. Concluding remarks

The purpose of this thesis was to investigate whether cellular senescence induced by oncogene-activation and by platinum-based chemotherapeutic conventional treatment can contribute to lung cancer progression, and to provide a novel therapeutic strategy to counteract such effects with reduced toxicities.

In Chapter 3, we employed the Kras-FSF^{G12V} model of NSCLC and demonstrated the increased expression of markers of cellular senescence in lung adenomas at the histological level, including higher SA-β-gal activity, p21 and p16 expressions. After verification of senescence induction in the lesions, we evaluated the impact of senescent cell ablation during lung tumorigenesis through senolytic ABT-737 treatment, and concluded that senolysis results in decreased lung tumour burden and enhanced animal survival, thereby demonstrating that senescence accumulation during NSCLC tumorigenesis supports lung tumour progression (**Figure 6.1**).

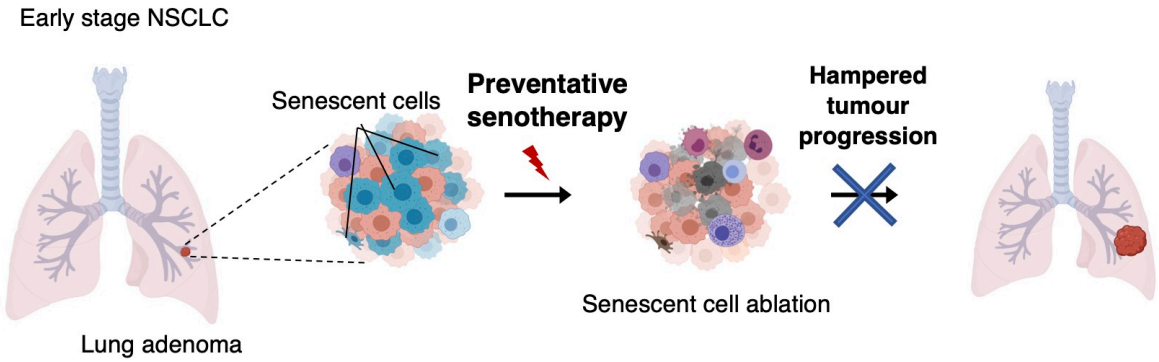

Figure 6.1. Cellular senescence accumulates during NSCLC tumorigenesis supporting cancer progression, and senolytic treatment can serve as a potential preventative therapy in NSCLC. In this thesis we confirm our working hypothesis and show that senescent cells accrue in lung adenomas, and their pharmacologic depletion effectively abrogates tumour progression.

In Chapter 4, we determined that cisplatin chemotherapeutic treatment results in a strong induction of cellular senescence in NSCLC human and murine cells, characterised by the implementation of a SASP enriched in TGF-β ligand secretion. This particular SASP was further demonstrated to drive the acquisition of enhanced malignant

properties in untreated or nearby lung cancer cells, both *in vitro* and *in vivo*, suggesting that this type of chemotherapy may contribute to tumour progression and subsequent treatment failure. Remarkably, we established that TGFβ-R1 inhibition and senolytic treatment efficiently prevent the enhanced proliferation of tumour cells derived from the exposure to cisplatin-induced senescence in human lung cancer xenografts and an orthotopic mouse model of lung adenocarcinoma (**Figure 6.2**).

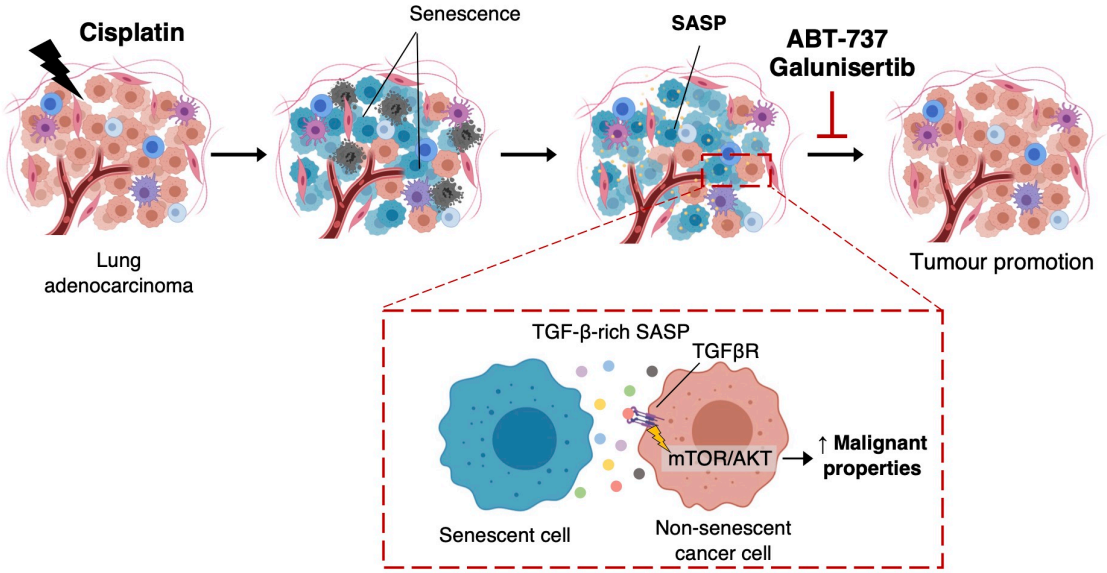

Figure 6.2. Cisplatin-induced senescence in lung adenocarcinoma promotes tumour progression through a TGF-β-rich SASP, which can be hampered with senolytic and TGF-βR inhibitory treatments. In Chapter 3 we provide compelling evidence of the acquisition of malignant traits in untreated lung adenocarcinoma cells upon exposure to cisplatin-derived SASP, which is rich in TGF-β ligands. We demonstrate that this is directed by the activation of TGF-βR-driven mTOR/Akt/P70S6K pathway, and show that senolytic treatment and TGF-βR inhibition with galunisertib effectively prevents enhanced tumour growth.

In Chapter 5, we evaluated a novel approach to selectively eliminate senescent tumour cells using a newly developed second-generation senolytic consisting of an acetylated-galactose covalently linked to navitoclax, named Nav-Gal (**Figure 6.3**). This novel pro-drug was systematically tested *in vitro* and in *in vivo* platforms, which confirmed its senolytic efficacy in combination with cisplatin treatment, as well as its markedly reduced systemic toxic effects with regards to navitoclax-induced

thrombocytopenia. We therefore obtained proof-of-principle of the therapeutic activity of this novel senotherapy in combination with senescence-inducing chemotherapy, thereby proposing galacto-conjugation of senolytics as a novel second-generation senolytic strategy to improve specificity and reduce senolytic-associated toxicities.

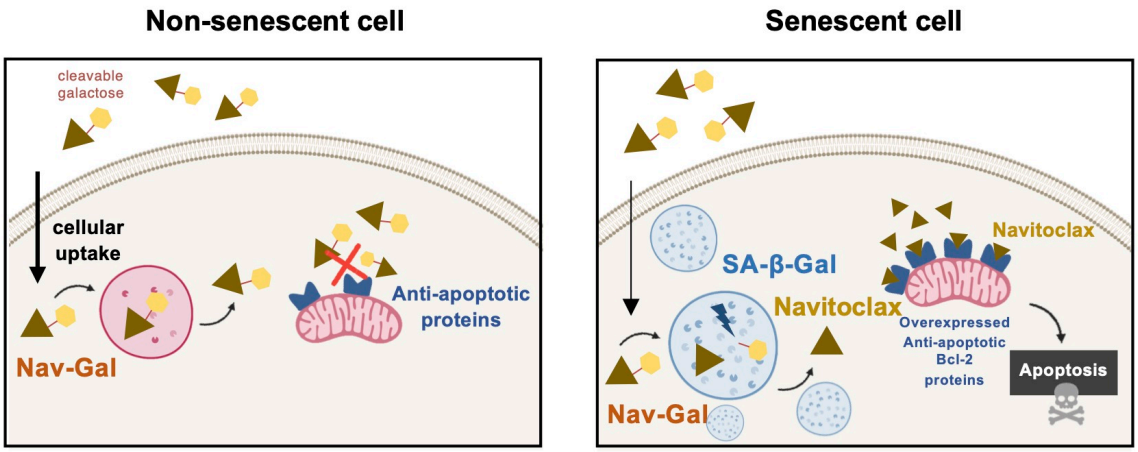

Figure 6.3. Galacto-conjugation of the senolytic navitoclax into a new generation senolytic prodrug, namely Nav-Gal, as an efficient second-generation strategy for selective senolysis. Schematic representation of the mechanism of action of Nav-Gal prodrug. Nav-Gal is passively taken up by both non-senescent and senescent cells. In non-senescent cells, its conjugation with a cleavable galactose renders it inactive and unable to inhibit anti-apoptotic proteins, such as BCL-2, preventing the induction of apoptosis. In senescent cells, the increased lysosomal and galactosidase activity, a hallmark of cellular senescence, allows the hydrolysis of the cleavable galactose, resulting in the release of active Navitoclax into the cytoplasm of senescent cells. Free navitoclax will inhibit anti-apoptotic BCL-2 proteins, which are overexpressed in senescent cells, driving specific apoptosis of these cells

Overall, the work hereby presented aims to place senescence detection, assessment and targeting as a therapeutic proxy for cancer management, and demonstrate that safer senolytic approaches can provide attractive strategies to control early-stage and advanced NSCLC.

REFERENCES

[1] D. K. Meyerholz, C. J. Suarez, S. M. Dintzis, and C. W. Frevert, "9 - Respiratory System," in *Comparative Anatomy and Histology (Second Edition)*, P. M. Treuting, S. M. Dintzis, and K. S. Montine Eds. San Diego: Academic Press, pp. 147-16, 2018.

[2] Cancer Research UK (CRUK). "Lung cancer statistics." http://www.cancerresearchkuk.org/health-professional/cancer-statistics/statistics-by-cancer-type/lung-cancer (accessed 25/08/2021).

[3] National Institute for Health and Care Excellence (NICE). "Suspected cancer: recognition and referral." https://www.nice.org.uk/guidance/ng12 (accessed 25/08/2021).

[4] B. H. Goulart *et al.*, "Referral and treatment patterns among patients with stages III and IV non-small-cell lung cancer," *J Oncol Pract,* vol. 9, no. 1, pp. 42-50, Jan 2013.

[5] S. Blandin Knight, P. A. Crosbie, H. Balata, J. Chudziak, T. Hussell, and C. Dive, "Progress and prospects of early detection in lung cancer," *Open Biol,* vol. 7, no. 9, Sep 2017.

[6] Z. Chen, C. M. Fillmore, P. S. Hammerman, C. F. Kim, and K. K. Wong, "Non-small-cell lung cancers: a heterogeneous set of diseases," *Nat Rev Cancer,* vol. 14, no. 8, pp. 535-46, Aug 2014.

[7] M. R. Davidson, A. F. Gazdar, and B. E. Clarke, "The pivotal role of pathology in the management of lung cancer," *J Thorac Dis,* vol. 5 Suppl 5, no. Suppl 5, pp. S463-78, Oct 2013.

[8] M. Paci *et al.*, "Large cell neuroendocrine carcinoma of the lung: a 10-year clinicopathologic retrospective study," *Ann Thorac Surg,* vol. 77, no. 4, pp. 1163-7, Apr 2004.

[9] S. Couraud, G. Zalcman, B. Milleron, F. Morin, and P. J. Souquet, "Lung cancer in never smokers--a review," *Eur J Cancer,* vol. 48, no. 9, pp. 1299-311, Jun 2012.

[10] F. Facciolo, G. Cardillo, M. Lopergolo, G. Pallone, F. Sera, and M. Martelli, "Chest wall invasion in non-small cell lung carcinoma: a rationale for en bloc resection," *J Thorac Cardiovasc Surg,* vol. 121, no. 4, pp. 649-56, Apr 2001.

[11] P. S. Hammerman *et al.*, "Comprehensive genomic characterization of squamous cell lung cancers," *Nature,* vol. 489, no. 7417, pp. 519-525, Sep 2012.

[12] W. D. Travis *et al.*, "The 2015 World Health Organization Classification of Lung Tumors: Impact of Genetic, Clinical and Radiologic Advances Since the 2004 Classification," *J Thorac Oncol,* vol. 10, no. 9, pp. 1243-1260, Sep 2015.

[13] I. I. Wistuba and A. F. Gazdar, "Lung cancer preneoplasia," *Annual Review of Pathology: Mechanisms of Disease,* vol. 1, no. 1, pp. 331-348, Feb 2006.

[14] A. Sweet-Cordero *et al.*, "An oncogenic KRAS2 expression signature identified by cross-species gene-expression analysis," *Nat Genet,* vol. 37, no. 1, pp. 48-55, Jan 2005.

[15] E. Izumchenko *et al.*, "Targeted sequencing reveals clonal genetic changes in the progression of early lung neoplasms and paired circulating DNA," *Nat Commun,* vol. 6, p. 8258, Sep 2015.

[16] A. K. Greenberg, H. Yee, and W. N. Rom, "Preneoplastic lesions of the lung," *Respiratory Research,* vol. 3, no. 1, p. 13, Apr 2004.

[17] H. Kadara, P. Scheet, I. I. Wistuba, and A. E. Spira, "Early Events in the Molecular Pathogenesis of Lung Cancer," *Cancer Prevention Research,* vol. 9, no. 7, p. 518, 2016.

[18] C. F. Kim *et al.*, "Identification of bronchioalveolar stem cells in normal lung and lung cancer," *Cell,* vol. 121, no. 6, pp. 823-35, Jun 2005.

[19] X. Xu *et al.*, "Evidence for type II cells as cells of origin of K-Ras-induced distal lung adenocarcinoma," *Proc Natl Acad Sci U S A,* vol. 109, no. 13, pp. 4910-5, Mar 2012.

[20] C. Tiozzo *et al.*, "Deletion of Pten expands lung epithelial progenitor pools and confers resistance to airway injury," *Am J Respir Crit Care Med,* vol. 180, no. 8, pp. 701-12, Oct 2009.

[21] J. J. Ventura *et al.*, "p38α MAP kinase is essential in lung stem and progenitor cell proliferation and differentiation," *Nature Genetics,* vol. 39, no. 6, pp. 750-758, Jun 2007.

[22] T. J. Desai, D. G. Brownfield, and M. A. Krasnow, "Alveolar progenitor and stem cells in lung development, renewal and cancer," *Nature,* vol. 507, no. 7491, pp. 190-4, Mar 2014.

[23] S. Mainardi, N. Mijimolle, S. Francoz, C. Vicente-Dueñas, I. Sánchez-García, and M. Barbacid, "Identification of cancer initiating cells in K-Ras driven lung adenocarcinoma," *Proc Natl Acad Sci U S A,* vol. 111, no. 1, pp. 255-60, Jan 2014.

[24] K. D. Sutherland, J.-Y. Song, M. C. Kwon, N. Proost, J. Zevenhoven, and A. Berns, "Multiple cells-of-origin of mutant K-Ras–induced mouse lung adenocarcinoma," *Proceedings of the National Academy of Sciences,* vol. 111, no. 13, p. 4952, 2014.

[25] National Institute for Health and Cancer Excellence (NICE). "Lung Cancer: Diagnosis and Management." https://www.nice.org.uk/guidance/ng12 (accessed 25/08/2021).

[26] S. Dasari and P. B. Tchounwou, "Cisplatin in cancer therapy: molecular mechanisms of action," *Eur J Pharmacol,* vol. 740, pp. 364-378, 2014.

[27] D. H. Johnson, "Evolution of cisplatin-based chemotherapy in non-small cell lung cancer: a historical perspective and the eastern cooperative oncology group experience," *Chest,* vol. 117, no. 4 Suppl 1, pp. 133s-137s, Apr 2000.

[28] H. Kenmotsu and Y. Tanigawara, "Pharmacokinetics, dynamics and toxicity of docetaxel: Why the Japanese dose differs from the Western dose," *Cancer Sci,* vol. 106, no. 5, pp. 497-504, May 2015.

[29] K. A. Cadoo, A. Gucalp, and T. A. Traina, "Palbociclib: an evidence-based review of its potential in the treatment of breast cancer," *Breast Cancer (Dove Med Press),* vol. 6, pp. 123-33, 2014.

[30] C. A. Stewart *et al.*, "Single-cell analyses reveal increased intratumoral heterogeneity after the onset of therapy resistance in small-cell lung cancer," *Nature Cancer,* vol. 1, no. 4, pp. 423-436, Apr 2020.

[31] K. L. Simpson *et al.*, "A biobank of small cell lung cancer CDX models elucidates inter- and intratumoral phenotypic heterogeneity," *Nature Cancer,* vol. 1, no. 4, pp. 437-451, Apr 2020.

[32] H. Pan *et al.*, "Comprehensive anatomic ontologies for lung development: A comparison of alveolar formation and maturation within mouse and human lung," *Journal of Biomedical Semantics,* vol. 10, no. 1, p. 18, Oct 2019.

[33] R. Meuwissen and A. Berns, "Mouse models for human lung cancer," *Genes Dev,* vol. 19, no. 6, pp. 643-64, Mar 2005.

[34] R. Safari and R. Meuwissen, "Practical use of advanced mouse models for lung cancer," *Methods Mol Biol,* vol. 1267, pp. 93-124, 2015.

[35] M. C. Kwon and A. Berns, "Mouse models for lung cancer," *Mol Oncol,* vol. 7, no. 2, pp. 165-77, Apr 2013.

[36] D. Hanahan and R. A. Weinberg, "The Hallmarks of Cancer," *Cell,* vol. 100, no. 1, pp. 57-70, 2000.

[37] H. Greulich, "The genomics of lung adenocarcinoma: opportunities for targeted therapies," *Genes Cancer,* vol. 1, no. 12, pp. 1200-10, Dec 2010.

[38] E. A. Akbay and J. Kim, "Autochthonous murine models for the study of smoker and neversmoker associated lung cancers," *Translational Lung Cancer Research,* vol. 7, no. 4, pp. 464-486, 2018.

[39] E. L. Jackson *et al.*, "Analysis of lung tumor initiation and progression using conditional expression of oncogenic K-ras," *Genes Dev,* vol. 15, no. 24, pp. 3243-8, Dec 2001.

[40] M. Sanclemente *et al.*, "c-RAF Ablation Induces Regression of Advanced Kras/Trp53 Mutant Lung Adenocarcinomas by a Mechanism Independent of MAPK Signaling," *Cancer Cell,* vol. 33, no. 2, pp. 217-228.e4, Feb 2018.

[41] V. Justilien and A. P. Fields, "Utility and applications of orthotopic models of human non-small cell lung cancer (NSCLC) for the evaluation of novel and emerging cancer therapeutics," *Curr Protoc Pharmacol,* vol. 62, pp. 14.27.1-14.27.17, Oct 2013.

[42] E. M. Kerr, E. Gaude, F. K. Turrell, C. Frezza, and C. P. Martins, "Mutant Kras copy number defines metabolic reprogramming and therapeutic susceptibilities," *Nature,* vol. 531, no. 7592, pp. 110-113, 2016.

[43] E. L. Jackson *et al.*, "The differential effects of mutant p53 alleles on advanced murine lung cancer," *Cancer Res,* vol. 65, no. 22, pp. 10280-8, Nov 2005.

[44] L. Hayflick and P. S. Moorhead, "The serial cultivation of human diploid cell strains," *Exp Cell Res,* vol. 25, pp. 585-621, Dec 1961.

[45] L. Hayflick, "The limited in vitro lifetime of human diploid cell strains," *Experimental Cell Research,* vol. 37, no. 3, pp. 614-636, Mar 1965.

[46] C. W. Greider and E. H. Blackburn, "Identification of a specific telomere terminal transferase activity in Tetrahymena extracts," *Cell,* vol. 43, no. 2 Pt 1, pp. 405-13, Dec 1985.

[47] V. Gorgoulis *et al.*, "Cellular Senescence: Defining a Path Forward," *Cell,* vol. 179, no. 4, pp. 813-827, Oct 2019.

[48] E. González-Gualda, A. G. Baker, L. Fruk, and D. Muñoz-Espín, "A guide to assessing cellular senescence in vitro and in vivo," *Febs j,* vol. 288, no. 1, pp. 56-80, Jan 2021.

[49] J. R. Nevins, "Toward an understanding of the functional complexity of the E2F and retinoblastoma families," *Cell Growth Differ,* vol. 9, no. 8, pp. 585-93, Aug 1998.

[50] R. Salama, M. Sadaie, M. Hoare, and M. Narita, "Cellular senescence and its effector programs," *Genes Dev,* vol. 28, no. 2, pp. 99-114, Jan 2014.

[51] R. Di Micco *et al.*, "Interplay between oncogene-induced DNA damage response and heterochromatin in senescence and cancer," *Nat Cell Biol,* vol. 13, no. 3, pp. 292-302, Mar 2011.

[52] M. Sadaie *et al.*, "Redistribution of the Lamin B1 genomic binding profile affects rearrangement of heterochromatic domains and SAHF formation during senescence," *Genes Dev,* vol. 27, no. 16, pp. 1800-8, Aug 2013.

[53] A. Ivanov *et al.*, "Lysosome-mediated processing of chromatin in senescence," *J Cell Biol,* vol. 202, no. 1, pp. 129-43, Jul 2013.

[54] L. Q. Cheng, Z. Q. Zhang, H. Z. Chen, and D. P. Liu, "Epigenetic regulation in cell senescence," *J Mol Med (Berl),* vol. 95, no. 12, pp. 1257-1268, Dec 2017.

[55] H. Paluvai, E. Di Giorgio, and C. Brancolini, "The Histone Code of Senescence," *Cells,* vol. 9, no. 2, 2020.

[56] P. Davalli, T. Mitic, A. Caporali, A. Lauriola, and D. D'Arca, "ROS, Cell Senescence, and Novel Molecular Mechanisms in Aging and Age-Related Diseases," *Oxid Med Cell Longev,* vol. 2016, p. 3565127, 2016.

[57] E. Wang, "Senescent human fibroblasts resist programmed cell death, and failure to suppress bcl2 is involved," *Cancer Res,* vol. 55, no. 11, pp. 2284-92, Jun 1995.

[58] Y. Y. Sanders *et al.*, "Histone modifications in senescence-associated resistance to apoptosis by oxidative stress," *Redox Biol,* vol. 1, no. 1, pp. 8-16, 2013.

[59] G. P. Dimri *et al.*, "A biomarker that identifies senescent human cells in culture and in aging skin in vivo," *Proc Natl Acad Sci U S A,* vol. 92, no. 20, pp. 9363-7, Sep 1995.

[60] T. Kuilman and D. S. Peeper, "Senescence-messaging secretome: SMS-ing cellular stress," *Nat Rev Cancer,* vol. 9, no. 2, pp. 81-94, Feb 2009.

[61] T. Tchkonia, Y. Zhu, J. van Deursen, J. Campisi, and J. L. Kirkland, "Cellular senescence and the senescent secretory phenotype: therapeutic opportunities," *J Clin Invest,* vol. 123, no. 3, pp. 966-72, Mar 2013.

[62] A. Krtolica, S. Parrinello, S. Lockett, P.-Y. Desprez, and J. Campisi, "Senescent fibroblasts promote epithelial cell growth and tumorigenesis: A link between cancer and aging," *Proceedings of the National Academy of Sciences,* vol. 98, no. 21, p. 12072, 2001.

[63] M. Rossi and K. Abdelmohsen, "The Emergence of Senescent Surface Biomarkers as Senotherapeutic Targets," *Cells,* vol. 10, no. 7, 2021.

[64] D. Muñoz-Espín and M. Serrano, "Cellular senescence: from physiology to pathology," *Nat Rev Mol Cell Biol,* vol. 15, no. 7, pp. 482-96, Jul 2014,.

[65] J. M. van Deursen, "The role of senescent cells in ageing," *Nature,* vol. 509, no. 7501, pp. 439-446, May 2014.

[66] N. V. Petrova, A. K. Velichko, S. V. Razin, and O. L. Kantidze, "Small molecule compounds that induce cellular senescence," *Aging Cell,* vol. 15, no. 6, pp. 999-1017, Dec 2016.

[67] Z. Lou and J. Chen, "Cellular senescence and DNA repair," *Exp Cell Res,* vol. 312, no. 14, pp. 2641-6, Aug 2006.

[68] X. L. Liu, J. Ding, and L. H. Meng, "Oncogene-induced senescence: a double edged sword in cancer," *Acta Pharmacol Sin,* vol. 39, no. 10, pp. 1553-1558, Oct 2018.

[69] F. d'Adda di Fagagna, "Living on a break: cellular senescence as a DNA-damage response," *Nat Rev Cancer,* vol. 8, no. 7, pp. 512-22, Jul 2008.

[70] A. Borodkina, A. Shatrova, P. Abushik, N. Nikolsky, and E. Burova, "Interaction between ROS dependent DNA damage, mitochondria and p38 MAPK underlies senescence of human adult stem cells," *Aging (Albany NY),* vol. 6, no. 6, pp. 481-95, Jun 2014.

[71] A. V. Borodkina, A. N. Shatrova, N. N. Nikolsky, and E. B. Burova, "The role of p38 MAP-kinase in stress-induced senescence of human endometrium-derived mesenchymal stem cells," *Cell and Tissue Biology,* vol. 10, no. 5, pp. 365-371, Sep 2016.

[72] N. Herranz *et al.*, "mTOR regulates MAPKAPK2 translation to control the senescence-associated secretory phenotype," *Nat Cell Biol,* vol. 17, no. 9, pp. 1205-17, Sep 2015.

[73] R. M. Laberge *et al.*, "MTOR regulates the pro-tumorigenic senescence-associated secretory phenotype by promoting IL1A translation," *Nat Cell Biol,* vol. 17, no. 8, pp. 1049-61, Aug 2015.

[74] N. Wajapeyee, R. W. Serra, X. Zhu, M. Mahalingam, and M. R. Green, "Oncogenic BRAF induces senescence and apoptosis through pathways mediated by the secreted protein IGFBP7," *Cell,* vol. 132, no. 3, pp. 363-374, 2008.

[75] R. M. Kortlever, P. J. Higgins, and R. Bernards, "Plasminogen activator inhibitor-1 is a critical downstream target of p53 in the induction of replicative senescence," *Nat Cell Biol,* vol. 8, no. 8, pp. 877-84, Aug 2006.

[76] M. Hoare *et al.*, "NOTCH1 mediates a switch between two distinct secretomes during senescence," *Nat Cell Biol,* vol. 18, no. 9, pp. 979-92, Sep 2016.

[77] C. Kang *et al.*, "The DNA damage response induces inflammation and senescence by inhibiting autophagy of GATA4," *Science,* vol. 349, no. 6255, p. aaa5612, 2015.

[78] A. Salminen, A. Kauppinen, and K. Kaarniranta, "Emerging role of NF-κB signaling in the induction of senescence-associated secretory phenotype (SASP)," *Cell Signal,* vol. 24, no. 4, pp. 835-45, Apr 2012.

[79] A. R. Davalos, J. P. Coppe, J. Campisi, and P. Y. Desprez, "Senescent cells as a source of inflammatory factors for tumor progression," *Cancer Metastasis Rev,* vol. 29, no. 2, pp. 273-83, Jun 2010.

[80] C. J. Sieben, I. Sturmlechner, B. van de Sluis, and J. M. van Deursen, "Two-Step Senescence-Focused Cancer Therapies," *Trends Cell Biol,* vol. 28, no. 9, pp. 723-737, Sep 2018.

[81] V. Krizhanovsky *et al.*, "Senescence of activated stellate cells limits liver fibrosis," *Cell,* vol. 134, no. 4, pp. 657-67, Aug 2008.

[82] J. I. Jun and L. F. Lau, "The matricellular protein CCN1 induces fibroblast senescence and restricts fibrosis in cutaneous wound healing," *Nat Cell Biol,* vol. 12, no. 7, pp. 676-85, Jul 2010.

[83] M. Demaria *et al.*, "An essential role for senescent cells in optimal wound healing through secretion of PDGF-AA," *Dev Cell,* vol. 31, no. 6, pp. 722-733, 2014.

[84] M. H. Yun, H. Davaapil, and J. P. Brockes, "Recurrent turnover of senescent cells during regeneration of a complex structure," *Elife,* vol. 4, May 2015.

[85] A. Chiche *et al.*, "Injury-Induced Senescence Enables In Vivo Reprogramming in Skeletal Muscle," *Cell Stem Cell,* vol. 20, no. 3, pp. 407-414.e4, Mar 2017.

[86] B. Ritschka *et al.*, "The senescence-associated secretory phenotype induces cellular plasticity and tissue regeneration," *Genes Dev,* vol. 31, no. 2, pp. 172-183, Jan 2017.

[87] M. Storer *et al.*, "Senescence is a developmental mechanism that contributes to embryonic growth and patterning," *Cell,* vol. 155, no. 5, pp. 1119-30, Nov 2013.

[88] D. Muñoz-Espín *et al.*, "Programmed cell senescence during mammalian embryonic development," *Cell,* vol. 155, no. 5, pp. 1104-18, Nov 2013.

[89] H. Davaapil, J. P. Brockes, and M. H. Yun, "Conserved and novel functions of programmed cellular senescence during vertebrate development," *Development,* vol. 144, no. 1, pp. 106-114, Jan 2017.

[90] R. Besancenot *et al.*, "A senescence-like cell-cycle arrest occurs during megakaryocytic maturation: implications for physiological and pathological megakaryocytic proliferation," *PLoS Biol,* vol. 8, no. 9, Sep 2010.

[91] A. Chuprin *et al.*, "Cell fusion induced by ERVWE1 or measles virus causes cellular senescence," *Genes Dev,* vol. 27, no. 21, pp. 2356-66, Nov 2013.

[92] J. M. Wolstein, D. H. Lee, J. Michaud, V. Buot, B. Stefanchik, and M. D. Plotkin, "INK4a knockout mice exhibit increased fibrosis under normal conditions and in response to unilateral ureteral obstruction," *Am J Physiol Renal Physiol,* vol. 299, no. 6, pp. F1486-95, Dec 2010.

[93] F. Zhu *et al.*, "Senescent cardiac fibroblast is critical for cardiac fibrosis after myocardial infarction," *PLoS One,* vol. 8, no. 9, p. e74535, 2013.

[94] S. M. Sanz-González *et al.*, "Increased p53 gene dosage reduces neointimal thickening induced by mechanical injury but has no effect on native atherosclerosis," *Cardiovasc Res,* vol. 75, no. 4, pp. 803-12, Sep 2007.

[95] H. González-Navarro *et al.*, "p19(ARF) deficiency reduces macrophage and vascular smooth muscle cell apoptosis and aggravates atherosclerosis," *J Am Coll Cardiol,* vol. 55, no. 20, pp. 2258-68, May 2010.

[96] J. Mercer, N. Figg, V. Stoneman, D. Braganza, and M. R. Bennett, "Endogenous p53 protects vascular smooth muscle cells from apoptosis and reduces atherosclerosis in ApoE knockout mice," *Circ Res,* vol. 96, no. 6, pp. 667-74, Apr 2005.

[97] A. K. Khanna, "Enhanced susceptibility of cyclin kinase inhibitor p21 knockout mice to high fat diet induced atherosclerosis," *J Biomed Sci,* vol. 16, no. 1, p. 66, Jul 2009.

[98] H. Noureddine *et al.*, "Pulmonary artery smooth muscle cell senescence is a pathogenic mechanism for pulmonary hypertension in chronic lung disease," *Circ Res,* vol. 109, no. 5, pp. 543-53, Aug 2011.

[99] S. Mizuno *et al.*, "p53 Gene deficiency promotes hypoxia-induced pulmonary hypertension and vascular remodeling in mice," *Am J Physiol Lung Cell Mol Physiol,* vol. 300, no. 5, pp. L753-61, May 2011.

[100] N. Mouraret *et al.*, "Activation of lung p53 by Nutlin-3a prevents and reverses experimental pulmonary hypertension," *Circulation,* vol. 127, no. 16, pp. 1664-76, Apr 2013.

[101] W. Xue *et al.*, "Senescence and tumour clearance is triggered by p53 restoration in murine liver carcinomas," *Nature,* vol. 445, no. 7128, pp. 656-60, Feb 2007.

[102] T. W. Kang *et al.*, "Senescence surveillance of pre-malignant hepatocytes limits liver cancer development," *Nature,* vol. 479, no. 7374, pp. 547-51, Nov 2011.

[103] H. J. Cooke and B. A. Smith, "Variability at the telomeres of the human X/Y pseudoautosomal region," *Cold Spring Harb Symp Quant Biol,* vol. 51 Pt 1, pp. 213-9, 1986.

[104] C. B. Harley, A. B. Futcher, and C. W. Greider, "Telomeres shorten during ageing of human fibroblasts," *Nature,* vol. 345, no. 6274, pp. 458-60, May 1990.

[105] M. Serrano, A. W. Lin, M. E. McCurrach, D. Beach, and S. W. Lowe, "Oncogenic ras provokes premature cell senescence associated with accumulation of p53 and p16INK4a," *Cell,* vol. 88, no. 5, pp. 593-602, Mar 1997.

[106] E. L. Schneider *et al.*, "Cellular replication and aging," *Mech Ageing Dev,* vol. 9, no. 3-4, pp. 313-24, Feb 1979.

[107] J. Krishnamurthy *et al.*, "Ink4a/Arf expression is a biomarker of aging," *J Clin Invest,* vol. 114, no. 9, pp. 1299-307, Nov 2004.

[108] U. Herbig and J. M. Sedivy, "Regulation of growth arrest in senescence: telomere damage is not the end of the story," *Mech Ageing Dev,* vol. 127, no. 1, pp. 16-24, Jan 2006.

[109] J. C. Jeyapalan, M. Ferreira, J. M. Sedivy, and U. Herbig, "Accumulation of senescent cells in mitotic tissue of aging primates," *Mech Ageing Dev,* vol. 128, no. 1, pp. 36-44, Jan 2007.

[110] C. Lawless, C. Wang, D. Jurk, A. Merz, T. Zglinicki, and J. F. Passos, "Quantitative assessment of markers for cell senescence," *Exp Gerontol,* vol. 45, no. 10, pp. 772-8, Oct 2010.

[111] J. Krishnamurthy *et al.*, "p16INK4a induces an age-dependent decline in islet regenerative potential," *Nature,* vol. 443, no. 7110, pp. 453-7, Sep 2006.

[112] D. J. Baker *et al.*, "Clearance of p16Ink4a-positive senescent cells delays ageing-associated disorders," *Nature,* vol. 479, no. 7372, pp. 232-6, Nov 2011.

[113] L. Hecker *et al.*, "Reversal of persistent fibrosis in aging by targeting Nox4-Nrf2 redox imbalance," *Sci Transl Med,* vol. 6, no. 231, p. 231ra47, Apr 2014.

[114] K. Aoshiba, T. Tsuji, and A. Nagai, "Bleomycin induces cellular senescence in alveolar epithelial cells," *Eur Respir J,* vol. 22, no. 3, pp. 436-43, Sep 2003.

[115] K. Aoshiba *et al.*, "Senescence-associated secretory phenotype in a mouse model of bleomycin-induced lung injury," *Exp Toxicol Pathol,* vol. 65, no. 7-8, pp. 1053-62, Nov 2013.

[116] P. Shivshankar, C. Brampton, S. Miyasato, M. Kasper, V. J. Thannickal, and C. J. Le Saux, "Caveolin-1 deficiency protects from pulmonary fibrosis by modulating epithelial cell senescence in mice," *Am J Respir Cell Mol Biol,* vol. 47, no. 1, pp. 28-36, Jul 2012.

[117] M. F. Gregor and G. S. Hotamisligil, "Inflammatory mechanisms in obesity," *Annu Rev Immunol,* vol. 29, pp. 415-45, 2011.

[118] T. Minamino *et al.*, "A crucial role for adipose tissue p53 in the regulation of insulin resistance," *Nat Med,* vol. 15, no. 9, pp. 1082-7, Sep 2009.

[119] H. Sone and Y. Kagawa, "Pancreatic beta cell senescence contributes to the pathogenesis of type 2 diabetes in high-fat diet-induced diabetic mice," *Diabetologia,* vol. 48, no. 1, pp. 58-67, Jan 2005.

[120] O. Tavana and C. Zhu, "Too many breaks (brakes): pancreatic β-cell senescence leads to diabetes," *Cell Cycle,* vol. 10, no. 15, pp. 2471-84, Aug 2011.

[121] P. Sousa-Victor *et al.*, "Geriatric muscle stem cells switch reversible quiescence into senescence," *Nature,* vol. 506, no. 7488, pp. 316-21, Feb 2014.

[122] B. D. Cosgrove *et al.*, "Rejuvenation of the muscle stem cell population restores strength to injured aged muscles," *Nat Med,* vol. 20, no. 3, pp. 255-64, Mar 2014.

[123] T. J. Bussian, A. Aziz, C. F. Meyer, B. L. Swenson, J. M. van Deursen, and D. J. Baker, "Clearance of senescent glial cells prevents tau-dependent pathology and cognitive decline," *Nature,* vol. 562, no. 7728, pp. 578-582, Oct 2018.

[124] J. A. Martin, T. D. Brown, A. D. Heiner, and J. A. Buckwalter, "Chondrocyte Senescence, Joint Loading and Osteoarthritis," *Clinical Orthopaedics and Related Research,* vol. 427, 2004.

[125] O. H. Jeon *et al.*, "Local clearance of senescent cells attenuates the development of post-traumatic osteoarthritis and creates a pro-regenerative environment," *Nat Med,* vol. 23, no. 6, pp. 775-781, Jun 2017.

[126] B. G. Childs, D. J. Baker, T. Wijshake, C. A. Conover, J. Campisi, and J. M. van Deursen, "Senescent intimal foam cells are deleterious at all stages of atherosclerosis," *Science,* vol. 354, no. 6311, pp. 472-477, Oct 2016.

[127] J. M. Gonzalez-Meljem, J. R. Apps, H. C. Fraser, and J. P. Martinez-Barbera, "Paracrine roles of cellular senescence in promoting tumourigenesis," *Br J Cancer,* vol. 118, no. 10, pp. 1283-1288, May 2018.

[128] M. K. Ruhland *et al.*, "Stromal senescence establishes an immunosuppressive microenvironment that drives tumorigenesis," *Nat Commun,* vol. 7, p. 11762, Jun 2016.

[129] D. Liu and P. J. Hornsby, "Senescent Human Fibroblasts Increase the Early Growth of Xenograft Tumors via Matrix Metalloproteinase Secretion," *Cancer Research,* vol. 67, no. 7, p. 3117, 2007.

[130] M. Demaria *et al.*, "Cellular Senescence Promotes Adverse Effects of Chemotherapy and Cancer Relapse," *Cancer Discovery,* vol. 7, no. 2, p. 165, 2017.

[131] J. Zhu, D. Woods, M. McMahon, and J. M. Bishop, "Senescence of human fibroblasts induced by oncogenic Raf," *Genes Dev,* vol. 12, no. 19, pp. 2997-3007, Oct 1998.

[132] M. Braig *et al.*, "Oncogene-induced senescence as an initial barrier in lymphoma development," *Nature,* vol. 436, no. 7051, pp. 660-5, Aug 2005.

[133] Z. Chen *et al.*, "Crucial role of p53-dependent cellular senescence in suppression of Pten-deficient tumorigenesis," *Nature,* vol. 436, no. 7051, pp. 725-30, Aug 2005.

[134] C. Michaloglou *et al.*, "BRAFE600-associated senescence-like cell cycle arrest of human naevi," *Nature,* vol. 436, no. 7051, pp. 720-4, Aug 2005.

[135] M. Collado *et al.*, "Senescence in premalignant tumours," *Nature,* vol. 436, no. 7051, pp. 642-642, Aug 2005.

[136] E. Lazzerini Denchi, C. Attwooll, D. Pasini, and K. Helin, "Deregulated E2F activity induces hyperplasia and senescence-like features in the mouse pituitary gland," *Mol Cell Biol,* vol. 25, no. 7, pp. 2660-72, Apr 2005.

[137] H.-L. Ou, R. Hoffmann, C. González-López, G. J. Doherty, J. E. Korkola, and D. Muñoz-Espín, "Cellular senescence in cancer: from mechanisms to detection," *Molecular Oncology,* Sep 2020.

[138] K. R. Jones *et al.*, "p53-Dependent accelerated senescence induced by ionizing radiation in breast tumour cells," *Int J Radiat Biol,* vol. 81, no. 6, pp. 445-58, Jun 2005.

[139] R. Mirzayans, A. Scott, M. Cameron, and D. Murray, "Induction of accelerated senescence by gamma radiation in human solid tumor-derived cell lines expressing wild-type TP53," *Radiat Res,* vol. 163, no. 1, pp. 53-62, Jan 2005.

[140] X. He *et al.*, "MiR-34a modulates ionizing radiation-induced senescence in lung cancer cells," *Oncotarget,* vol. 8, no. 41, pp. 69797-69807, Sep 2017.

[141] B. C. Kim *et al.*, "Evaluation of premature senescence and senescence biomarkers in carcinoma cells and xenograft mice exposed to single or fractionated irradiation," *Oncol Rep,* vol. 31, no. 5, pp. 2229-35, May 2014.

[142] R. H. te Poele, A. L. Okorokov, L. Jardine, J. Cummings, and S. P. Joel, "DNA damage is able to induce senescence in tumor cells in vitro and in vivo," *Cancer Res,* vol. 62, no. 6, pp. 1876-83, Mar 2002.

[143] R. Sidi *et al.*, "Induction of senescence markers after neo-adjuvant chemotherapy of malignant pleural mesothelioma and association with clinical outcome: an exploratory analysis," *Eur J Cancer,* vol. 47, no. 2, pp. 326-32, Jan 2011.

[144] J. P. Coppé *et al.*, "Senescence-associated secretory phenotypes reveal cell-nonautonomous functions of oncogenic RAS and the p53 tumor suppressor," *PLoS Biol,* vol. 6, no. 12, pp. 2853-68, Dec 2008.

[145] H. K. Sanoff *et al.*, "Effect of cytotoxic chemotherapy on markers of molecular age in patients with breast cancer," *J Natl Cancer Inst,* vol. 106, no. 4, p. dju057, Apr 2014.

[146] R. S. Roberson, S. J. Kussick, E. Vallieres, S. Y. Chen, and D. Y. Wu, "Escape from therapy-induced accelerated cellular senescence in p53-null lung cancer cells and in human lung cancers," *Cancer Res,* vol. 65, no. 7, pp. 2795-803, Apr 2005.

[147] J. C. Acosta *et al.*, "Chemokine signaling via the CXCR2 receptor reinforces senescence," *Cell,* vol. 133, no. 6, pp. 1006-18, Jun 2008.

[148] T. Kuilman *et al.*, "Oncogene-induced senescence relayed by an interleukin-dependent inflammatory network," *Cell,* vol. 133, no. 6, pp. 1019-31, Jun 2008.

[149] J. C. Acosta *et al.*, "A complex secretory program orchestrated by the inflammasome controls paracrine senescence," *Nat Cell Biol,* vol. 15, no. 8, pp. 978-90, Aug 2013.

[150] Z. Dou *et al.*, "Cytoplasmic chromatin triggers inflammation in senescence and cancer," *Nature,* vol. 550, no. 7676, pp. 402-406, Oct 2017.

[151] J. van Tuyn *et al.*, "Oncogene-Expressing Senescent Melanocytes Up-Regulate MHC Class II, a Candidate Melanoma Suppressor Function," *J Invest Dermatol,* vol. 137, no. 10, pp. 2197-2207, Oct 2017.

[152] G. Ferbeyre, E. de Stanchina, E. Querido, N. Baptiste, C. Prives, and S. W. Lowe, "PML is induced by oncogenic ras and promotes premature senescence," *Genes & Development,* vol. 14, no. 16, pp. 2015-2027, August 2000.

[153] M. Narita *et al.*, "Rb-Mediated Heterochromatin Formation and Silencing of E2F Target Genes during Cellular Senescence," *Cell,* vol. 113, no. 6, pp. 703-716, Jun 2013,

[154] R. Di Micco *et al.*, "Oncogene-induced senescence is a DNA damage response triggered by DNA hyper-replication," *Nature,* vol. 444, no. 7119, pp. 638-642, Nov 2006.

[155] J. Bartkova *et al.*, "Oncogene-induced senescence is part of the tumorigenesis barrier imposed by DNA damage checkpoints," *Nature,* vol. 444, no. 7119, pp. 633-637, Nov 2006.

[156] M. Narita *et al.*, "A Novel Role for High-Mobility Group A Proteins in Cellular Senescence and Heterochromatin Formation," *Cell,* vol. 126, no. 3, pp. 503-514, Aug 2006.

[157] J. Guillon, C. Petit, B. Toutain, C. Guette, E. Lelièvre, and O. Coqueret, "Chemotherapy-induced senescence, an adaptive mechanism driving resistance and tumor heterogeneity," *Cell Cycle,* vol. 18, no. 19, pp. 2385-2397, Oct 2019.

[158] L. W. Elmore, X. Di, C. Dumur, S. E. Holt, and D. A. Gewirtz, "Evasion of a single-step, chemotherapy-induced senescence in breast cancer cells: implications for treatment response," *Clin Cancer Res,* vol. 11, no. 7, pp. 2637-43, Apr 2005.

[159] S. Achuthan, T. R. Santhoshkumar, J. Prabhakar, S. A. Nair, and M. R. Pillai, "Drug-induced senescence generates chemoresistant stemlike cells with low reactive oxygen species," *J Biol Chem,* vol. 286, no. 43, pp. 37813-29, Oct 2011.

[160] Q. Wang *et al.*, "Survivin and escaping in therapy-induced cellular senescence," *Int J Cancer,* vol. 128, no. 7, pp. 1546-58, Apr 2011.

[161] Q. Wang *et al.*, "Polyploidy road to therapy-induced cellular senescence and escape," *International Journal of Cancer,* vol. 132, no. 7, pp. 1505-1515, Apr 2013.

[162] H. Was *et al.*, "Bafilomycin A1 triggers proliferative potential of senescent cancer cells in vitro and in NOD/SCID mice," *Oncotarget,* vol. 8, no. 6, pp. 9303-9322, Feb 2017.

[163] M. Sabisz and A. Skladanowski, "Cancer stem cells and escape from drug-induced premature senescence in human lung tumor cells: implications for drug resistance and in vitro drug screening models," *Cell Cycle,* vol. 8, no. 19, pp. 3208-17, Oct 2009.

[164] M. Milanovic *et al.*, "Senescence-associated reprogramming promotes cancer stemness," *Nature,* vol. 553, no. 7686, pp. 96-100, Jan 2018.

[165] Z. V. Chitikova, S. A. Gordeev, T. V. Bykova, S. G. Zubova, V. A. Pospelov, and T. V. Pospelova, "Sustained activation of DNA damage response in irradiated apoptosis-resistant cells induces reversible senescence associated with mTOR downregulation and expression of stem cell markers," *Cell Cycle,* vol. 13, no. 9, pp. 1424-39, 2014.

[166] R. A. Busuttil, M. Rubio, M. E. T. Dollé, J. Campisi, and J. Vijg, "Mutant frequencies and spectra depend on growth state and passage number in cells cultured from transgenic lacZ-plasmid reporter mice," *DNA Repair,* vol. 5, no. 1, pp. 52-60, Jan 2006.

[167] D. V. Faget, Q. Ren, and S. A. Stewart, "Unmasking senescence: context-dependent effects of SASP in cancer," *Nature Reviews Cancer,* vol. 19, no. 8, pp. 439-453, Aug 2019.

[168] J. P. Coppe *et al.*, "A role for fibroblasts in mediating the effects of tobacco-induced epithelial cell growth and invasion," *Mol Cancer Res,* vol. 6, no. 7, pp. 1085-98, Jul 2008.

[169] M. Demaria *et al.*, "Cellular Senescence Promotes Adverse Effects of Chemotherapy and Cancer Relapse," *Cancer Discov,* vol. 7, no. 2, pp. 165-176, Feb 2017.

[170] I. Tamm, T. Kikuchi, I. Cardinale, and J. G. Krueger, "Cell-adhesion-disrupting action of interleukin 6 in human ductal breast carcinoma cells," *Proc Natl Acad Sci U S A,* vol. 91, no. 8, pp. 3329-33, Apr 1994.

[171] J. Cahu, S. Bustany, and B. Sola, "Senescence-associated secretory phenotype favors the emergence of cancer stem-like cells," *Cell Death Dis,* vol. 3, no. 12, p. e446, Dec 2012.

[172] L. J. Castro-Vega *et al.*, "The senescent microenvironment promotes the emergence of heterogeneous cancer stem-like cells," *Carcinogenesis,* vol. 36, no. 10, pp. 1180-92, Oct 2015.

[173] L. Mosteiro *et al.*, "Tissue damage and senescence provide critical signals for cellular reprogramming in vivo," *Science,* vol. 354, no. 6315, Nov 2016.

[174] J. M. Gonzalez-Meljem *et al.*, "Stem cell senescence drives age-attenuated induction of pituitary tumours in mouse models of paediatric craniopharyngioma," *Nature Communications,* vol. 8, no. 1, p. 1819, Nov 2017.

[175] A. Toso *et al.*, "Enhancing chemotherapy efficacy in Pten-deficient prostate tumors by activating the senescence-associated antitumor immunity," *Cell Rep,* vol. 9, no. 1, pp. 75-89, Oct 2014.

[176] J. L. Kirkland and T. Tchkonia, "Senolytic drugs: from discovery to translation," *Journal of Internal Medicine,* vol. 288, no. 5, pp. 518-536, Nov 2020.

[177] Y. Zhu *et al.*, "The Achilles' heel of senescent cells: from transcriptome to senolytic drugs," *Aging Cell,* vol. 14, no. 4, pp. 644-58, Aug 2015.

[178] Y. Zhu *et al.*, "Identification of a novel senolytic agent, navitoclax, targeting the Bcl-2 family of anti-apoptotic factors," *Aging Cell,* vol. 15, no. 3, pp. 428-35, Jun 2016.

[179] J. Chang *et al.*, "Clearance of senescent cells by ABT263 rejuvenates aged hematopoietic stem cells in mice," *Nat Med,* vol. 22, no. 1, pp. 78-83, Jan 2016.

[180] Y. Zhu *et al.*, "New agents that target senescent cells: the flavone, fisetin, and the BCL-X(L) inhibitors, A1331852 and A1155463," *Aging (Albany NY),* vol. 9, no. 3, pp. 955-963, Mar 2017.

[181] R. Yosef *et al.*, "Directed elimination of senescent cells by inhibition of BCL-W and BCL-XL," *Nat Commun,* vol. 7, p. 11190, Apr 2016.

[182] Y. Wang *et al.*, "Discovery of piperlongumine as a potential novel lead for the development of senolytic agents," *Aging (Albany NY),* vol. 8, no. 11, pp. 2915-2926, Nov 2016.

[183] L. Samaraweera, A. Adomako, A. Rodriguez-Gabin, and H. M. McDaid, "A Novel Indication for Panobinostat as a Senolytic Drug in NSCLC and HNSCC," *Sci Rep,* vol. 7, no. 1, p. 1900, May 2017.

[184] H. N. Kim *et al.*, "DNA damage and senescence in osteoprogenitors expressing Osx1 may cause their decrease with age," *Aging Cell,* vol. 16, no. 4, pp. 693-703, Aug 2017.

[185] P. Zhang *et al.*, "Senolytic therapy alleviates Aβ-associated oligodendrocyte progenitor cell senescence and cognitive deficits in an Alzheimer's disease model," *Nat Neurosci,* vol. 22, no. 5, pp. 719-728, May 2019.

[186] J. D. Leverson *et al.*, "Exploiting selective BCL-2 family inhibitors to dissect cell survival dependencies and define improved strategies for cancer therapy," *Sci Transl Med,* vol. 7, no. 279, p. 279ra40, Mar 2015.

[187] F. Triana-Martínez *et al.*, "Identification and characterization of Cardiac Glycosides as senolytic compounds," *Nat Commun,* vol. 10, no. 1, p. 4731, Oct 2019.

[188] A. Guerrero *et al.*, "Cardiac glycosides are broad-spectrum senolytics," *Nat Metab,* vol. 1, no. 11, pp. 1074-1088, Nov 2019.

[189] D. G. A. Burton and A. Stolzing, "Cellular senescence: Immunosurveillance and future immunotherapy," *Ageing Res Rev,* vol. 43, pp. 17-25, May 2018.

[190] S. Radaeva, R. Sun, B. Jaruga, V. T. Nguyen, Z. Tian, and B. Gao, "Natural killer cells ameliorate liver fibrosis by killing activated stellate cells in NKG2D-dependent and tumor necrosis factor-related apoptosis-inducing ligand-dependent manners," *Gastroenterology,* vol. 130, no. 2, pp. 435-52, Feb 2006.

[191] A. Sagiv *et al.*, "NKG2D ligands mediate immunosurveillance of senescent cells," *Aging (Albany NY),* vol. 8, no. 2, pp. 328-44, Feb 2016.

[192] C. Amor *et al.*, "Senolytic CAR T cells reverse senescence-associated pathologies," *Nature,* vol. 583, no. 7814, pp. 127-132, Jul 2020.

[193] G. Pellegrini *et al.*, "Telomerase activity is sufficient to bypass replicative senescence in human limbal and conjunctival but not corneal keratinocytes," *Eur J Cell Biol,* vol. 83, no. 11-12, pp. 691-700, Dec 2004.

[194] N. Dietrich *et al.*, "Bypass of senescence by the polycomb group protein CBX8 through direct binding to the INK4A-ARF locus," *Embo j,* vol. 26, no. 6, pp. 1637-48, Mar 2007.

[195] M. Abad *et al.*, "Reprogramming in vivo produces teratomas and iPS cells with totipotency features," *Nature,* vol. 502, no. 7471, pp. 340-5, Oct 2013.

[196] L. Lapasset *et al.*, "Rejuvenating senescent and centenarian human cells by reprogramming through the pluripotent state," *Genes Dev,* vol. 25, no. 21, pp. 2248-53, Nov 2011.

[197] M. Paez-Ribes, E. González-Gualda, G. J. Doherty, and D. Muñoz-Espín, "Targeting senescent cells in translational medicine," *EMBO Mol Med,* vol. 11, no. 12, p. e10234, Dec 2019.

[198] J. Hou, C. Cui, S. Kim, C. Sung, and C. Choi, "Ginsenoside F1 suppresses astrocytic senescence-associated secretory phenotype," *Chem Biol Interact,* vol. 283, pp. 75-83, Mar 2018.

[199] C. D. Wiley *et al.*, "Small-molecule MDM2 antagonists attenuate the senescence-associated secretory phenotype," *Scientific Reports,* vol. 8, no. 1, p. 2410, Feb 2018.

[200] N. N. Mohamad Anuar, N. S. Nor Hisam, S. L. Liew, and A. Ugusman, "Clinical Review: Navitoclax as a Pro-Apoptotic and Anti-Fibrotic Agent," *Front Pharmacol,* vol. 11, p. 564108, 2020.

[201] L. J. Niedernhofer and P. D. Robbins, "Senotherapeutics for healthy ageing," *Nat Rev Drug Discov,* vol. 17, no. 5, p. 377, May 2018.

[202] A. K. Sharma *et al.*, "The Senolytic Drug Navitoclax (ABT-263) Causes Trabecular Bone Loss and Impaired Osteoprogenitor Function in Aged Mice," *Front Cell Dev Biol,* vol. 8, p. 354, 2020.

[203] A. Agostini *et al.*, "Targeted cargo delivery in senescent cells using capped mesoporous silica nanoparticles," *Angew Chem Int Ed Engl,* vol. 51, no. 42, pp. 10556-60, Oct 2012.

[204] D. Muñoz-Espín *et al.*, "A versatile drug delivery system targeting senescent cells," *EMBO Mol Med,* vol. 10, no. 9, Sep 2018.

[205] R. K. Thapa *et al.*, "Progressive slowdown/prevention of cellular senescence by CD9-targeted delivery of rapamycin using lactose-wrapped calcium carbonate nanoparticles," *Sci Rep,* vol. 7, p. 43299, Apr 2017.

[206] A. E. Ekpenyong-Akiba *et al.*, "Detecting and targeting senescent cells using molecularly imprinted nanoparticles," *Nanoscale Horizons,* 10.1039/C8NH00473K vol. 4, no. 3, pp. 757-768, 2019.

[207] B. Lozano-Torres *et al.*, "An OFF-ON Two-Photon Fluorescent Probe for Tracking Cell Senescence in Vivo," *J Am Chem Soc,* vol. 139, no. 26, pp. 8808-8811, Jul 5 2017.

[208] S. U. Lee *et al.*, "Increasing cell permeability of N-acetylglucosamine via 6-acetylation enhances capacity to suppress T-helper 1 (TH1)/TH17 responses and autoimmunity," *PLoS One,* vol. 14, no. 3, p. e0214253, 2019.

[209] L. Su *et al.*, "Potential role of senescent macrophages in radiation-induced pulmonary fibrosis," *Cell Death Dis,* vol. 12, no. 6, p. 527, May 2021.

[210] J. Massagué, "TGFbeta in Cancer," *Cell,* vol. 134, no. 2, pp. 215-30, Jul 2008..

[211] S. Cheifetz *et al.*, "The transforming growth factor-beta system, a complex pattern of cross-reactive ligands and receptors," *Cell,* vol. 48, no. 3, pp. 409-15, Feb 1987.

[212] L. E. Gentry, M. N. Lioubin, A. F. Purchio, and H. Marquardt, "Molecular events in the processing of recombinant type 1 pre-pro-transforming growth factor beta to the mature polypeptide," *Mol Cell Biol,* vol. 8, no. 10, pp. 4162-8, Oct 1988,.

[213] A. M. Gray and A. J. Mason, "Requirement for activin A and transforming growth factor--beta 1 pro-regions in homodimer assembly," *Science,* vol. 247, no. 4948, pp. 1328-30, Mar 1990.

[214] K. Miyazono, U. Hellman, C. Wernstedt, and C. H. Heldin, "Latent high molecular weight complex of transforming growth factor beta 1. Purification from human platelets and structural characterization," *J Biol Chem,* vol. 263, no. 13, pp. 6407-15, May 1988.

[215] L. Kubiczkova, L. Sedlarikova, R. Hajek, and S. Sevcikova, "TGF-β – an excellent servant but a bad master," *Journal of Translational Medicine,* vol. 10, no. 1, p. 183, Sep 2012.

[216] Y. E. Zhang, "Non-Smad pathways in TGF-β signaling," *Cell Research,* vol. 19, no. 1, pp. 128-139, Jan 2009.

[217] C. Porta, C. Paglino, and A. Mosca, "Targeting PI3K/Akt/mTOR Signaling in Cancer," *Frontiers in Oncology,* Review vol. 4, no. 64, Apr 2014.

[218] E. Batlle and J. Massagué, "Transforming Growth Factor-β Signaling in Immunity and Cancer," *Immunity,* vol. 50, no. 4, pp. 924-940, Apr 2019.

[219] S. Biswas *et al.*, "Inhibition of TGF-beta with neutralizing antibodies prevents radiation-induced acceleration of metastatic cancer progression," *J Clin Invest,* vol. 117, no. 5, pp. 1305-13, May 2007.

[220] N. M. Muñoz *et al.*, "Transforming growth factor beta receptor type II inactivation induces the malignant transformation of intestinal neoplasms initiated by Apc mutation," *Cancer Res,* vol. 66, no. 20, pp. 9837-44, Oct 2006.

[221] H. Ijichi *et al.*, "Aggressive pancreatic ductal adenocarcinoma in mice caused by pancreas-specific blockade of transforming growth factor-β signaling in cooperation with active Kras expression," *Genes & Development,* vol. 20, no. 22, pp. 3147-3160, November 2006.

[222] G. Guasch, M. Schober, H. A. Pasolli, E. B. Conn, L. Polak, and E. Fuchs, "Loss of TGFbeta signaling destabilizes homeostasis and promotes squamous cell

carcinomas in stratified epithelia," *Cancer Cell,* vol. 12, no. 4, pp. 313-27, Oct 2007.

[223] Y.-S. Yoon, J.-H. Lee, S.-C. Hwang, K. S. Choi, and G. Yoon, "TGF β1 induces prolonged mitochondrial ROS generation through decreased complex IV activity with senescent arrest in Mv1Lu cells," *Oncogene,* vol. 24, no. 11, pp. 1895-1903, Mar 2005.

[224] B. Hu, D. C. Tack, T. Liu, Z. Wu, M. R. Ullenbruch, and S. H. Phan, "Role of Smad3 in the regulation of rat telomerase reverse transcriptase by TGFβ," *Oncogene,* vol. 25, no. 7, pp. 1030-1041, Feb 2006.

[225] H. Li, D. Xu, J. Li, M. C. Berndt, and J.-P. Liu, "Transforming Growth Factor Beta Suppresses Human Telomerase Reverse Transcriptase (hTERT) by Smad3 Interactions with c-Myc and the hTERT Gene," *Journal of Biological Chemistry,* vol. 281, no. 35, pp. 25588-25600, 2006.

[226] H. I. Suzuki, "MicroRNA Control of TGF-β Signaling," *International Journal of Molecular Sciences,* vol. 19, no. 7, 2018.

[227] G. Lyu *et al.*, "TGF-β signaling alters H4K20me3 status via miR-29 and contributes to cellular senescence and cardiac aging," *Nature Communications,* vol. 9, no. 1, p. 2560, Jul 2018.

[228] J. Wu, J. Niu, X. Li, X. Wang, Z. Guo, and F. Zhang, "TGF-β1 induces senescence of bone marrow mesenchymal stem cells via increase of mitochondrial ROS production," *BMC Developmental Biology,* vol. 14, no. 1, p. 21, May 2014.

[229] G. Lyu *et al.*, "TGF-β signaling alters H4K20me3 status via miR-29 and contributes to cellular senescence and cardiac aging," *Nat Commun,* vol. 9, no. 1, p. 2560, Jul 2018.

[230] H. Zhao, J. Wei, and J. Sun, "Roles of TGF-β signaling pathway in tumor microenvirionment and cancer therapy," *Int Immunopharmacol,* vol. 89, no. Pt B, p. 107101, Dec 2020.

[231] J. Seoane and R. R. Gomis, "TGF-β Family Signaling in Tumor Suppression and Cancer Progression," *Cold Spring Harbor Perspectives in Biology,* vol. 9, no. 12, Dec 2017.

[232] R. Derynck and R. J. Akhurst, "Differentiation plasticity regulated by TGF-beta family proteins in development and disease," *Nat Cell Biol,* vol. 9, no. 9, pp. 1000-4, Sep 2007.

[233] G. A. Stouffer and G. K. Owens, "TGF-beta promotes proliferation of cultured SMC via both PDGF-AA-dependent and PDGF-AA-independent mechanisms," *The Journal of clinical investigation,* vol. 93, no. 5, pp. 2048-2055, 1994.

[234] E. J. Battegay, E. W. Raines, R. A. Seifert, D. F. Bowen-Pope, and R. Ross, "TGF-beta induces bimodal proliferation of connective tissue cells via complex control of an autocrine PDGF loop," *Cell,* vol. 63, no. 3, pp. 515-24, Nov 1990.

[235] A. F. Kells, S. R. Coats, H. S. Schwartz, and R. L. Hoover, "TGF-β and PDGF Act Synergistically in Affecting the Growth of Human Osteoblast-Enriched Cultures," *Connective Tissue Research,* vol. 31, no. 2, pp. 117-124, Jan 1995.

[236] M. T. Jennings and J. A. Pietenpol, "The role of transforming growth factor beta in glioma progression," *J Neurooncol,* vol. 36, no. 2, pp. 123-40, Jan 1998.

[237] L. T. Diemel, S. J. Jackson, and M. L. Cuzner, "Role for TGF-beta1, FGF-2 and PDGF-AA in a myelination of CNS aggregate cultures enriched with macrophages," *J Neurosci Res,* vol. 74, no. 6, pp. 858-67, Dec 2003.

[238] A. Mazzocca, E. Fransvea, G. Lavezzari, S. Antonaci, and G. Giannelli, "Inhibition of transforming growth factor beta receptor I kinase blocks hepatocellular carcinoma growth through neo-angiogenesis regulation," *Hepatology,* vol. 50, no. 4, pp. 1140-51, Oct 2009.

[239] M. Zhang *et al.*, "Trimodal glioblastoma treatment consisting of concurrent radiotherapy, temozolomide, and the novel TGF-β receptor I kinase inhibitor LY2109761," *Neoplasia,* vol. 13, no. 6, pp. 537-49, Jun 2011.

[240] A. Akbari *et al.*, "Evaluation of antitumor activity of a TGF-beta receptor I inhibitor (SD-208) on human colon adenocarcinoma," *Daru,* vol. 22, no. 1, p. 47, Jun 2014.

[241] K. Miyazono, Y. Katsuno, D. Koinuma, S. Ehata, and M. Morikawa, "Intracellular and extracellular TGF-β signalin.

[242] M. A. Friese *et al.*, "RNA interference targeting transforming growth factor-beta enhances NKG2D-mediated antiglioma immune response, inhibits glioma cell

migration and invasiveness, and abrogates tumorigenicity in vivo," *Cancer Res,* vol. 64, no. 20, pp. 7596-603, Oct 2004.

[243] N. Oshimori, D. Oristian, and E. Fuchs, "TGF-β Promotes Heterogeneity and Drug Resistance in Squamous Cell Carcinoma," *Cell,* vol. 160, no. 5, pp. 963-976, Feb 2015.

[244] R. J. Forsey *et al.*, "Plasma cytokine profiles in elderly humans," *Mech Ageing Dev,* vol. 124, no. 4, pp. 487-93, Apr 2003.

[245] G. Carrieri *et al.*, "The G/C915 polymorphism of transforming growth factor beta1 is associated with human longevity: a study in Italian centenarians," *Aging Cell,* vol. 3, no. 6, pp. 443-8, Dec 2004.

[246] K. Tominaga and H. I. Suzuki, "TGF-β Signaling in Cellular Senescence and Aging-Related Pathology," *International journal of molecular sciences,* vol. 20, no. 20, p. 5002, 2019.

[247] V. Rapisarda *et al.*, "Integrin Beta 3 Regulates Cellular Senescence by Activating the TGF-β Pathway," *Cell Rep,* vol. 18, no. 10, pp. 2480-2493, Mar 2017.

[248] M. Hoare and M. Narita, "Notch and Senescence," in *Molecular Mechanisms of Notch Signaling*, T. Borggrefe and B. D. Giaimo Eds. Cham: Springer International Publishing, 2018.

[249] W. Sterlacci *et al.*, "High transforming growth factor β expression represents an important prognostic parameter for surgically resected non-small cell lung cancer," *Hum Pathol,* vol. 43, no. 3, pp. 339-49, Mar 2012.

[250] A. E. González-Santiago, L. A. Mendoza-Topete, F. Sánchez-Llamas, R. Troyo-Sanromán, and C. M. Gurrola-Díaz, "TGF-β1 serum concentration as a complementary diagnostic biomarker of lung cancer: establishment of a cut-point value," *J Clin Lab Anal,* vol. 25, no. 4, pp. 238-43, 2011.

[251] H. S. Jeon *et al.*, "SMAD6 contributes to patient survival in non-small cell lung cancer and its knockdown reestablishes TGF-beta homeostasis in lung cancer cells," *Cancer Res,* vol. 68, no. 23, pp. 9686-92, Dec 2008.

[252] B. N. Kim *et al.*, "TGF-β induced EMT and stemness characteristics are associated with epigenetic regulation in lung cancer," *Sci Rep,* vol. 10, no. 1, p. 10597, Jun 2020.

[253] D. M. Wu, S. H. Deng, T. Liu, R. Han, T. Zhang, and Y. Xu, "TGF-β-mediated exosomal lnc-MMP2-2 regulates migration and invasion of lung cancer cells to the vasculature by promoting MMP2 expression," *Cancer Med,* vol. 7, no. 10, pp. 5118-5129, Oct 2018.

[254] A. Saito, M. Horie, and T. Nagase, "TGF-β Signaling in Lung Health and Disease," *Int J Mol Sci,* vol. 19, no. 8, Aug 2018.

[255] P. Micke and A. Ostman, "Tumour-stroma interaction: cancer-associated fibroblasts as novel targets in anti-cancer therapy?," *Lung Cancer,* vol. 45 Suppl 2, pp. S163-75, Aug 2004.

[256] W. Huang *et al.*, "Circular RNA cESRP1 sensitises small cell lung cancer cells to chemotherapy by sponging miR-93-5p to inhibit TGF-β signalling," *Cell Death Differ,* vol. 27, no. 5, pp. 1709-1727, May 2020.

[257] M. Zheng *et al.*, "ESRP1 regulates alternative splicing of CARM1 to sensitize small cell lung cancer cells to chemotherapy by inhibiting TGF-β/Smad signaling," *Aging (Albany NY),* vol. 13, no. 3, pp. 3554-3572, Jan 2021.

[258] D. V. F. Tauriello *et al.*, "TGFβ drives immune evasion in genetically reconstituted colon cancer metastasis," *Nature,* vol. 554, no. 7693, pp. 538-543, Feb 2018.

[259] S. Mariathasan *et al.*, "TGFβ attenuates tumour response to PD-L1 blockade by contributing to exclusion of T cells," *Nature,* vol. 554, no. 7693, pp. 544-548, Feb 2018.

[260] K. Leventakos *et al.*, "Management of Multifocal Lung Cancer: Results of a Survey" *Journal of Thoracic Oncology,* vol. 12, no. 9, pp. 1398-1402, 2017.

[261] S. Y. El Sharouni, H. B. Kal, and J. J. Battermann, "Accelerated regrowth of non-small-cell lung tumours after induction chemotherapy," *Br J Cancer,* vol. 89, no. 12, pp. 2184-9, Dec 2003.

[262] Y. Zhao *et al.*, "Cytotoxicity enhancement in MDA-MB-231 cells by the combination treatment of tetrahydropalmatine and berberine derived from Corydalis yanhusuo W. T. Wang," *J Intercult Ethnopharmacol,* vol. 3, no. 2, pp. 68-72, Apr 2014.

[263] B. Vogelstein and K. W. Kinzler, "The multistep nature of cancer," *Trends Genet,* vol. 9, no. 4, pp. 138-41, Apr 1993.

[264] P. Vermylen, C. Roufosse, V. Ninane, and J. P. Sculier, "Biology of pulmonary preneoplastic lesions," *Cancer Treat Rev,* vol. 23, no. 4, pp. 241-62, Jul 1997.

[265] M. Collado and M. Serrano, "Senescence in tumours: evidence from mice and humans," *Nat Rev Cancer,* vol. 10, no. 1, pp. 51-57, 2010.

[266] P. A. Pérez-Mancera, A. R. Young, and M. Narita, "Inside and out: the activities of senescence in cancer," *Nat Rev Cancer,* vol. 14, no. 8, pp. 547-58, Aug 2014.

[267] S. He and N. E. Sharpless, "Senescence in Health and Disease," *Cell,* vol. 169, no. 6, pp. 1000-1011, Jun 2017.

[268] V. J. Carpenter, T. Saleh, and D. A. Gewirtz, "Senolytics for Cancer Therapy: Is All That Glitters Really Gold?," *Cancers (Basel),* vol. 13, no. 4, p. 723, 2021.

[269] E. O. Wissler Gerdes, Y. Zhu, T. Tchkonia, and J. L. Kirkland, "Discovery, development, and future application of senolytics: theories and predictions," *Febs j,* vol. 287, no. 12, pp. 2418-2427, Jun 2020.

[270] B. G. Childs *et al.*, "Senescent cells: an emerging target for diseases of ageing," *Nat Rev Drug Discov,* vol. 16, no. 10, pp. 718-735, 2017.

[271] P. J. Thompson, A. Shah, V. Ntranos, F. Van Gool, M. Atkinson, and A. Bhushan, "Targeted Elimination of Senescent Beta Cells Prevents Type 1 Diabetes," *Cell Metab,* vol. 29, no. 5, pp. 1045-1060.e10, May 2019.

[272] B. Ritschka *et al.*, "The senotherapeutic drug ABT-737 disrupts aberrant p21 expression to restore liver regeneration in adult mice," *Genes Dev,* vol. 34, no. 7-8, pp. 489-494, Apr 2020.

[273] N. K. Altorki *et al.*, "The lung microenvironment: an important regulator of tumour growth and metastasis," *Nat Rev Cancer,* vol. 19, no. 1, pp. 9-31, Jan 2019.

[274] D. D. Tippimanchai *et al.*, "Adenoviral vectors transduce alveolar macrophages in lung cancer models," *Oncoimmunology,* vol. 7, no. 6, pp. e1438105-e1438105, 2018.

[275] B. M. Hall *et al.*, "p16(Ink4a) and senescence-associated β-galactosidase can be induced in macrophages as part of a reversible response to physiological stimuli," *Aging (Albany NY),* vol. 9, no. 8, pp. 1867-1884, 2017.

[276] J. Y. Liu *et al.*, "Cells exhibiting strong p16 (INK4a) promoter activation in vivo display features of senescence," *Proc Natl Acad Sci U S A,* vol. 116, no. 7, pp. 2603-2611, Feb 2019.

[277] G. Jia, A. R. Aroor, C. Jia, and J. R. Sowers, "Endothelial cell senescence in aging-related vascular dysfunction," *Biochim Biophys Acta Mol Basis Dis,* vol. 1865, no. 7, pp. 1802-1809, Jul 2019.

[278] X. Sun and M. W. Feinberg, "Vascular Endothelial Senescence: Pathobiological Insights, Emerging Long Noncoding RNA Targets, Challenges and Therapeutic Opportunities," *Front Physiol,* vol. 12, p. 693067, 2021.

[279] J. C. Reed, "Dysregulation of Apoptosis in Cancer," *Journal of Clinical Oncology,* vol. 17, no. 9, pp. 2941-2941, Jan 1999.

[280] L. Yang, J. Fang, and J. Chen, "Tumor cell senescence response produces aggressive variants," *Cell Death Discov,* vol. 3, p. 17049, 2017.

[281] T. Saleh *et al.*, "Tumor cell escape from therapy-induced senescence," *Biochemical Pharmacology,* vol. 162, pp. 202-212, Apd 2019.

[282] R. Saab, "Senescence and pre-malignancy: how do tumors progress?," *Semin Cancer Biol,* vol. 21, no. 6, pp. 385-91, Dec 2011.

[283] K. Lawrenson, B. Grun, E. Benjamin, I. J. Jacobs, D. Dafou, and S. A. Gayther, "Senescent fibroblasts promote neoplastic transformation of partially transformed ovarian epithelial cells in a three-dimensional model of early stage ovarian cancer," *Neoplasia,* vol. 12, no. 4, pp. 317-25, Apr 2010.

[284] E. Pazolli *et al.*, "Senescent stromal-derived osteopontin promotes preneoplastic cell growth," *Cancer Res,* vol. 69, no. 3, pp. 1230-9, Feb 2009.

[285] M. Casanova-Acebes *et al.*, "Tissue-resident macrophages provide a pro-tumorigenic niche to early NSCLC cells," *Nature,* vol. 595, no. 7868, pp. 578-584, Jul 2021.

[286] D. Yang, P. Guo, T. He, and C. A. Powell, "Role of endothelial cells in tumor microenvironment," *Clin Transl Med,* vol. 11, no. 6, pp. e450-e450, 2021.

[287] D. R. Brenner, J. R. McLaughlin, and R. J. Hung, "Previous lung diseases and lung cancer risk: a systematic review and meta-analysis," *PloS one,* vol. 6, no. 3, pp. e17479-e17479, 2011.

[288] T. Tsuji, K. Aoshiba, and A. Nagai, "Alveolar cell senescence in patients with pulmonary emphysema," *Am J Respir Crit Care Med,* vol. 174, no. 8, pp. 886-93, Oct 2006.

[289] M. J. Schafer *et al.*, "Cellular senescence mediates fibrotic pulmonary disease," *Nature Communications,* vol. 8, no. 1, p. 14532, Feb 2017.

[290] P. J. Barnes, "Senescence in COPD and Its Comorbidities," *Annu Rev Physiol,* vol. 79, pp. 517-539, Feb 12017.

[291] R. S. Herbst, D. Morgensztern, and C. Boshoff, "The biology and management of non-small cell lung cancer," *Nature,* vol. 553, no. 7689, pp. 446-454, Jan 2018.

[292] R. S. Roberson, S. J. Kussick, E. Vallieres, S.-Y. J. Chen, and D. Y. Wu, "Escape from Therapy-Induced Accelerated Cellular Senescence in p53-Null Lung Cancer Cells and in Human Lung Cancers," *Cancer Research,* vol. 65, no. 7, p. 2795, 2005.

[293] T. Saleh *et al.*, "Therapy-Induced Senescence: An "Old" Friend Becomes the Enemy," *Cancers (Basel),* vol. 12, no. 4, p. 822, 2020.

[294] B. Wang, J. Kohli, and M. Demaria, "Senescent Cells in Cancer Therapy: Friends or Foes?," *Trends Cancer,* vol. 6, no. 10, pp. 838-857, Oct 2020.

[295] Z.-Y. Li, Z.-L. Chen, T. Zhang, C. Wei, and W.-Y. Shi, "TGF-β and NF-κB signaling pathway crosstalk potentiates corneal epithelial senescence through an RNA stress response," *Aging (Albany NY),* vol. 8, no. 10, pp. 2337-2354, 2016.

[296] H. Chen *et al.*, "TGF-β1/IL-11/MEK/ERK signaling mediates senescence-associated pulmonary fibrosis in a stress-induced premature senescence model of Bmi-1 deficiency," *Experimental & Molecular Medicine,* vol. 52, no. 1, pp. 130-151, Jan 2020.

[297] Y. V. Teo *et al.*, "Notch Signaling Mediates Secondary Senescence," *Cell Rep,* vol. 27, no. 4, pp. 997-1007.e5, Apr 2019.

[298] C. J. David and J. Massagué, "Contextual determinants of TGFβ action in development, immunity and cancer," *Nat Rev Mol Cell Biol,* vol. 19, no. 7, pp. 419-435, Jul 2018.

[299] J. A. Ewald, J. A. Desotelle, G. Wilding, and D. F. Jarrard, "Therapy-Induced Senescence in Cancer," *JNCI: Journal of the National Cancer Institute,* vol. 102, no. 20, pp. 1536-1546, 2010.

[300] F. K. Turrell *et al.*, "Lung tumors with distinct p53 mutations respond similarly to p53 targeted therapy but exhibit genotype-specific statin sensitivity," *Genes Dev,* vol. 31, no. 13, pp. 1339-1353, Jul 2017.

[301] A. Calcinotto, J. Kohli, E. Zagato, L. Pellegrini, M. Demaria, and A. Alimonti, "Cellular Senescence: Aging, Cancer, and Injury," *Physiological Reviews,* vol. 99, no. 2, pp. 1047-1078, Apr 2019.

[302] H. K. Sanoff *et al.*, "Effect of Cytotoxic Chemotherapy on Markers of Molecular Age in Patients With Breast Cancer," *JNCI: Journal of the National Cancer Institute,* vol. 106, no. 4, 2014.

[303] M. Fane and A. T. Weeraratna, "How the ageing microenvironment influences tumour progression," *Nature Reviews Cancer,* vol. 20, no. 2, pp. 89-106, Jan 2020.

[304] R. Smith *et al.*, "Using Microarrays to Interrogate Microenvironmental Impact on Cellular Phenotypes in Cancer," *J Vis Exp,* no. 147, p. 10.3791/58957, 2019.

[305] E. González-Gualda *et al.*, "Galacto-conjugation of Navitoclax as an efficient strategy to increase senolytic specificity and reduce platelet toxicity," *Aging Cell,* vol. 19, no. 4, p. e13142, Apr 2020.

[306] A. Rossi and M. Di Maio, "Platinum-based chemotherapy in advanced non-small-cell lung cancer: optimal number of treatment cycles," *Expert Rev Anticancer Ther,* vol. 16, no. 6, pp. 653-60, Jun 2016.

[307] Y. Zhang, J. Gundelach, L. D. Lindquist, D. J. Baker, J. van Deursen, and R. J. Bram, "Chemotherapy-induced cellular senescence suppresses progression of Notch-driven T-ALL," *PLoS One,* vol. 14, no. 10, p. e0224172, 2019.

[308] A. E. Vilgelm *et al.*, "Connecting the Dots: Therapy-Induced Senescence and a Tumor-Suppressive Immune Microenvironment," *J Natl Cancer Inst,* vol. 108, no. 6, p. djv406, Jun 2016.

[309] F. Rodier *et al.*, "Persistent DNA damage signalling triggers senescence-associated inflammatory cytokine secretion," *Nat Cell Biol,* vol. 11, no. 8, pp. 973-9, Aug 2009.

[310] P. A. Toste *et al.*, "Chemotherapy-Induced Inflammatory Gene Signature and Protumorigenic Phenotype in Pancreatic CAFs via Stress-Associated MAPK," *Mol Cancer Res,* vol. 14, no. 5, pp. 437-447, 2016.

[311] X. Sun *et al.*, "Senescence-associated secretory factors induced by cisplatin in melanoma cells promote non-senescent melanoma cell growth through activation of the ERK1/2-RSK1 pathway," *Cell Death Dis,* vol. 9, no. 3, p. 260, Feb 2018.

[312] J. G. Hou, B. M. Jeon, Y. J. Yun, C. H. Cui, and S. C. Kim, "Ginsenoside Rh2 Ameliorates Doxorubicin-Induced Senescence Bystander Effect in Breast Carcinoma Cell MDA-MB-231 and Normal Epithelial Cell MCF-10A," *Int J Mol Sci,* vol. 20, no. 5, Mar 2019.

[313] M. P. Mongiardi, M. Pellegrini, R. Pallini, A. Levi, and M. L. Falchetti, "Cancer Response to Therapy-Induced Senescence: A Matter of Dose and Timing," *Cancers (Basel),* vol. 13, no. 3, Jan 2021.

[314] X. Luo *et al.*, "Stromal-Initiated Changes in the Bone Promote Metastatic Niche Development," *Cell Rep,* vol. 14, no. 1, pp. 82-92, Jan 2016/

[315] J. Campisi, "Aging, cellular senescence, and cancer," *Annu Rev Physiol,* vol. 75, pp. 685-705, 2013.

[316] S. Senturk, M. Mumcuoglu, O. Gursoy-Yuzugullu, B. Cingoz, K. C. Akcali, and M. Ozturk, "Transforming growth factor-beta induces senescence in hepatocellular carcinoma cells and inhibits tumor growth," *Hepatology,* vol. 52, no. 3, pp. 966-74, Sep 2010.

[317] S. Lamouille and R. Derynck, "Cell size and invasion in TGF-β–induced epithelial to mesenchymal transition is regulated by activation of the mTOR pathway," *Journal of Cell Biology,* vol. 178, no. 3, pp. 437-451, 2007.

[318] L. Zhang, F. Zhou, and P. ten Dijke, "Signaling interplay between transforming growth factor-β receptor and PI3K/AKT pathways in cancer," *Trends Biochem Sci,* vol. 38, no. 12, pp. 612-20, Dec 2013.

[319] S. Herbertz *et al.*, "Clinical development of galunisertib (LY2157299 monohydrate), a small molecule inhibitor of transforming growth factor-beta signaling pathway," *Drug Des Devel Ther,* vol. 9, pp. 4479-4499, 2015.

[320] G. Azzam, S. Samuels, A. Ahmad, and B. Marples, "Notch-high Senescence Induction Occurs Early After Radiation (RT), and its TGFB-rich Senescence-

Associated Secretory Phenotype (SASP) Increases Over Time," *International Journal of Radiation Oncology, Biology, Physics,* vol. 108, no. 3, p. e559, 2020.

[321] D. V. Faget, Q. Ren, and S. A. Stewart, "Unmasking senescence: context-dependent effects of SASP in cancer," *Nat Rev Cancer,* vol. 19, no. 8, pp. 439-453, Aug 2019.

[322] S. Lee and C. A. Schmitt, "The dynamic nature of senescence in cancer," *Nat Cell Biol,* vol. 21, no. 1, pp. 94-101, Jan 2019.

[323] B. Lozano-Torres *et al.*, "The chemistry of senescence," *Nature Reviews Chemistry,* vol. 3, no. 7, pp. 426-441, Jul 2019.

[324] M. J. Yousefzadeh *et al.*, "Fisetin is a senotherapeutic that extends health and lifespan," *EBioMedicine,* vol. 36, pp. 18-28, Oct 2018.

[325] M. P. Baar *et al.*, "Targeted Apoptosis of Senescent Cells Restores Tissue Homeostasis in Response to Chemotoxicity and Aging," *Cell,* vol. 169, no. 1, pp. 132-147.e16, Mar 2017.

[326] H. Fuhrmann-Stroissnigg *et al.*, "Identification of HSP90 inhibitors as a novel class of senolytics," *Nat Commun,* vol. 8, no. 1, p. 422, Sep 2017.

[327] S. Cang, C. Iragavarapu, J. Savooji, Y. Song, and D. Liu, "ABT-199 (venetoclax) and BCL-2 inhibitors in clinical development," *J Hematol Oncol,* vol. 8, p. 129, Nov 2015.

[328] A. Hernandez-Segura, J. Nehme, and M. Demaria, "Hallmarks of Cellular Senescence," *Trends Cell Biol,* vol. 28, no. 6, pp. 436-453, Jun 2018.

[329] X. Liu, Y. Zhang, W. Huang, W. Tan, and A. Zhang, "Design, synthesis and pharmacological evaluation of new acyl sulfonamides as potent and selective Bcl-2 inhibitors," *Bioorg Med Chem,* vol. 26, no. 2, pp. 443-454, Jan 2018.

[330] W. H. Wilson *et al.*, "Navitoclax, a targeted high-affinity inhibitor of BCL-2, in lymphoid malignancies: a phase 1 dose-escalation study of safety, pharmacokinetics, pharmacodynamics, and antitumour activity," *Lancet Oncol,* vol. 11, no. 12, pp. 1149-59, Dec 2010.

[331] M. Vogler *et al.*, "BCL2/BCL-X(L) inhibition induces apoptosis, disrupts cellular calcium homeostasis, and prevents platelet activation," *Blood,* vol. 117, no. 26, pp. 7145-54, Jun 2011.

[332] D. J. Baker *et al.*, "Naturally occurring p16(Ink4a)-positive cells shorten healthy lifespan," *Nature,* vol. 530, no. 7589, pp. 184-9, Feb 2016.

[333] N. E. Sharpless and C. J. Sherr, "Forging a signature of in vivo senescence," *Nat Rev Cancer,* vol. 15, no. 7, pp. 397-408, Jul 2015.

[334] J. Shi, P. W. Kantoff, R. Wooster, and O. C. Farokhzad, "Cancer nanomedicine: progress, challenges and opportunities," *Nat Rev Cancer,* vol. 17, no. 1, pp. 20-37, Jan 2017.

[335] C. Tse *et al.*, "ABT-263: a potent and orally bioavailable Bcl-2 family inhibitor," *Cancer Res,* vol. 68, no. 9, pp. 3421-8, May 2008.

[336] K. D. Mason *et al.*, "Programmed anuclear cell death delimits platelet life span," *Cell,* vol. 128, no. 6, pp. 1173-86, Mar 2007.

[337] S. Khan *et al.*, "A selective BCL-X(L) PROTAC degrader achieves safe and potent antitumor activity," *Nat Med,* vol. 25, no. 12, pp. 1938-1947, Dec 2019.

[338] Y. He *et al.*, "Using proteolysis-targeting chimera technology to reduce navitoclax platelet toxicity and improve its senolytic activity," *Nat Commun,* vol. 11, no. 1, p. 1996, Apr 2020.

[339] J. A. Eggert, M. Palavanzadeh, and A. Blanton, "Screening and Early Detection of Lung Cancer," *Semin Oncol Nurs,* vol. 33, no. 2, pp. 129-140, May 2017.

[340] J. A. Barta, C. A. Powell, and J. P. Wisnivesky, "Global Epidemiology of Lung Cancer," *Ann Glob Health,* vol. 85, no. 1, Jan 2019.

[341] P. Nanavaty, M. S. Alvarez, and W. M. Alberts, "Lung cancer screening: advantages, controversies, and applications," *Cancer Control,* vol. 21, no. 1, pp. 9-14, Jan 2014.

[342] P. Hofman, "Liquid biopsy for early detection of lung cancer," *Curr Opin Oncol,* vol. 29, no. 1, pp. 73-78, Jan 2017.

[343] C. Goebel, C. L. Louden, R. McKenna, Jr., O. Onugha, A. Wachtel, and T. Long, "Diagnosis of Non-small Cell Lung Cancer for Early Stage Asymptomatic Patients," *Cancer Genomics Proteomics,* vol. 16, no. 4, pp. 229-244, Jul 2019.

[344] W. De Wever, J. Coolen, and J. A. Verschakelen, "Imaging techniques in lung cancer," *Breathe,* vol. 7, no. 4, p. 338, 2011.

[345] D. Kolodkin-Gal *et al.*, "Senolytic elimination of Cox2-expressing senescent cells inhibits the growth of premalignant pancreatic lesions," *Gut,* Mar 2021.

[346] K. D. Sutherland and A. Berns, "Cell of origin of lung cancer," *Mol Oncol,* vol. 4, no. 5, pp. 397-403, Oct 2010.

[347] C. R. Goding, D. Pei, and X. Lu, "Cancer: pathological nuclear reprogramming?," *Nat Rev Cancer,* vol. 14, no. 8, pp. 568-73, Aug 2014.

[348] D. Friedmann-Morvinski and I. M. Verma, "Dedifferentiation and reprogramming: origins of cancer stem cells," *EMBO Rep,* vol. 15, no. 3, pp. 244-253, 2014.

[349] L. Mosteiro, C. Pantoja, A. de Martino, and M. Serrano, "Senescence promotes in vivo reprogramming through p16(INK)(4a) and IL-6," *Aging cell,* vol. 17, no. 2, p. e12711, 2018.

[350] C. Li *et al.*, "Programmed cell senescence in skeleton during late puberty," *Nature Communications,* vol. 8, no. 1, p. 1312, Mar 2017.

[351] L. Grosse *et al.*, "Defined p16(High) Senescent Cell Types Are Indispensable for Mouse Healthspan," *Cell Metab,* vol. 32, no. 1, pp. 87-99.e6, Jul 2020.

[352] S. Ball, M. Arevalo, E. Juarez, J. D. Payne, and C. Jones, "Breast cancer chemoprevention: An update on current practice and opportunities for primary care physicians," *Prev Med,* vol. 129, p. 105834, Dec 2019.

[353] L. Ombrato *et al.*, "Metastatic-niche labelling reveals parenchymal cells with stem features," *Nature,* vol. 572, no. 7771, pp. 603-608, Aug 2019.

[354] R. Liu *et al.*, "PI3K/AKT pathway as a key link modulates the multidrug resistance of cancers," *Cell Death & Disease,* vol. 11, no. 9, p. 797, Sep 2020.

[355] E. Pleasance *et al.*, "Pan-cancer analysis of advanced patient tumors reveals interactions between therapy and genomic landscapes," *Nature Cancer,* vol. 1, no. 4, pp. 452-468, Apr 2020.

[356] E. Frei, 3rd *et al.*, "The effectiveness of combinations of antileukemic agents in inducing and maintaining remission in children with acute leukemia," *Blood,* vol. 26, no. 5, pp. 642-56, Nov 1965.

[357] R. Bayat Mokhtari *et al.*, "Combination therapy in combating cancer," *Oncotarget,* vol. 8, no. 23, pp. 38022-38043, 2017.

[358] L. Wang *et al.*, "High-Throughput Functional Genetic and Compound Screens Identify Targets for Senescence Induction in Cancer," *Cell Rep,* vol. 21, no. 3, pp. 773-783, Oct 2017.

[359] T. Saleh *et al.*, "Clearance of therapy-induced senescent tumor cells by the senolytic ABT-263 via interference with BCL-X(L) -BAX interaction," *Mol Oncol,* vol. 14, no. 10, pp. 2504-2519, Oct 2020.

[360] H. Fleury *et al.*, "Exploiting interconnected synthetic lethal interactions between PARP inhibition and cancer cell reversible senescence," *Nat Commun,* vol. 10, no. 1, p. 2556, Jun 12019.

[361] N. Malaquin *et al.*, "DNA Damage- But Not Enzalutamide-Induced Senescence in Prostate Cancer Promotes Senolytic Bcl-xL Inhibitor Sensitivity," *Cells,* vol. 9, no. 7, Jul 2020.

[362] A. Shahbandi *et al.*, "BH3 mimetics selectively eliminate chemotherapy-induced senescent cells and improve response in TP53 wild-type breast cancer," *Cell Death Differ,* vol. 27, no. 11, pp. 3097-3116, Nov 2020.

[363] S. S. Gayle *et al.*, "Targeting BCL-xL improves the efficacy of bromodomain and extra-terminal protein inhibitors in triple-negative breast cancer by eliciting the death of senescent cells," *J Biol Chem,* vol. 294, no. 3, pp. 875-886, Jan 2019.

[364] V. Suvarna, V. Singh, and M. Murahari, "Current overview on the clinical update of Bcl-2 anti-apoptotic inhibitors for cancer therapy," *Eur J Pharmacol,* vol. 862, p. 172655, Nov 2019.

[365] A. Guerrero *et al.*, "Galactose-modified duocarmycin prodrugs as senolytics," *Aging Cell,* vol. 19, no. 4, p. e13133, 2020.

[366] Y. Cai *et al.*, "Elimination of senescent cells by β-galactosidase-targeted prodrug attenuates inflammation and restores physical function in aged mice," *Cell Research,* vol. 30, no. 7, pp. 574-589, Jul 2020.

[367] S. Acklin *et al.*, "Depletion of senescent-like neuronal cells alleviates cisplatin-induced peripheral neuropathy in mice," *Sci Rep,* vol. 10, no. 1, p. 14170, Aug 2020.

[368] Z. Yao *et al.*, "Therapy-Induced Senescence Drives Bone Loss," *Cancer Res,* vol. 80, no. 5, pp. 1171-1182, Mar 2020.

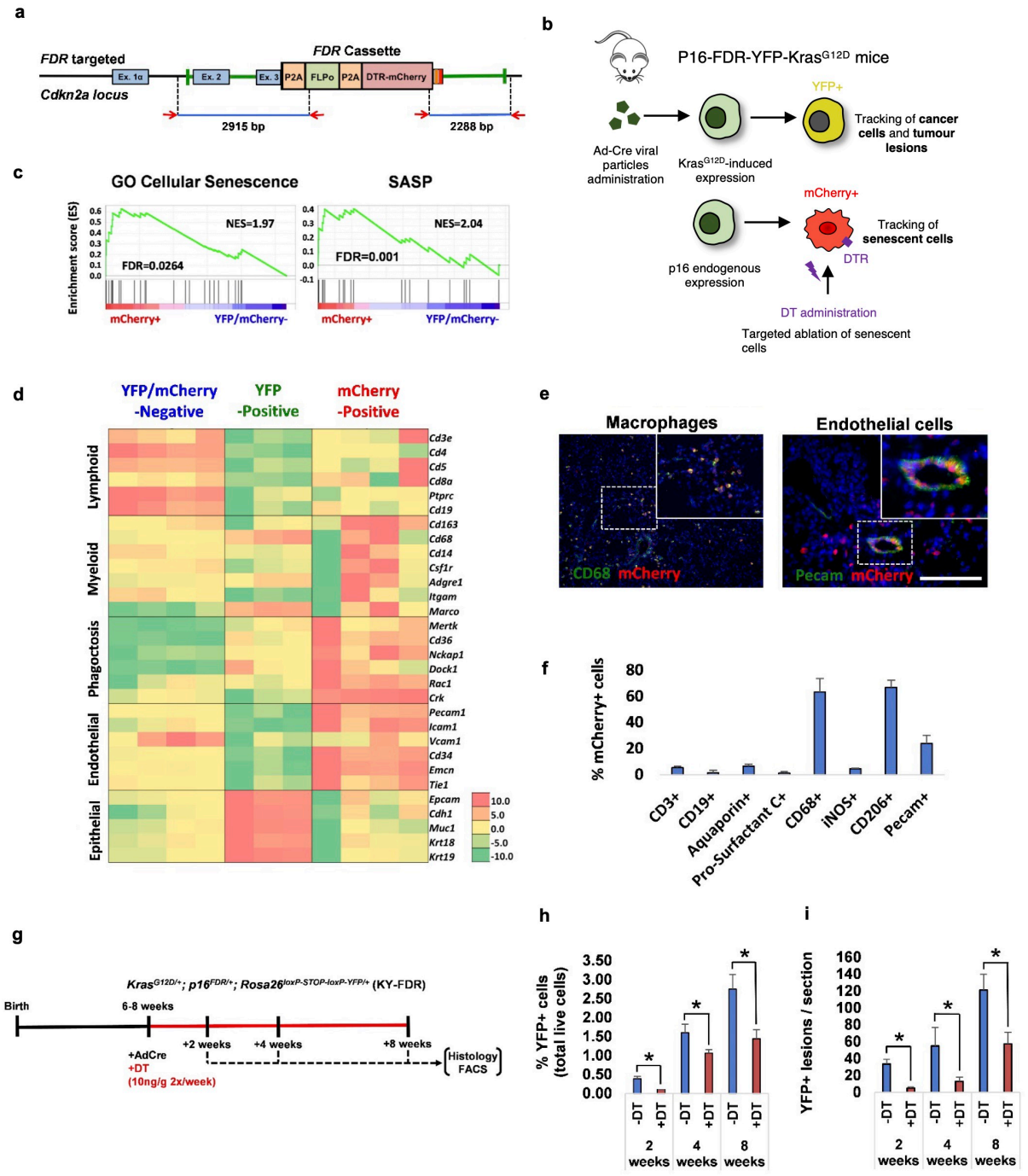

Supplementary Figure 3.1. Novel *p16-FDR* mouse model and relevant findings during Kras^{G12D}-driven lung tumorigenesis. a. Schematic representation of newly generated *p16-FDR* allele, inserted within Exon 3 of *Cdkn2a* locus. P2A; 2A self-cleaving peptide, FLPo; mammalian optimised FLP-recombinase, DTR; diphtheria toxin receptor. **b.** Schematic representation of strategy for the tracking of G12D-positive (tumour) cells

and p16-positive (senescent) cells, as well as the targeted ablation of p16-positive cells, in *p16-FDR-Kras^{G12D}* mouse model. DT, diphtheria toxic; DTR, diphtheria toxin receptor. **c.** GSEA comparing transcriptomic data from mCherry-positive and YFP/mCherry-negative cell fractions showing an enrichment of senescence-associated pathways in mCherry-positive cells (senescence, SASP). **d.** Heatmap of differentially expressed genes showing that senescence markers (notably *Cdkn2a*, *Cdkn2b* and *Cdkn1a*), as well as SASP and lysosome markers are enriched in the mCherry-positive cell fraction, which shows down-regulation of proliferation-associated genes. **e.** Double immunofluorescence staining of mCherry expression in KY-FDR lungs 8 weeks after tumour induction with macrophages (CD68+) and endothelial cells (Pecam+). **f**. Quantification of the degree of colocalisation between mCherry and the different lung cell type markers from (e). **g.** Experimental schematic for pharmacogenetic ablation of mCherry (p16^{INK4a})-expressing cells with DT. DT treatment was initiated in *Kras$^{G12D/+}$;p16$^{FDR/+}$*;*Rosa26$^{loxP\text{-}STOP\text{-}loxP\text{-}YFP/+}$* (KY-FDR) mice the day after AdCre administration and lungs analysed 2, 4 and 8 weeks post viral induction. **h.** FACS analysis of the proportion of YFP-positive tumour cells (relative to total live cells) between KY-FDR mice treated with either vehicle control or DT, showing a reduction in the number of YFP-positive cells after DT treatment. **i.** Quantification of number of tumour lesions in KY-FDR mice treated with either vehicle control or DT, showing a reduction in the number of lesions. *Note that these data belong to Dr Scott Haston (Martínez-Barberá group, UCL) and have been included in this thesis to show the results obtained in parallel to our experiments in Chapter 3, and to facilitate the understanding of the rationale behind our assessments of the macrophage and endothelial cell compartment in our model.*

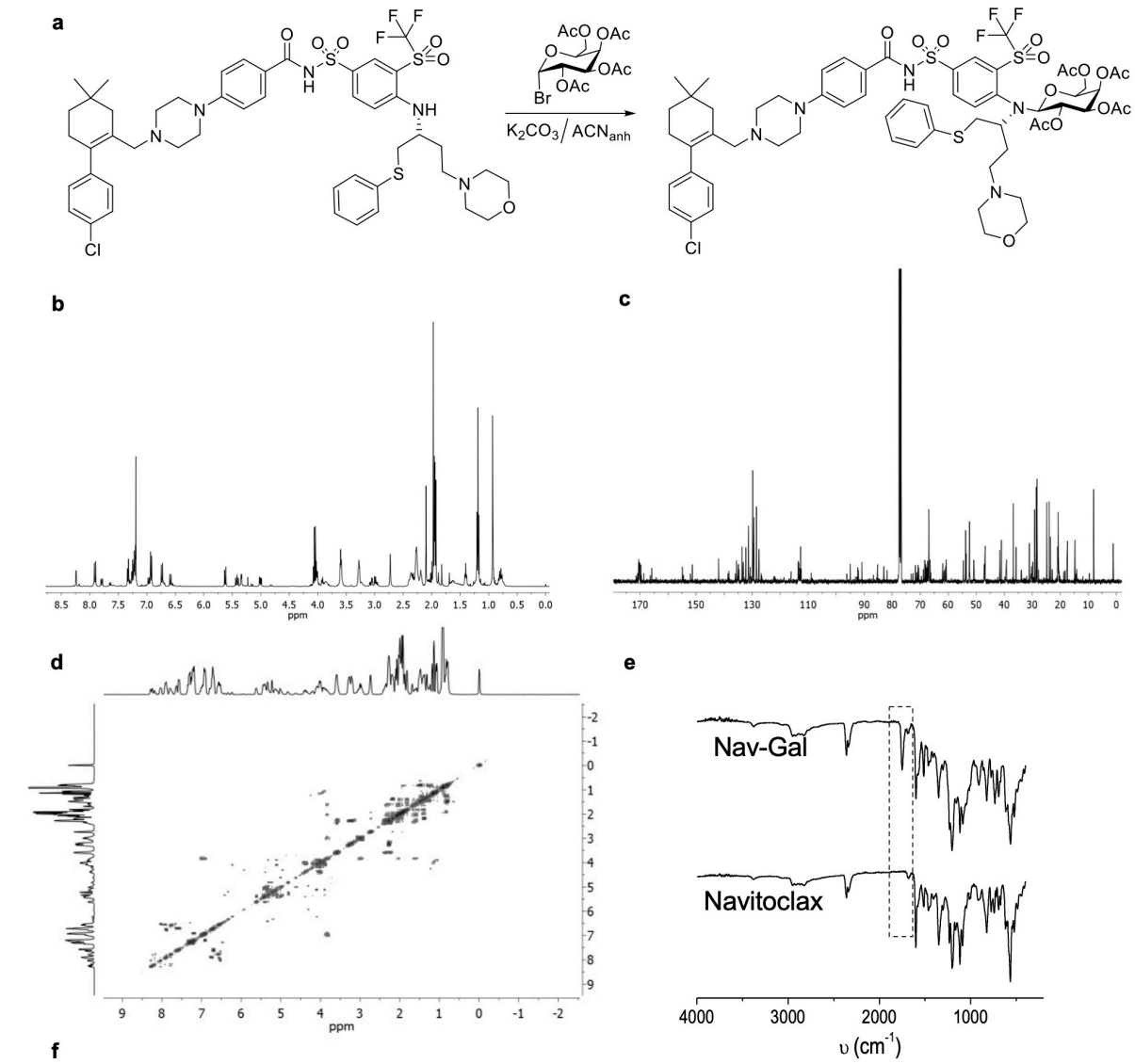
a
b
c
d
e
f
Nav-Gal
Navitoclax
υ (cm-1)
ppm
652.7035
487.6554
804.1578
974.3040
1134.2538
1304.4007
Mass/Charge, Da

Supplementary Figure 5.1. Molecular characterisation of Nav-Gal. a. Schematic chemical structural representation of synthesis of Nav-Gal prodrug. **b, c.** Chemical shifts of the signals of proton **(b)** and carbon **(c)** atoms of Nav-Gal observed in 1H and 13C NMR recorded in a 400MHz NMR spectrometer using deuterated chloroform (CDCl3) as solvent. 1H NMR (400 MHz, CDCl3) δ = 8.25 (d, J=2.19Hz, 1H), 7.98 (d, J=9.18Hz, 1H), 7.86 (dd, J= 2.19, 9.18Hz, 1H), 7.41-7.26 (m, 5H), 7.03 (d, J=8.43,2H), 7.01 (d, J=8.43Hz,2H), 6.80 (d, J=9.4Hz, 2H), 6.65 (d, J=9.4Hz, 2H), 5.71 (d, J=8.24 Hz,1H), 5.48 (dd, J=10.37, 8.24 Hz, 1H), 5.41 (d, J=2.72 Hz, 1H), 5.07 (dd, J=3.41, 10.4 Hz, 1H), 4.09-4.06 (m, 1H), 4.00-3.94 (m, 2H), 3.80 (t, J=4.51 Hz, 4H), 3.28 (t, J=5.15 Hz, 4H), 3.10-2.92 (m, 3H), 2.73 (s, 2H), 2.43-2.14 (m, 12H), 2.04 (s, 3H), 2.02 (s, 3H), 2.01 (s, 3H), 1.99 (s,3H), 1.82 (s, 2H), 1.69-1.50 (m, 2H), 1.4 (m, 3H), 0.99 (s, 6H) ppm. **c.** 13C NMR (400 MHz, CDCl3) δ =170.24, 170.48, 170.26, 170.05, 169.21, 154.90, 151.31, 141.97, 135.55, 134.93, 133.63, 132.22, 131.34, 131.30, 131.29, 131.15, 129.83, 129.49, 129.44, 129.41, 129.39, 128.46, 127.62, 127.52, 113.60, 113.38, 112.67, 94.76, 90.80, 71.72, 70.76, 68.64, 68.35, 66.92, 60.68, 54.59, 53.79, 53.74, 53.56, 52.42, 50.86, 50.95, 46.82, 41.64, 41.00, 39.22, 36.77, 35.79, 31.00, 29.83, 29.11, 28.58, 28.26. **d.** Homonuclear bidimensional correlated spectroscopy 1H-1H (2D) COSY NMR (400MHz, CDCl3). Signals outside of the diagonal arises from the protons that are coupled together in neighbouring carbons. **e.** Attenuated total reflectance (ATR) spectra of Nav-Gal and Navitoclax compounds, the signal centred at ca. 1795 cm-1 are assigned to the C=O stretching vibration present in Nav-Gal structure. **f.** The high-resolution mass spectra shows molecular fragments obtained after Nav-Gal ionization corroborating the chemical structure of Nav-Gal. HRMS-EI m/z: calculated:(M+H) = 1304.3979 m/z, measured:(M+H) = 1304.4001 m/z. *This work was performed by Dr Beatriz Lozano-Torres (Polytechnic University of Valencia).*